The University Of Sheffield.

The role of *Gata3* in the functional development of cochlear hair cells

By:
Tanaya Bardhan

A thesis submitted in partial fulfilment of the requirements for the degree of Doctor of Philosophy

The University of Sheffield
Faculty of Science
Department of Biomedical Science

September 2016

Abstract

Developmental mechanisms provide insight into potential therapies for auditory regeneration. *Gata3* is one of the earliest expressed transcription factors during auditory development and it is essential for the development of the auditory sensory epithelium. Haploinsufficiency in man manifests as hypoparathyroidism, sensorineural deafness and renal dysplasia (HDR) syndrome. In a heterozygous mouse model of this condition, hearing loss has an early onset that is apparently associated with functional defects in outer hair cells but the cause of hearing loss is unknown. Our aims were to identify the earliest electrophysiological deficits in hair cells to explain the observed hearing loss in HDR syndrome and to characterize the developmental function of *Gata3* in the auditory sensory epithelium. We then proposed to identify factors that might upregulate *Gata3* and restore hearing. Electrophysiological recordings of embryonic, neonatal and young adult outer hair cells showed that they differentiate normally in heterozygous mice, although some die at very early postnatal stages. However, inner hair cells suffer deficits in the function of the potassium conductances $I_{k,f}$ and $I_{k,n}$ at the onset of normal hearing. When *Gata3* was knocked down selectively in inner hair cells from around embryonic day E16, similar deficits were observed. This is the first evidence that *Gata3* has a cell autonomous function in the physiological differentiation of hair cells.

Conditionally immortal, *Gata3* reporter cell lines were then derived from otocysts of mice carrying the SV40 immortalising gene and a BAC construct with the *Gata3* enhancer region linked to *Egfp*. The *Gata3* reporter faithfully reproduces the expression pattern of endogenous *Gata3* in the BAC transgenic mouse during

normal inner ear development and it correlates with GATA3 protein in the reporter cell lines. These lines can thus be used for more detailed studies on how *Gata3* regulates functional expression of potassium conductances in hair cells. More importantly, they can be used to screen for small molecules and drugs that might be able to upregulate *Gata3 in vitro*, which could potentially rescue the phenotype of HDR syndrome and provide an important therapeutic component for sensory regeneration.

Acknowledgements

I would like to express my sincerest gratitude to my supervisor, Prof. Matthew Holley, for continually believing in me and giving me the freedom to carry out this study, when I wanted to take it down a different path than was originally intended. His keen insight, frank honesty and sense of perspective have been invaluable life lessons; his sense of humor and ready wit made the lab a fun place to be in.

I am deeply indebted to Prof. Walter Marcotti for enduring my endless, often silly questions, when I turned into the accidental physiologist. He welcomed me into his 'family of physiologists' and kept me focussed, challenged, excited and nurtured my eagerness (occasionally annoying) about all things related to electrophysiology.

Jenny has been my patch *guru*, and because of her, today, I feel like I can patch anything! I am thankful to Stuart, my go-to person for any rig issues, and to Laura for always being around to answer my unending stream of questions and also for reading drafts of my thesis. I am grateful to Maria for her positive attitude towards my infinite genotyping requests, and also to Paul for helping out tirelessly with the cell lines.

This would certainly not have been possible without the unconditional support of my partner, Shann, who uprooted his life in Singapore to be by my side, and has been my chef, chauffeur, ATM, sounding board and my 'frenemy' all at once.

Finally, I would like to acknowledge Deafness Research UK for providing us with the funding necessary to carry out the work, and also extending the timeline of the project when the odds were against us.

Contents

Glossary

ABR	Auditory Brainstem Recordings. 28
ACh	acetylcholine. 38
BAC	Bacterial Artificial Chromosome. 32
bHLH	basic helix-loop-helix. 17
BMP	Bone Morphogenetic Protein. 16
CDH23	Cadherin23. 11
DBD	DNA Binding Domain. 22
DMEM	Dulbecco's Modified Eagle Medium. 49
DPOAE	Distortion Product Oto-acoustic Emissions. 29
EP	endocochlear potential. 12
ER	endoplasmic reticulum. 145
EYFP	Enhanced Yellow Flourescent Protein. 121
FACS	Flourescence Assisted Cell Sorting. vii, 55
FCS	Fetal Calf Serum. 51
FGF	Fibroblast Growth Factor. 15
GER	Greater Epithelial Ridge. 8
HC	hair cells. 8
HDR	hypoparathyroidism, deafness and renal anomaly. 28
HL	hearing loss. 18
IHC	inner hair cells. 7
IL-4	Interleukin 4. 147
MET	mechanoelectrical transducer. 11
OAE	Oto-acoustic Emissions. 58
OHC	outer hair cells. 8

PCDH15	Protocadherin15. 11
PKB	Protein Kinase B. 168
PTS	permanent threshold shift. 29
SERCA	smooth endoplasmic reticulum calcium ATP-ase. 145
SHH	Sonic Hedghehog. 15

List of Figures

List of Tables

Chapter 1

Introduction

Our sense of hearing is an exquisite product of evolutionary engineering, which helps us to negotiate our environment, interpret its acoustic stimuli, and respond to them. It enables us to process speech, learn, and communicate effectively. Along with the other four special senses, it allows us to decode the nature of our environments continuously. Being a vital sense that allows us to process and respond to extrinsic stimuli, any form of impairment has a direct impact on the way we interact with our environment.

Prevention of hearing loss or restoration of our auditory capabilities has been an enduring challenge to the scientific community. Mammals, although equipped with a highly sophisticated organ for hearing, fail to regenerate their sensory cells in the event of damage or loss, a feat easily accomplished by lower vertebrates like fish, amphibians, reptiles and birds [Edge and Chen, 2008]. Their regenerative ability has sparked tremendous interest into studying the process of cell death, restoration and their fundamental underlying properties, with the ultimate goal of functional replacement of sensory cells in humans. To this end, gene therapy [Fukui and Raphael, 2013], stem cell therapy [Shi and Edge, 2013] and the administration of neurotrophic factors into the inner ear [Ramekers et al., 2015] have emerged as experimental treatments. Despite proof-of-principle studies in these areas, these interventions are fraught with challenges that include, but are not limited to the delivery of agents, target specificity, side effects and inefficient functional recovery.

The astoundingly high statistical prevalence, intractable nature and poor prognosis of hearing loss highlights the need for both preventative measures as well as better intervention methods than the ones that currently exist. Central to the idea of better management of this condition is the need to understand the process of development of the auditory system, and the intrinsic molecular cascades that instruct the formation, function and survival of the different types of specialized cells constituting it. Over the past 150 years or so, although our knowledge of the anatomy and physiology of the system has expanded, the inductive events and the genetic and molecular aspects of auditory development are still not entirely understood. Understanding the role of transcription factors and the signaling mechanisms they regulate during early development could potentially provide insight into regeneration of the auditory system.

Whilst a majority of work in regeneration has focused on sensory epithelia, most forms of hearing loss concern homeostatic aspects of the whole hearing organ. Thus to look at potential regeneration, it is important to study mechanisms of development at earlier stages. In this work I attempt to dissect the role of an essential inner ear transcription factor called GATA3. GATA3 is expressed in all major tissues of the ear from the earliest stages of development to maturity. We believe that understanding its function could enlighten ways in which to stimulate regeneration. To put this into context it is necessary to describe inner ear development, structure and function, which is the purpose of the introduction. At the end of the chapter I shall state the goals of my study, and will then go on to explain in more detail the approach, methods and conclusions in subsequent chapters.

1.1 Sound reception and interpretation: how and where it happens in the mammalian auditory system

Pressure oscillations in air are responsible for the sound that we perceive. The outer ear consists of a cartilaginous structure called the pinna and a resonant cavity called the concha which leads into the ear canal, terminating at the eardrum or tympanic membrane. Together the concha and ear canal form a complex acoustic cavity. The pinna collects acoustic vibrations from our environment, which then bounce off the concha and are then funnelled inwards along the external auditory canal. This causes the thin and pliable tympanic membrane to move inwards and outwards due to the impinging sound waves (Figure 1-1).

The effect of the outer ear on the incoming sound waves is two-fold. The resonances of the outer ear increase the sound pressure of the incoming sound waves at the eardrum by 15-20 decibels (dB), especially the lower frequencies between two and seven kilohertz which correspond to human speech. It also provides directionality cues which aid in sound localization in space - the ability to distinguish the source of sound from front or behind, and above from below. The more important binaural cues about sound localization are derived from timing and intensity differences between the two ears [Middlebrooks and Green, 1991].

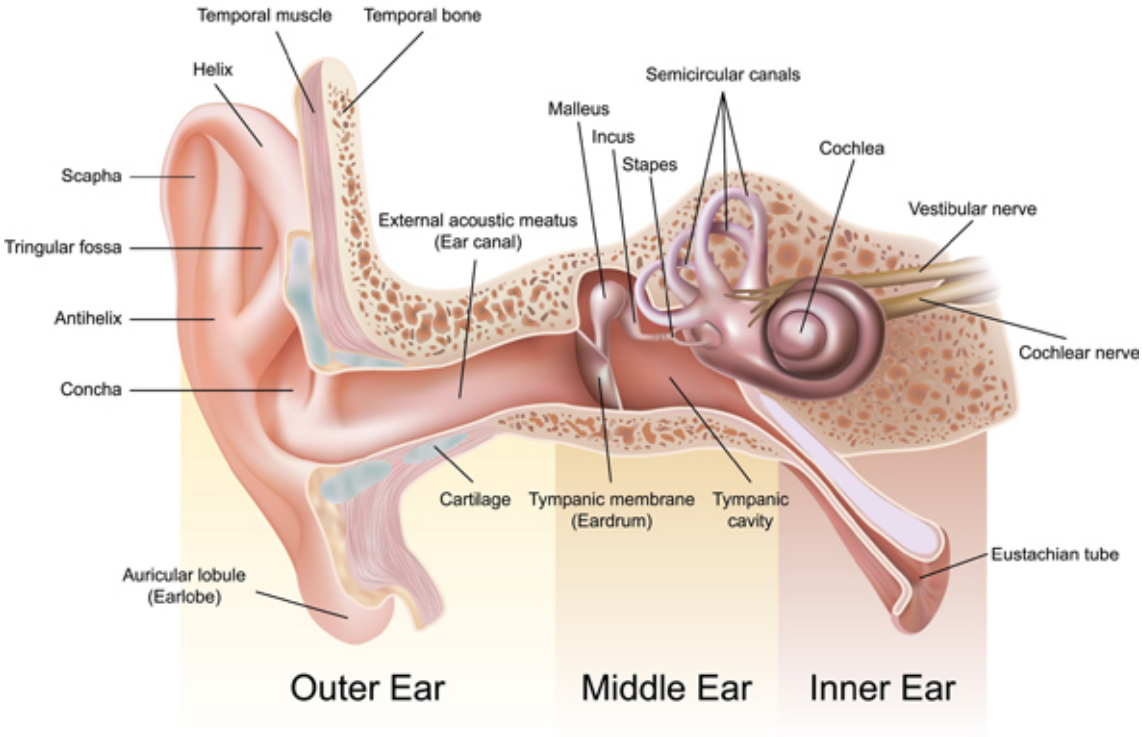

Figure 1-1: Anatomy of the peripheral auditory system in humans. It is divided into three sections: the outer ear is composed of the external pinna/earlobe and the auditory canal; the middle ear is composed of the ear drum and the ossicles; and the inner ear comprises of the vestibular organ for balance, and the cochlea for hearing (www.headfi.org).

This movement of the tympanic membrane sets in motion the three inner ear ossicles - the malleus, incus and stapes, which together function as a system of levers. The interlocking ear ossicles are suspended in the air-filled middle ear cavity and contact the tympanic membrane on one end and the oval window at the other, forming a continuous connection between the outer and inner ear chambers. Since sound waves travel from a low impedance air-filled environment to the high impedance fluid-filled environment in the inner ear, it would lose most of its incident energy at the air-fluid interface. The middle ear apparatus serves to primarily act as an acoustic impedance transformer in order to compensate for this loss while transferring the sound pressure characteristics in the external ear to the sound pressure variations in the inner ear. The smaller area of the oval window in comparison to the tympanic membrane, the lever action of the ossicles, and the conical shape of the tympanic membrane - all contribute to this impedance matching.

The middle ear also has two sets of striated muscles, the tensor tympani attached to the malleus and the stapedius muscle attached to the stapes. Contraction of these muscles increases the stiffness of the middle ear ossicular chain. This functions to dampen potentially harmful sounds and thereby prevent them from reaching the inner ear. This is called the middle ear/acoustic reflex [Møller, 1974].

The inner ear comprises the highly organised coiled cochlea, the three semi-circular canals and two maculae. The spiral cochlea is divided into three fluid-filled chambers that run along its entire length, from the base of the cochlea to the apex. The outer perilymph-filled chambers are the scala vestibuli and scala tympani, and the central endolymph-filled chamber is the scala media. While the scala media is partitioned from the scala vestibuli above by the Reissner's membrane, it is separated by the reticular lamina from the scala tympani below it (Figure 1-2). The scala vestibuli and scala tympani are joined at the apex by an opening called the helicotrema. The reticular lamina is the apical surface of the organ of Corti, which in turn rests upon the fibrous basilar membrane.

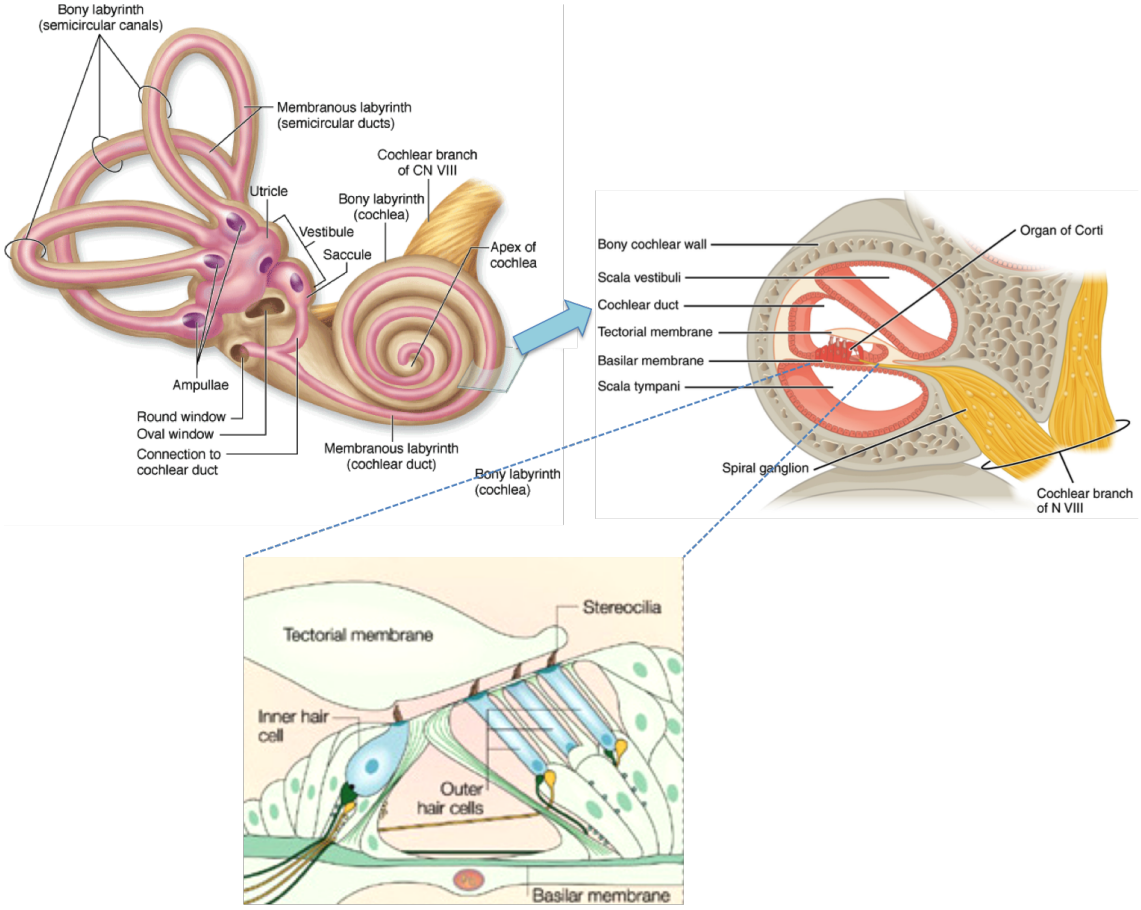

Figure 1-2: Diagram illustrating the vestibulo-cochlear apparatus, and a cross section of the cochlear duct. The cochlear duct has three compartments, two perilymph-filled peripheral chambers, and the central endolymph-containing scala media. The organ of Corti is located in the scala media. Zoomed in view of the organ of Corti shows the sensory hair cells and the supporting cells (image modified from www.cns.org and [Mescher, 2010; Hudspeth, 2014])

When sound vibrations cause the oval window to move, this causes the fluid inside the scala vestibuli to be displaced to a second window called the round window opening into the scala tympani. This causes the movement of the cochlear partition and fluids, and generates a wave-like motion of the basilar membrane (Figure 1-3) that corresponds to the incoming sound frequency, which travels apically along the basilar membrane as a passive travelling wave [Von Békésy and Wever, 1960]. For a pure tone, the membrane displacement reaches a peak at a narrow region, in a frequency-dependent manner. For a lower frequency, this wave travels farther along the membrane before it reaches its maximal amplitude near the apex, and the reverse is true for a high frequency sound. Simply put, each narrow region

along the basilar membrane displaces maximally to only a certain frequency (called its characteristic frequency), like a band pass filter, thereby contributing to the sensitivity and frequency discrimination of the incoming signals.

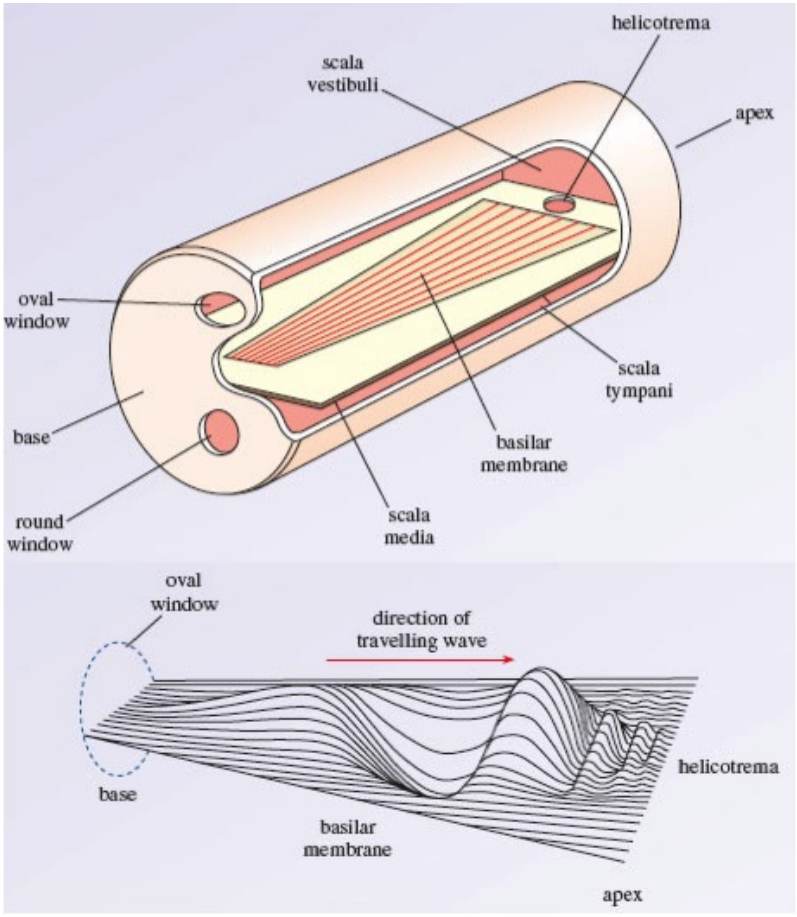

Figure 1-3: Schematic diagram of the travelling wave along the basilar membrane. Upper panel shows the variation in width of the basilar membrane along the uncoiled cochlear duct. The lower panel shows the movement of sound-induced travelling wave along the basilar membrane. Lower frequency sounds travel further along the membrane towards the apex (image modified from www.open.edu)

The organ of Corti, the mammalian sensory epithelium, has a highly specialized structure with receptor cells called hair cells (HCs), supporting cells and nerve fibres. In the human organ of Corti there are about 15,000 HCs in each ear [Úlehlová et al., 1987]. Two different kinds of HCs are arranged in three to five concentric rows. In humans, there are generally three rows of outer hair cells (OHCs) and one row of inner hair cells (IHC). Structural rigidity is maintained within the organ of Corti due to an arch formed by the rod-like pillar cells which

form the Tunnel of Corti. On the modiolar side of the structure, inner phalangeal cells surround the IHCs and on the other side of the tunnel, Deiter's cells form a cup-like structure to dock the base of each OHC, and also extend longer phalangeal processes to the reticular lamina. Other supporting cells are also present - like the inner sulcus cells and interdental cells on the modiolar side of the inner hair cells (HC) and Claudius' cells, Hensen's cells and external sulcus cells external to the outer hair cells (OHC) [Raphael and Altschuler, 2003].

Supporting cells serve a diverse range of functions [Wan et al., 2013]. They span the entire depth of the sensory epithelium, from the basal end to the lumen, thereby collectively providing structural stability to the entire system. They help maintain an optimal ionic climate within the organ of Corti by recycling potassium ions. They also serve as tissue-resident phagocytes to clear up hair cell debris following injury and trauma [Anttonen et al., 2014]. Supporting cells in conjunction with interdental cells of the Greater Epithelial Ridge (GER) produce and generate the elements of the tectorial membrane, a gelatinous structure composed of collagens and tectorins that overlie the HCs.

HCs are responsible for the reception of auditory stimuli. The flask-shaped IHCs serve as the primary auditory receptors. They are about 35 microns in length and 10 microns (in chinchilla) wide at their widest point, with a centrally located nucleus and most mitochondria and cellular organelles concentrated at the apical pole of the cell. Within the presynaptic site, are electron-dense elements called synaptic ribbons. Several neurotransmitter-filled synaptic vesicles remain closely tethered to these ribbons so as to effectively coordinate the release of glutamate onto the afferent terminals associated with each ribbon [Liberman et al., 1990]. Afferent neurons at the base of the IHCs carry information to the brain via the auditory pathway through several brain nuclei, as the raw data is decoded and continually processed before reaching the auditory cortex of the brain.

OHCs, on the other hand, are cylindrical in shape, and 20 - 100 microns in length depending on their position along the cochlea in the guinea pig [Pujol et al., 1998], with the longer cells being at the apical end. They have a basally located nucleus, with mitochondria arranged in groups at the basal, apical and lateral areas of the cells. The apical surface of both IHCs and OHCs is marked by the presence of actin-dense microvilli-like structures bathed in endolymph that project through the reticular lamina, called the stereociliary bundle. This is from where the hair cell derives its name. They form a V-shaped 'staircase' structure on the surface of OHCs and crescent-shape on IHCs, with a very precise orientation and height-ranked arrangement of rows of stereocilia within the hair bundle on the surface of each hair cell. All the stereocilia within each row are connected by fine extracellular links so that they tend to move together. Tip links also project from the tips of shorter stereocilia to connect them to the tips of longer stereocilia in adjacent rows [Hackney and Furness, 1995; Kachar et al., 2000].

Fluid displacement coupled with basilar membrane movement, causes movement of the partition, and the architecture results in shear movement between the basilar membrane and reticular lamina. The direction of deflection alters the gating of mechano-sensitive ion channels located on the stereociliary bundles of IHCs, triggering a series of events finally responsible for eliciting currents; thereby transducing mechanical information contained in sound stimulus into a chemical signal, which further gets transformed into an electrical signal as it is carried away from the hair cells via afferent fibres towards the brain via an ascending pathway. The stereociliary bundles of OHCs are embedded into the overhanging collagenous tectorial membrane. Generation of shear force at the stereociliary bundle and the displacement of the basilar membrane, causes OHCs to rapidly change in length in response to changes in membrane potential (Figure 1-4), due to a motor protein in their lateral wall, called prestin [Ashmore, 1987; Dallos and Evans, 1995; Dallos

et al., 2006]. This active form of cochlear mechanics, called electromotility, serves to amplify mechanical inputs and further sharpen frequency selectivity.

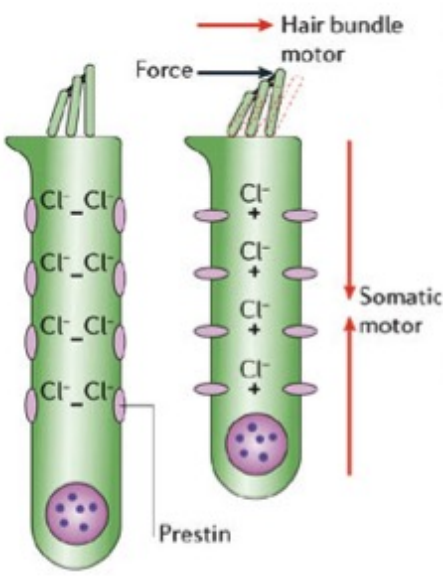

Figure 1-4: Schematic diagram showing the mode of action of a cochlear outer hair cell. Prestin allows the hair cells to shorten in length upon depolarisation, and elongate upon hyperpolarisation, a phenomenon called electromotility. This allows the outer hair cell to mechanically amplify sound-induced vibrations of the basilar membrane, and augment frequency tuning (modified from [Fettiplace and Hackney, 2006])

1.2 Functional properties of the hair cell

Mechanotransduction, the ability to transduce mechanical force into cellular electrochemical signals, forms the basis of sound perception. The inner ear represents a highly specialized form of mechanoreception, detecting a wide range of sound stimuli and converting these into electrical signals with remarkable sensitivity, speed and precision. The initial step in the sound transduction cascade is accomplished by the hair bundle that crowns the HC.

At the onset of hair bundle morphogenesis, the entire apical surface of the HC is covered with numerous microvilli-like structures, which initially all grow to a comparable height around a taller centrally located kinocilium, which migrates to

the cell periphery, thereby establishing bundle polarity. After a period of sequential staggered stereociliary elongation [Kaltenbach et al., 1994; Nishida et al., 1998], and subsequent increase of width, the mature hair bundle consists of two or more rows of stereocilia, in a staircase-like arrangement, with their vertices positioned away from the centre of the cochlea.

Hair bundles transduce sound, linear and rotational acceleration into receptor potentials, which are further translated into neurotransmitter release at the base of the HCs. In the mammalian cochlea, deflection of the hair bundle towards the tallest stereocilia in the excitatory direction leads to the stretching of the oblique tip links that connect shorter stereocilia to their counterparts in the adjacent taller row. Cadherin23 (CDH23) and Protocadherin15 (PCDH15) comprise the intertwined elements of the tip links [Kazmierczak et al., 2007]. Tension due to deflection in the excitatory direction, opens non-selective mechanosensitive cation channels, located within close proximity to PCDH15 near the top of the shorter stereocilia, generating a rapidly activating inward transducer current, carried predominantly by K^+, from the K^+ rich-endolymph that bathes the stereociliary bundles; however, there is a smaller but important contribution from Ca^{2+}. The channels are open to various degrees at rest, depending on numerous conditions such as the endolymphatic Ca^{2+} concentration, and can be closed when the bundle is deflected in the opposite inhibitory direction towards the shorter stereocilia. The exact molecular properties of the HC mechanoelectrical transducer (MET) channel remain elusive.

When HCs are initially specified and differentiate within the sensory epithelium, they are virtually indistinguishable from each other. However, in order to undergo their distinct functional specializations, they physiologically diverge starting from birth (in mice), and functionally mature at P8 and P12 for OHC and IHCs respectively, just before the onset of hearing (in mice).

The endolymphatic fluid bathing the stereociliary bundle of the HCs contains 150 mM K^+ ions [Wangemann, 2006]. This produces an endocochlear potential (EP) within the scala media, of approximately +100 mV, depending on the position along the cochlea. This unusually high EP is maintained by the active injection of K^+ ions into the endolymph by the stria vascularis, the lateral epithelium of the scala media. The high EP causes the flow of K^+ ions out of the scala media - this may be through the non-selective MET channel of the hair cells or through ion transporters and gap junctions in other cells of the system.

Intracellular depolarization of the HC, caused by the entry of K^+ ions through the MET channel due to the excitatory displacement of the hair bundle leads to a series of events, which ultimately triggers the fusion of synaptic vesicles at the cell membrane for neurotransmitter release. K^+ ions now have to be extruded from the HC in order for it to revert to its ground state, and this is effected by dedicated K^+ channels located in the cell membrane (Figure 1-5). HCs undergo extensive changes in their complement of ion channels as development progresses from immature HCs to fully functional mechanotransducers. Further details about these ion channels will be reviewed in chapters 3 and 4.

Immature IHCs are capable of generating spontaneous Ca^{2+}-dependent action potentials. This is because their MET channels remain partially open due to resting tension, and their membrane potentials lie close to threshold. The pattern of spiking is not consistent, and varies as a function of position along the cochlea [Johnson et al., 2011b]. This spontaneous spiking activity is proposed to provide instructional cues for maturation of the synaptic machinery, refinement of tonotopic circuitry and also influence gene expression. At later stages of postnatal development, when the membrane becomes more hyperpolarised due to the expression of the inward rectifier K^+ current, this pattern of repetitive action potential activity is abolished.

Mature HCs within the organ of Corti do not fire action potentials. Instead they respond with rapid and graded receptor potentials proportional to the magnitude of bundle displacement, which accurately encodes the properties of the incoming sound stimulus [Marcotti, 2012].

All information contained within sound stimuli, including frequency, intensity and timing has to be faithfully represented across the HC ribbon synapse before it is processed by higher centres in the brain. Ribbon synapses are designed for coordinated multivesicular and sustained neurotransmitter release. They are also found in the vestibular and visual systems. They dock several synaptic vesicles near the active sites for transmission. In mice HCs, they change their shape from round to ellipsoid upon maturation [Sobkowicz et al., 1982]. In the IHCs, each ribbon is associated with a type I afferent spiral ganglion neuron, which is activated upon glutamate release across the synaptic cleft. Fusion of synaptic vesicles with the cell membrane is triggered by the influx of Ca^{2+} into the cell body through $Ca_v1.3$ channels located close to the ribbons.

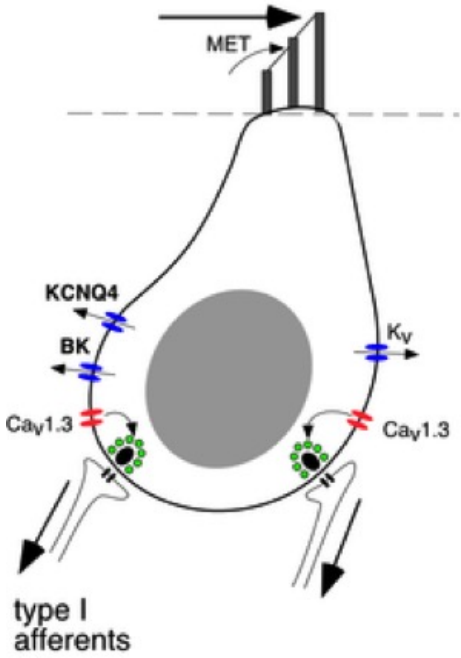

Figure 1-5: Schematic representation of a mature inner hair cell. The apical pole bears the stereociliary bundle and the basolateral membrane contains ion channels. The basal pole of the cell harbours the synaptic machinery, and is contacted by type I afferent fibres (modified from http://sfb894.uni-saarland.de/en/projects/a8-engel-2011-2014/)

As the biophysical properties of HCs change from firing spontaneous Ca^{2+}-dependent action potentials to responding with small, graded changes in receptor potentials, their synaptic machinery undergoes refinement by altering its Ca^{2+}-dependence from high-order to linear-dependence for exocytosis [Johnson et al., 2005], effectively improving the efficiency of transduction. Ribbon synapses in the auditory system possess their own set of nonclassical novel synaptic proteins like bassoon [Khimich et al., 2005], synaptotagmins [Safieddine et al., 2012], ribeye [Schmitz, 2009] and otoferlin [Pangršič et al., 2012].

1.3 Development of the inner ear

The development of the inner ear is a precise spatially and temporally monitored programme controlled by the complex interplay of signaling molecules which direct proliferation, growth, migration, morphogenesis, cell specification, differentiation,

survival and apoptosis. The first morphologically distinguishable event of otogenesis is the formation of an ectodermal thickening, called the otic placode, on either side of the rhombencephalon [Noramly and Grainger, 2002], adjacent to rhombomeres 5 and 6. The otic placode invaginates to form an otic cup (Figure 1-6), and just after neural tube closure, it pinches off from the ectodermal surface to form an otocyst by E9.5 in mice [Kelley, 2006]. Placode induction and early otocyst formation is directed by secreted Fibroblast Growth Factor (FGF) molecules from the neural plate and surrounding mesoderm [Schimmang et al., 2007]. Sonic Hedghehog (SHH), a morphogen secreted by the notochord and floor plate is important in activating paired homeobox containing family (*Pax*) genes, which are critical for vertebrate otic vesicle development [Torres et al., 1996]. The otocyst is a transient autonomous structure that contains all the information to effect the development and subsequent differentiation of most of the cell types of the inner ear. Other signaling pathways like Notch and Wnt are activated at this time to control placode size and otocyst patterning [Ohyama et al., 2006]. During placode invagination, otic neuroblasts delaminate from the anteroventral wall of the otocyst to form the cochleovestibular ganglion [Rubel and Fritzsch, 2002; Sánchez-Calderón et al., 2007], which serves to wire the inner ear to the central nervous system. SHH itself plays a critical role in neuroblast proliferation and in conferring a ventral identity within the otocyst [Riccomagno et al., 2005].Ventral otocyst identity is also promoted and maintained by GATA3, OTX2 and inhibition of WNT signaling in this domain [Groves and Fekete, 2012].

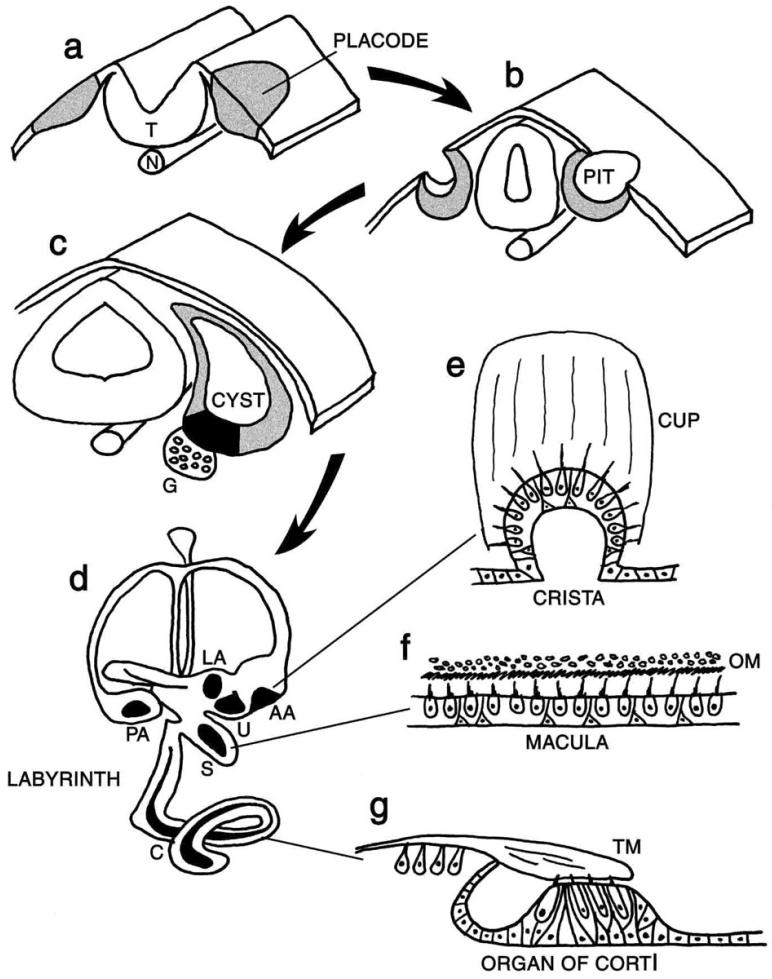

Figure 1-6: Scheme of the early development of the vertebrate inner ear (a-d), and the structure of the three types of sensory organ (e-g). The inner ear develops from the otic placode (a) an ectodermal thickening that invaginates to form the otic pit (b), which then pinches off from the surface ectoderm to form the otic vesicle (c). A complex series of events transforms the otic vesicle (c) into the structure (d) containing three cristae (e), two maculae (f), and an organ of Corti (g). Abbreviations: G, VIIIth ganglion; AA, anterior ampulla; LA, lateral ampulla; PA, posterior ampulla;, U, utricle; S, saccule; C, cochlea; CUP, cupula; OM, otoconial membrane; TM, tectorial membrane (www.researchgate.edu)

Dorsal identity, on the other hand, is promoted by another set of secreted signals - GBX2, DLX5/6, HMX2/3, GLI3 and bone morphogenetic protein Bone Morphogenetic Protein (BMP)4 [Bok et al., 2007]. At E13.5, the cochleovestibular ganglion splits to form the spiral ganglion that innervates the organ of Corti at the ventral aspect of the inner ear, and the vestibular ganglion, which innervates the five sensory organs at of the vestibular system at the dorsal aspect of the inner ear.

The otocyst undergoes a series of precisely orchestrated events during the course of the next three weeks that lead to the formation of an elaborate fluid-filled three-dimensional labyrinth housing the mature cochlear and vestibular sensory organs [Morsli et al., 1998]. The cochlea extends from the ventral region of the developing otocyst and coils 2.5 times around itself in mice [Morsli et al., 1998] as it projects anteriorly.

The specification of the prosensory domain within the cochlea is brought about by a dynamic interplay of factors. NOTCH signaling via JAG1 is critical in prosensory domain specification [Kiernan et al., 2001]. The HMG-box transcription factor SOX2 is also expressed in proliferating cells in this region, and mutations in *Sox2* results in an almost complete obliteration of sensory cell types [Dabdoub et al., 2008; Kiernan et al., 2005]. Later in development, SOX2, JAG1 are restricted only to the supporting cells. BMP4 has also been shown to play a key role in otic prosensory specification in vertebrates [Cole et al., 2000; Liu et al., 2005]. *Eye absent Eya1* plays an important role in prosensory specification. Its deletion causes a failure of prosensory specification and a gross perturbation of prosensory markers [Zou et al., 2008].

HCs and supporting cells arise from the newly specified neurosensory domain. The *Atoh1* gene, member of the *atonal* basic helix-loop-helix (bHLH) family of transcription factors is one of the earliest markers of newly specified HCs [Bermingham et al., 1999]. *Atoh1* expression is inhibited by the expression of *Id* (inhibitors of differentiation) proteins. Once ID proteins are downregulated, *Atoh1* activity is allowed and HCs form [Jones et al., 2006]. ATOH1-expressing cells then express Notch ligands *Jagged 2* (*Jag2*) and *Dl1*, which leads to activation of Notch signaling in adjacent cells, and expression of Notch targets *Hes1*, *Hes5*, *Hey1* and *Hey2*. Neighbouring cells are thus restricted to the fate of supporting cells by the

process of Notch-mediated lateral inhibition [Bryant et al., 2002].

Mammalian ears have six sensory patches once mature: three cristae associated with the semi-circular canals for detecting angular acceleration; two maculae in the utricle and saccule for the detection of linear acceleration; and the organ of Corti which lies within the cochlear duct, for detecting sound.

1.4 The Hearing Loss problem

According to estimates by the World Health Organisation (2015), 360 million of the global population suffers from disabling hearing loss (HL). This figure reflects more than 5% of the population worldwide and will continue on its upward trend as a consequence of living in societies with increasing noise levels [Daniel, 2007], exposure to ototoxic drugs [Freeland et al., 2010] and a longer average lifespan.

HL can be categorized in a few different ways. According to the anatomy of the ear affected, it can be divided into: conductive or sensorineural HL. Conductive HL results from a physical blockage of the outer and/or middle ear apparatus that impedes the transmission of sounds waves to the organ of Corti. This could be due to cerumen, excessive fluid due to infection, otosclerosis, tympanosclerosis and tumors. Sensorineural abnormalities are by far the greater threat, causing HL in the majority of cases. This results from the damage or loss of the sensory HCs of the inner ear and/or their associated neurons. HL of a mixed nature can also arise due to a combination of conductive and sensorineural defects.

According to severity of the audiological impairment, HL may be classified into mild (26 -40 dB HL), moderate (41 -70 dB HL), severe (71 -90 dB HL) or profound (exceeding 90 dB HL) [Alzahrani et al., 2015].

Causes of HL can be congenital or acquired. Congenital HL may be due to hereditary or non-hereditary factors at birth or soon after, and acquired HL refers to HL that develops at any age. Either may result in conductive and/or sensorineural HL.

The limited number of sensory HCs coupled with their inability to be replaced within the cochlea, makes HL an irreversible condition in mammals [Warchol, 2011]. The most widely available treatments to manage HL is the usage of hearing aids and cochlear implants. Modern hearing aids are small and discreet, are worn externally, and amplify sound from the external environment. There are however, several drawbacks to this line of treatment. Besides being ineffective for profound deafness and some other conditions, they often do not offer good resolution between background and foreground sounds, although this technology is continually being improved upon.

Cochlear implants, on the other hand, work by electrically exciting the auditory nerve and serve to partially substitute for the HCs only in the presence of functional spiral ganglion neurons. In cases where these neurons are damaged, there remains no therapy. Limitations of their use include high cost, compression of the entire auditory dynamic range and poor frequency resolution. Currently in the United Kingdom, only 5% of the adults that need cochlear implants are being fitted with one (www.earfoundation.org.uk)

Regeneration of HCs in the sensory epithelium has been an area of intensive research. *Atoh1* has been shown to be necessary for the differentiation of HCs in vertebrates [Bermingham et al., 1999]. However, the efficacy of *Atoh1* to induce the formation of new HCs is directly dependent upon the developmental stage of the animal investigated, with more success in embryonic [Woods et al., 2004] and neonatal animals [Zheng and Gao, 2000] than in mature animals [Atkinson et al.,

2014]. This reflects the idea that the efficacy of HC differentiation affected by *Atoh1* is directly related to the molecular context in which it acts. And knowledge of the complement of genes active within this molecular environment is scant as far as the vertebrate context is concerned. A more logical approach to instruct differentiation of HCs would be perhaps to identify earlier transcription factors, such as those seen to be expressed in the prosensory domain (wherefrom the precursor pool of hair and supporting cells are derived) such as *Sox2*, *Eya1* [Driver and Kelley, 2009] or *Gata3*, thereby recapitulating an earlier developmental molecular state, which may impart competence to uncommitted cells in the epithelium to respond to inductive extrinsic and intrinsic signals (like *Atoh1* for example), and guide their development along sensory or non-sensory pathways.

While *Sox2* and *Eya1* are involved in the specification of the prosensory domain, and are expressed relatively later on in the chronology of events in auditory development, *Gata3* is one of the earliest expressed transcription factors in the auditory system. The fly homolog of the *Gata* transcription factor, *pannier*, has been shown to be able to upregulate bHLH genes [García-Bellido and de Celis, 2009; Asmar et al., 2008]. The extensive expression of *Gata3* in the different constituent compartments of the auditory system during early ontogenesis suggests an instructive role in coordinating development across the entire system, via a common signaling mechanism. Moreover, *Gata* null mutants are entirely devoid of HCs in the cochlear sensory epithelium and exhibit an overall arrest of otocyst development [Duncan et al., 2011]. Critical regulation of precise levels of GATA3 is evident in neurosensory deafness in humans, which is a result of the presence of one copy of *Gata3*.

Few studies have addressed the role of *Gata3* in the inner ear in general and its role in the sensory epithelium in particular. The rationale for focusing on *Gata3* can be underpinned by the following fundamental observations:

1. The widespread and early expression pattern of *Gata3* in the developing otocyst, which then evolves in a dynamic spatio-temporal manner (Karis et al., 1999)

2. The complete absence of functional protein leading to a gross perturbation in normal otic development, and the complete lack of sensory HCs in the cochlea

3. The manifestation of sensorineural HL in the event of presence of only one functional copy of *Gata3*

   The above observations, taken together, argue for a role in coordinating the development of the auditory system and potentially in the specification and/or functional differentiation of cochlear cell types.

1.5 *Gata3*

Gata3 belongs to a highly conserved family of structurally homologous vertebrate transcription factors identified by their affinity to bind to the consensus DNA sequence GATA. The *Gata* family of six transcription factors (Gata1 through Gata6) are vital potentiators of specific gene expression during development and differentiation of a multitude of tissue systems. While GATA1 to 3 are broadly involved in development and survival of cells of the haematopoietic and immune system, GATA4 to 6 can be classified as endodermal factors.

Gata1 is essential for erythrocyte production [Pevny et al., 1991], maturation and differentiation [Pevny et al., 1995], and in the differentiation of megakaryocytes [Shivdasani et al., 1998]. It is also important in the development of Sertoli cells in the testes [Wakabayashi et al., 2003]. *Gata2* is critical for the proliferation and maintenance of haematopoietic stem cell progenitors [Vicente et al., 2012]. *Gata3* is considered to be a master regulator in the development and differentiation of the T-cell lineage in the blood system [Hosoya et al., 2010]. *Gata4* to 6 are expressed in

the heart, gut and adrenal glands [Xu et al., 2011; Jiang et al., 2008; Bossard and Zaret, 1998; Nakamura et al., 2007].

1.5.1 Structure of GATA3

GATA3 belongs to a class of zinc finger transcription factors, characterised by the presence of two highly conserved zinc finger motifs, each followed by basic regions. The gene is located in region 15 of P arm of chromosome 10. At the amino end (proximal) of the protein it harbours two transactivation domains (Figure 1-7), which enable it to interact with other factors and co-regulators. The carboxyl (distal) zinc finger is followed by its DNA Binding Domain (DBD) located within the basic region. This region can directly interact with the WGATAR sequence on a DNA strand. W can be replaced by nucleotides A or T, and R can be nucleotides A or G. Its proximal zinc finger is also capable of interaction with GATC sequences on DNA [Ho et al., 2009].

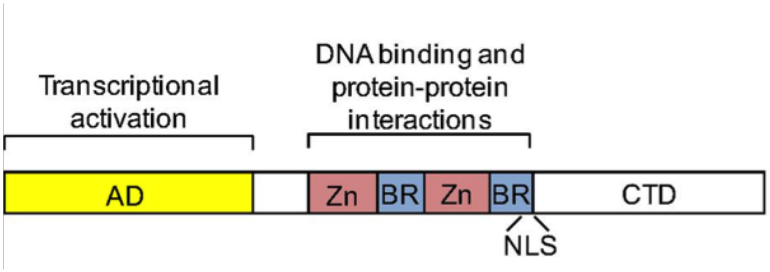

Figure 1-7: Schematic diagram showing the general structure of vertebrate GATA factors. Vertebrate GATA factors contain activation domains (AD) at the NH_2 terminus (yellow), 2 highly conserved zinc fingers (pink) with adjacent basic regions (BR, light blue), a nuclear localization signal (NLS), and a COOH-terminal domain (CTD). Modified from [Aronson et al., 2014]

X-ray crystallography and nuclear resonance imaging studies have attempted to shed light on the specific details of physical interactions of GATA3 with DNA. Thus far, two modes of interaction have been revealed: both zinc fingers can either bind or wrap around a specific DNA region in the 'wrapping mode', or each finger can interact separately so as to bridge two regions of DNA which may be located on different molecules in the 'bridging mode'[Chen et al., 2012].

1.5.2 Mammalian expression of *Gata3*

In the mammalian vertebrate system, *Gata3* exhibits a highly dynamic temporal and wide spatial expression. In human embryos, it is expressed from the beginning of the fourth week of gestation (a stage corresponding to embryonic day E8.5 in mice), when it is expressed in the foregut, nephric duct of the transient embryonic kidneys and rostro-caudal neural tube. By the end of the fourth week, its expression is seen in the otic vesicle, pharynx, parathyroid, primitive thymus, the prospective kidney tubules and frontonasal bud. During the fifth week, at a stage equivalent to E10.5 in mice, it's expression in the eye region, ectodermal thickenings of the olfactory placode, a specific population of postmitotic motor neurons in the rhomboncephalon on either side of the floor plate, and the branchial arches. In the trunk, expression in noticed in the ventral aortic wall, stomach and mesonephric branches [Debacker et al., 1999]. In the embryonic kidney, it is a direct target of *Pax2/8* and is required for the formation and guidance of the nephric duct [Grote et al., 2006]. In addition to the above, it is important in skin and hair follicle development [Fuchs, 2007], in proliferation and differentiation of luminal epithelial cells in mammary glands [Abba et al., 2006] and vital in the development of the nervous system [Lim et al., 2000].

With such a pleiotropic expression pattern, it is unsurprising that the homozygous null condition leads to mid-gestation lethality around E11-12 with several severe abnormalities[Pandolfi et al., 1995].

1.5.3 Expression in the auditory system

In the murine auditory system, the earliest expression of *Gata3* is noted in the otic placode at E8. As the otic cup forms, this expression is retained until the otic vesicle is formed at about E9.5. *Gata3* expression is localized along the walls of the otic vesicle apart from its dorso-lateral region [Lawoko-Kerali et al., 2002]. At

about E10.5, when the endolymphatic duct is formed from the dorsomedial region of the otocyst, the dorsolateral part of the otocyst expresses *Gata3*. In addition, the developing vestibular and cochlear pouch express *Gata3* at this stage. Within the elongating cochlear duct, only the posterior-medial edge, which forms the sensory epithelium, expresses *Gata3*. Outside the otic vesicle, *Gata3* is also expressed in the periotic mesenchyme [Lawoko-Kerali et al., 2002].

As development progresses, *Gata3* defines the epithelial tracts that would form the future posterior and anterior canals at the dorsal aspect of the otocyst. Simultaneously, the intensity of its expression in the vestibular atrium decreases while its cochlear expression increases considerably at E11.5. Expression in the vestibule continues to decline progressively, till it is barely detectable at E12.5. The striolar region of the utricle and the cruciate eminence of the semi-circular canals also express *Gata3* [Karis et al., 2001]. A GATA3-positive periotic population is seen in the area corresponding to the cochleovestibular ganglion [Lawoko-Kerali et al., 2002].

The cochleovestibular ganglion, which is initially formed by the accumulation of delaminating neuroblasts from the otic epithelium, morphologically separates into two distinct neuronal entities at about E14.5. It forms the GATA3-positive spiral ganglion that innervates the organ of Corti within the cochlea, and the GATA3-negative vestibular ganglion that innervates the five sensory organs of the vestibule [Lawoko-Kerali et al., 2004].

1.5.4 Within the sensory epithelium of the organ of Corti

The cochlear duct elongates by a morphogenetic process called convergent extension [Jones and Chen, 2007]. The short and thick sensory epithelium reorganises itself to become thin and long as it extends along its longitudinal axis and narrows

in the perpendicular medio-lateral direction. The distal end of the elongating cochlear duct will subsequently become the apical low frequency end of the sensory epithelium, while the proximal region will form the basal high frequency end of the mature organ of Corti [Echteler et al., 1989].

Cells in the primordial organ of Corti progressively exit the cell cycle from the distal end at about E12 and reach the proximal end following a two-day delay, at E14 [Ruben, 1967]. This Zone of Non-Proliferating Cells [Chen et al., 2002] encompasses the precursor domain from which HCs and supporting cells will differentiate. Differentiation of HCs however, commences soon after the last terminal mitoses from the basal end at around E14 and reaches the apex following a two-day delay again, thus establishing a longitudinal gradient [Rivolta and Holley, 1998]. Terminally differentiated HCs are identified by the expression of *Atoh1* and *MyosinVIIa* [Kelley, 2006].

There is conflicting evidence in the literature about the expression of *Gata3* in nascent HCs and the postnatal organ of Corti. Rivolta & Holley (1998), report the decline of GATA3 protein level as HCs differentiate from the base to the apex, while being maintained at high levels in the neighbouring supporting cells [Rivolta and Holley, 1998]. This downregulation in *Gata3* levels coincide with the innervation of HCs [Lawoko-Kerali et al., 2002]. In neonatal mice, GATA3 is not detected in HCs but is still present in the supporting cells. However, this expression too progressively diminishes until about P14, when GATA3 protein levels become undetectable in the entire sensory epithelium [Rivolta and Holley, 1998]. However, van der Wees'group has demonstrated that *Gata3* mRNA persists in HCs, spiral ganglion, supporting cells and the GER into adulthood, without showing any indication of diminished expression [van der Wees et al., 2004].

1.5.5 Hair cells and *Gata3*

Mammalian HCs in the cochlea, once formed, remain in a quiescent terminally differentiated state throughout life. They do not possess the capacity to spontaneously regenerate in the event of loss or injury. In lower vertebrates like fish and birds, the sensory epithelium is able to spontaneously give rise to new HCs [Brignull et al., 2009] by cell division or direct transdifferentiation of supporting cells [Roberson et al., 2004]. The mammalian vestibular sensory epithelia too exhibit limited plasticity in terms of HC regeneration [Forge et al., 1993].

HC production can however be induced by the ectopic over-expression of certain proteins. Retinoic acid has been shown to influence the production of supernumerary HCs within the organ of Corti [Lefebvre et al., 1993; Kelley et al., 1993]. The number of HCs produced varies with the dosage and timing of exposure, with the maximum yield being at E14. Thereafter, the capacity of extraneous HC production dramatically decreases, until P1 when retinoic acid seemingly has no effect [Kelley et al., 1993]. Interestingly, this precise temporal regulation of additional HC induction overlaps with the downregulation of *Gata3*. This suggests that *Gata3* might confer some kind of competency to cells in the prosensory epithelium within a specific developmental window and molecular context, to be recruited as HCs. Although other studies have demonstrated the production of HCs upon transfection of ATOH1 in postnatal mammalian inner ears [Zheng and Gao, 2000; Izumikawa et al., 2005], the ease and robustness of HC production in the embryonic stages seem greater. More recently Shh has been shown to be able to induce cell cycle re-entry and subsequent HC production in postnatal rat cochlea by attenuating protein retinoblastoma function [Lu et al., 2013].

1.5.6 Inner ear defects in *Gata3* null mutants

Gata3 null mutants die at an early embryonic stage of E10.5 to E13.5 [Karis et al., 2001; Pandolfi et al., 1995] due to noradrenaline deficiency in their sympathetic nervous systems [Lim et al., 2000], showing variable severity in phenotype associated with inner ear development. However, in all cases, the size of the otocyst is small compared to wild type animals and their subsequent morphogenesis is affected. The semicircular canals in the vestibular region of the otocyst do not develop as the periotic-mesenchyme interaction mediated by GATA3 is obliterated [Karis et al., 2001; Haugas et al., 2012], resulting in the failure to induce FGF10, a well-established requirement for semicircular canal formation [Lilleväli et al., 2006]. In addition to poor growth and development of the vestibular region, cochlear extension and coiling seem to be severely affected.

Gata3 is expressed only in the cochlear sensory neurons and not in the sensory afferents of the vestibular ganglion. Null mutation of *Gata3* seems to result in a limited formation of sensory neurons. Projection of efferent neurons into the vestibular nerve is also affected, suggesting a possible role of *Gata3* in efferent pathfinding [Karis et al., 2001].

As embryonic lethality precludes further analysis of sensory organ formation in null mutants, catecholamine-rescued mutants can provide insights into the development of sensory epithelium until E16.5. Rescued animals have demonstrated the formation of a shortened cochlear duct devoid of HCs and nervous innervation in the absence of GATA3 [Duncan et al., 2011]. Few HCs form in the maculae and reduced cristae in these rescued mutants, showing that vestibular HCs can form in the absence of GATA3 [Haugas et al., 2012]. The sensory epithelia often fail to separate efficiently in these mice, and cochlear HCs and supporting cells fail to differentiate, showing that this process is critically dependent on GATA3 [Haugas et al., 2012].

1.5.7 *Gata3* haploinsufficiency

Haploinsufficiency, caused by the presence of only one functional *Gata3* allele, is responsible for hypoparathyroidism, deafness and renal anomaly (HDR) syndrome in humans [Van Esch et al., 2000]. This autosomal dominant disease is inherited [Bilous et al., 1992] due to deactivation of a single allele resulting from intragenic deletions [Van Esch et al., 2000; Mejia et al., 2014; Fukai et al., 2013], missense [Gomes et al., 2012] or nonsense mutations [Nanba et al., 2013; Zhu et al., 2014].

The prevalence of HDR Syndrome (also known as Barakat disease) is unknown, but is reportedly quite rare, with only a handful of cases. Apart from the triad of complications after which the condition is named, other clinical symptoms range from cerebral infarction, hypocalcemia [Mejia et al., 2014], vestibular symptoms [van Beelen et al., 2014], craniofacial defects [Sheehan-Rooney et al., 2013] and seizures [Sau et al., 2013]. Due to the variability of the genetic mutations causing this condition, not all symptoms are present in every patient investigated. HL is the most penetrant complication presented [Van Esch and Devriendt, 2001], may be unilateral or bilateral, and is often seen to exist alone [Ali et al., 2007]. This highlights the requirement for stringent regulation of GATA3 protein levels for normal auditory function.

HL is usually detected by mandatory newborn screens, and this is followed by genetic screens to identify mutations in specific genes potentially causing the impairment. Because of the pleiotropic nature of HDR Syndrome and the serious nature of its secondary complications, it is important to understand the underlying genetic and molecular cause behind this condition to enable therapeutic intervention and management.

Auditory Brainstem Recordings (ABR) have revealed *Gata3* heterozygous

(*Gata3*$^{+/-}$) mice to have a 30 dB permanent threshold shift (PTS) in their hearing, making them a good model to study this condition. HL progressively deteriorates with age, as the architecture of the organ of Corti undergoes cellular degeneration. Interestingly, the rate of deterioration of hearing in haploinsufficient animals is similar to control animals [van der Wees et al., 2004], pointing towards a developmental role of *Gata3*. The OHCs at the apex are the first to deteriorate followed by IHCs, supporting cells and underlying nerve terminals, which also express GATA3 [van der Wees et al., 2004]. Distortion Product Oto-acoustic Emissions (DPOAE), considered to be an accurate measure of OHC function [Schrott et al., 1991], point towards dysfunction of the same [van Looij et al., 2005]. There are no apparent abnormalities associated with the auditory regions of the central nervous system.

1.6 Aims of the study

The objective of this study is to understand the role of *Gata3* in the mammalian cochlear sensory epithelium in the context of is potential role in regeneration. This requires a focus on the precise function of *gata3* in the development of the sensory epithelia. It also requires development of translational tools for screening regulators of *gata3* and for testing potential therapeutic interventions. I have addressed part of this question by focusing on the role of *gata3* in the most important cell population of the sensory epithelium, the HCs, in the first part of my project.

We hypothesize that HL in *Gata3*$^{+/-}$ animals is due to a developmental defect caused due to dose-shortage of GATA3, and not due to loss of GATA3 specifically in HCs. Secondly, we hypothesize that *Gata3* is not functionally important for HC maturation or in the functioning of mature HCs.

To test the hypotheses, I have used the following complementary approaches: Firstly, I have used *Gata3 tauLacZ* mice, which have a *LacZ* knock-in in one of the *Gata3* alleles, effectively rendering it heterozygous for *Gata3*, to model the audiological phenotypes of the HDR Syndrome. This allows us to model the effects of a knock-down or reduction of GATA3 levels. These mice have been used previously, and display hearing loss [van der Wees et al., 2004]. While the studies published have reported gross physiological and morphological analyses that are a result of reduction of GATA3 levels [van der Wees et al., 2004], there have been no studies to investigate the exact functional defect. Although malfunction of OHCs in particular have been suggested [van Looij et al., 2005], there have been no efforts to elucidate if IHCs contribute at all to this observed phenotype.

Here, I have established a comprehensive physiological screen of both OHCs and IHCs. To do this I have used whole cell patch clamp electrophysiology on acutely dissected organ of Corti preparations, whereby I have taken electrical readings directly from our cells of interest. Basolateral membrane properties have been recorded for a range of ages from pre-hearing to adult, to generate a developmental profile of characteristics, and present the most sensitive assay of HC function. This approach would help us understand the effects of a global GATA3 dose manipulation from the very beginning of the *Gata3* transcription process. It allows us:

- To study the possible differential effects of this condition on the OHCs and IHCs.
- To potentially help identify the earliest physiological signature of HDR Syndrome
- To attempt to rectify this phenotype *in vitro* with drugs or small compounds.

Secondly, we have genetically deleted *Gata3* specifically in HCs, using a HC-specific *Cre* driver, to then investigate the downstream effects of such a deletion on their

physiology. This study investigates the effects of a complete knockout of *Gata3* only from HCs (while leaving the supporting cells and neurons with normal GATA3 levels). It is important to note that this *Gata3* knock-out occurs only after *Gata3* has been allowed to exert its effects in the system for some time. A more detailed discussion about the procedure will follow in chapter 5. A combination of both these approaches would help us to elucidate:

- The effects of a systemic GATA3 dose reduction versus complete *Gata3* knockout only in HCs
- Whether *Gata3* exerts its effects on HCs in a cell autonomous or non-autonomous way
- There have been opposing reports of *Gata3* expression in differentiated HCs [van der Wees et al., 2004; Rivolta and Holley, 1998]. This method allows us to address the issue of whether *Gata3* has a role in HCs after their differentiation.

The second part of my project deals with establishing an *in vitro* system to validate the inferences from studies into the role of *Gata3* in the sensory epithelium. To this end, we have established an otic *Gata3 Egfp* reporter cell line, where *Egfp* is under the control of the *Gata3* promoter. This cell line can be used to test small drugs and compounds to screen for molecules that are able to modulate *Gata3* expression *in vitro*. The ultimate aim is to identify compounds which will be able to upregulate *Gata3*, and thus develop an assay whereby it will be possible to reverse the effects of *Gata3* haploinsufficiency. This can also serve as a tool to investigate signaling networks that GATA3 interacts with at a later stage.

Chapter 2

General Methods

2.1 Animal breeding and husbandry

All animal studies were licensed under the UK Home Office, under the Animals (Scientific Procedures) Act 1986, and had prior approval of The University of Sheffield Ethical Review Committee. Animals used in the study were housed at The University of Sheffield according to the Home Office guidelines. Transgenic animals were maintained and bred under a dedicated project licence issued to the Principal Investigator. Tissue was harvested from animals culled by a Schedule 1 method by a registered Schedule 1 practitioner, after completion of modules 1 and 2 of the Home Office animal handling course.

Heterozygous *Gata3 tauLacZ* knockout mice have one of their alleles replaced by a *tauLacZ* reporter construct which allows β-galactosidase to hydrolyse X-gal, and thereby yield an easily detectable insoluble reaction product [Hendriks et al., 1999]. All *Gata3 tauLacZ* mice were bred on a FVB/N background, reported to be a good hearing strain [Zheng et al., 1999]. Heterozygous *Gata3 tauLacZ* mice (hereafter referred to as $Gata3^{+/-}$) were bred with wild type mice so as to yield only wild type and $Gata3^{+/-}$ offspring as *Gata3* null mutants die at mid-gestation [Pandolfi et al., 1995].

Homozygous *Gata3 Egfp* mice and were generated by Bacterial Artificial

Chromosome (BAC) recombination as described previously [Panayi et al., 2010] and kindly gifted by Dr. Stavros Malos from the Cyprus Institute of Neurology and Genetics. For characterization of embryos, homozygous *Gata3 Egfp* mice were interbred and were checked for vaginal plugs regularly since the day they were mated. The time of earliest detection of plugs was considered to be E0.5. Embryos were harvested at E10.5, E12.5, E14.5 and E16.5.

Immortomouse (a kind gift from Dr. Md. Nassar at The University of Sheffield) were bred with C57BL/6 mice to generate mice heterozygous for the *T Antigen*. This was then cross-bred with homozygous *Gata3 Egfp* mice to yield embryos heterozygous for both *Gata3 Egfp* and *T Antigen* transgenes. Embryos were harvested at E10.5, E11.5, E13.5 and E15.5 for deriving conditionally immortal reporter cell lines for *Gata3*.

$Gata3^{flox}$, $Otof^{cre}$ and *Rosa26R Eyfp* transgenic mouse lines were also used and will be described in chapter 5. All animals were maintained in 12-hour light/dark cycles throughout the experiments. Adult and neonatal mice were killed by rapid cervical dislocation, and embryos beyond the age of E12.5 were decapitated, in accordance with UK Home Office (Animal Procedures) Act 1986.

2.2 Genotyping

2.2.1 Genotyping by protein staining

Gata3 tauLacZ - Ear clips or tails from *Gata3 tauLacZ* were incubated in glutaraldehyde (Agar Scientific, UK) fixative for 30 minutes followed by a couple of 10 minute washes in PBS (Thermo Scientific, UK). To this was added X-gal (Sigma Aldrich, UK) dissolved in buffer solution followed by incubation at 30°C in the dark. A blue reaction product indicated the presence of the knocked-in *tau LacZ*

construct for *Gata3*$^{+/-}$ animals. Tissue from wild type animals remained colourless.

2.2.2 Genotyping by visible phenotype

Gata3 Egfp - These animals were checked for EGFP by shining ultraviolet light into the eyes of the animals [Maeda et al., 2009]. These animals were further characterized for faithful reporter expression as detailed in chapter 6.

2.2.3 Genotyping by PCR

All other strains of mice were genotyped by polymeric chain reaction (PCR) amplification of genomic DNA. For adult experimental or breeding animals, DNA was extracted from earclips taken after P14. Tail samples from experimental animals were kept, to confirm the genotype if required. For animals younger than two weeks old, tail samples were kept after experiments for genotyping.

PCR reactions were set up in 10μl with 1X DreamTaq Buffer KCl, $(NH_4)_2SO_4$, 20 mM $MgCl_2$), primers at a final concentration of 0.4 μM, 0.2 mM dNTPs and 0.07 U DreamTaq polymerase (ThermoFischer Scientific, UK). Negative controls contained 1μl of PCR clean H_2O. For each reaction, 1μl DNA at a concentration of 50-100 ng/μl was added. PCR programmes (in Bio-Rad Thermo Cycler) varied according to genotyping protocols as exemplified in Table 2.1. Both, *Otof*^{cre} and *Rosa26R Eyfp* reactions were set up containing all three primers. *Gata3*^{flox} reactions were separated, i.e. primer pair 1 and 2 and primer pair 1 and 3 were set up in two different reactions.

TABLE 2.1: *Genotyping protocol*

Strain	Primer	Primer sequence 5'- 3'	Protocol	Expected bands
Rosa26R Eyfp	P1 P2 P3	AAGACCGCGAAGAGTTTGTC AAAGTCGCTCTGAGTTGTTAT GGAGCGGGAGAAATGGATATG	1) 94°C, 3 min; 2) 94°C, 30 sec; 3) 58°C, 1 min; 4) 72°C, 1 min; repeat 2-4, X 35; 5) 72°C, 2 min	Wt 600bp Het 320 & 600bp Mutant 320bp
$Gata3^{Flox}$	P1 P2 P3	TCAGGGCACTAAGGGTTGTTAACTT GAATTCCATCCATGAGACACACAA GTGCAGCAGAGCAGGAAACTCTCAC	1) 94°C, 3 min; 2) 94°C, 30 sec; 3) 58°C, 1 min; 4) 72 °C, 1 min; repeat 2-4, X 35; 5) 72°C, 2 min	Wt 150bp Het 150bp & 220bp Mutant 220bp Del 240bp
$Otof^{Cre}$	P1 P2 P3	CAGCACACTGGCGGCCGTTACTA AGAGAAACACAAGGTCGGGCTCAATCT TGGTCGGGTCTGTGGTGTTACAACT	1) 94°C, 3 min; 2) 94°C, 30 sec; 3) 61°C, 30 sec; 4) 72°C, 30 sec; repeat 2-4, X 30; 5) 72°C, 5 min	Wt 561bp Het 561bp & 418bp Mutant 418bp
Immortomouse	P1 P2 P3	GATCTGCCTGAGGTGTTACTTG GGATGGCATCACTAGTCATGAC AGTCCTCACAGTCTGTTCATGATC	1) 94°C, 3 min; 2) 94°C, 30 sec; 3) 61°C, 30 sec; 4) 72°C, 30 sec; repeat 2-4, X 30; 5) 72°C, 5 min	Wt 500bp Het 300bp & 500bp Mutant 300bp

2.3 Tissue preparation for electrophysiology

IHC and OHCs were studied in apical coils of acutely dissected organs of Corti from *Gata3 tauLacZ* mice between P6 and P50. All mice were killed by rapid cervical dislocation and the vestibulo-cochlear system was removed (Figure 2-1A)from the temporal bone and placed in small petri dishes containing ice-cold extracellular solution, and further dissected under a dissection microscope (Leica, Germany).

The cartilaginous or bony covering the cochlea (depending on developmental stage) was removed to expose the cochlear spiral still connected to the modiolus (Figure 2-1B). The coil was usually separated from the modiolus as a single entity (in stages younger than P8) and the stria vascularis was removed to expose the scala media.This allowed access to the organ of Corti. Usually in more mature stages (P8 and onwards), it was increasingly difficult to isolate the entire organ of Corti as a single entity, and the apical coil was selectively isolated.

The relevant cochlear coil was then placed in a recording chamber containing approximately 2 ml of extracellular solution. The coils were immobilized under a stainless steel grid (25 mm internal diameter) with nylon mesh stretched over it (1 mm distance between the nylon threads; Figure 2-1C) [Marcotti and Kros, 1999]. The tectorial membrane overlying the hair cells was carefully removed with fine forceps to gain direct access to the hair cells. The recording chamber was then placed upon the stage of an experimental microscope mounted upon an anti-vibration table. Cells were observed to remain healthy (in terms of appearance and low leak currents) for approximately 3 hours depending upon the age of the animal. Preparations from older animals were seen to decline in health sooner. All experiments were conducted at room temperature (21 - 25°C).

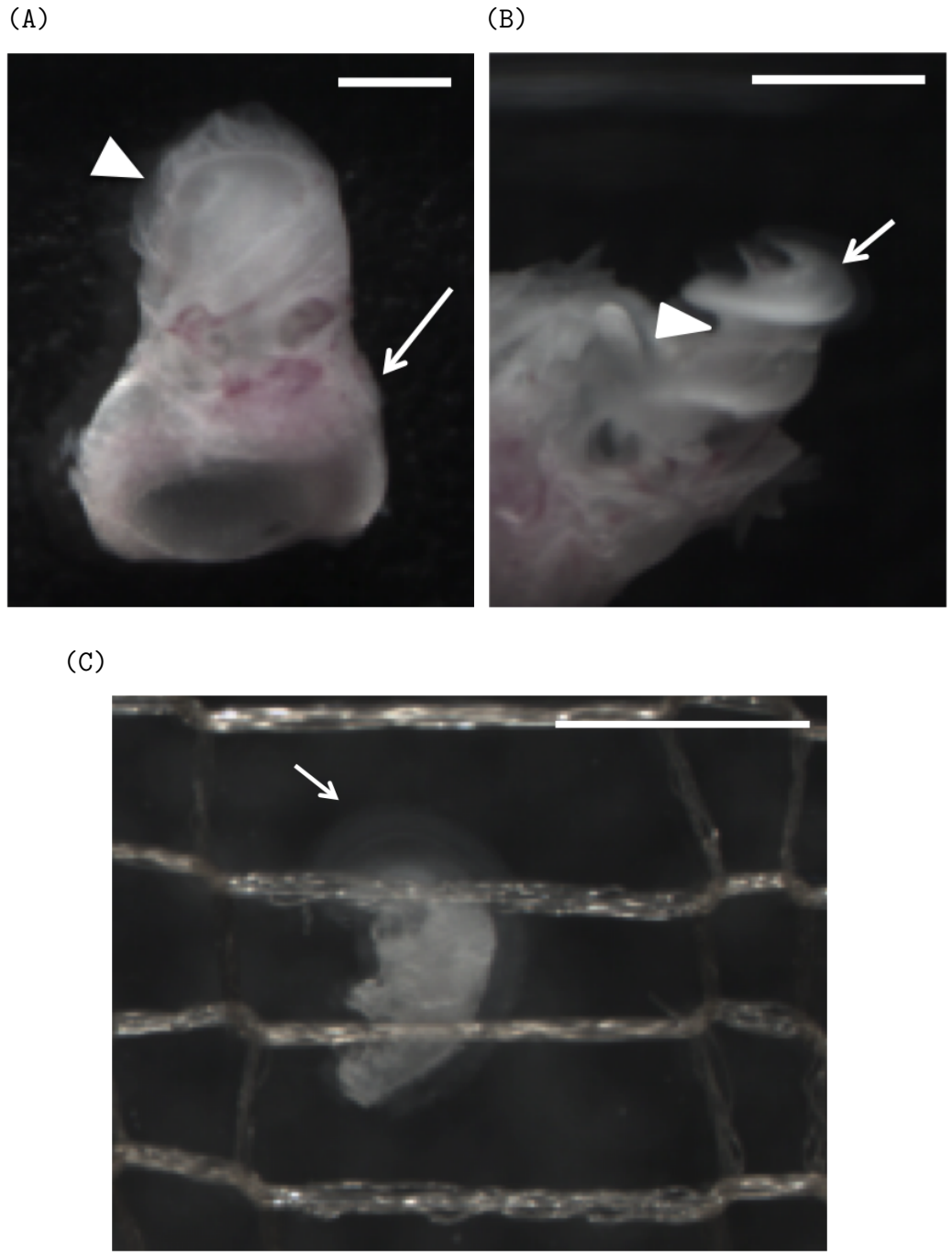

Figure 2-1: Photograph showing preparation of the cochlear tissue before recording electrical properties of hair cells.
(A) The entire vestibulo-cochlear apparatus of a P18 mouse after isolation from the temporal bone of the skull. The spiral structure of the cochlea can be clearly observed (arrowhead). The vestibular system (arrow) is helpful for holding on to during dissection
(B) The exposed organ of Corti (arrow) after removal of the bony covering and the stria vascularis. All electrical recordings in our study have been made from the apical coil (arrow), which has been left undamaged, and shall be removed from the modiolus (arrowhead)
(C) The apical region of the organ of Corti (arrow), containing the inner and outer hair cells has been placed under a nylon mesh on a recording chamber. Scale bars represent 1 mm

2.4 Experimental equipment

The recording chamber with the organ of Corti coil was placed on a custom-made rotating stage (Olympus, Tokyo, Japan) affixed to an upright microscope (Leica DM LFS, Leica Instruments, UK) with Nomarski DIC optics (X63/0.90 water-immersion objective). The microscope was placed on anti-vibration table (TMC, MA, USA) to prevent slippage of the recording electrode (Figure 2-2A). This entire set-up was placed in a Faraday cage that had a curtain interwoven with copper-mesh to provide isolation from noise while conducting experiments.

The tissue preparation was continuously perfused with fresh extracellular solution by a peristaltic pump (Cole-Palmer, IL, USA) at approximately 9 ml/hour connected to the recording chamber. The pump was placed outside the Faraday cage to prevent electrical interference during perfusion of extracellular solution. To ensure total isolation from the pump a 65 μF capacitor was connected in series with the inlet tube of the recording chamber and ground electrode.

A small number of experiments were conducted to study the effect of acetylcholine (ACh) on hair cells. Superfusion of ACh near hair cells in the recording region was accomplished using a gravity-driven solution changer with a large diameter (500 μm) plastic tip connected to five plastic inlets embedded in dental cement. The inlet tubes were in turn connected to 10 ml plastic syringe reservoirs (containing ACh and control extracellular solutions) attached to the cage and placed slightly higher than the perfusion tip level.The perfusion tip was carefully placed near the recording region, taking care not to cause any tissue movements, and three-way valves controlled the flow of solution into the chamber. The flow rate was maintained at approximately 4-6 ml/min by keeping the height and volume of the syringe reservoirs unchanged. Immediately before establishing the patch-clamp configuration, inflow from the peristaltic pump was diverted, and extracellular

solution was perfused from the gravity-driven syringe reservoir. After the patch-clamp configuration was achieved, the chamber was perfused with ACh solution.

2.5 Electrical recording

Whole cell patch clamp recordings of IHC and OHCs in the voltage and current clamp configurations were recorded with an Axopatch 200B amplifier (Molecular Devices, CA, USA). The recording configuration used for all experiments are illustrated in Figure 2-2B.

2.5.1 Recording electrodes

Cells in the apical coil of the organ of Corti were recorded in all experiments described here. Patch or recording electrodes were pulled from soda glass capillaries (Harvard Apparatus Ltd, Edenbridge, UK) with a vertical pipette puller (Narishige Instruments, Tokyo, Japan). They had typical resistances between 2 - 4 MΩ when immersed in extracellular solution using KCl-based intracellular solutions. The shank of the patch electrode was coated with surf wax (coconut flavour Mr. Zoggs SexWax, CA, USA) to minimise fast electrode capacitance transients. Pipettes were filled with KCl-based intracellular solutions for all experiments, except for mechanotransduction experiments, where they were filled with cesium glutamate-based intracellular. Patch electrodes were mounted into a pipette holder (Axon Instruments, CA, USA) with a chlorodized silver wire making electrical contact between the headstage circuit and the intracellular solution. A Patchstar micro manipulator (Scientifica Instruments, UK) was employed for making fine adjustments to the pipette movements.

(A)

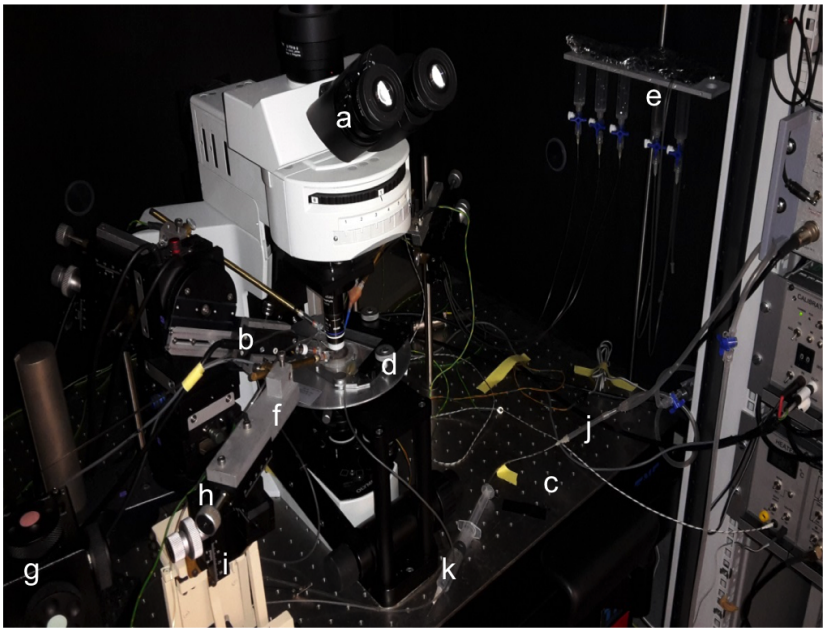

(B)

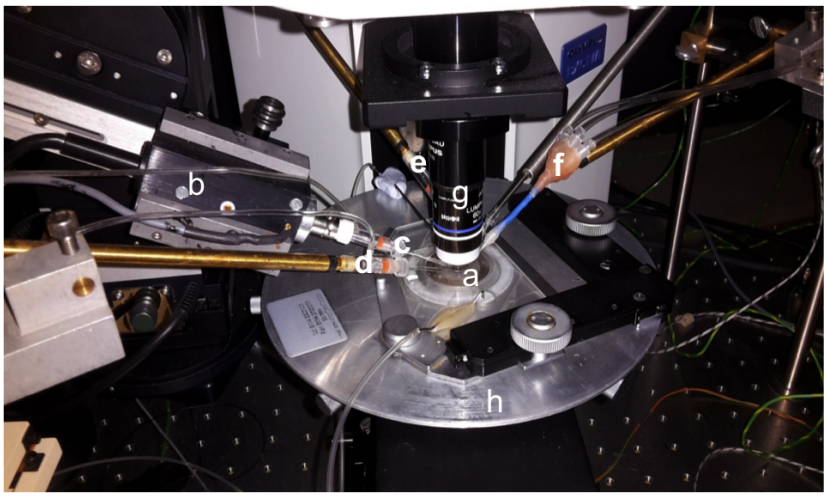

Figure 2-2: Photograph showing electrophysiology set-up used for recording electrical properties of hair cells.
(A) Components of the rig as labelled are: a) Olympus BX51 water immersion microscope, b) Headstage of Axopatch amplifier, c) TMC anti-vibration table, d) Custom-made rotating stage, e) 10ml reservoirs for solution changer for superfusion, f) Holder for cleaning pipette, g) Patchstar micromanipulator control for recording electrode, h) Marzhauser manipulators, i) Intracel micromanipulator for the cleaning pipette, j) Plastic tubing for applying pressure to patch pipette, k) Syringe for applying pressure to cleaning pipette.
(B) Closer view of the rotating stage with the tissue preparation. Components labelled are: a) Recording chamber with nylon mesh, b) Headstage of the Axopatch amplifier, c) Recording electrode, d) Cleaning electrode, e) Ground electrode, f) Home-made multi-inlet superfusion system for application of drugs, g) Eyepiece of the microscope, and h) Custom-made rotating stage

2.5.2 Cleaning electrodes

Cleaning electrodes or crudsuckers, with a tip diameter of 3 - 4 μm were pulled from borosilicate glass (Harvard Apparatus, UK) and were used to clean the area immediately surrounding the target hair cell to be recorded. In order to do this, crudsuckers were filled with extracellular solution and connected to a syringe through which positive or negative pressure allowed the formation of holes in the epithelium to facilitate cleaning of the cells before patching.

2.5.3 Establishment of the patch clamp configuration

Once the area had been cleaned of any debris, the patch electrode was lowered into the solution. At the beginning of the experiments, a +10 mV command voltage was applied to the patch pipette using the pClamp software to assess the pipette resistance, seal formation and generation of whole cell configuration. Positive pressure was maintained in the patch electrode to prevent blocking of the tip. The resistance of the pipette was confirmed on the oscilloscope, and fast capacitive transients caused by the build-up of charge were cancelled using the fast capacitance cancelling circuitry of the Axopatch amplifier.

In voltage clamp mode, the pipette offset, as visualised on the oscilloscope, was compensated using the offset dial on the amplifier. The tip of the patch pipette was brought into focus and carefully lowered down to the focal plane of the cell of interest. The fine control knobs on the micro manipulator were then used to advance the pipette to the target cell membrane until a dimple was observed due to the positive pressure from the pipette. Positive pressure was released and seal formation was observed by the current response changing to zero. Resistances above 4 GΩ were considered to be a good seal. During the 'gigaseal', the holding potential was stepped down to to -84 mV (taking into account the liquid junction potential

of -4 mV in KCl-based intracellular solutions). Holding potentials could be changed using an external calibrator that applied a known DC voltage shift to the cell. Gentle suction allowed the patch pipette to break a small area of the cell membrane connected to it to obtain the whole-cell recording mode. This was confirmed by the larger current response and the appearance of slow membrane transients in response to the +10 mV voltage step. The transients were minimised using the slow capacitance cancelling circuitry of the Axopatch amplifier, which also allowed measurements of the cell membrane capacitance and the series resistance. During current clamp recordings, the calibrator was set to zero to enable measurement of the cell's resting membrane potential.

2.6 Experimental solutions

2.6.1 Extracellular solution

Voltage and current clamp experiments were conducted using an extracellular solution that resembled as closely as possible the perilymph that bathes the basolateral membrane of HCs *in vivo*. This solution is referred to as 'normal' extracellular solution and its composition is tabulated in Table 2.2. It was supplemented with 20 ml/L Amino Acids (from concentrate, 50X) and 10 ml/L vitamins (from concentrate, 10X). The pH of the solution was adjusted to 7.48 with 4M NaOH, and the osmolality was 308 mOsm/kg measured with an osmometer (Advanced Instruments, MA, USA). Normal extracellular solution was used for all dissections and continuous bath perfusion via the peristaltic pump.

TABLE 2.2: *Composition of extracellular solution for electrophysiological recordings*

Component	Final concentration (mM)
NaCl	135
$CaCl_2$	1.3
KCl	5.8
$MgCl_2$	0.9
Hepes	10
Glucose	5.6
NaH_2PO_4	0.7
Na Pyruvate	2
Amino acids	
Vitamins	

2.6.2 Intracellular solutions

The intracellular solution for most experiments was KCl-based and is shown in Table 2.3. The composition of the extracellular and intracellular solutions used provided the naturally occurring gradients between hair cells and perilymph. The pH of the intracellular solution was adjusted to 7.28 using 1M KOH and had an osmolality of around 280 - 290 mOsm/kg. Intracellular solution was passed through a 0.2 μm pore filter before filling patch electrodes to eliminate pipette blockage.

TABLE 2.3: *Composition of KCl-based intracellular solution for electrophysiological recordings*

Component	Final concentration (mM)
KCl	131
$Na_2Phosphocreatine$	10
$MgCl_2$	10
EGTA-KOH	1
Na_2ATP	5
Hepes	5

A cesium glutamate-based intracellular solution was used for mechanotransduction experiments (Table 2.4). The pH of the intracellular solution was adjusted to 7.28 using 1 M cesium hydroxide and had an osmolality of around 294 mOsm/kg.

TABLE 2.4: *Composition of cesium glutamate-based intracellular solution for electrophysiological recordings*

Component	Final concentration (mM)
L-Glutamic acid	106
CsCl	20
$Na_2Phosphocreatine$	10
$MgCl_2$	3
EGTA-CsOH	1
Na_2ATP	5
Hepes	5
GTP	0.3

In some experiments, the effects of ACh (Sigma, Dorset, UK) on hair cells were investigated. ACh was superfused at a concentration of 10 μM from a stock solution of 10 mM acetylcholine (Sigma Aldrich, UK).

2.7 Mechanotransduction experiments

The outermost row of OHCs from P6 or P7 mice were studied for their mechanotransduction properties. MET currents were elicited by stimulating the hair bundles of OHCs with a fluid jet connected to a borosilicate glass pipette, driven by a piezo-electric disc [Kros et al., 1992]. Mechanical stimulus applied was as a 45 Hz sinusoid (filtered at 1 kHz, 8-pole Bessel) with a driving voltage of $\pm$ 40 V.

The fluid jet was placed on the modiolar side of the tissue preparation. The pipette tip was 7 - 10 μm in diameter and was placed around 8 μm away from the hair bundles. Positive driver voltage caused fluid to escape the fluid jet and stimulate the HCs, due to which the bundle was displaced towards the tallest stereocilia forcing the opening of the MET channels, mimicking an *in vivo*-like excitatory stimulus. Negative driver voltage, on the other hand, caused fluid to be sucked into the fluid jet, pulling hair bundles in the inhibitory direction, thereby closing the MET channels.

During these experiments, the fluid jet was filled with normal extracellular solution (Table 2.2). The recording electrode was filled with cesium glutamate intracellular in order to be able to record the MET currents without contamination by K^+ currents.

2.8 Data acquisition and analysis

Data acquisition by the application of current or voltage clamp protocols were carried out using the Clampex 10.3 software (Molecular Devices, CA, USA) connected to the Digidata 1440A (Axon Instruments, CA, USA), analogue to digital converter. Responses were filtered at 2.5 kHz or 10 kHz (8-pole Bessel) and sampled at 5 kHz. The responses were digitized at the sampling frequency and stored offline for later analysis.

The initial fast electrode capacitance was compensated before the whole-cell configuration. The cell membrane capacitance (C_m) and series resistance (R_s) were manually compensated upon membrane rupture using the Axopatch manual compensation controls.

Data analysis was performed offline using Clampfit software (version 10.3, Molecular Devices, CA, USA) and OriginPro (10.3 and 10.5 versions; OriginLab, MA, USA). Clampfit enabled quantification of holding currents, peak currents and leak conductances. All membrane potentials for voltage clamp experiments were corrected for the liquid junction potentials which arise from the different ion mobilities at the liquid interface [Neher, 1992]. This was -4 mV for Cl^- based intracellular solutions and -11 mV for glutamate-based intracellular solution. The membrane potential for voltage clamp experiments were corrected for the voltage drop across the R_s. OriginPro was used to calculate the actual command voltages by correcting them for the voltage drop across the uncompensated series resistance.

This was done using Ohm's law:

$$V = R\ X\ I, \tag{2.1}$$

where V is the voltage, R is the resistance and I is the current.

For analysis of MET currents, the fits through the current - voltage curves are according to a single-energy-barrier model:

$$I(V) = k\ [exp\ ((1 - \gamma)(V - V_r)/V_r - exp\ (-\gamma(V - V_r)/V_r)], \tag{2.2}$$

where k is a proportionality constant, V_r is the reversal potential, V_s is a measure for the steepness of the rectification, and γ is the fractional distance within the membrane's electrical field of an energy barrier, as measured from the outside [Kros et al., 1992]. The values of the fits are as follows: k = 444 pA, V_r = 1.3 mV, V_s = 38 mV, γ = 0.41.

All statistical analyses were carried out using Graphpad Prism 6 software. Statistical comparison of means were made using Student's t-test for independent data-sets. For comparison between multiple data-sets, one-way or two-way analysis of variance (ANOVA) tests were used followed by relevant post-hoc tests, as specified. For the above tests, the p-value for statistical significance was set at 0.05 in order to reject or accept the null-hypothesis. The statistical tests have been specified where used. All averages are reported as mean ± S.E.M. Statistical significance is indicated in figures by asterisks.

2.9 Organotypic cultures of the organ of Corti

Mice aged P0, P4, P7 and P8 were killed by rapid cervical dislocation and doused in 80% ethanol for a few minutes to rid the skin of bacteria. Mice were then

transferred to a couple of large petri dishes containing Hank's solution (Stock Hank's solution was prepared previously by adding 5 ml Hepes Buffer (Gibco, UK) to 500 ml HBSS (Gibco, UK) for sequential washes, after which the cochleae were isolated and dissected in fresh Hank's solution. Each organ of Corti was separated into apical and basal coils, and cochleae from each individual animal transferred onto a coverslip covered with collagen (Corning, MA, USA) with a tiny amount of Dulbecco's Modified Eagle Medium (Gibco, UK). Coverslip with the cochlear coils were then placed inside a Maximou slide and sealed with a mixture of vaseline and wax. This was then kept flat and placed inside an incubator maintained at 33°C and 5% CO_2 for a period of 24 hours. All the above steps were carried out in sterile conditions with sterile tools and equipment in the laminar air flow unit.

2.10 Immunofluorescence

2.10.1 Phalloidin staining

After a period of 24 hours, the cultures described above were rinsed in Hank'solution and fixed with 4% paraformaldehyde (Agar Scientific, UK) in PBS solution for a period of one hour at room temperature. After three PBS rinses, the cultures were incubated in a solution containing 0.1% Triton X-100 and Alexa Flour 488 Phalloidin (ThermoFischer Scientific Cat. no. A12379) in PBS at a dilution of 1:100 for two hours, to enable visualization of hair cell bundles and subsequent counting of HCs (Section 2.12) under a fluorescent microscope.

2.10.2 Antibody labelling

Cryosections between 8 μm - 12 μm were either used immediately after sectioning or after removal from -80°C storage. Sections were first brought up to room temperature, re-hydrated with PBS and re-fixed with 4% paraformaldehyde in

PBS solution for about 20 minutes. They were then incubated in blocking buffer containing 5% goat serum (Sigma Aldrich, UK) and 0.1% Triton X-100 (Sigma Aldrich, UK) in PBS for 20 - 30 minutes. Following a couple of rinses in PBS, cryosections were left in primary antibodies overnight at 4°C. The next day, after three PBS washes, they were incubated in relevant secondary antibodies for one hour at room temperature, to enable detection of proteins of interest.

Primary antibodies used were rabbit anti-BK polyclonal antibody (at a dilution of 1: 300; Alomone Labs APC-021), rabbit anti-MyosinVIIa (at a dilution of 1:300; Abcam 3481), mouse anti-GFP monoclonal (at a dilution of 1:300, DSHB-GFP-4C9), and were detected with goat anti-rabbit IgG Alexa Flour 488 conjugate (1:500; Invitrogen), goat anti-rabbit IgG Cy3-conjugate (1:500; Invitrogen) and goat anti-mouse IgG FITC-conjugate (1:500; Life Tecnologies), respectively. Excess unbound antibodies were washed away with PBS, and sections were mounted on glass coverslips with Vectashield medium containing DAPI (Vector Labs, UK) to stain cell nuclei. Coverslips were sealed with clear varnish before imaging. For negative controls, primary antibodies were left out and the overnight incubation was carried out in blocking buffer. Secondary antibodies were used as normal.

For characterizing cells from the *Gata3 Egfp* X *Immortomouse* cross, cells were grown directly on multi-chamber slides to allow simultaneous labeling of different samples. The same protocol as above was followed. Primary antibodies used were mouse SV40 T Antigen antibody (1:400; Santa Cruz-58665), rabbit anti-Gata3 (1:100; Santa Cruz H-48 SC-9009), mouse anti-GFP monoclonal (at a dilution of 1:300, DSHB-GFP-4C9) and were detected with goat anti-mouse Alexa 568 (1:500; Invitrogen), goat anti-rabbit Cy3 (1:250; Invitrogen), goat anti-mouse IgG FITC-conjugate (1:500; Life Tecnologies), respectively.

2.11 Imaging

Immunolabelled or EGFP-expressing cryosections, cochlear cultures and cells were mounted onto a glass slide and covered with Vectashield medium containing DAPI for imaging. They were imaged using an upright Olympus epifluorescence microscope equipped with the appropriate filters and objectives (20X, 40X and 60X). Images were captured using Volocity software connected to microscope and further processed using ImageJ or Adobe Photoshop for image analysis.

2.12 Hair cell counting and analysis

After being maintained in controlled conditions as described in section 2.9, the cultured cochlear epithelium was divided into four regions for ease of analysis. A1 corresponds to the apical-most region of the cochlear spiral; A2 corresponds to the apical region lying immediately basal to A1; A3 represented the basal part of the apical coil, and B1 corresponded to the basal region of the epithelium.

A region of 150 μm in each of the above A1, A2, A3 and B1 regions was selected and the HCs within it counted. OHCs in each row (three rows of outer hair cells - OHC1: innermost, OHC2: middle and OHC3: outermost), IHCs (single row) and the total number of OHCs (OHC1 + OHC2 + OHC3) along this length were recorded.

2.13 Isolation and freezing of mouse embryos

Pregnant females were culled by cervical dislocation, doused in alcohol several times for a few minutes, and peritoneally cut open to reveal embryos in the uterus. The uterus was removed and placed in a large petri dish containing plain Dulbecco's Modified Eagle Medium (DMEM). Within the uterus, each embryo was contained in its own amniotic sac. After all embryos had been released from their individual sacs, they were transferred to another medium-sized petri dish containing 4% PFA

(fixative) and kept at 4°C for 30 minutes. At the end of 30 minutes, fixative was removed and replaced with PBS for 5 minutes. This was done three times to properly wash away the fixative. Embryos were next transferred to a small dish and passed through an increasing sucrose gradient at 4°C (sucrose is a cryoprotectant and partial dehydrant. It draws water out of the tissue so that ice crystals do not form within the tissue). A 10% sucrose solution in PBS was used for 1 hour, followed by 30% for 1 hour, followed by 50% for 1-2 hours, all at 4°C until the embryos sank. Embryos were placed in 1:1 solution of OCT:50% sucrose solution overnight in numbered plastic moulds. Next day, heads/bodies were placed in 100% OCT for a couple of hours in numbered plastic moulds, and then frozen. Snap freezing was performed in isopentane (2-methylbutane), as it preserved tissue elements very well and prevented ice crystal artefact formation. After freezing, they were transferred to the -80°C freezer until sectioning. Before sectioning, moulds were placed in the cryostat for at least 24 to 36 hours to raise them to cryostat temperature to ensure smooth sectioning.

After sectioning, Kaufman, 1992 was used as a guide for the identification of all embryonic structures in the case of *Gata3 Egfp* embryos, as described in Section 6.2.1.

2.14 Generation of reporter mice

2.14.1 Generation of reporter mice for testing *Cre* activation

Rosa26R Eyfp mice carry the coding sequence for Enhanced Yellow Flourescent Protein (EYFP) downstream of a floxed stop codon inserted into the ubiquitous *Gt(ROSA)26Sor* locus. The termination signal prevents expression of *Eyfp* under normal circumstances. Mice homozygous for the *Eyfp* transgene were maintained on

a C57BL/6 background (https://www.jax.org/strain/006148) and were crossed into the homozygous *Otof*^{Cre} line to yield first generation offspring heterozygous for both *Eyfp* and *Cre* transgene. The progeny was then back-crossed into the homozygous floxed father to produce knockout test animals and controls to test for the activation of *Cre recombinase*.

2.14.2 Generation of mice carrying floxed *Gata3* alleles and *Cre* transgenes

Gata3 floxed mice used in our study have been described previously (Zhu et al., 2004). These transgenic animals harbour loxP sites flanking exon 4, that encodes the first DNA-binding zinc finger motif. Deletion of exon 4 also introduces a reading frame-shift that causes a termination codon in exon 5, thereby preventing the expression of exon 5 and more distal exons. Mice homozygous for the *Gata3* floxed allele were viable and healthy, and analysis of their immune systems showed no differences compared to wild type mice [Zhu et al., 2004].

Mice homozygous for the floxed *Gata3* allele and *Cre* insertion were individually maintained on a 129/SvJ and C57BL/6 background, respectively, and were found to be viable and fertile. The homozygous *Otof*$^{Cre/Cre}$ had normal ABR responses (https://www.mmrrc.org/), ruling out any toxic effects of the *Cre* transgene in hair cells. The first generation of crosses between the floxed line and the *Cre* driver line yielded animals heterozygous for both the floxed allele and *Cre* transgene. The F1 progeny was then back-crossed into the homozygous floxed animal to yield offspring both homozygous and heterozygous for the floxed alleles (our test animals, each driven by one *Cre* transgene) and wild type controls without a *Cre* driver. The knockout animal from the above cross was further crossed into the homozygous floxed animal to yield knockout and control animals in a 1:1 ratio. The *Cre* was maternally transferred in every cross.

2.15 Harvesting embryos from *Otof*^{Cre} X *Rosa26R Eyfp* cross

F2 generation embryos were harvested from pregnant dams from as described in section 2.13, at E17.5, E18.5 and E19.5, to ascertain expression of *Cre recombinase* by *Eyfp* expression. Embryos were frozen down and cryo-sectioned before labelling with anti-GFP antibody according to the procedure outlined in section 2.10.2. Anti-GFP antibody also recognises EYFP protein as it has been raised against a common epitope (http://dshb.biology.uiowa.edu).

2.16 Derivation of otic tissue from *Immortomouse* X *Gata3 Egfp* embryos and initial culture of cells

Timed matings were set up between heterozygous *Immortomouse* X homozygous *Gata3 Egfp* mice and detected by vaginal plugs. The day the plug was dicovered was considered E0.5. Embryos were harvested from pregnant females as described in Section 2.13 and transferred in MEM. Embryos were transferred again after rinsing in MEM to small individual plastic petri dishes. Here otocysts were removed as cleanly as possible from the surrounding mesenchyme, using microscissors and forceps under sterile conditions. A pipette was used to transfer otocysts of each embryo into a 24-well tissue culture plate containing growth medium containing MEM with Earle's Salts (Gibco MEM-1X + Glutamax + Earle's Salts, Cat. no. 41090), 20% Fetal Calf Serum (FCS), 50 units/ml γ-interferon and 100X penicillin-streptomycin antibiotic cocktail (this is henceforth referred to as 'full growth medium'). The otocysts were pooled into the central chambers (one animal, one well) of a polystyrene 24-well plate leaving a border of empty wells surrounding these chambers. These empty wells were then filled with sterile pre-warmed water

to prevent evaporation of medium from the central chambers. Explants were maintained for 10-12 days in full growth medium containing 50 units/ml γ–IFN at 33°C to ensure expression of the immortalizing gene. They were monitored regularly for feeding. Water levels in surrounding wells were checked daily for evaporation.

This above protocol was followed for derivation of otic tissue from E10.5 embryos. It was modified to use dispase (containing 1 unit/ml in calcium magnesium-free PBS) for 10 - 15 minutes on ice to help loosen the otic tissue from the surrounding connective tissue. However, this method was abandoned as our tissue failed to survive at later stages, probably due to incomplete removal of dispase, which interferes with growth. For tissue from E16.5 embryos, the organ of Corti from the ventral otocyst was dissected out.

2.17 Cloning

2.17.1 Cell type selection

Existing medium was discarded from the well and replaced with fresh plain MEM containing Earle's Salt, swirled and discarded twice. This was done to wash away all debris in the well and also to wash away all traces of serum that inhibits trypsin. Next, 0.25% trypsin (Sigma Aldrich, UK) was added to the relevant wells and kept in the 33°C incubator for 10-15 mins. Wells were observed periodically for detachment of cells. Upon detachment of cells, contents of each well were mechanically dissociated and removed into a labelled falcon tube. Medium containing 10% fetal calf serum (FCS, Bio Whittaker, Belgium) was added into the wells to further wash away remaining traces of trypsin. This was removed and added into respective falcon tubes. Medium containing 10% FCS (trypsin inhibition medium) was added into the falcon tube, and centrifuged at 1000 RCF for 3 minutes, and the supernatant

carefully discarded. The pellet was re-suspended in full growth medium, and added to the first well of a labelled 6-well plate (one 6-well plate per animal). After a few cells had attached to the floor of the well (after approximately 1 hour), all medium was removed from the first well and put into the second well, while the first well was re-filled with fresh medium. Next, 200 μl, 150 μl, 100 μl and 75 μl (total removed from second well is 525 μl) of medium containing cells from second well was removed and added into the 3rd, 4th, 5th and 6th wells respectively. Full growth medium was added in all of these wells. Removed full growth medium was replaced in the second well. In order to get well separated epithelial colonies that could be further ring-cloned, all the plates were allowed to grow undisturbed for a few days.

2.17.2 Selection of epithelial sheets and coherent patches of cells potentially derived from a clone

Some plates had large sheets of epithelia growing, with a few other cell types. In high levels of serum epithelial cells adhere to each other and to the dish much more strongly than other cell types (based upon observation), thus one can use trypsin for a measured time and lift epithelia as coherent clumps. We decided to separate the cell types based on the differences in their relative weights (instead of serially diluting them like above), taking advantage of the fact that the more abundant lumps and sheets epithelia would sink quicker to the bottom of the tube compared to the other cell types.

Medium was discarded and trypsin was added as in Section 2.17.1. The plates were then placed in the incubator for 7 minutes and periodically observed under the microscope for the rolling up of epithelial sheets. Once all epithelial edges had lifted, MEM containing 10% FCS was added to the well. A plastic pipette was used to suck this up and down a few times (without bubble formation) to dislodge all epithelia. This was re-confirmed under the microscope. This cell suspension

was lifted into a falcon tube containing fresh MEM, and were left undisturbed for 5 minutes to allow the epithelial sheets to settle to the bottom. Cell suspension from the very bottom of the tube was removed and put into the first well of a 6-well plate. MEM and 10% fetal calf serum was added into this well and the entire suspension was removed and put into new falcon tube. This was topped up with MEM and 10% FCS, spun at 1000 RCF for 3 minutes, supernatent was discarded and replaced with full growth medium, and added back into the first well of the 6-well plate. This was the epithelial fraction of the original cell suspension. 200 μl, 150 μl, 100 μl and 75 μl (total: 525 μl) of medium containing cells from the this well was removed and added into the 3rd, 4th, 5th and 6th wells respectively.

The remaining suspension in the original tube was spun at 1000 RCF for 3 minutes, supernatent was discarded and replaced with full growth medium, and added back into the second well of the 6-well plate. This suspension contains most cells other than the epithelial cells. In order to get well separated epithelial colonies that could be further ring-cloned, the cells were allowed to grow undisturbed for a few days.

2.17.3 Cloning by limiting dilution

Existing medium was removed, washed twice with MEM, replaced with trypsin, and placed in the incubator at 39°C for 10-15 minutes and monitored for cell detachment. After cell detachment, trypsin inhibition medium was added to the well. Cells were resuspended with 1 ml pipette and then added into a tube containing trypsin inhibition medium. The tubes were then centrifuged for 3 minutes at 1000 RCF. The supernatant was carefully removed and replaced with full growth medium, and resuspended. 8 μl from each tube was removed into individual eppendorf tubes and 2 μl of trypan blue was added and mixed well. 10 μl mixture of cells and trypan blue was placed under the cover slip of a haemocytometer and cells were counted in all 5 squares and averaged. Dark blue dead cells were ignored. The dilution

was determined by the formula : 10000 μl/(Average number of cells per square of haemocytometer X volume of a single drop from a 10 ml strippete) Volume of a single drop from a 10 ml strippete was previously measured. This volume was taken from the sample and add to a tube containing 10 ml of full growth medium and mixed well: this suspension now had 10 cells/ml. 1 ml from above mixture was added to the next tube containing 10 ml full growth medium and mixed: this suspension now had 1 cell/ml. 1 ml from above mixture was taken from above tube and added to the next tube containing 10 ml full growth medium and mixed: this suspension now had 0.1 cell/ml. A 10 ml pipette was used to dispense solution from each of the above tubes, one drop per well, into the corresponding numbered 96-well plate. Plates were left undisturbed for 10 - 14 days, and medium levels were carefully monitored to prevent drying out.

2.17.4 Cloning by FACS

Cells were trypsinised and lifted from flasks, counted and centrifuged as mentioned above. Cells were resuspended in full growth medium at a final concentration of 1,000,000 cells/ml. The suspension was then filtered through a 70 μm cell strainer and poured into sterile FACS tubes. The FACS machine sorted cells individually according to high or low EGFP expression directly into 96-well U-bottomed plates containing 100 μl of full growth medium. This was then allowed to grow for 10-14 days undisturbed and monitored for drying of medium.

2.18 Expansion of clones

Cells were lifted from 96-well plate with a small amount of trypsin, just to lift cells from well. The cells were then either centrifuged, or depending on number were transferred to 24-well plates and maintained in full growth medium.

2.19 Cryo-preservation of cells

The same steps as in Section 2.17.3 were followed until discarding of the supernatent. Thereafter, 0.5 or 0.75 ml of FCS + 10% DMSO was added to the cells, resuspended and put into cryovials. Cryovials were transferred to -80°C freezer for 24 - 48 hours before transferring to liquid nitrogen stores to preserve cell viability.

Chapter 3

Gata3 is essential for the survival of outer hair cells

3.1 Introduction

Although IHCs are the primary acoustic transducers of the mammalian cochlea, OHCs have an important role in refining the cochlear mechanics during the sound transduction process. They are distinct from IHCs in terms of their structural anatomy, electrophysiological functions, innervation pattern and timescale of development. Only 5 - 10% of the total population of afferent fibres, called Type II spiral ganglion neurons, synapse with OHCs in the adult cochlea. In contrast, efferent neurons of the medial olivocochlear bundle (MOC), arising from the brainstem, provides the major innervation in mature OHCs [Liberman et al., 1990].

The dominant K^+ current expressed in OHCs from the time of their birth until P8 is an outward delayed rectifier current (I_k) that shows slow activation and inactivation kinetics [Marcotti and Kros, 1999]. Hyperpolarising potentials from the resting potential at this stage elicit small inwardly rectifying currents (I_{k1}) [Marcotti and Kros, 1999]. The amplitude of the I_k conductance increases during the first postnatal week until around P6 and reaches a minimum at P9 [Marcotti and Kros, 1999]. Immature OHCs have been shown to fire spontaneous Ca^{2+}-dependent action potentials that are able to trigger exocytosis [Beurg et al., 2008]. In elevated Ca^{2+}, they generate evoked action potentials in response to current injections,

followed by large oscillations in membrane potential [Marcotti and Kros, 1999].

The next stage (from about P8) is marked by the onset of $I_{k,n}$, carried through KCNQ4 channels [Marcotti and Kros, 1999; Kubisch et al., 1999] at negative potentials [Marcotti and Kros, 1999].This conductance increases in size, such that it becomes the major contributor towards the total current in these cells from the second postnatal week. This in turn influences the excitability of the cells such that $I_{k,n}$-expressing cells rest at more negative potentials, and current injections now generate smaller and quicker responses [Marcotti and Kros, 1999].

The onset of functional maturity in OHCs occurs at P8 when the expression of $I_{k,n}$ coincides with the commencement of electromotility, a unique phenomenon that allows OHCs to undergo rapid changes in their shape and size in response to changes in membrane potential [Santos-Sacchi and Dilger, 1988]. Elongation during hyperpolarisation and contraction during depolarisation generates forces within the cochlea that fine-tunes the cochlear mechanics such that its characteristic frequency is amplified [Kachar et al., 1985]. *Prestin*, a novel motor protein [Dallos et al., 2008; Liberman et al., 2002], expressed in the lateral walls of the OHCs, underlies this amplification process.

This efferent pathway mediates a negative-feedback loop which exercises modulatory control over the gain-control mechanisms of OHCs [Guinan Jr, 2010]. Upon activation of the efferents, ACh causes Ca^{2+} entry through $\alpha 9\alpha 10$nAChRs on the postsynaptic OHC membrane, which in turn causes membrane hyperpolarisation via the activation of Ca^{2+}-dependent K^+ channels (SK2) [Oliver et al., 2000].

Rationale for our study

$Gata3^{+/-}$ mice reveal haploinsufficiency, which causes a local peripheral cochlear defect [van der Wees et al., 2004]. The organ of Corti degenerates almost completely

by 15 months of age, starting with the OHCs at the apex of the cochlea as early as one month of age. This is followed by loss of pillar cells, IHCs and nerve fibres [van der Wees et al., 2004]. ABRs show that the average threshold elevation compared to age-matched wild type controls is 30 dB at all ages investigated (from 1 - 19 months) and across all frequencies [van der Wees et al., 2004].

The involvement of OHCs in the HDR phenotype is evident in the formation of vacuoles, and through their subsequent degeneration [van Looij et al., 2005]. Compelling evidence provided by distortion product otoacoustic emissions (DPOAEs) has led previous investigators to conclude that dysfunction of OHCs contributes towards the observed HL in *Gata3*$^{+/-}$ mice [van Looij et al., 2005]. Oto-acoustic Emissions (OAE) are generated from within the cochlea, most likely from the amplification processes of OHCs. These emissions can be measured non-invasively by placing a microphone in the ear canal, and serve as a clinical indicator for cochlear health [Probst et al., 1991].

Since the morphological and physiological abnormalities in *Gata3*$^{+/-}$ OHCs are detectable at one month postnatally [van Looij et al., 2005; van der Wees et al., 2004], we hypothesized that there should be much earlier, quantifiable deficits. We speculated that morphological changes in OHCs would be accompanied by changes in the biophysical properties of the cells, and this would be measurable under whole cell patch clamp electrophysiology. In order to accomplish this, we investigated the biophysical properties of OHCs in *Gata3*$^{+/-}$ mice at different stages encompassing pre-hearing (before P12), newly-hearing (P12 - P14) and adult animals (beyond P19).

3.2 Results

3.2.1 Mechanotransduction in OHCs in *Gata3*$^{+/-}$ mice is normal

Investigations into the MET properties of OHCs from *Gata3*$^{+/-}$ mice were carried out in order to ascertain the functionality of the MET apparatus, which serves to introduce the depolarising stimulus into the HC.

OHCs were chosen according to good bundle morphology, and stimulated with a sinusoidal force stimulus via a piezo-electric disc driving a fluid jet (as described previously in section 2.7), in order to elicit MET currents. A fluid jet was preferred over a fixed probe as this accomplishes a more uniform and physiological representation of the movement of fluid across the hair bundles [Johnson et al., 2011a]. Positive driver voltages moved hair bundles in the excitatory direction and caused large inward currents at negative potentials (at -121 mV; Figure 3-1).

In response to depolarising voltage steps, the elicited MET current initially decreased and then reversed in direction to become outward near the 0 mV potential. At positive potentials the resting transducer current was larger when compared to the resting current at negative potentials. This is due to the increased open probability of the MET channels due to the reduced Ca^{2+} influx at positive potentials, which is known to drive channel adaptation [Corns et al., 2014]. At positive potentials, Ca^{2+} entry is reduced into the cell because of its equilibrium potential (+99 mV under our experimental conditions) which strongly reduces its entry through the MET channels [Corns et al., 2014]. Negative driver voltages moved hair bundles in the inhibitory direction, shutting the MET channels and thereby abolishing the resting transducer current (arrows in Figure 3-1A and B).

Maximal transducer currents at -121 mV in *Gata3*$^{+/-}$ mice were comparable to their age-matched wild type counterparts (Table 3.1; Student's t-test, $p < 0.05$). Comparison between the genotypes of transducer currents elicited at different potentials are shown in Figure 3-1C.

TABLE 3.1: *Saturating MET currents at -121 mV in OHCs*

Genotype	Mean (pA)	S.E.M	N
Wt	-1294.6	125	5
Gata3$^{+/-}$	-1290.7	40	3

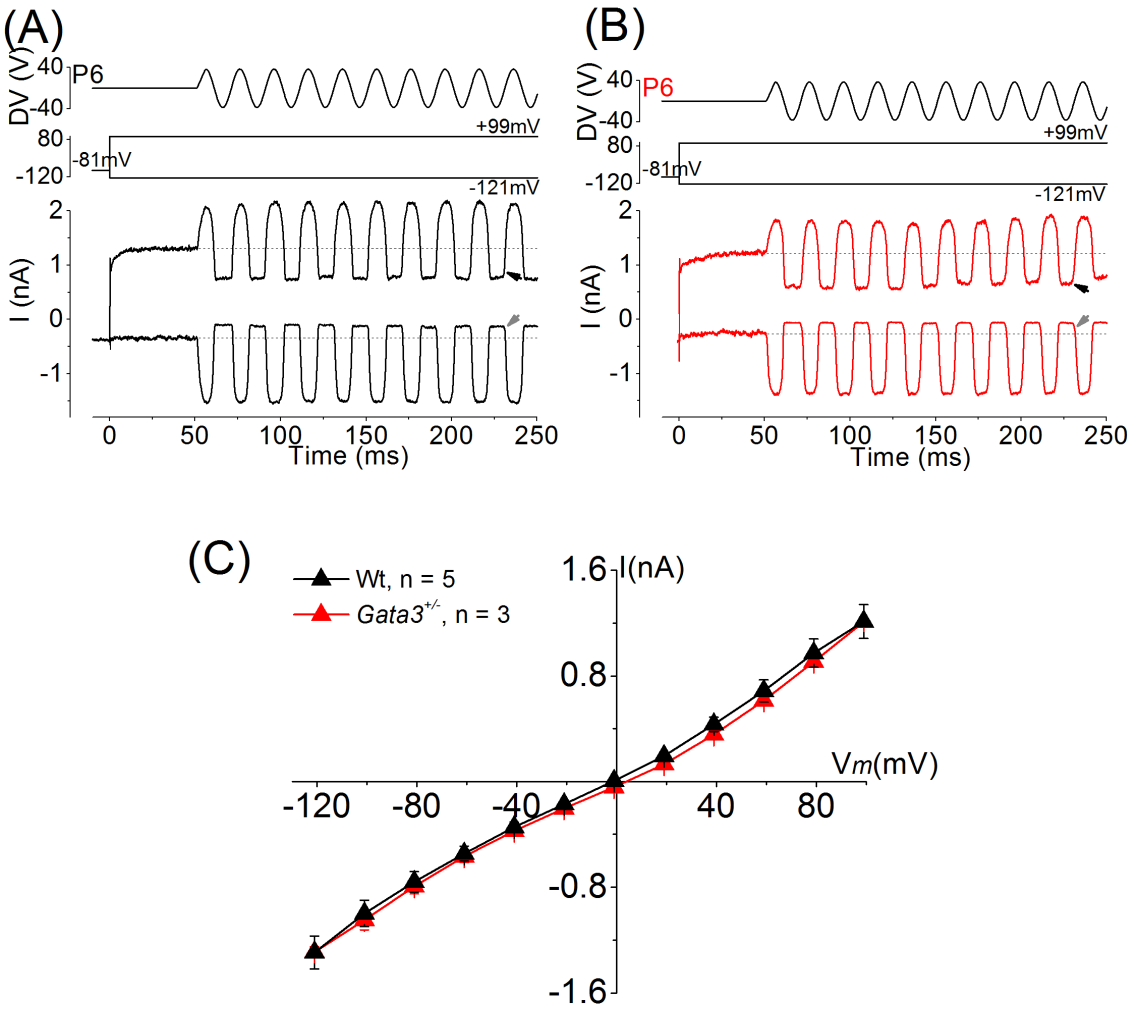

Figure 3-1: MET currents in *Gata3*$^{+/-}$ OHCs is normal
(A) Saturating MET currents recorded from voltage clamped wild type P6 OHCs, (B) And P6 *Gata3*$^{+/-}$ OHCs, in response to 50-Hz sinusoidal force stimuli to hair bundles. The driver voltage (DV) signal of ± 40 V has been indicated above the traces. Positive driver voltages stimulated bundles in the excitatory direction. The arrows indicate closure of the MET channels and disappearance of the resting current, during inhibitory bundle displacement, in response to negative driver voltages at -121 and +99 mV, respectively. Dashed lines indicate the holding current.
(C) Peak-to-peak MET I-V curves obtained from 5 wild type and 3 *Gata3*$^{+/-}$ OHCs.

3.2.2 Development of K^+ currents in *Gata3*$^{+/-}$ mice is normal

To study the basolateral membrane properties of OHCs from *Gata3*$^{+/-}$ mice, their current responses were studied from P6 to P24 from apical regions of the cochlea, under the voltage clamp configuration.

OHCs were held in patch clamp configuration and a series of depolarizing and hyperpolarizing voltage steps of 170 ms duration were applied from the holding potential of -84 mV, in 10 mV nominal increments (Figure 3-2A), in order to elicit K^+ currents. Steady-state values of the outward currents were measured towards the end of each test pulse (160 ms from the start of the voltage step) and plotted against the corresponding membrane potential to generate a current-voltage (I-V) relationship curve.

During the first postnatal week (at P6 - P7), when OHCs are immature, outward currents showed slow activation kinetics and partial voltage-dependent decay characteristics (3-2B). Average current size at 0 mV between the two groups was comparable at this stage (3-2C). Upon the onset of electromotility at P8, the outward K^+ currents were similar in amplitude to the previous stage investigated (Figure 3-3A) and the current sizes between both groups were also comparable (Figure 3-3B). By P10 - P11, the current amplitude decreased and the voltage-dependent relaxation of the outward current was abolished (Figure 3-4A). At P14 - P16, when OHCs are functionally mature, and at adult stages of P22 - P24, the oldest age studied, the total current increased in size (Figure 3-5 and 3-6). At all time-points investigated, OHCs from *Gata3*$^{+/-}$ mice were comparable to their wild type littermates (Two-way ANOVA, $p < 0.05$; Table 3.2; Figure 3-7).

TABLE 3.2: *Outward K^+ currents at 0 mV in OHCs*

Age	Wt (nA)	S.E.M	N	*Gata3*$^{+/-}$ (nA)	S.E.M	N
P6 - 7	1.93	0.26	6	2.48	0.14	20
P8	1.8	0.10	20	1.89	0.42	14
P10 - 11	1.93	0.17	7	1.31	0.09	13
P14 - 16	2.39	0.25	15	2.37	0.41	7
P22 - 24	3.0	0.9	12	2.37	0.38	5

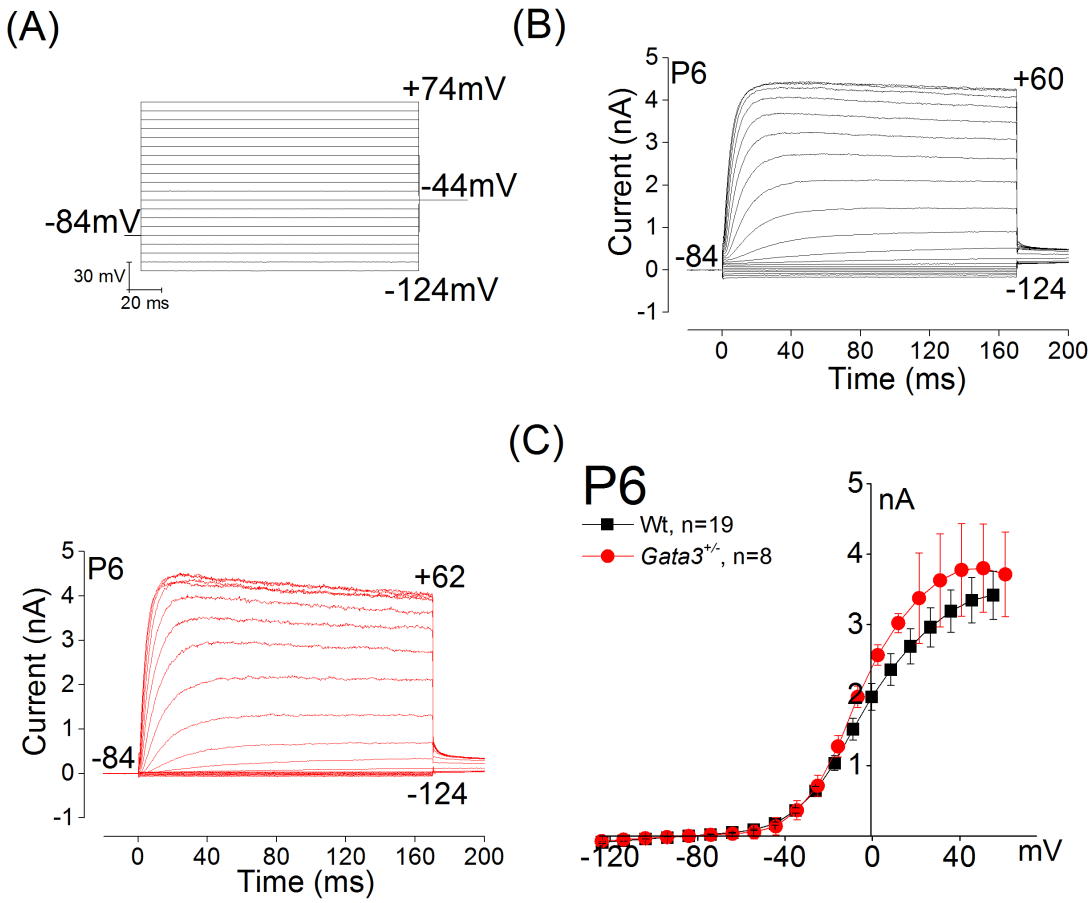

Figure 3-2: Outward K^+ currents in OHCs from neonatal (P6 - P7) mice
(A) The step protocol applied to elicit outward K^+ currents. Cells were referred to a holding potential of -84 mV, and stepped to different potentials from a potential of -124 mV in nominal increments of 10 mV. The duration of each voltage step was 170 ms.
(B) Example of the current responses of an OHC from wild type (black) and *Gata3*$^{+/-}$ (red) P6 mouse, in response to the voltage step protocol described in (A). In this trace and all subsequent traces, the holding current has been zeroed, and the actual test potentials reached are shown for a couple of the sweeps. The command voltage for each voltage step was corrected for the voltage drop across the series resistance.
(C) Average steady-state current-voltage (I-V) relationship curves for wild type (n = 19) and *Gata3*$^{+/-}$ (n = 8) OHCs from P6 - P7 mice. Error bars represent ± S.E.M values.
No significant difference was observed in the amplitude of the K^+ currents of OHCs in response to voltage steps, from control and *Gata3*$^{+/-}$ mice at this stage.

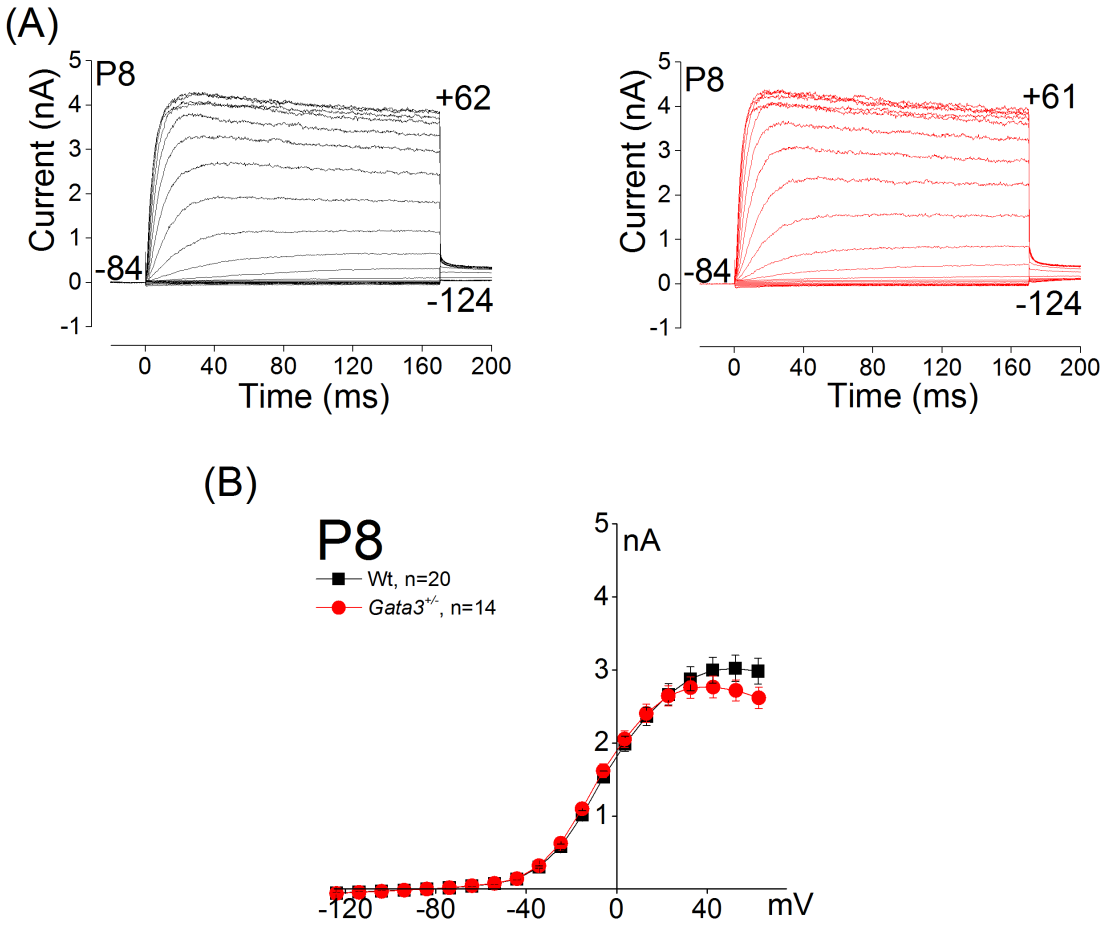

Figure 3-3: Outward K^+ currents in OHCs at the end of the first postnatal week, upon the onset of electromotility

(A) Example of the current responses of an OHC from wild type (black) and $Gata3^{+/-}$ (red) P8 mouse.

(B) Average steady-state current-voltage (I-V) relationship curves for wild type (n = 20) and $Gata3^{+/-}$ (n = 14) OHCs from P8 mice. Error bars represent ± S.E.M values.

No significant difference was observed in the amplitude of the K^+ currents of OHCs in response to voltage steps, from control and $Gata3^{+/-}$ mice at this stage.

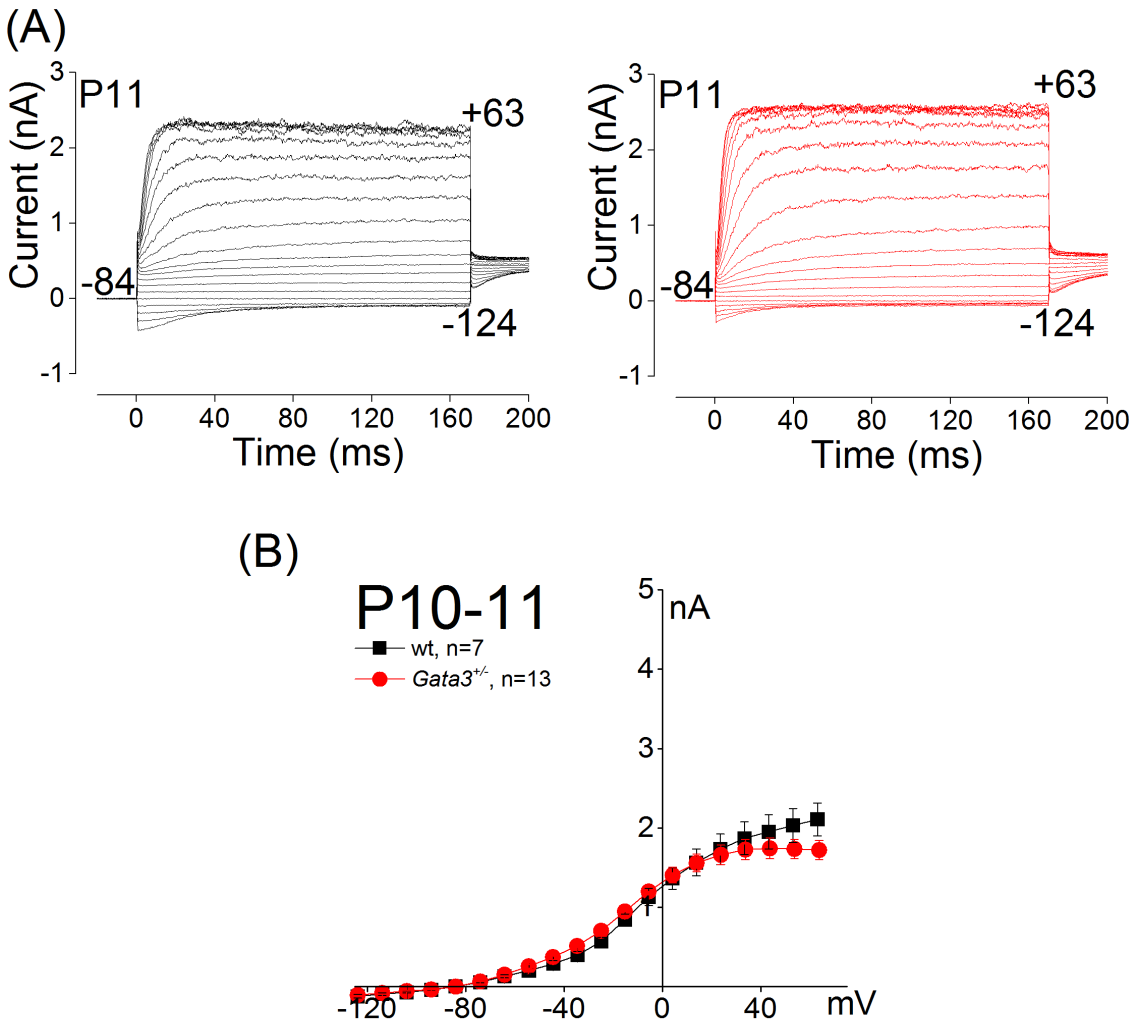

Figure 3-4: Outward K^+ currents in OHCs from P10 - P11 mice
(A) Example of the current responses of an OHC from wild type (black) and *Gata3*$^{+/-}$ (red) P11 mouse.
(B) Average steady-state current-voltage (I-V) relationship curves for wild type (n = 7) and *Gata3*$^{+/-}$ (n = 13) OHCs from P10 - P11 mice. Error bars represent ± S.E.M values.
No significant difference was observed in the amplitude of the K^+ currents of OHCs in response to voltage steps, from control and *Gata3*$^{+/-}$ mice at this stage.

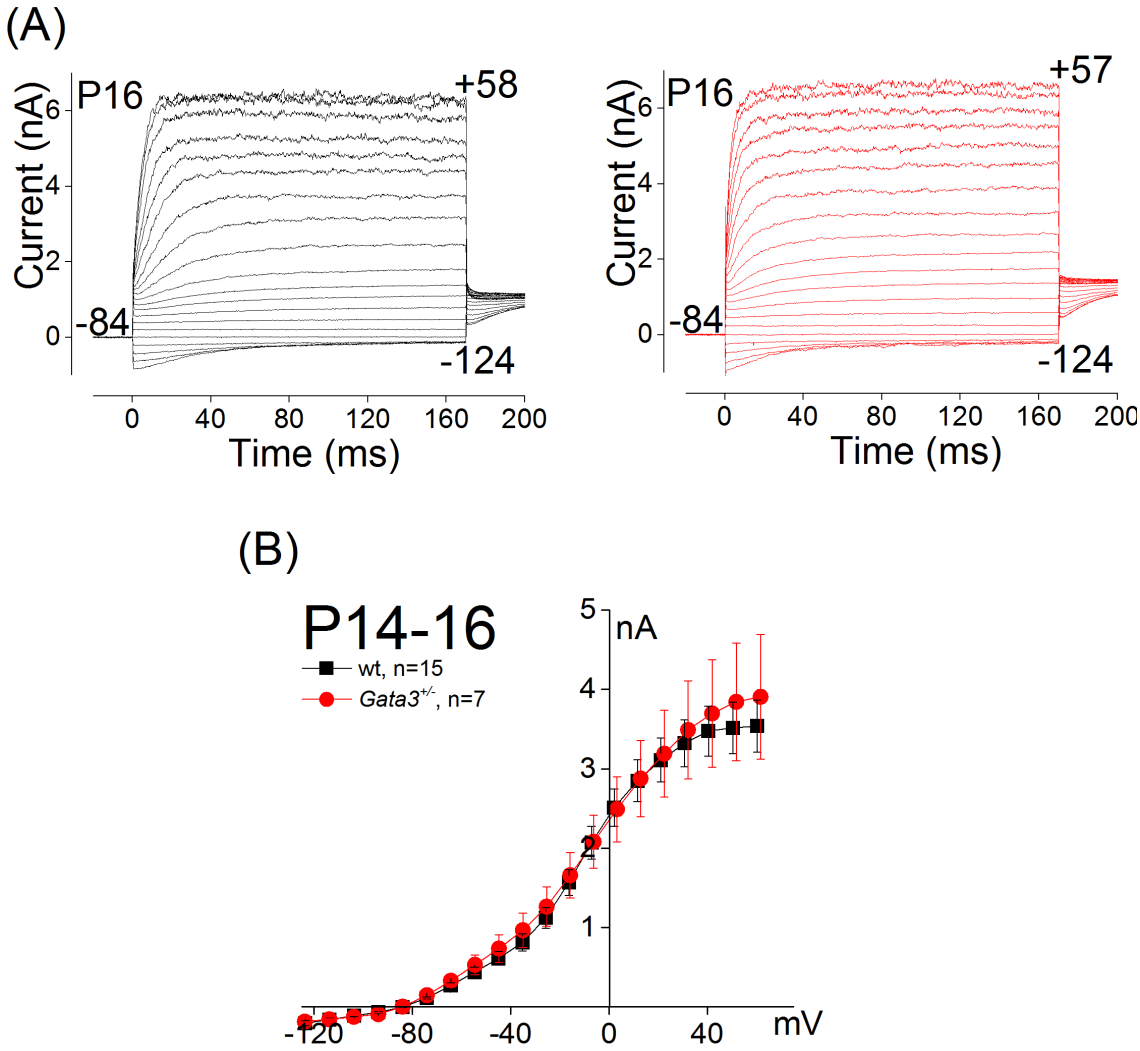

Figure 3-5: Outward K^+ currents in OHC from newly hearing (P14 - P16) mice
(A) Example of the current responses of an OHC from wild type (black) and $Gata3^{+/-}$ (red) P16 mouse.
(B) Average steady-state current-voltage (I-V) relationship curves for wild type (n = 15) and $Gata3^{+/-}$ (n = 7) OHCs from P14 - P16 mice. Error bars represent ± S.E.M values.
No significant difference was observed in the amplitude of the K^+ currents of OHCs in response to voltage steps, from control and $Gata3^{+/-}$ mice at this stage.

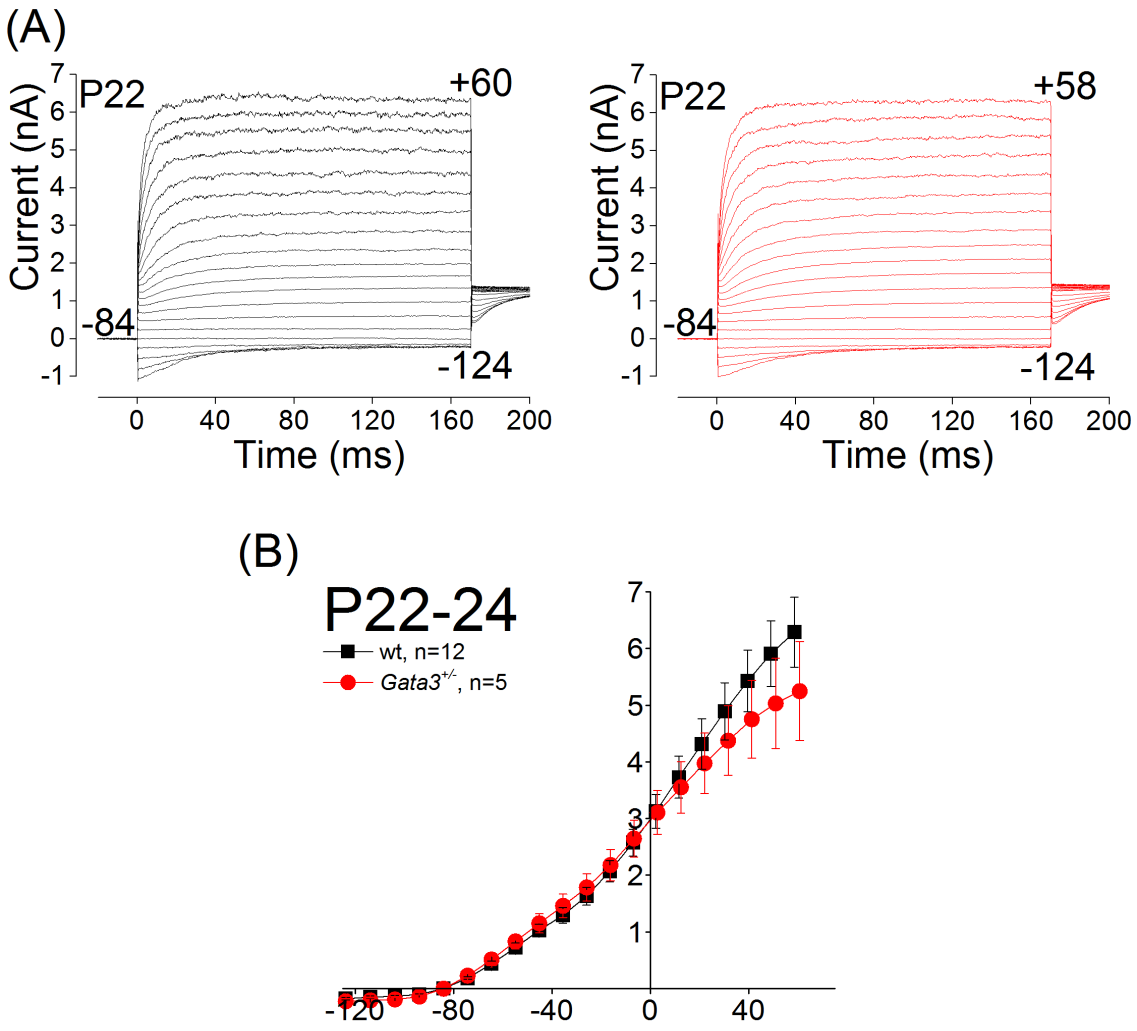

Figure 3-6: Outward K^+ currents in OHCs from adult (P22 - P24) mice
(A) Example of the current responses of an OHC from wild type (black) and *Gata3*$^{+/-}$ (red) P22 mouse.
(B) Average steady-state current-voltage (I-V) relationship curves for wild type (n = 12) and *Gata3*$^{+/-}$(n = 5) OHCs from P22 - P24 mice. Error bars represent ± S.E.M values.
No significant difference was observed in the amplitude of the K^+ currents of OHCs in response to voltage steps, from control and *Gata3*$^{+/-}$ mice at this stage.

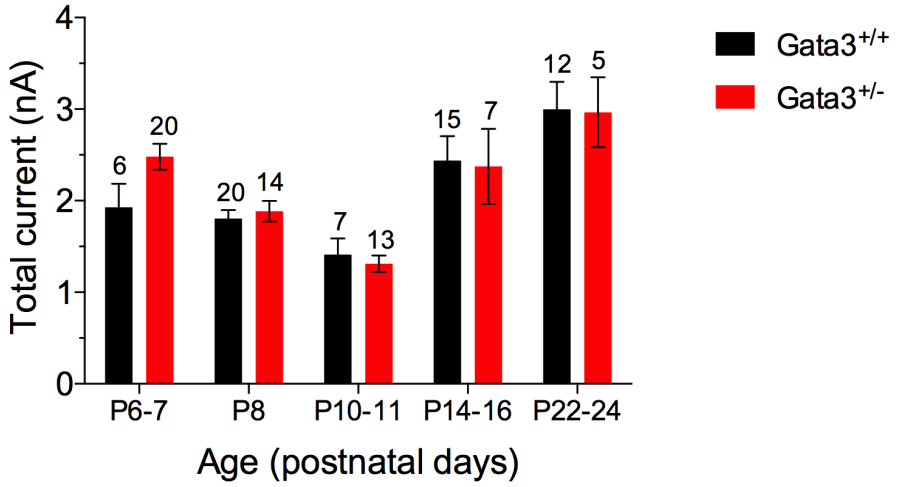

Figure 3-7: Outward K^+ current profile in *Gata3*$^{+/-}$ mouse OHCs shows normal postnatal development
Bar graph showing average steady-state currents at 0 mV of wild type (black) and *Gata3*$^{+/-}$ (red) OHCs at different postnatal ages. Note the reduction in total current size until P10 - P11, followed by subsequent increase thereafter. N numbers are written above individual columns, and error bars indicate ± S.E.M values. No differences were observed in current size between control and test animals at each age investigated (Two-way ANOVA, p <0.05).

The overall current response characteristics elicited by *Gata3*$^{+/-}$ OHCs at the above stages were similar to those in previous reports [Marcotti and Kros, 1999]. In conclusion, outward K^+ currents develop normally with age in *Gata3*$^{+/-}$ OHCs (Figure 3-7).

3.2.3 $I_{k,n}$ conductance shows normal development in *Gata3*$^{+/-}$ OHCs

We studied the properties of $I_{k,n}$ in OHCs to investigate if the principal conductance responsible for OHC maturity develops normally and is maintained in *Gata3*$^{+/-}$ mice. $I_{k,n}$ was elicited by depolarizing voltage steps of 170 ms duration, from -154 mV in 10 mV increments, from the holding potential of -64 mV (Figure 3-8A). Current size was measured as the difference between the peak and steady-state deactivating currents at a fixed potential of -125 mV (arrows in Figure 3-8B).

At the stages investigated, hyperpolarising steps from the holding potential of -64 mV caused large rapid inward currents that decayed slowly and reached a steady state (Figure 3-8B), consistent with previous observations [Marcotti and Kros, 1999]. At more depolarised potentials, the current changed direction to become outward, thus providing an efficient exit route for K^+ and determining the OHC time constant [Marcotti and Kros, 1999].

There were no differences observed between the two groups at the time-points studied (Two-way ANOVA, $p < 0.05$; Table 3.3; Figure 3-9), showing that the conductance developed normally and was maintained in *Gata3*$^{+/-}$ OHCs.

TABLE 3.3: $I_{k,n}$ *conductance in OHCs*

Age	Wt (pA)	S.E.M	N	*Gata3*$^{+/-}$ (pA)	S.E.M	N
P22 - 24	-1034.8	109.3	5	-1132.5	41.07	5
P28 - 30	-1073.14	55.8	7	-934.63	186.0	4

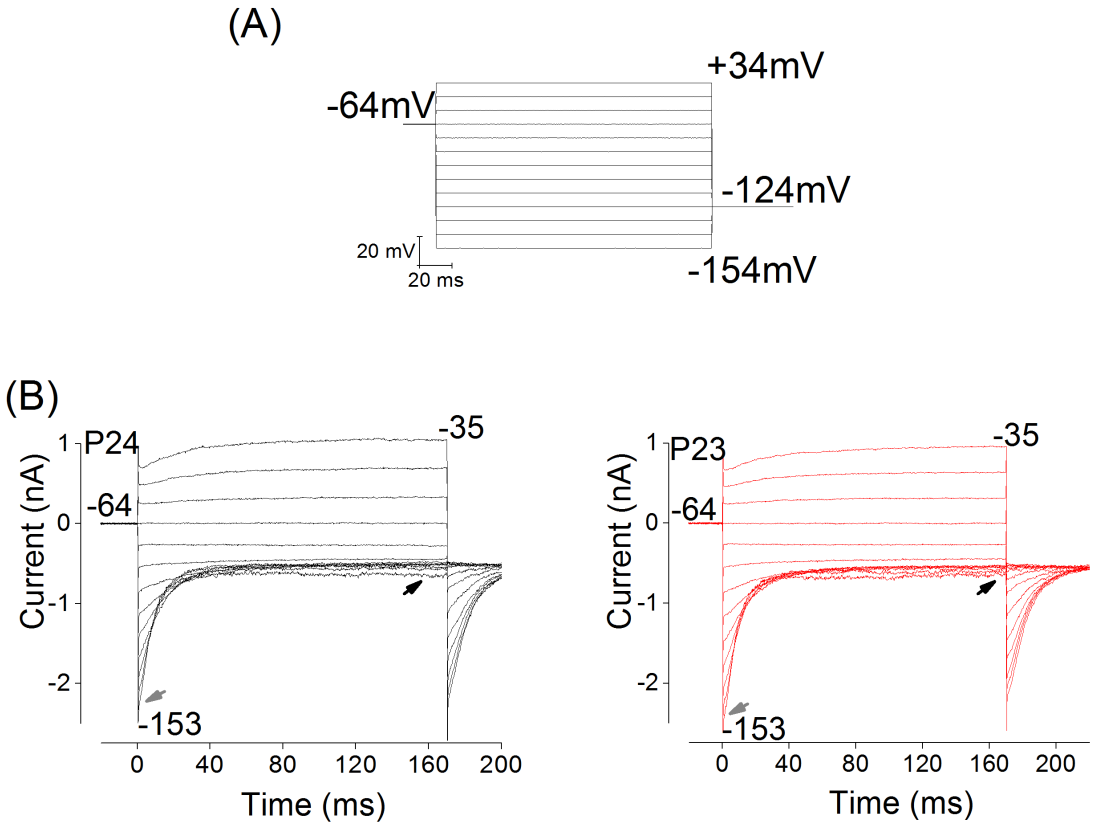

Figure 3-8: Negatively-activating inward K^+ current ($I_{k,n}$) is normal in $Gata3^{+/-}$ OHCs

(A) The voltage protocol applied to HCs to elicit $I_{k,n}$. Cells were referred to a holding potential of -64 mV, and stepped to different potentials from a potential of -154 mV in increments of 10 mV. The duration of each voltage step was 170 ms.

(B) Example of K^+ currents measured from a wild type (black) and $Gata3^{+/-}$ (red) OHCs, in response to the voltage step protocol as described in (A). The $I_{k,n}$ amplitude was quantified in isolation as the difference between the instantaneous (black arrow) and deactivating steady-state (grey arrow) inward currents at a fixed potential of -125 mV.

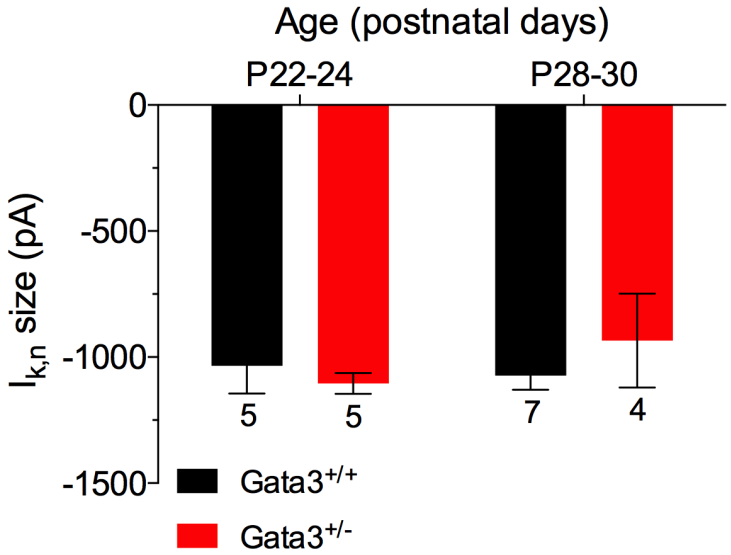

Figure 3-9: Comparison of $I_{k,n}$ amplitude between control and *Gata3*$^{+/-}$ OHCs
Bar graph showing the size of $I_{k,n}$ conductance of wild type (black bars) and *Gata3*$^{+/-}$ (red bars) OHCs. There are no differences between $I_{k,n}$ amplitude from *Gata3*$^{+/-}$ and wild type OHCs at the time-points investigated (Two-way ANOVA, $p < 0.05$). N numbers are written below individual columns, and and error bars indicate ± S.E.M values.

3.2.4 Voltage responses of OHCs in *Gata3*$^{+/-}$ mice are normal

Voltage responses of apical HCs were investigated under current clamp conditions to study if the progressive developmental changes in the K^+ currents shaped the voltage responses in a predictable fashion, as studied previously [Marcotti and Kros, 1999].

Cells were stimulated from their resting potential with current injections that ranged from -100 pA to +900 pA in 100 pA increments for a duration of 250 ms (Figure 3-10A), at an age when the animals had reached adulthood. Action potentials were not evoked at this stage, as has been established previously [Marcotti and Kros, 1999]. Large current injections caused the voltage to rise rapidly to a peak and then sustain a steady depolarization, similar to wild type cell behaviour (Figure 3-10B).

The resting membrane potential was measured by averaging the voltage of the clamped cell before current injection. Resting membrane potentials between wild type and *Gata3*$^{+/-}$ OHCs were found to be comparable in adult mice, between P22 - P24 (Table 3.4; Student's t-test, $p < 0.05$).

Steady-state vales of the voltage responses were measured by averaging the voltage of the cell over the last 25 ms of the current injections, to allow for comparisons between the two groups. Responses of wild type and *Gata3*$^{+/-}$ OHCs were comparable (Figure 3-11)

TABLE 3.4: *Resting membrane potential of OHCs*

Genotype	R_m (mV)	S.E.M	N
Wt	-68.20	0.99	5
Gata3$^{+/-}$	-66.78	2.75	5

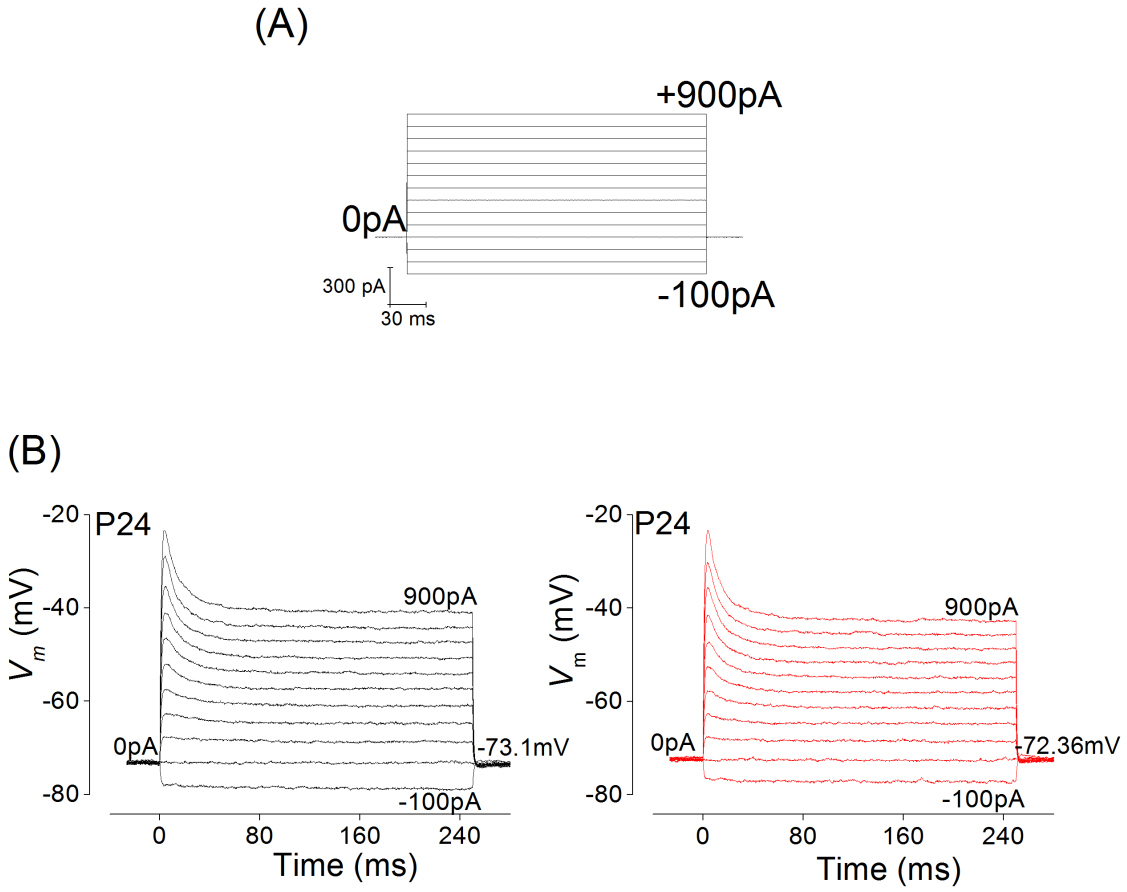

Figure 3-10: Resting membrane potentials of *Gata3*$^{+/-}$ OHCs are normal
(A) Step protocol applied to current clamped HCs. After averaging the voltage of the clamped cell, a range of currents from -100 pA to +900 pA was injected into the cell, in increments of 100 pA. The duration of the step is 250 ms.
(B) Current clamp recordings of an OHC from a P23 control (black) and P24 *Gata3*$^{+/-}$ (red) mouse
The average resting membrane potential of control OHCs (-68.20 ± 0.99 mV, n = 5) was not different from that in *Gata3*$^{+/-}$ mice (-66.78 ± 2.75 mV, n = 5)

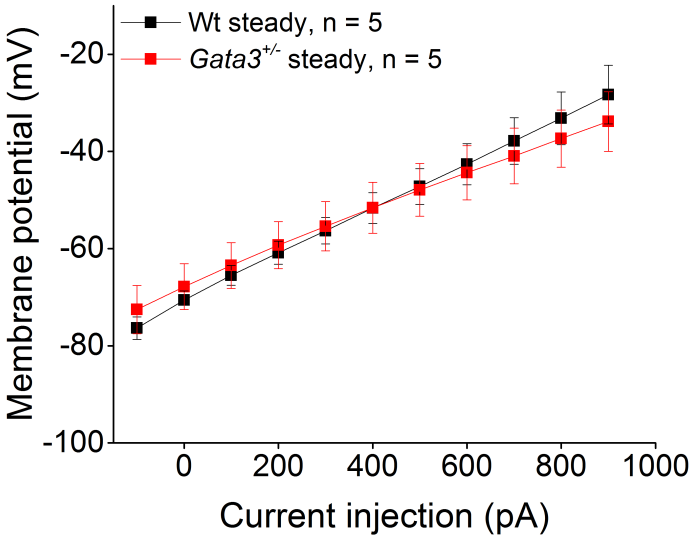

Figure 3-11: Steady-state voltage responses of $Gata3^{+/-}$ OHCs are normal
Average steady-state voltage responses measured from P22 - P24 wild type (black, n = 5) and $Gata3^{+/-}$ (red, n = 5) mice. Values plotted are the mean voltages over the last 25 ms of the current injection. Error bars represent ± S.E.M.

3.2.5 The ACh-activated current is normal in *Gata3*$^{+/-}$ OHCs

OHCs become responsive to ACh release from efferent synapses from P8, and retain this characteristic into adulthood, mirroring the persistence of their efferent connections. The ACh-activated current provides OHCs with an inhibitory mechanism to control their voltage-dependent electromotile activity [Wersinger and Fuchs, 2011].

Presynaptic ACh release from efferent fibres causes Ca^{2+} influx via $\alpha9\alpha10$nAChRs, which in turn activates SK2 channels to trigger a hyperpolarizing K^+ current [Oliver et al., 2000]. More recently it has been shown that this is the case in apical OHCs, while in basal high frequency regions of the cochlea, BK channels underlie this synaptic inhibition (in rats: [Wersinger et al., 2010; Rohmann et al., 2015]).

Basolateral membrane currents were recorded from mature OHCs (between P17 and P21) before, during and after the superfusion of 100 μM ACh in the presence of 1.3 mM Ca^{2+}, in response to voltage steps in 10 mV increments (of 170 ms pulse duration), from a potential of -154 mV (protocol as in Figure 3-8A). The cells were referred to a holding potential of -64 mV, and all recordings were conducted at room temperature. The ACh-sensitive current (Figure 3-12C and 3-13C) was calculated by subtracting the control current (before ACh superfusion; Figure 3-12A and 3-13A) from the current in the presence of 100 μM ACh (Figure 3-12B and 3-13B). The steady state current was measured at 160 ms from the start of the voltage step, and I-V curves were plotted for the currents before and during ACh perfusion, and also of the ACh-activated current (Figure 3-12D and 3-13D). The ACh -sensitive current was calculated as the steady-state slope conductance at the potential of -84 mV.

The steady state slope conductance at -84 mV was not found to be different between the two groups tested (Table 3.5; Student's t-test, $p < 0.05$) indicating that mature OHCs from *Gata3*$^{+/-}$ animals respond normally to cholinergic input via $\alpha 9\alpha 10$nAChRs by expressing an outward SK2 conductance.

TABLE 3.5: *Steady-state slope conductance of the ACh-activated current in OHCs*

Genotype	Slope conductance (nS)	S.E.M	N
Wt	9.42	3.3	4
Gata3$^{+/-}$	7.41	1.92	5

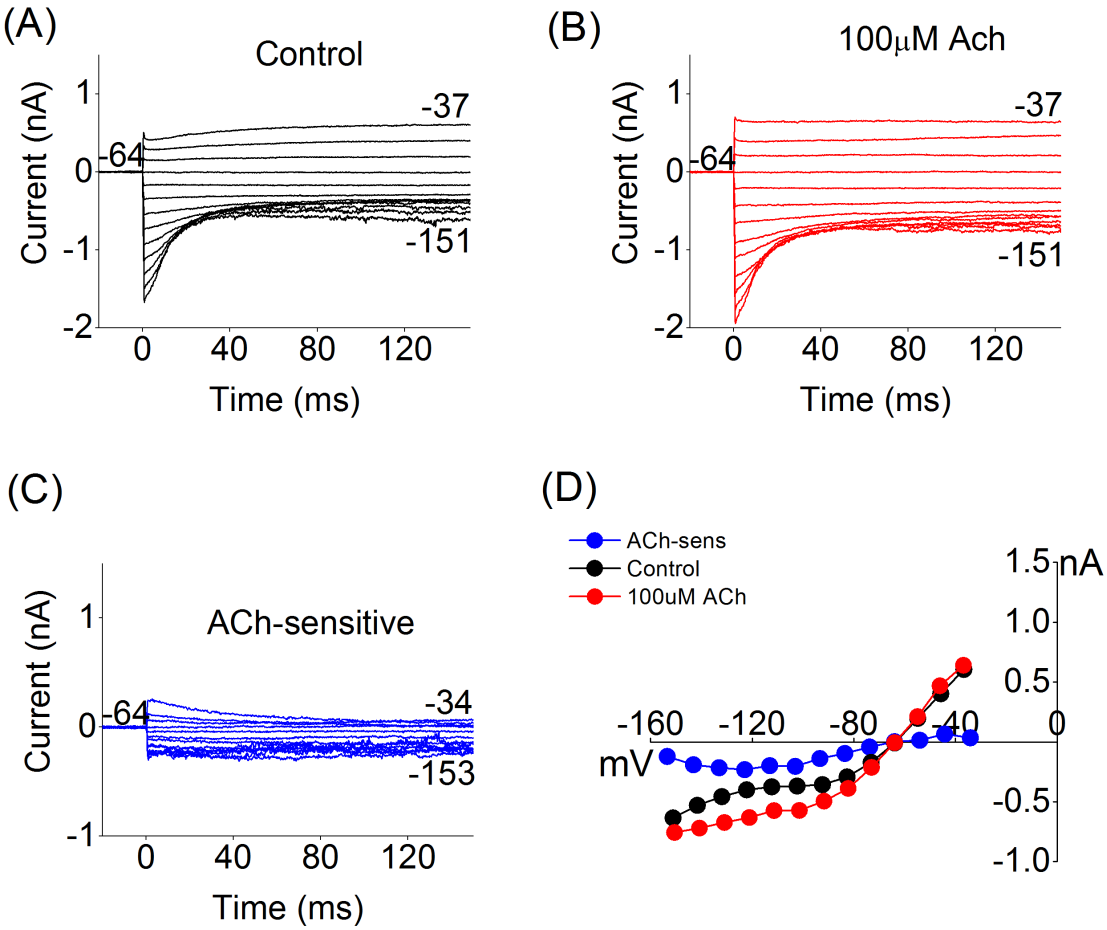

Figure 3-12: ACh-activated current in mature wild type OHCs
Membrane currents recorded from a wild type apical P22 OHC before (A), and during (B) the perfusion of 100 μM ACh, in response to depolarising voltage steps of 170 ms duration from -154 mV, from a holding potential of -64 mV, in nominal increments of 10 mV.
(C) ACh-activated current is obtained by subtracting the control current (A) from the current in the presence of 100 μM ACh (B).
(D) I-V curves of the currents recorded before and during the perfusion of 100 μM ACh, and also the ACh-activated current of the traces shown for the wild type OHC.

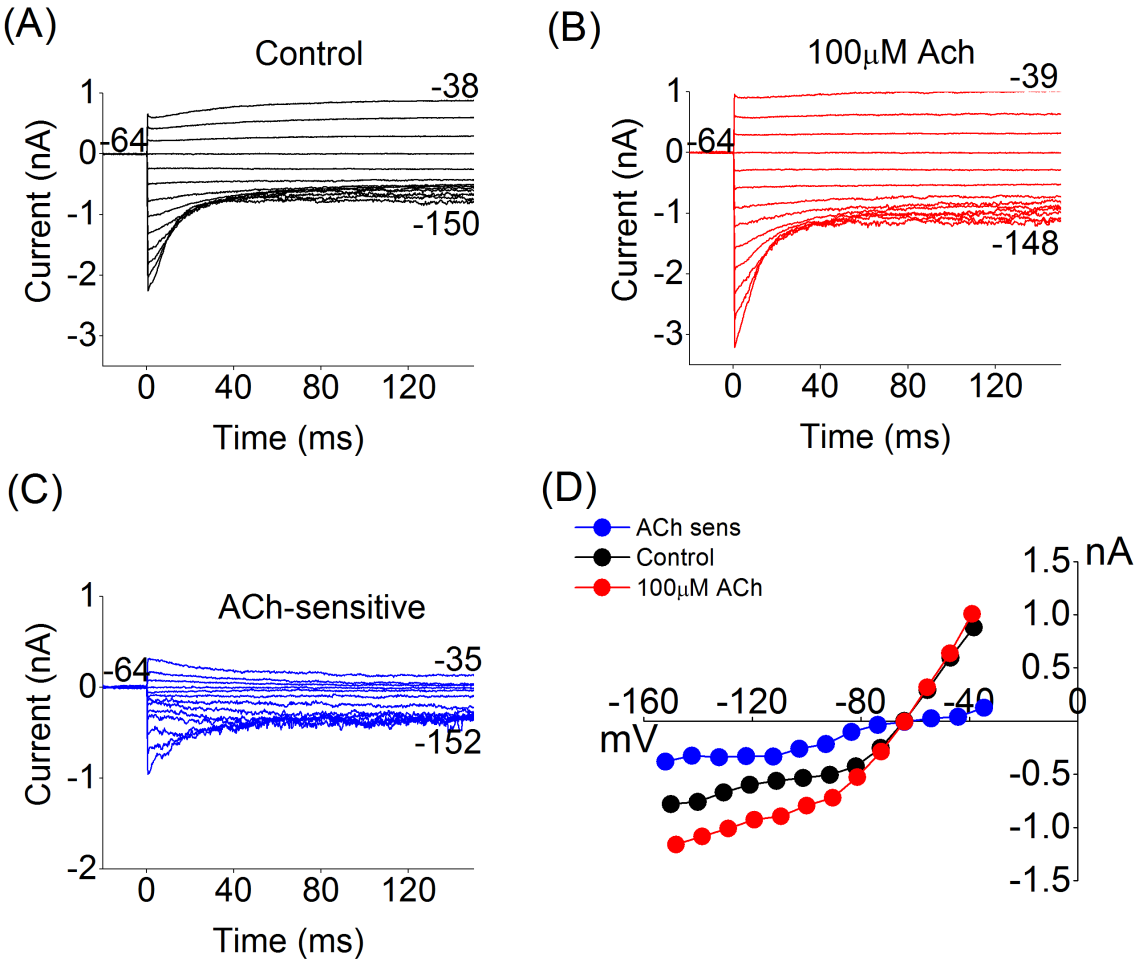

Figure 3-13: ACh-activated current in mature *Gata3*$^{+/-}$ OHCs
Membrane currents recorded from a *Gata3*$^{+/-}$ apical P22 OHC before (A), and during (B) the perfusion of 100 μM ACh, in response to depolarising voltage steps of 170 ms duration from -154 mV, from a holding potential of -64 mV, in nominal increments of 10 mV.
(C) ACh-activated current is obtained by subtracting the control current (A) from the current in the presence of 100 μM ACh (B).
(D) I-V curves of the currents recorded before and during the perfusion of 100 μM ACh, and also the ACh-activated current of the traces shown for the *Gata3*$^{+/-}$ OHC.

3.2.6 OHC numbers are lower in *Gata3*$^{+/-}$ animals

Missing apical OHCs have been reported in *Gata3*$^{+/-}$ animals from the age of two months onwards [van der Wees et al., 2004]. Therefore, we investigated whether OHC loss occurred at neonatal stages.

The organ of Corti was dissected from the mouse cochlea at different ages immediately after birth, between P0 and P8, and cultured for a period of 24 hours, as described in Section 2.9. HC counts were then performed on different regions along the epithelium (refer to Section 2.12). IHCs and all three rows of OHCs were counted to allow for comparisons between wild type and *Gata3*$^{+/-}$ animals, to investigate the function of postnatal age and position on the loss of OHCs.

The most striking differences observed involved missing OHCs from the outermost row (OHC3) in *Gata3*$^{+/-}$ mice (Figure 3-14) from as early as the day of birth. HCs were counted along a length of 150 μm within each specified region, and OHC counts from only OHC3 are presented here for clarity.

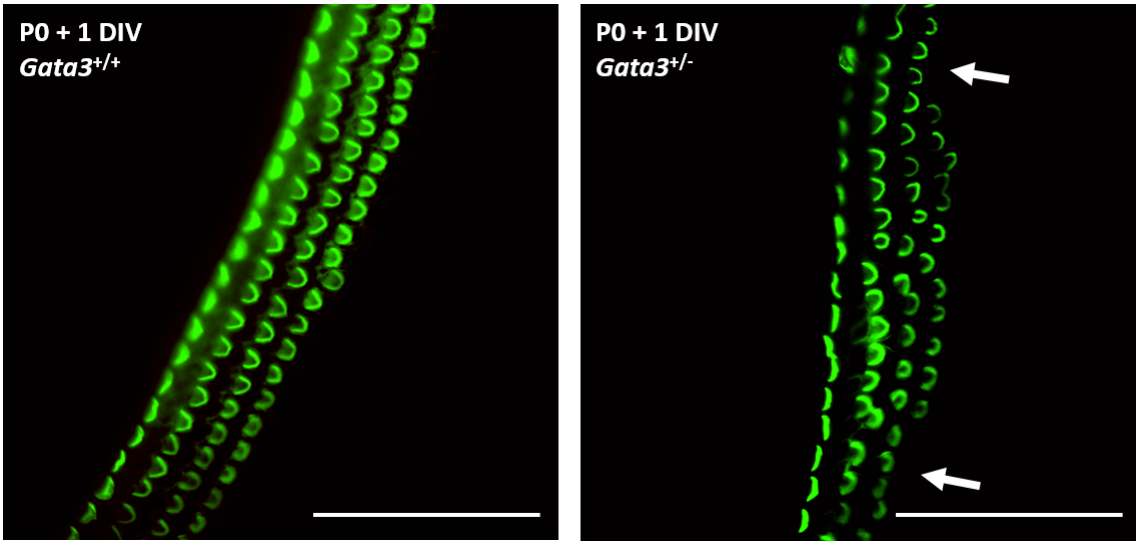

Figure 3-14: OHC numbers are reduced in *Gata3*$^{+/-}$ mice
Cultures of the organ of Corti from P0 *Gata3*$^{+/+}$ (wild type) and *Gata3*$^{+/-}$ mice, after being kept under culture conditions for 1 day *in vitro* (DIV). A number of OHCs are missing from the outermost row (OHC3) in cultures from the *Gata3*$^{+/-}$ animal (white arrows). The remaining HCs also appear to be misaligned compared to the wild type control. Scale bar is 60 μm.

At the P0 - P1 stage, it was difficult to quantify the number of HCs in the apical-most region (A1 region) as the cells appeared to have either not stained or the tissue had folded in such as a way so as to interfere with counting. This region was therefore excluded from subsequent analysis.

At the A2 apical region which lies slightly basal to the A1, *Gata3*$^{+/-}$ OHCs were significantly reduced in number at each stage investigated, and the number of missing OHCs at P4 - P8 exceeded that of the earlier time-point (Table 3.6; Figure 3-15A; two-way ANOVA followed by Tukey's post-test, $p < 0.05$).

TABLE 3.6: *OHC number in A2 region of the cochlea*

Age	Genotype	Mean	S.E.M	N
P0 - 1	Wt	22.3	0.69	19
	Gata3$^{+/-}$	15.85	1.8	13
P4 - 8	Wt	21.81	0.48	16
	Gata3$^{+/-}$	9.0	1.28	10

The A3 region lying basal to the A2 section, and representing the basal part of the apical coil, similarly showed a reduction in the number of OHCs from *Gata3*$^{+/-}$ animals at both time-points studied. Similar to the A2 region, the number of missing OHCs at P4 - P8 exceeded that of the earlier time-point, showing that postnatal age had a significant effect. (Table 3.7; Figure 3-15B; two-way ANOVA followed by Tukey's post-test, $p < 0.05$).

TABLE 3.7: *OHC number in A3 region of the cochlea*

Age	Genotype	Mean	S.E.M	N
P0 - 1	Wt	21.4	0.43	15
	Gata3$^{+/-}$	15.8	1.4	10
P4 - 8	Wt	20.47	0.7	15
	Gata3$^{+/-}$	11.17	1.51	6

From the basal B1 region of the epithelium, the results seen were similar to those observed in A2 and A3, with fewer OHCs from *Gata3*$^{+/-}$ animals at each time-point studied, but this time age did not seem to have an effect on the number of missing OHCs (Table 3.8; Figure 3-15C; two-way ANOVA followed by Tukey's test, $p < 0.05$).

TABLE 3.8: *OHC number in B1 region of the cochlea*

Age	Genotype	Mean	S.E.M	N
P0 - 1	Wt	19.5	0.53	18
	Gata3$^{+/-}$	10.93	1.09	14
P4 - 8	Wt	18.13	0.58	8
	Gata3$^{+/-}$	10.67	1.26	6

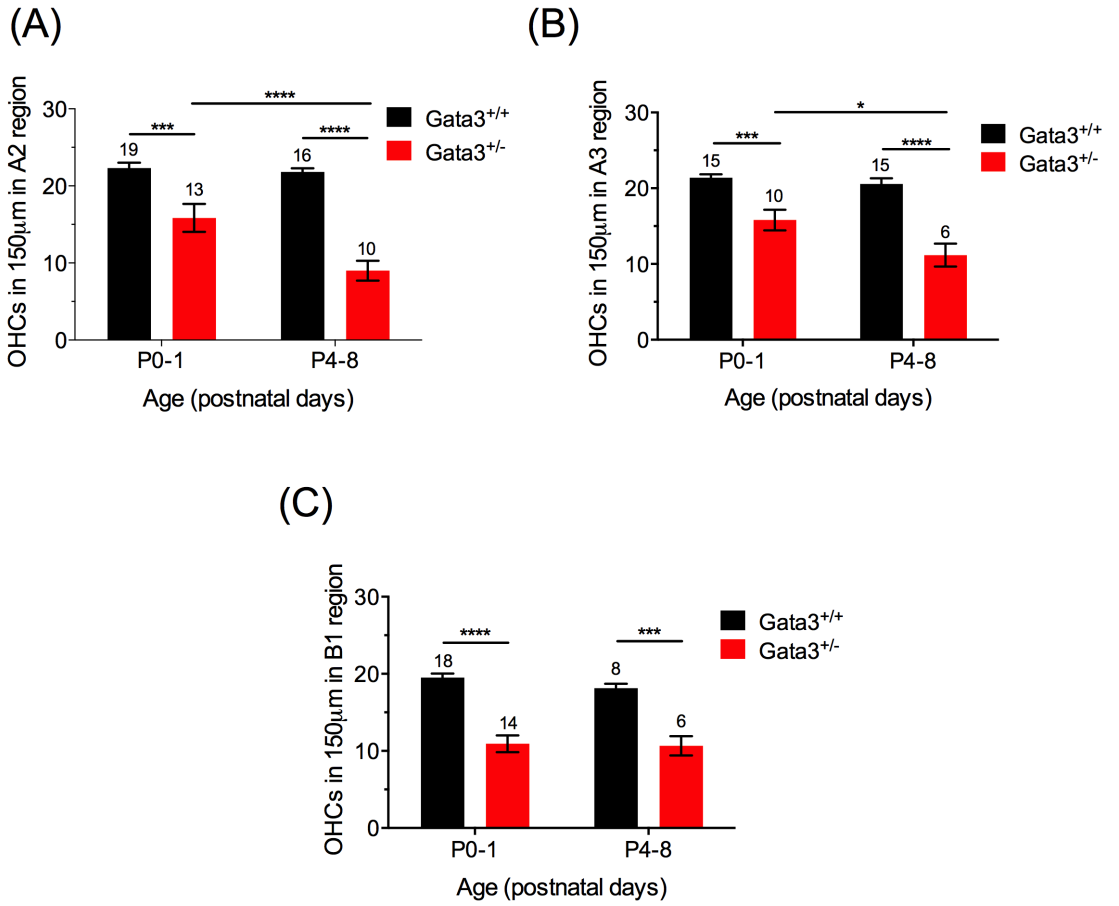

Figure 3-15: Number of OHCs as a function of age
OHCs were counted along a length of 150 μm along different regions of the cochlear spiral. Bar graph representing the OHC count in the A2 region (A), A3 region (B), and B1 region (C). At each region and time-point studied, OHCs were lower in number from *Gata3*$^{+/-}$ animals. N numbers are written above each column and error bars represent ± S.E.M. * indicates p<0.05, ** indicates $p \leq .01$, *** indicates $p \leq .001$ and **** indicates $p \leq .0001$.

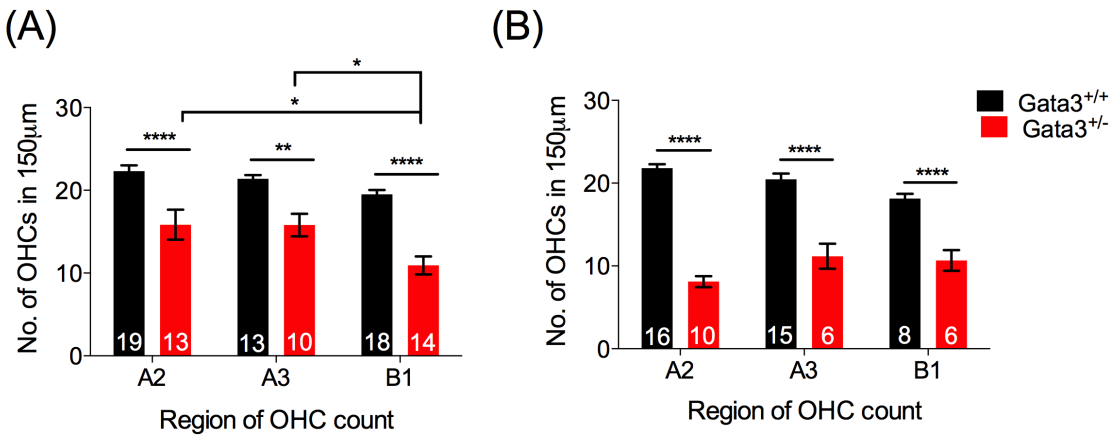

Figure 3-16: Number of OHCs as a function of position
Bar graph representing the OHC count along the different regions at the beginning of the first postnatal week between P0 and P1 (A), and end end of the first postnatal week between P4 and P8 (B). Although OHC numbers were reduced at each region investigated, there was no clear positional effect on their loss. N numbers are written at the base of each column and error bars represent ± S.E.M. * indicates $p<0.05$, ** indicates $p \leq .01$, *** indicates $p \leq .001$ and **** indicates $p \leq .0001$.

IHC numbers were unaffected at each region and time-point studied, indicating that OHCs were more vulnerable to loss by a reduction of GATA3 levels, corroborating previous work [van der Wees et al., 2004]. There did not appear to be a very obvious longitudinal gradient to the loss of OHCs, as cells were found to be missing from all regions of the cochlear spiral (Figure 3-16). This is in contradiction to the earlier finding of a positional gradient of HC loss, which started in the apex and progressed towards the base as a function of postnatal age [van der Wees et al., 2004]. In fact, at birth the base had significantly fewer OHCs than the apex (Figure 3-16A). However, our studies were conducted at two time-points relatively close to each other, at the beginning and end of the first postnatal week, perhaps not allowing enough time to monitor such a positional effect on HC death.

3.3 Discussion

In summary, our analysis shows the following:

1. Outer hair cells have normal basolateral currents, even at P22. But they appear to die earlier

2. The complement of outer hair cells is reduced at least from the day of birth (the earliest time investigated)

3. The loss of outer hair cells demonstrates a clear radial gradient, with outer hair cells from the outermost row disappearing preferentially to the two inner rows.

4. The MET current is normal

3.3.1 *Gata3* haploinsufficiency does not affect basolateral membrane properties or MET of OHCs

By the above analyses we attempted to establish a physiological basis for the hearing impairment phenotype that is observed in *Gata3*$^{+/-}$ animals [van der Wees et al., 2004]. The development of membrane properties of *Gata3*$^{+/-}$ mice over time, as exemplified by the ion channels underlying the conductances expressed in OHCs, closely matched wild type littermates and are consistent with previous observations [Marcotti and Kros, 1999].

It should be noted that all the above physiological data have been collected from OHCs residing in the low frequency apical region of the cochlear sensory epithelium. The highest ABR threshold elevations [van der Wees et al., 2004] and the poorest signal-noise DPOAE ratios [van Looij et al., 2005] were observed in low frequency regions of *Gata3*$^{+/-}$ animals. So any potential physiological malfunction harboured by these cells could be expected to be revealed in our data. However, it should also be mentioned that *Gata3* is purportedly downregulated by HCs as they differentiate from base to apex along the longitudinal gradient of the sensory epithelium from E14 to E16 following a two three day delay [Rivolta and Holley, 1998]. Thus, HCs at the basal high frequency region at any given point in time have lived longer with lower levels of GATA3 than those in the apex. Perhaps, our studies, if conducted upon basal HCs might reveal slightly different results.

Sensitivity to ACh implies the presence and normal function of both $\alpha 9\alpha 10$nAChRs and SK2 channels, but it does not provide information about endogenous efferent innervation in these animals. Immunofluorescence studies on efferent terminals would be more instructive in this regard.

In addition to the basolateral membrane properties, the MET channel seems to

develop and function normally in these animals. However, MET measurements are not instructive about the endocochlear potential operating *in vivo*, as patch clamp measurements necessitate destruction of the endolymph.

Electromotility in OHCs from these animals has not been studied, and remains to be investigated. *Prestin* mutants demonstrate normal MET, however they are not electromotile due to the lack of prestin from their lateral walls [Liberman et al., 2002]. There have been no previous reports of a reduction in size of OHCs in *Gata3*$^{+/-}$ animals, as would be expected from the lack of PRESTIN [Liberman et al., 2002]. It is possible, however, that PRESTIN may be reduced or malfunctional in our system [Gross et al., 2010]. Taken together, our physiological data suggest that *Gata3* seemingly has very little or no role in the expression of ion channels underlying the basolateral membrane or MET properties as far as OHCs are concerned, at least within the time frame studied.

3.3.2 Essential role for *Gata3* in the maintenance and survival of cochlear OHCs

The expression of *Gata3* in the developing auditory system is almost concomitant with formation of the auditory placode [Lawoko-Kerali et al., 2002]. This expression is maintained in all sensory cell progenitors until they differentiate as HCs [Rivolta and Holley, 1998]. Thereafter, its expression is maintained at high levels in the adjacent supporting cell population. Thus, it is highly plausible that *Gata3* is somehow involved in the initial specification and generation of HCs.

Our data indicate that the number of OHCs is deregulated in animals with a dose shortage of GATA3, resulting in:

1. Fewer numbers of OHCs from birth in GATA3-deficient animals

2. A disordered arrangement of OHC rows, and

3. A preferential loss of OHCs from the outermost row

4. A reduction or degeneration of OHCs from all regions of the cochlear turns

Conditional *Gata3*-null mice demonstrate abnormalities in the specification of the prosensory domain (*Sox2*-positive) accompanied by cell death in this region from as early as E12.5. From E18.5, OHCs appear to be missing [Luo et al., 2013]. Therefore, it is no surprise that in our system, *Gata3* haploinsufficiency leads to a similar result. This still begs the question of whether a reduced number of HCs is due to a developmental defect - whereby fewer HCs are born to begin with, perhaps because their precursors were never specified; or a maintenance issue - whereby the HCs fail to survive after having been born due to a postnatal role of *Gata3*, or a combination of both.

The misalignment of OHCs in $Gata3^{+/-}$ animals could be an indication of an accumulation of molecular changes within the cells before their morphological degeneration. A more likely explanation could be the degeneration of the underlying Dieter's cells, which also arise from the *Sox2*-positive domain. If this is the case, is the loss of OHCs an issue secondary to the death of supporting cells, where *Gata3* is expressed at higher levels and for a longer duration?

An additional observation was the preferential loss of HCs from the outermost row (OHC3) of OHCs. If vacuolation is considered as an indication of a progressively degenerating cell, then this evidence is in direct contrast to the observation of the innermost row (OHC1) containing the most vacuoles [van Looij et al., 2005]. In the absence of a distinct radial gradient of *Gata3* expression in OHCs, an initial preferential loss of the outermost row could suggest a differential requirement for the protein in the different rows of OHCs. Alternatively, *Gata3* may modulate the expression of another molecule that is expressed in a radial gradient and is required

for their maintenance. It is also likely that *Gata3*$^{+/-}$ phenotypes are variable and highly dependent upon background and growth conditions. Haploinsufficiency suggests sensitivity to dose and the large number of indirect effects via cell signaling could lead to variability.

Dying cells could be expected to harbour physiological defects. However, we have been unable to detect any such issues. From these studies, it can be concluded that while there is a critical requirement for the normal levels of GATA3 for the generation and/or survival of the full complement of OHCs, the OHCs that exist, albeit for a limited time, appear to differentiate normally and mediate their physiological roles without quantifiable abnormalities. It has been previously observed that as long as IHCs function, a 40 - 60 dB threshold elevation can be expected in the absence of OHC function [Lonsbury-Martin et al., 1990; Spektor et al., 1991]. The 30 - 40 dB HL observed [van der Wees et al., 2004] in *Gata3*$^{+/-}$ is well within this range.

Additionally, the peripheral loss of cochlear OHCs could affect the downstream central auditory processing of incoming signals. A functional set of OHCs is partly responsible for the generation of a sharply tuned frequency curve and the preservation of tonotopicity in the nuclei of the auditory pathway [Sterbing and Schrott-Fischer, 2002].

Since OHCs in *Gata3*$^{+/-}$ mice appear to be normal in their biophysical characteristics, we next looked at IHCs to understand if deficits in these animals could be attributable to them.

Chapter 4

Gata3 haploinsufficiency prevents normal physiological development of inner hair cells

4.1 Introduction

IHCs receive 90 - 95% of the afferent fibre innervation. The basal pole of each cell is contacted by 20 - 30 myelinated bipolar afferent fibres [Liberman et al., 1990], which serve to couple the IHCs to the cochlear nuclei in the hindbrain. These fibres are called Type I spiral ganglion neurons as their cell bodies form the spiral ganglion within the modiolus (for a review, see [Coate and Kelley, 2013]).

HCs begin to differentiate at around E14 in the basal coil of the mouse cochlea [Anniko, 1983] and the onset of hearing occurs 3 weeks later, at around P12 in most altricial rodents. Throughout this time their biophysical characteristics change considerably [Marcotti et al., 2003] to adapt with the changing environmental demands imposed upon them. The progressive changes through development can be broken down into stages associated with distinct biophysical properties.

At very early stages of differentiation, around E14.5, basal IHCs respond to depolarising voltage steps with a small, slowly activating outward voltage-dependent K^+ current. This delayed rectifier-type current gradually increases in amplitude over the next few weeks, and can be pharmacologically dissected to

reveal two distinct components that are either sensitive or insensitive to 4-AP [Marcotti et al., 2003]. Over the next couple of days, it is also accompanied by a rapidly activating inward Ca^{2+} current and a fast activating inward-rectifier K^+ current (I_{k1}) [Marcotti et al., 2003]. The interplay between the inward Ca^{2+} and the outward K^+ current causes spontaneous occurring spiking behaviour. As the Ca^{2+} and K^+ currents increase in size, the action potential spikes become narrower and faster [Marcotti et al., 2003]. The combination of the gradually increasing delayed rectifier and inward rectifier I_{k1}, result in the initial hyperpolarisation of the resting membrane potential of the cells during the late embryonic stages. Concurrently, afferent fibres organise themselves into synapse-like contacts around the base of IHCs [Pujol et al., 1998].

The increase of the Ca^{2+} current during the first postnatal week sustains spontaneous action potential activity. This behaviour persists during the second postnatal week. Low endolymphatic Ca^{2+} concentration (0.3 mM) causes a larger resting current through the partially open but fully functional MET channels. The interplay between the resting MET current and the outward K^+ currents continues to drive action potential activity [Johnson et al., 2012] *in vivo* in the absence of sensory stimuli until the onset of hearing. This second week of sensory-independent firing represents a critical window in the development of the synaptic machinery of IHCs, which becomes more efficient by changing from a high-order Ca^{2+}-dependence for exocytosis to a linear relationship [Johnson et al., 2008].

During this time, afferent neurons undergo pruning in order to establish an unbranched pattern of axo-somatic connections, such that each Type I neuron synapses with only one IHC[Echteler et al., 1989].

In addition to the afferent circuitry, the efferent system that exercises modulatory control over action potential activity of the IHCs develops during this period.

Cholinergic efferent fibres from the superior olivary complex within the brainstem make transitory axo-somatic connections with IHCs [Shnerson et al., 1981] from birth until just before the onset of hearing [Simmons, 2002].

$\alpha 9\alpha 10$nAChRs are expressed by IHCs [Elgoyhen et al., 2001] from birth [Roux et al., 2011], and allow the entry of Ca^{2+} into the cell upon the release of ACh from efferent fibres. As $\alpha 9\alpha 10$nAChRs become functionally associated with the small conductance Ca^{2+}-dependant K^+ channel (SK2) from P2 [Marcotti et al., 2004b], this Ca^{2+} influx activates outward K^+ currents in SK2 channels. This hyperpolarises the cell and inhibits further action potential activity [Glowatzki and Fuchs, 2000]. The SK2 conductance appears to play a dual role in the context of development - it allows the firing of repetitive action potentials by making the shape of the repolarisation phase of action potentials more efficient; and when the efferents exert their inhibitory control over excitability of cells, they modulate this firing activity [Marcotti et al., 2004b]. This central control mediated by the efferent system is unique to the auditory system and has been shown to be critical in the maturation of ribbon synapses [Johnson et al., 2013]

The final steps in the transition of IHCs, from immature to functionally efficient, high frequency sensory transducers, occurs at P12 at the onset of hearing. $I_{k,f}$, the large conductance Ca^{2+}-activated outward K^+ current mediated by the BK channel, begins to appear at the base of the cochlea by P10, and by P13 is an established feature in all IHCs. It is chiefly responsible for the suppression of action potential activity [Kros et al., 1998]. The K^+ outward delayed rectifier remains, although now the 4AP-sensitive fraction emerges as the major constituent of this current. Another hallmark of these mature cells is the expression of the linopirdine-sensitive $I_{k,n}$ conductance carried via the KCNQ4 channels [Kharkovets et al., 2000]. Both the $I_{k,n}$ and the 4AP-sensitive components of the delayed rectifier contribute to the resting membrane potential mature IHCs [Marcotti

et al., 2003; Oliver et al., 2003]. IHCs by this stage are equipped to respond to incoming stimuli with continual, rapid and graded changes in receptor potential that are directly proportional to the extent of hair bundle displacement. By about P16, efferent connections rearrange themselves to form axo-dendritic contacts on IHC afferent fibres, and HCs stop responding to ACh [Marcotti et al., 2004b]. Refinement of the number of afferent neural connections under IHCs is complete by this stage [Pujol et al., 1998].

Rationale for our study

Given the lack of functional deficit in OHCs, which had more obvious structural defects, we turned our attention to the IHCs as the potential source of observed HL. Measurable deficits may not only be informative regarding the function of *Gata3* but also provide the basis of an assay for rescuing the effects of haploinsufficiency. Thus we undertook a systematic investigation of the membrane properties of IHCs. Here we report our findings from whole-cell patch clamp electrophysiological recordings of IHCs from *Gata3*$^{+/-}$ mice from the first postnatal week to two months of age. These were then compared to age-matched, wild type littermates to build a developmental profile of membrane properties of IHCs and also to investigate any progressive changes that may occur with age.

4.2 Results

4.2.1 Total outward K^+ currents in *Gata3*$^{+/-}$ mouse IHCs are affected

We recorded whole cell time and voltage-dependent current responses from apical IHCs of P6 to P50 *Gata3*$^{+/-}$ mice and their wild type littermates, in order to study the current profile of IHCs in these animals as a function of development.

The voltage step protocol employed was the same as that used for OHCs (Figure 3-2A). Steady-state values of the outward currents were measured towards the end of each test pulse (160 ms from the start of the voltage step) and plotted against the corresponding membrane potential to construct an I-V curve.

For the first two postnatal weeks (between P6 and P14), the average steady-state current at 0 mV from IHCs of *Gata3*$^{+/-}$ mice was comparable to their age-matched wild type controls (Table 4.1; Figure 4-1 and Figure 4-2). However, from P16 onwards, there was a reduction in the total current in IHCs observed in *Gata3*$^{+/-}$ mice at each time-point studied (two-way ANOVA followed by Bonferroni's post-hoc test, $p < 0.05$; Table 4.1; Figure 4-3 and Figure 4-4).

TABLE 4.1: *Outward K^+ currents at 0 mV in IHCs*

Age	Wild type (nA)	S.E.M	N	*Gata3*$^{+/-}$ (nA)	S.E.M	N
P6 - 9	3.48	0.18	21	4.4	0.73	6
P12 - 14	8.17	0.77	8	9.79	0.92	11
P16 - 20	11.38	1.09	7	7.75	1.91	7
P28 - 50	16.25	0.88	8	11.03	0.62	11

For IHCs from wild type animals, the total current generally increased in amplitude with age, however from P16 onwards *Gata3*$^{+/-}$ animals demonstrated an abnormal K^+ current profile (Figure 4-5).

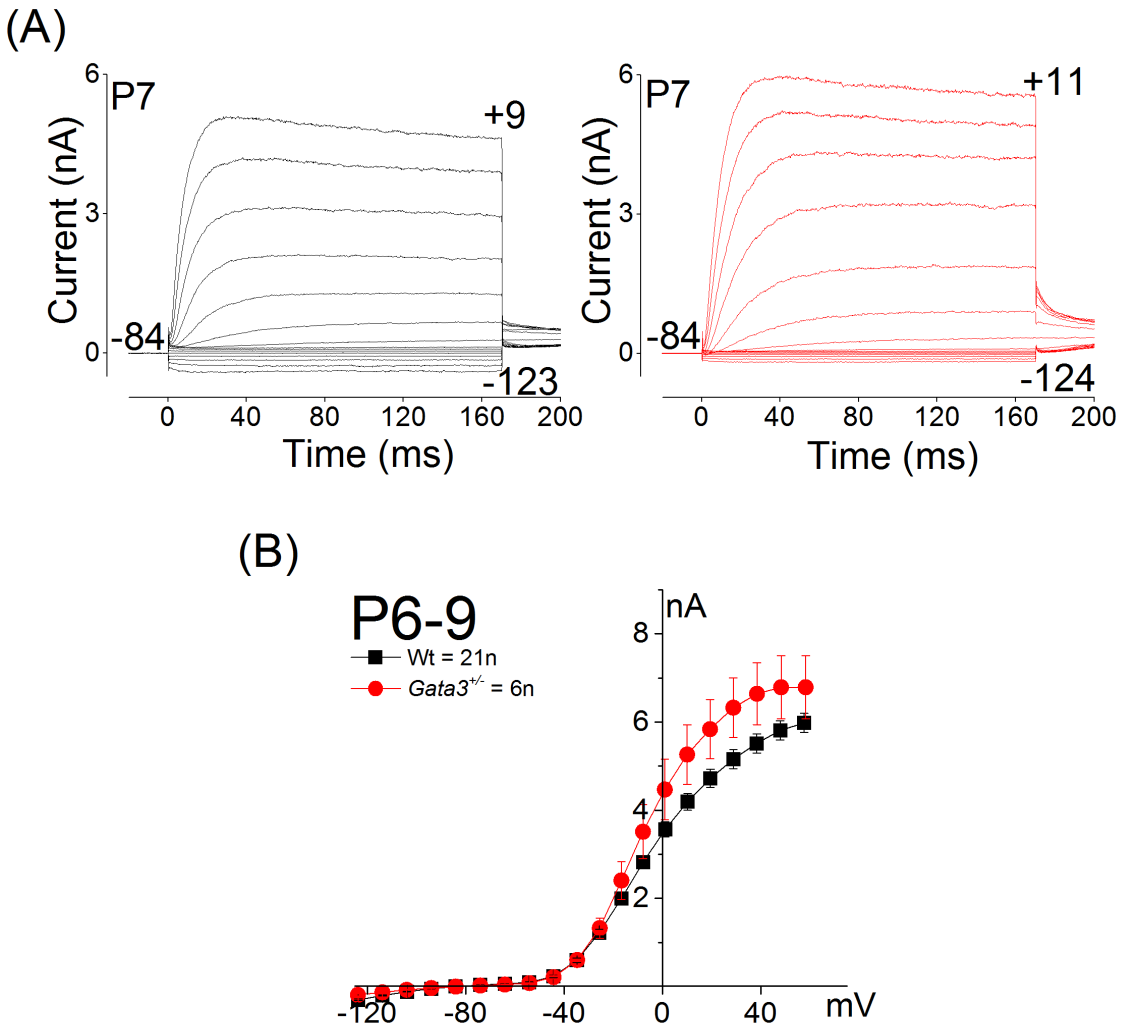

Figure 4-1: Outward K^+ currents in IHCs from neonatal (P6 - P9) mice
(A) Example of the current responses of an IHC from wild type (black) and $Gata3^{+/-}$ (red) P7 mouse.
(B) Average steady-state I-V relationship curves for wild type (n = 21) and $Gata3^{+/-}$ (n = 6) IHCs from P6 - P9 mice. Error bars represent ± S.E.M values.
No significant difference was observed in the amplitude of the K^+ currents of IHCs in response to voltage steps, from control and $Gata3^{+/-}$ mice at this stage.

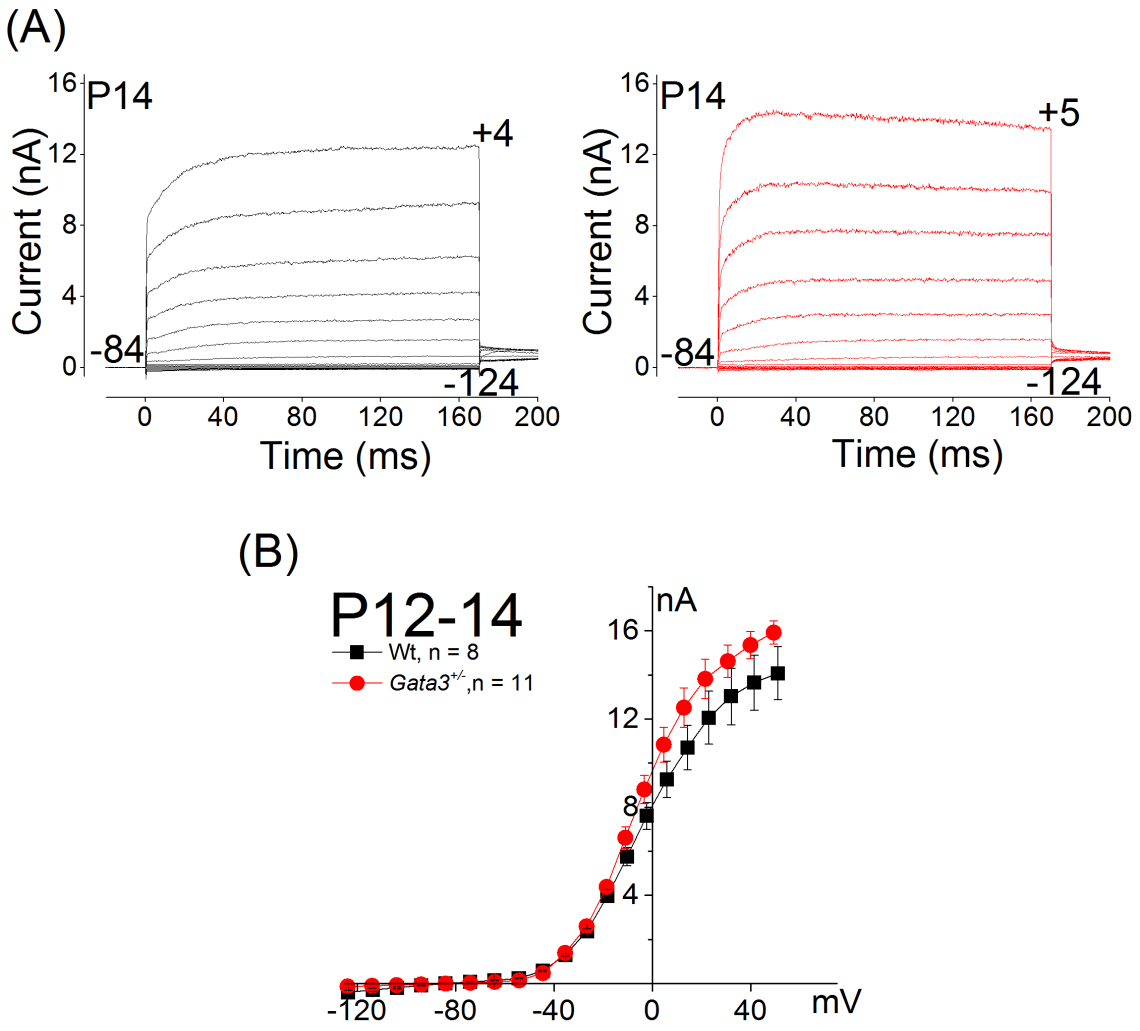

Figure 4-2: Outward K^+ currents in IHCs from newly hearing (P12 - P14) mice
(A) Example of the current responses of an IHC from wild type (black) and $Gata3^{+/-}$ (red) P14 mouse.
(B) Average steady-state current-voltage (I-V) relationship curves for wild type (n = 8) and $Gata3^{+/-}$ (n = 11) IHCs from P12 - P14 mice. Error bars represent ± S.E.M values.
No significant difference was observed in the amplitude of the K^+ currents of IHCs in response to voltage steps, from control and $Gata3^{+/-}$ mice.

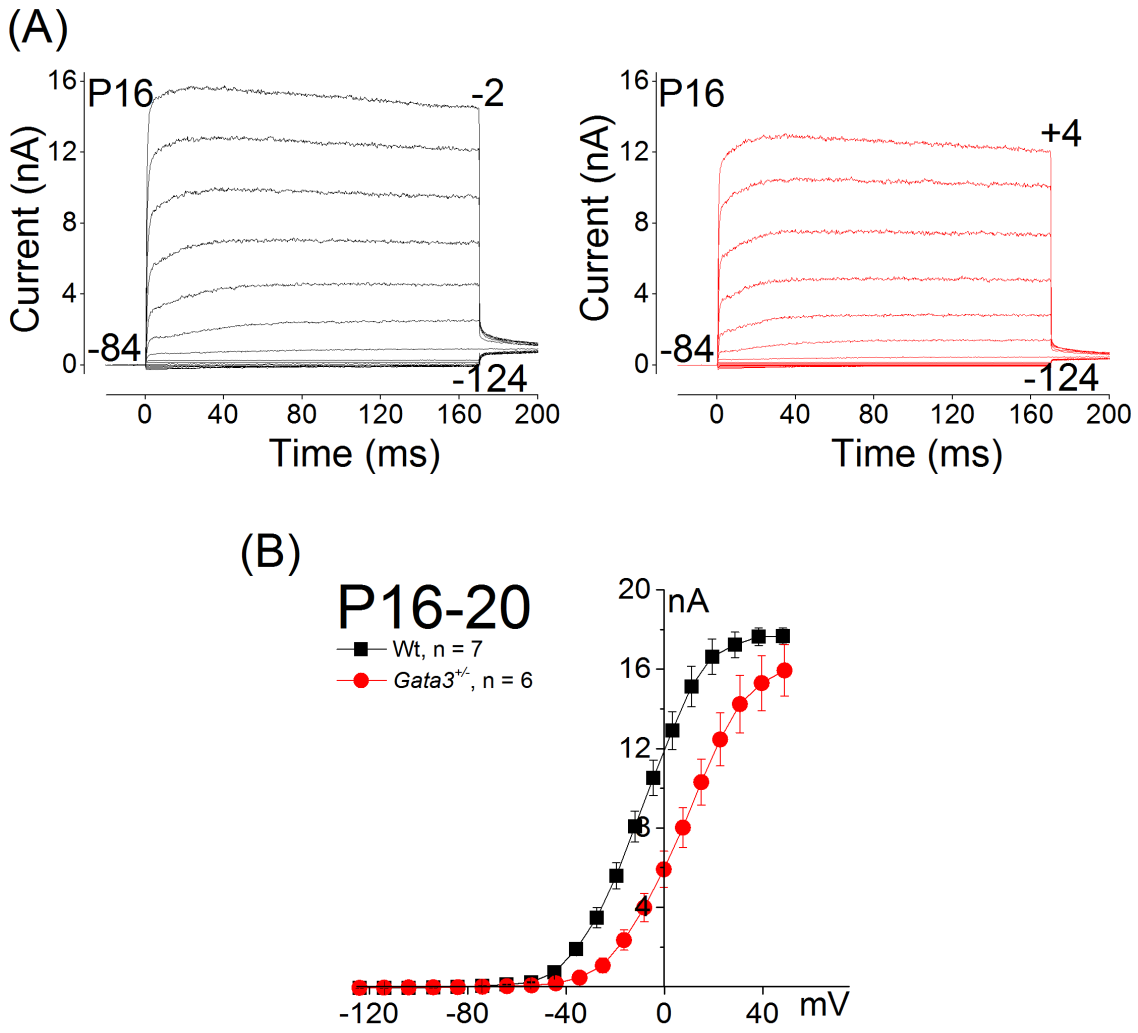

Figure 4-3: Outward K^+ currents in IHCs from newly hearing (P16 - P20) mice
(A) Example of the current responses of an IHC from wild type (black) and $Gata3^{+/-}$ (red) P16 mouse.
(B) Average steady-state current-voltage (I-V) relationship curves for wild type (n = 7) and $Gata3^{+/-}$ (n = 6) IHCs from P16 - P20 mice. Error bars represent ± S.E.M values. Note that the plateau effect of the curve from the control group is due to the operational range of the Axopatch 200B amplifier (18 nA).
Total steady state currents were reduced in IHCs from $Gata3^{+/-}$ mice compared to their age-matched controls (Student's t-test, p <0.05).

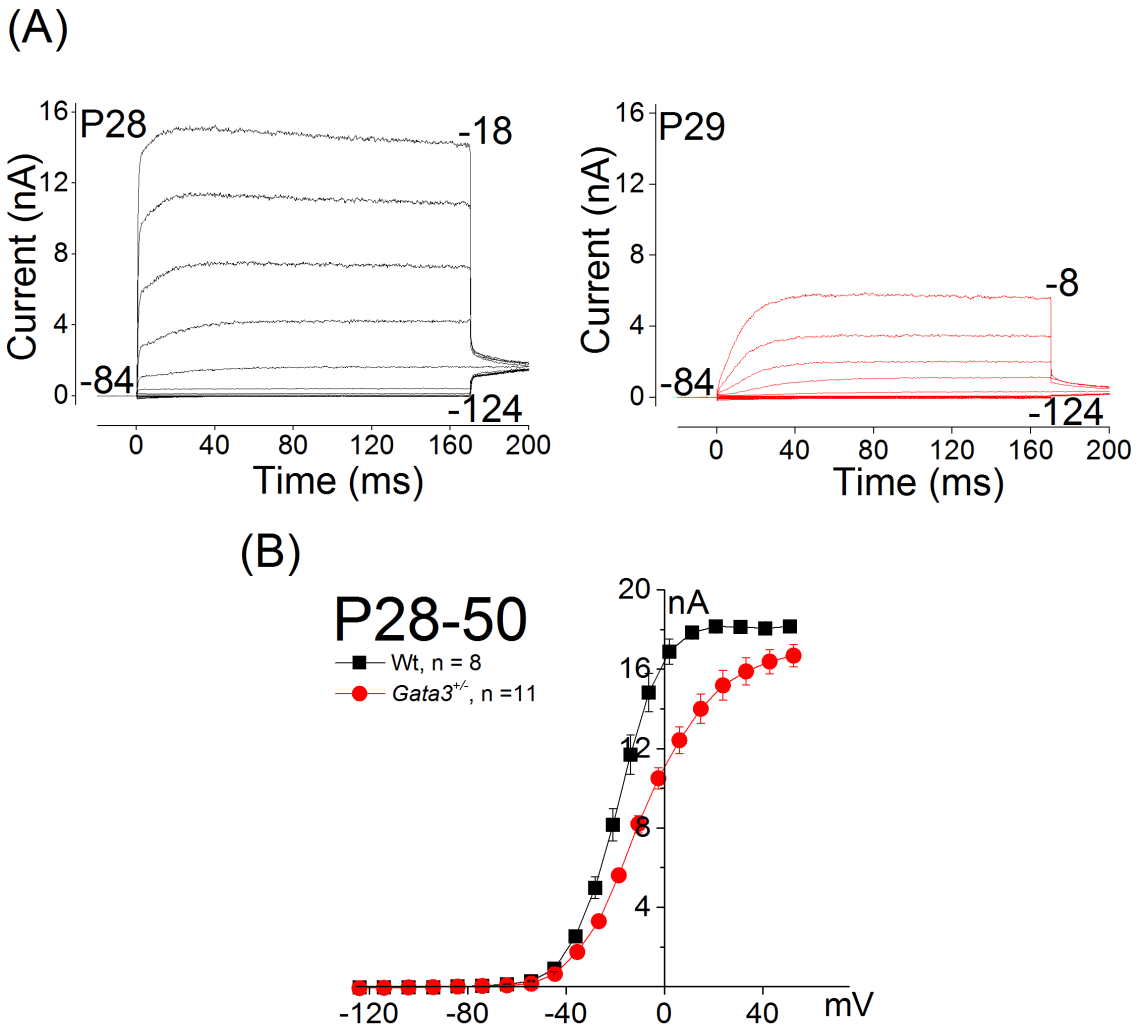

Figure 4-4: Outward K^+ currents in IHCs from adult (P28 - P50) mice
(A) Example of the current responses of an IHC from wild type (black) and $Gata3^{+/-}$ (red) P28 mouse.
(B) Average steady-state I-V relationship curves for wild type (n = 8) and $Gata3^{+/-}$ (n = 11) IHCs from P28 - P50 mice. Error bars represent ± S.E.M values. Note that the plateau effect of the curve from the control group is due to the operational range of the Axopatch 200B amplifier (18 nA).
Total steady state currents were reduced in IHCs from $Gata3^{+/-}$ mice compared to their age-matched controls (Student's t-test, p <0.05).

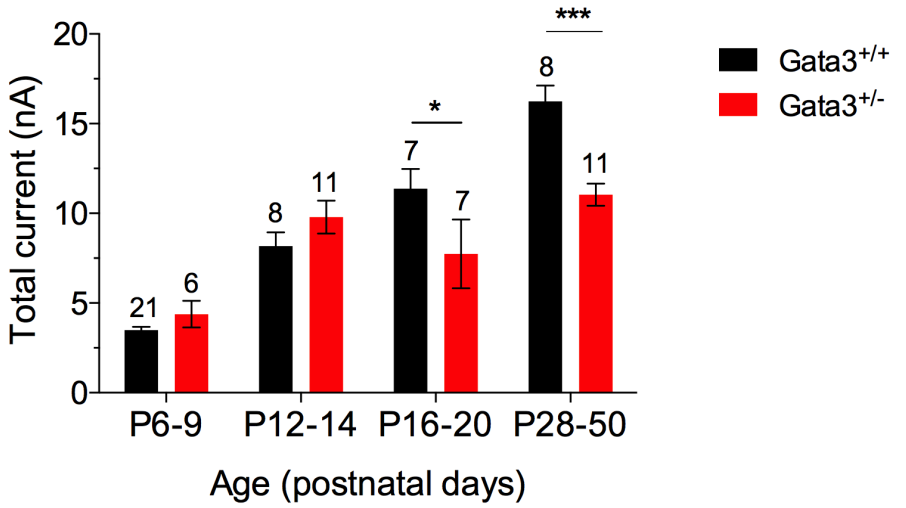

Figure 4-5: Outward K^+ currents in $Gata3^{+/-}$ mouse IHCs are reduced during postnatal development
Bar graph showing average steady-state currents at 0 mV of wild type (black) and $Gata3^{+/-}$ (red) IHCs at different postnatal ages. Note the increase in total current in wild type IHCs as a function of age, while $Gata3^{+/-}$ IHCs from P16 onwards show a significant reduction in total outward current compared to their wild type counterparts (Two-way ANOVA followed by Bonferroni's post-hoc test, p <0.05). N numbers are written above individual columns, and error bars are ± S.E.M values. * indicates p<0.05 and *** indicates $p \leq 0.001$

4.2.2 Fast activating $I_{k,f}$ conductance is drastically reduced in $Gata3^{+/-}$ IHCs

During development, the increase in total membrane current in IHCs from the second postnatal week is chiefly due to the increase in $I_{k,f}$, the large conductance Ca^{2+}-activated K^+ current [Kros et al., 1998]. It begins to appear in the apical cells by P12 and influences the rapid functional maturation of IHCs [Kros et al., 1998]. To examine the basis of the total K^+ current size reduction in $Gata3^{+/-}$ IHCs, we looked at the development of the $I_{k,f}$ conductance.

In control IHCs, $I_{k,f}$ was first recorded from P12, and its size increased as a function of age. To isolate the $I_{k,f}$ conductance, we measured its amplitude at 1.5 ms from the start of the voltage step at the membrane potential of -25 mV. At this time-point $I_{k,f}$ had almost reached steady-state, and the slower delayed

rectifier component of the total current was beginning to activate. I-V curves were constructed for each recording and the size of the current was measured from non-leak subtracted traces. We found the $I_{k,f}$ amplitude in *Gata3*$^{+/-}$ IHCs to be significantly reduced from P28 onwards (two-way ANOVA followed by Bonferroni's post-test, $p < 0.05$; Table 4.2; Figure 4-6B).

TABLE 4.2: *$I_{k,f}$ conductance amplitude in IHCs*

Age	Wild type (nA)	S.E.M	N	*Gata3*$^{+/-}$ (nA)	S.E.M	N
P12 - 14	0.9238	0.2076	8	0.8891	0.1555	11
P16 - 20	1.5956	0.3032	9	0.7	0.2211	7
P28 - 50	4.6538	0.9772	8	1.2282	0.1923	11

The difference in the total whole cell current between control and *Gata3*$^{+/-}$ IHCs could be accounted for largely in terms of the reduced $I_{k,f}$. The residual current in *Gata3*$^{+/-}$ IHCs, showing a sigmoidal activation is the delayed rectifier-type current.

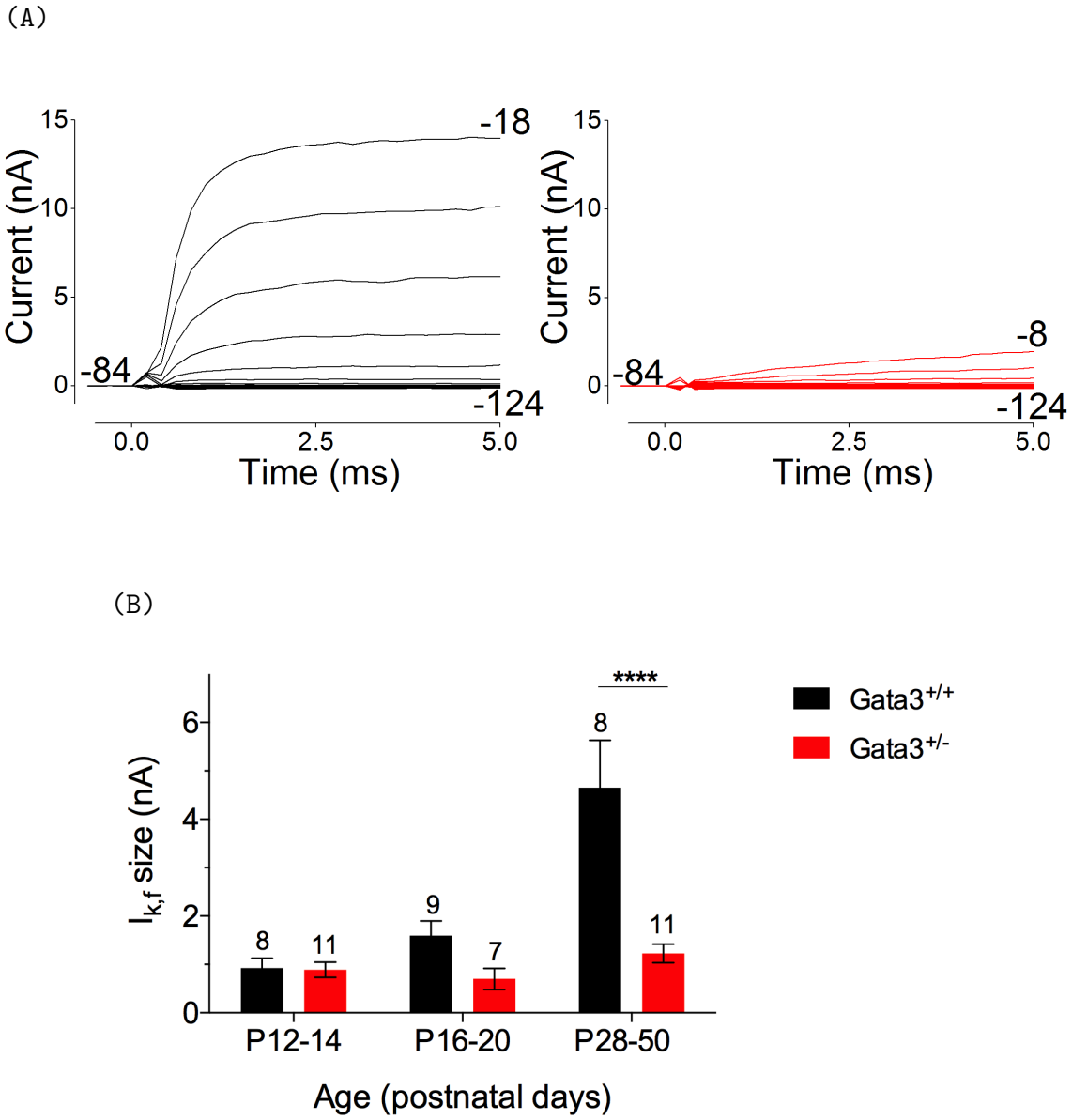

Figure 4-6: Fast-activating outward K^+ current ($I_{k,f}$) is reduced in *Gata3*$^{+/-}$ IHCs
(A) The first 5 ms of the P28 voltage clamped control (black) and *Gata3*$^{+/-}$ (red) IHC from Figure 4-4, showing the amplitude of the $I_{k,f}$ conductances. $I_{k,f}$ is severely diminished in *Gata3*$^{+/-}$ IHCs compared to their wild type littermates.
(B) Developmental profile of average peak $I_{k,f}$ amplitudes from control (black) and *Gata3*$^{+/-}$ (red) IHCs, measured at 1.5 ms from the start of the voltage step. Note the increase of $I_{k,f}$ size in control IHCs as a function of postnatal development, while its size in *Gata3*$^{+/-}$ IHCs remains almost consistent amongst all three age groups examined. $I_{k,f}$ size is observed to be smaller in *Gata3*$^{+/-}$ IHCs from P16, and this reaches significance from P28 onwards ($p < 0.05$, two-way ANOVA followed by Bonferroni's post-hoc test). N numbers are written above individual columns, and error bars are ± S.E.M values. **** indicates $p \leq 0.0001$.

4.2.3 BK channel is expressed in *Gata3*$^{+/-}$ IHCs

We checked for the expression of BK channels that underlie the $I_{k,f}$ conductance, to understand if its lack of expression could explain the large reduction of this current. At P30, the pore-forming α-subunit of the BK channel was localized to the supranuclear region in IHCs in the apical coil of the organ of Corti and to the basal region of OHCs. There were no differences in the expression pattern of the channel between wild type control and *Gata3*$^{+/-}$ IHCs (Figure 4-7)

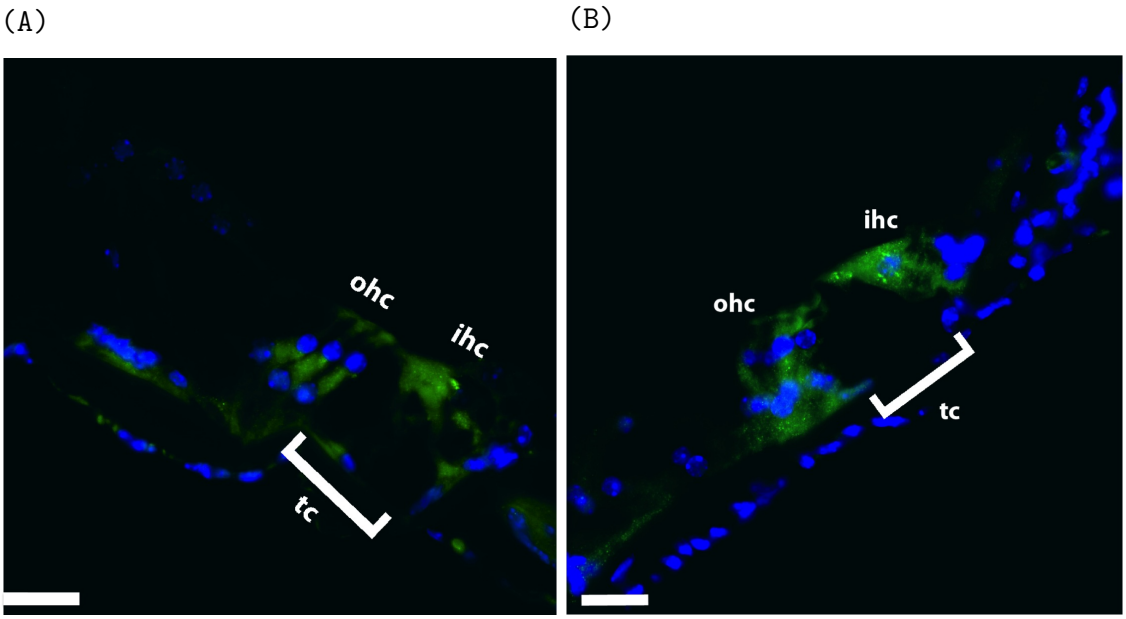

Figure 4-7: BK channel expression in *Gata3*$^{+/-}$ IHCs
(A) In cryosections of the apical coil from wild type P30 animals, BK channel expression (green) is observed in the basal region of OHCs. In IHCs, BK localises in a punctate fashion in the region above the nucleus. Nuclei have been labelled in blue by DAPI. HCs were identified by their morphology and position on either side of the Tunnel of Corti (tc).
(B) The BK expression pattern in *Gata3*$^{+/-}$ IHCs is comparable to age-matched wild type controls. Scale bar is 16 μm.

4.2.4 $I_{k,n}$ conductance is reduced in *Gata3*$^{+/-}$ IHCs

Along with the onset of the $I_{k,f}$ and increase in the amplitude of the delayed rectifier, $I_{k,n}$ conductance contributes to the functional maturation of IHCs. It is expressed from around P12, is active at rest, and sets the resting membrane

potential of the IHC [Marcotti et al., 2003; Oliver et al., 2003].

Since we observed a decrease in total membrane currents in *Gata3*$^{+/-}$ IHCs as a result of the impaired development of $I_{k,f}$, we wanted to determine if the $I_{k,n}$ conductance, another signature of functional IHCs, develops normally.

$I_{k,n}$ was elicited as described before by depolarizing voltage steps of 170 ms duration from -154 mV to -34 mV, in 10 mV increments, from the holding potential of -64 mV (Figure 3-8A). Steady- state currents were calculated as the mean current over 20 ms towards the end of each voltage step, and the peak currents were measured individually. $I_{k,n}$ size was quantified as the difference between the instantaneous and steady-state deactivating currents at a fixed potential of -125 mV (arrows in Figure 4-8A). I-V plots of the peak and steady currents have been shown in Figure 4-8B - C.

TABLE 4.3: *$I_{k,n}$ conductance in IHCs*

Age	Wild type (pA)	S.E.M	N	*Gata3*$^{+/-}$ (pA)	S.E.M	N
P28 - 30	-237.8	15.96	5	-160.0	28.6	5
P49 - 50	-218.75	19.35	4	-123.0	13.12	4

Table 4.3 shows the size of $I_{k,n}$ in IHCs at one month and two months of age, in *Gata3*$^{+/-}$ and age-matched wild type mouse IHCs. While the size of $I_{k,n}$ in wild type mice is comparable to previous reports [Marcotti et al., 2003], at each age examined $I_{k,n}$ was smaller in *Gata3*$^{+/-}$ IHCs (two-way ANOVA and Bonferroni's post-hoc test, $p < 0.05$; Figure 4-9). There does not appear to be a progressive decline in the size of this current with age.

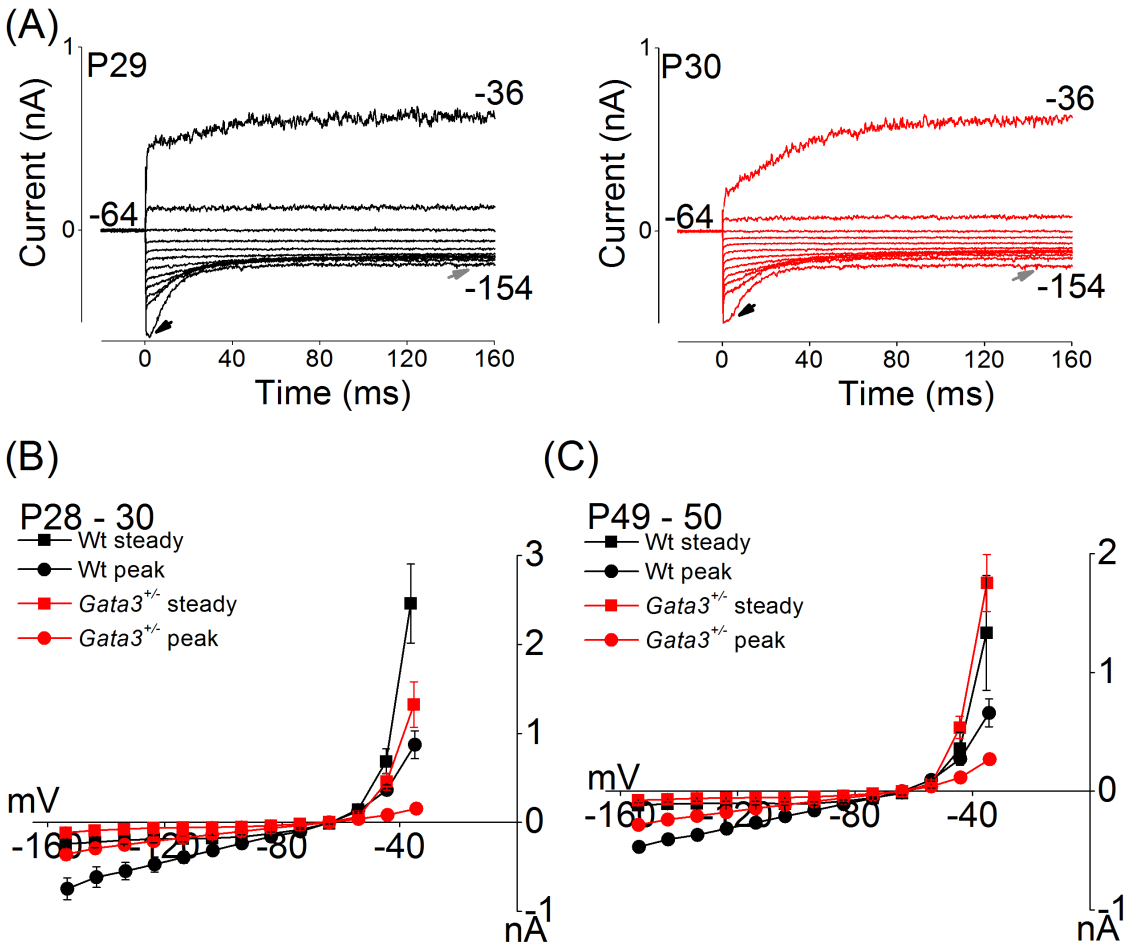

Figure 4-8: Negatively-activating inward K^+ current ($I_{k,n}$) is reduced in *Gata3*$^{+/-}$ IHCs

(A) Example of $I_{k,n}$ recorded from a wild type (black) and *Gata3*$^{+/-}$ (red) IHCs. The $I_{k,n}$ amplitude was quantified in isolation as the difference between the instantaneous (black arrow) and deactivating steady-state (grey arrow) inward currents at a fixed potential of -125 mV.

(B) Averaged steady-state (measured towards the end of the voltage step, square symbol) and peak (circle symbol) inward currents from control (n = 5) and *Gata3*$^{+/-}$ (n = 5) IHCs at one month of age (between P28 - P30).

(C) Averaged steady-state (square symbol) and peak (circle symbol) inward currents from control (n = 4) and *Gata3*$^{+/-}$ (n = 4) IHCs between P49 - P50.

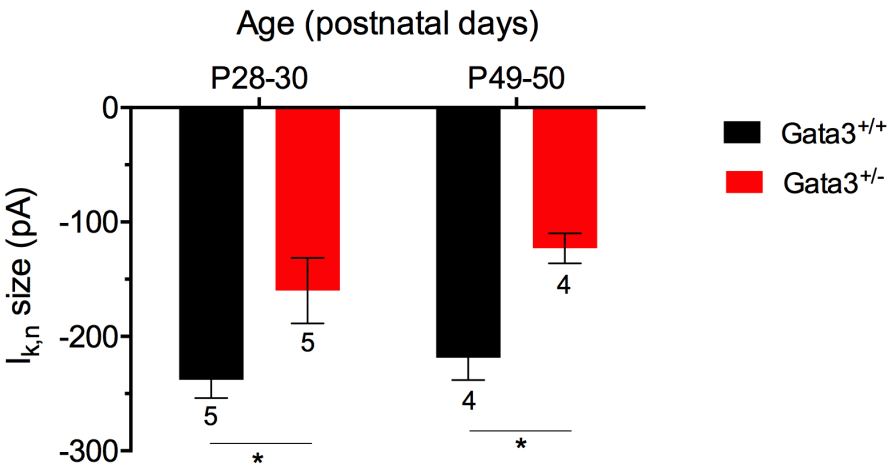

Figure 4-9: Bar graph showing the effect of genotype and age on the amplitude of $I_{k,n}$.
$I_{k,n}$ is reduced in *Gata3*$^{+/-}$ (red bars) IHCs at each time-point investigated, however age does not seem to have an effect on the reduction ($p < 0.05$, two-way ANOVA and Bonferroni's post-hoc test). * indicates $p<0.05$.

4.2.5 Voltage responses of *Gata3*$^{+/-}$ IHCs are altered

Voltage responses of apical IHCs were studied under current clamp conditions to evaluate the functional consequence of the diminished $I_{k,f}$ and $I_{k,n}$ conductances in *Gata3*$^{+/-}$ animals.

Cells were stimulated from their resting potential with current injections that ranged from -100 pA to +900 pA in 100 pA increments for a duration of 250 ms (Figure 3-10A). The resting membrane potential of IHCs was measured by averaging the voltage of the cell before current injection. We found no differences in the resting membrane potential between *Gata3*$^{+/-}$ animals and controls at each age investigated (Table 4.4; Figure 4-11; Two-way ANOVA, $p < 0.05$).

Regenerative spiking behaviour was not observed in response to current injections in *Gata3*$^{+/-}$ animals, consistent with responses from wild type cells of this age [Kros et al., 1998]. In the case of the wild type, with the largest current injections (+900 pA), IHCs responded with an initial fast voltage transient which then

declined to a steady state level (black trace in Figure 4-10). In contrast, *Gata3*$^{+/-}$ IHCs responded with larger voltage responses (red trace in Figure 4-10), with a clear slower relaxation (grey arrows) consistent with the absence of $I_{k,f}$, the role of which is to reduce the repolarization time constant in mature IHCs [Kros et al., 1998], a function that serves to improve their frequency response.

In response to hyperpolarizing current injections (-100 pA), *Gata3*$^{+/-}$ IHCs responded with a large passive response, being unable to curb the change in the membrane voltage. This was in contrast to the wild type (black arrows in Figure 4-10).

To quantify the altered voltage response of IHCs, the peak of the membrane potential was manually calculated for each current injection, and the steady state voltage response was quantified as the mean voltage over the last 25 ms of each current injection. While the steady state voltages are comparable between the two groups studied, their peak responses are much larger, being almost double that of the responses of their wild type counterparts (compare Figure 4-10C to B).

TABLE 4.4: *Resting membrane potential of IHCs*

Age	Wild type (mV)	S.E.M	N	*Gata3*$^{+/-}$ (mV)	S.E.M	N
P28 - 30	-74.95	1.66	5	-75.58	1.04	3
P49 - 50	-74.71	0.47	4	-74.09	1.42	5

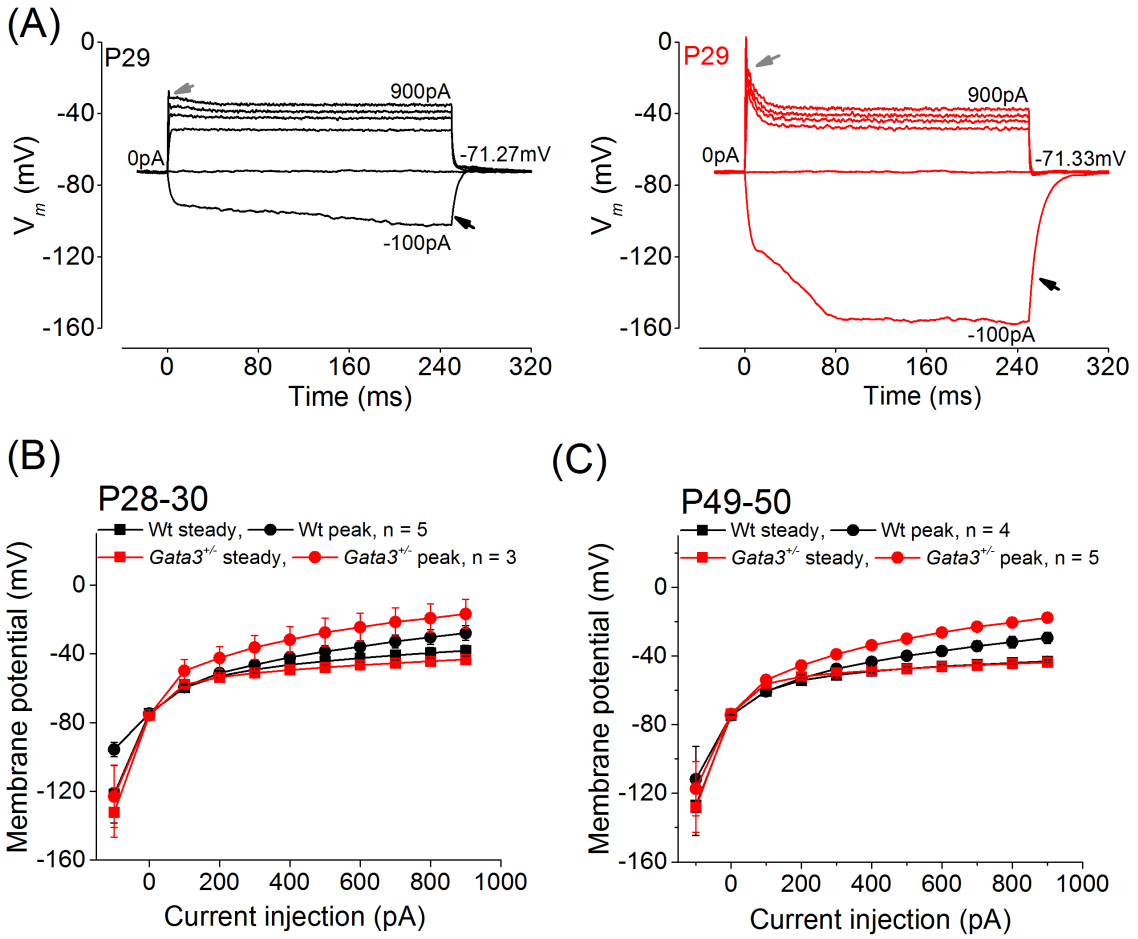

Figure 4-10: Voltage responses of *Gata3*$^{+/-}$ IHCs are altered
(A) Voltage response of an IHC from a P29 control (black) and *Gata3*$^{+/-}$ (red) mouse. In the recording from *Gata3*$^{+/-}$ IHC, note the larger amplitude of voltage responses and delayed repolarization phase (grey arrow) in response to depolarising current injections, and also the larger voltage fluctuation (black arrow) in response to negative current injection.
(B) Average peak and steady-state voltage responses measured from one month old (P28 - 30) wild type (n = 5) and *Gata3*$^{+/-}$ (n = 3) mice. Steady-state values plotted are the mean voltages over the last 25 ms of the current injection, while peak currents were individually measured.
(C) Average peak and steady-state voltage responses measured from P48 - 50 wild type (n = 4) and *Gata3*$^{+/-}$ (n = 5). Error bars represent ± S.E.M. Note the larger voltage change for *Gata3*$^{+/-}$ IHCs in response to current injections at all levels

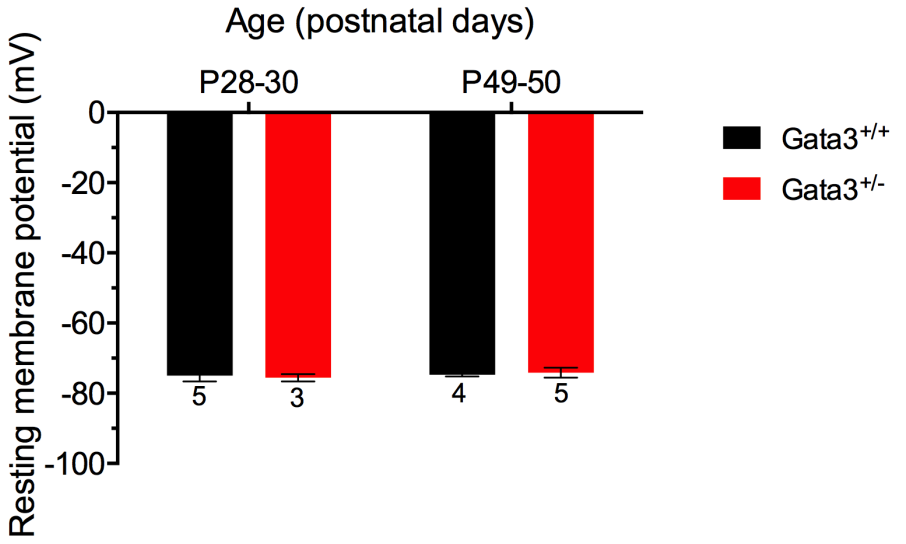

Figure 4-11: Resting membrane potentials of *Gata3*$^{+/-}$ IHCs are comparable to wild type
Comparison between resting membrane potential of wild type and *Gata3*$^{+/-}$ IHCs at two time-points. No differences were observed in the resting membrane potential between the two groups at each time-point investigated (Two-way ANOVA, p <0.05)

4.2.6 The ACh-activated current is normal in immature *Gata3*$^{+/-}$ IHCs

Immature IHCs in mice express a transient ACh-sensitive current from very soon after birth until about P16 [Glowatzki and Fuchs, 2000; Marcotti et al., 2004b], while efferents make axo-somatic connections with IHCs, coinciding with the expression of Ca^{2+}-dependent small conductance SK2 channels [Marcotti et al., 2004b]. The ACh-sensitive current itself has two components: an inward component carried by Ca^{2+} and Na^{+} via $\alpha9\alpha10$nAChRs and L-type Ca^{2+} channels, and an outward current carried via K^{+} mediated via SK2 channels (SK current) located within close proximity of $\alpha9\alpha10$nAChRs [Marcotti et al., 2004b]. Since the SK current is believed to contribute towards the normal development of IHCs, we studied their responses in *Gata3*$^{+/-}$ mice to ACh.

Basolateral membrane currents were recorded from P9 IHCs before, during and after the superfusion of 100 μM ACh in the presence of 1.3 mM Ca^{2+}, in response

to voltage steps in 10 mV increments (of 170 ms pulse duration) from a potential of -143 mV. The cells were referred to a holding potential of -84 mV. The ACh -sensitive current was calculated by subtracting the control current (before ACh superfusion) from the current in the presence of 100 μM ACh. The steady state current was measured at 160 ms from the start of the voltage step before and during ACh perfusion. The ACh-sensitive current was calculated as the steady-state slope conductance at around the holding potential of -84 mV.

The ACh-sensitive current was found to be comparable between both groups tested (table 4.5; Student's t-test, p <0.05) indicating that *Gata3*$^{+/-}$ IHCs respond to the influx of Ca^{2+} via functional $\alpha9\alpha10$nAChRs and $Ca_v1.3$ channels, and express a hyperpolarising SK current in response.

TABLE 4.5: *Steady-state slope conductance of the ACh-activated current in IHCs*

Genotype	Slope conductance (nS)	S.E.M	N
Wt	11.25	1.09	5
Gata3$^{+/-}$	10.55	2.51	6

Figures 4-12 and 4-13 show typical examples of current traces of IHCs before, during and after the application of 100 μM ACh from wild type and *Gata3*$^{+/-}$ mice, respectively, and also show their corresponding steady-state I-V curves.

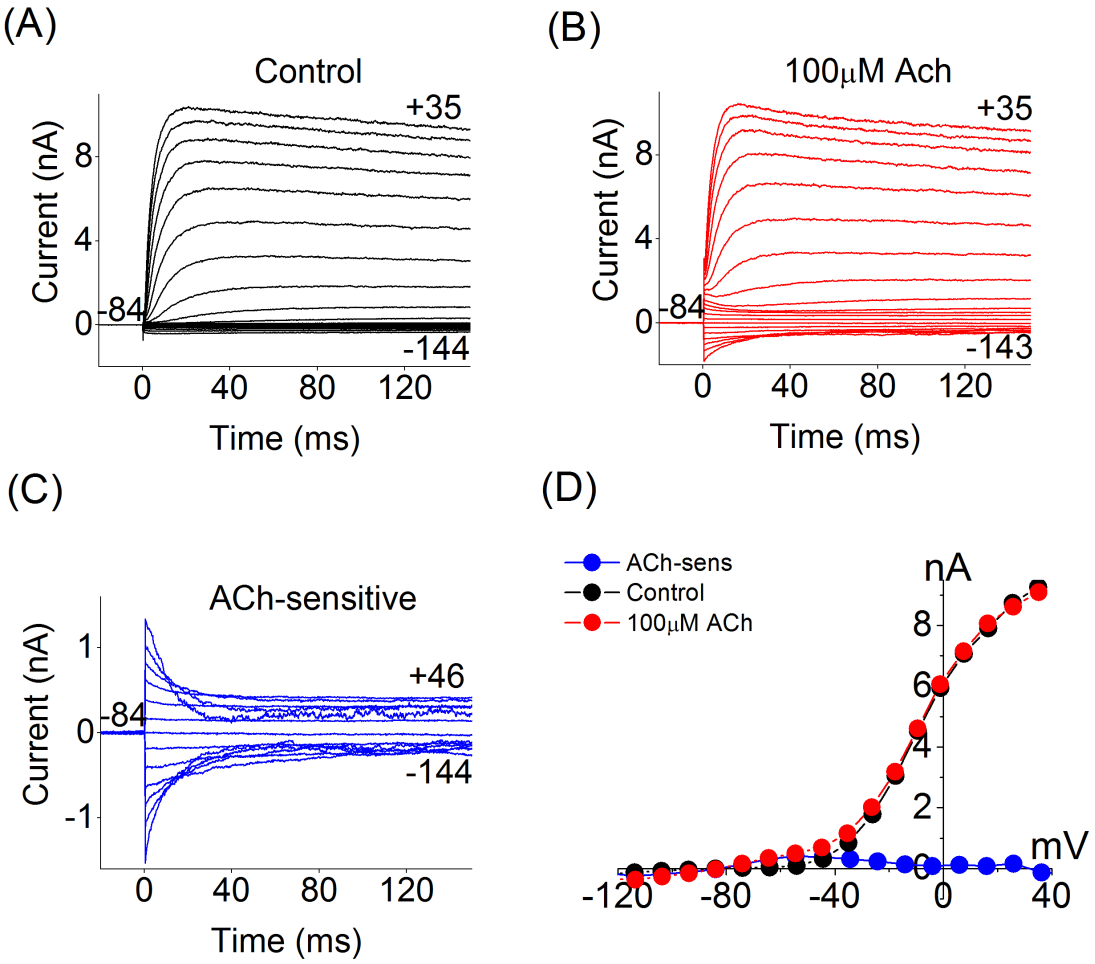

Figure 4-12: ACh-activated current in immature wild type IHCs
(A)Membrane currents recorded from a control apical P9 IHC before,
(B) and during the perfusion of 100 μM ACh, in response to depolarising voltage steps of 170 ms duration from -154 mV, from a holding potential of -84 mV, in nominal increments of 10 mV.
(C) ACh-activated current is obtained by subtracting the control current (A) from the current in the presence of 100 μM ACh (B).
(D) I-V curves of the currents recorded before and during the perfusion of 100 μM ACh, and also the ACh-activated current of the traces shown for the wild type IHC.

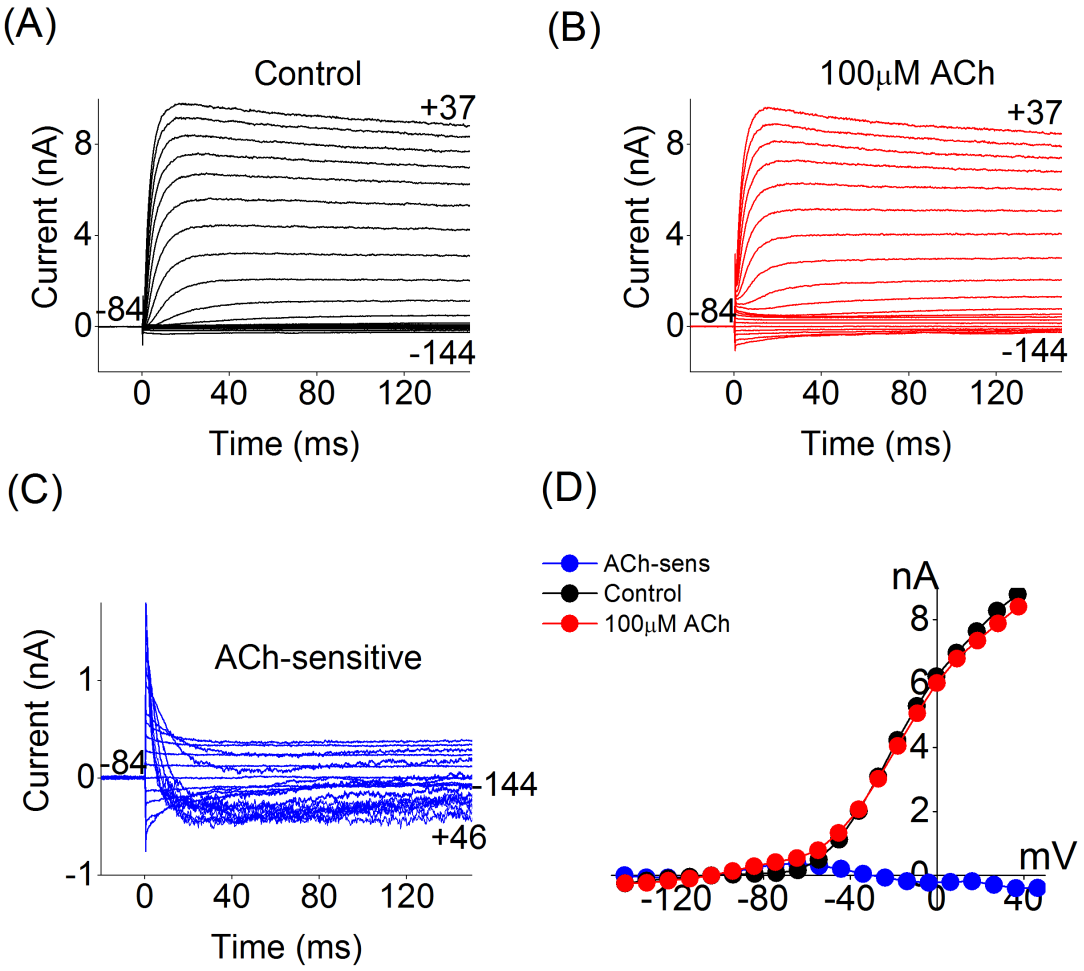

Figure 4-13: ACh-activated current in immature *Gata3*$^{+/-}$ IHCs
(A)Membrane currents recorded from a *Gata3*$^{+/-}$ apical P9 IHC before,
(B) and during the perfusion of 100 μM ACh, in response to depolarising voltage steps of 170 ms duration from -154 mV, from a holding potential of -84 mV, in nominal increments of 10 mV.
(C) ACh-activated current is obtained by subtracting the control current (A) from the current in the presence of 100 μM ACh (B).
(D) I-V curves of the currents recorded before and during the perfusion of 100 μM ACh, and also the ACh-activated current of the traces shown for the *Gata3*$^{+/-}$ IHC.

4.3 Discussion

Our results suggest that IHCs in *Gata3*$^{+/-}$ mice are functionally defective. This is surprising as OHCs in these mice have been purported to underlie the HL observed (van der Wees et al., 2004; van Looij et al., 2005); and there is no evidence to suggest that IHCs may be affected. Additionally, HCs started to differentiate within the sensory epithelium much earlier, so any deregulation in HC function three weeks later, could point towards a specific requirement for *Gata3* in postnatal HCs.

Gata3$^{+/-}$ IHCs differentiate normally up to the onset of hearing at P12-14. Thereafter, at each time-point examined, there was a clear reduction in the total current size in *Gata3*$^{+/-}$ IHCs. The total whole cell K^+ currents at this stage (P16 onwards) would be expected to be a mixture of $I_{k,f}$, $I_{k,n}$ and the delayed-rectifier type K^+ current. $I_{k,f}$ is activated at depolarized potentials and mediates the fast time constant of the receptor potential in response to stimulus onset. This conductance increases in magnitude until around P20 [Kros et al., 1998]. $I_{k,n}$ is an inward current, much smaller in size, is active at rest and at more hyperpolarized potentials, and contributes towards establishing the resting membrane potential of the cell [Oliver et al., 2003]. The delayed rectifier type K^+ current has a much slower time constant and thus activates much later than $I_{k,f}$, also at depolarised potentials. The increase of this conductance with development follows a slower time course than $I_{k,f}$ [Kros et al., 1998].

$I_{k,f}$ in IHCs is essential for the sharp time course of the onset of the receptor potential, due to its fast activation kinetics. The receptor potential drives neurotransmitter release onto afferent neurons causing them to spike and propagate this signal along the auditory chain. The consequence of an impaired $I_{k,f}$ is evident in the voltage responses of the cell. Our results show that both the time course of

onset and the amplitude of voltage responses are altered, suggesting that receptor potentials *in vivo* could be affected.

Firstly, the increased amplitude of voltage responses are consistent with a strong reduction of $I_{k,f}$. At depolarized potentials rapid activation of $I_{k,f}$ serves to clamp down the voltage excursion, thereby restricting the receptor potential. Even with a depolarizing stimulus of 1 nA, the voltage fluctuation is no more than 10 mV in wild type animals [Oliver et al., 2006]. In the case of the affected IHCs, due to a strong reduction of $I_{k,f}$, the cell is unable to attenuate the receptor potential at more depolarized conditions, thereby resulting in larger amplitudes.

Secondly, the reduction of $I_{k,f}$ results in a delay of onset of voltage responses. Unlike in lower vertebrates where BK channels and their associated Ca^{2+} channels underlie the intrinsic frequency tuning of HCs [Fettiplace and Fuchs, 1999], in the mammalian system BK channels have been linked to the remarkable temporal precision of the ear [Oliver et al., 2006; Kurt et al., 2012]. Its rapid activation kinetics [Kros and Crawford, 1990; Marcotti et al., 2004a] allows them to accomplish this impressive feature. Thus, with the loss of $I_{k,f}$ in the affected IHCs, the onset of the receptor potential in response to stimulus is delayed.

Functionally, these findings could translate to a more sustained depolarization of the HCs *in vivo* leading to increased spike rates in the downstream neurons, a reduction in dynamic range of the HC receptor potential, and deterioration in signal/noise ratio, as observed previously in HC-specific BK channel deletion [Kurt et al., 2012]. Diminished signal/noise ratio levels observed in *Gata3*$^{+/-}$ mice [van Looij et al., 2005] corroborate these results. However, it is interesting to note that spiral ganglion neurons also express BK channels [Hafidi et al., 2005] in addition to *Gata3* [Appler et al., 2013]. In case of an accompanying reduction of BK channel function in afferent neurons, the temporal accuracy

of spike timing would be expected to be reduced. This would translate into reduced amplitude of cochlear neural responses and prolonged first peak latency as evidenced by wave I of ABR measurements [Oliver et al., 2006; Maison et al., 2013], which have been observed to be normal in these animals [van Looij et al., 2005] arguing against a concomitant reduction of BK channel function in afferent neurons.

Genetically knocking out the pore-forming α-subunit of the BK channel does not alter cochlear thresholds for up to eight weeks [Rüttiger et al., 2004; Pyott et al., 2007]. However, in one study, loss-of-function of BK resulted in age-related, progressive high frequency hearing loss, and was attributed to the loss of KCNQ4 channels from the OHCs [Rüttiger et al., 2004]. However, normal cochlear thresholds were recorded at least until 12 weeks [Pyott et al., 2007], the maximum age tested. The contrast between the two studies could be attributed to the use of 129/SvJ background in the first study with a predisposition to age related hearing loss [Johnson et al., 1997] as opposed to the FVB/NJ background used in the other study (also used in our study), considered to be a good hearing strain.

The above result implicates the involvement of *Gata3* in either the development and/or function of BK channels. However, the mechanism by which *Gata3* could potentially influence the function of BK channels in HCs is uncertain. $I_{k,f}$ in apical IHCs depends predominantly upon the release of Ca^{2+} from intracellular stores [Marcotti et al., 2004a]. As BK channel expression in *Gata3*$^{+/-}$ IHCs is no different to that in control cells [Hafidi et al., 2005; Rüttiger et al., 2004] , it might be plausible that *Gata3* regulates the availability of intracellular Ca^{2+} or regulates some component involved in the release of Ca^{2+} from cytosolic stores.

The expression of BK channels and *Gata3* [Lilleväli et al., 2004] also overlap in the stria vascularis [Shen et al., 2004]. The stria vascularis is the source of the EP and is involved in K^+ recycling, thereby maintaining optimal ionic homeostasis of

the system. A potential influence of *Gata3* on BK channel function in the stria vascularis could reduce the EP, effectively reducing the transduction current into the cell. This would in turn reduce the spontaneous rates of the afferent nerves. However, it is possible that *Gata2*, also present in the stria vascularis, could compensate for the loss of *Gata3* [Lilleväli et al., 2004]. It is also plausible that haploinsufficiency may not be a problem in all cells, as protein expression levels differ between cells.

Hyperpolarizing current injections (-100 pA) to *Gata3*$^{+/-}$ IHCs give rise to a large passive response. This is due to the reduction of $I_{k,n}$, known to have a negative activation range (Marcotti et al., 2003). The smaller $I_{k,n}$ is unable to clamp the changing potential, thereby causing a large membrane voltage excursion.

As expected from earlier studies cells [Marcotti et al., 2003; Oliver et al., 2003; Marcotti et al., 2004a], even a large reduction of the $I_{k,f}$ would not impact the resting membrane potential of *Gata3*$^{+/-}$ IHCs. Although $I_{k,f}$ is 50% active at the resting potential of IHCs [Marcotti et al., 2004a], it does not contribute to the resting membrane potential, which is set by $I_{k,n}$ [Oliver et al., 2003]. A complete block of $I_{k,n}$, brought about by linopirdine, shifts the membrane potential by 7 mV [Oliver et al., 2003] towards positive values. It is conceivable that a reduction of $I_{k,n}$ size observed in our studies is not large enough to change the resting membrane potential.

KCNQ4 has been implicated in autosomal dominant non-syndromic hearing loss (DFNA2) [Kubisch et al., 1999], where the complete loss of $I_{k,n}$ gradually leads to a chronic overload of K^+ in the HCs, progressively leading to their degeneration [Kubisch et al., 1999]. This would in turn lead to a persistent depolarisation of the cell. It has also been suggested that *in vivo*, in the presence of the resting transducer current, the absence of $I_{k,f}$ would cause HCs to be more depolarized

[Oliver et al., 2006]. The reduction of $I_{k,f}$ and $I_{k,n}$ in inner HCs of *Gata3*$^{+/-}$ animals could act synergistically to cause sustained depolarization of IHCs *in vivo*, causing prolonged neurotransmitter release.

Furthermore, a reduced $I_{k,n}$ favours the influx of Ca^{2+} influx via $Ca_v1.3$ channels [Oliver et al., 2003]. Continued Ca^{2+} influx, without an efficient exit route for K^+ could induce apoptosis of the HC. Increased presynaptic activity of the IHCs could in turn prolong glutamate release onto afferent neurons, which could lead to excitotoxicity. Auditory nerve fibres have been found to be missing in *Gata3*$^{+/-}$ animals [van der Wees et al., 2004].

Normal responses to ACh by *Gata3*$^{+/-}$ IHCs rules out the involvement of $\alpha 9\alpha 10$nAChRs and SK2 channels in the reported phenotype. Although this is not informative regarding the presence and normal function of efferent neurons, it has been reported that the normal complement of SK2 channels in HCs is essential for the establishment and maintenance of efferent fibres [Kong et al., 2008]. Transient cholinergic activity of efferent neurons is responsible for fine-tuning the tonotopic properties IHCs during the first postnatal week [Johnson et al., 2011b], and during the second postnatal week it drives the maturation of the synaptic machinery of the cells [Johnson et al., 2013].

Overall, Gata3 appears to influence in the normal physiology of IHCs. Complete maturation of the normal current profile mediated via BK and KCNQ4 appears to be stalled due to a partial reduction of GATA3 in the system. It is not clear from these results whether this influence is direct or indirect and *Gata3* has not previously been linked to either KCNQ4 or BK. Considering that *Gata3* regulates various processes in mammalian systems and is thus capable of interacting with a wide variety of signaling molecules, an indirect role in mediating ion channel function is more likely.

These results show the surprising conclusion that IHCs, rather than OHCs, contribute to HL. However, it is not clear if this is a cell autonomous effect of *Gata3* haploinsufficiency. Given the apparent down regulation of *Gata3* in IHCs it would seem to be non-cell autonomous. A good way to test this would be to knock *Gata3* out of IHCs.

Chapter 5

Gata3 is essential for the complete functional maturation of inner hair cells

5.1 Introduction

Chapters 3 and 4 probe the differential effects of a systemic GATA3 dose reduction on the two HC populations, and provide the first evidence for a role of *Gata3* in the normal physiological function of HCs, which could partially explain the HL observed in HDR patients. Questions unanswered by this approach remain: does *Gata3* exert its influence on HC function in a cell-autonomous or non-autonomous way (i.e., via its presence in HCs itself, or indirectly via its expression in supporting cells)? Conflicting reports regarding the sustained expression of *Gata3* in HCs [Rivolta and Holley, 1998; van der Wees et al., 2004; Luo et al., 2013] implores the distinction of whether the observed anomalies arising due to GATA3 dose shortage is due to a developmental or maintenance defect.

Investigation into the direct/cell-autonomous role of *Gata3* on potential HC phenotypes necessitates manipulation of GATA3 levels explicitly from target HCs. Genetically downregulating GATA3 levels in HCs after their differentiation (when GATA3 levels have been debated) is informative regarding the developmental versus maintenance function of *Gata3*.

Atoh1 and *Gata3* are the only two transcription factors, in the absence of which, HCs are not produced in the cochlear sensory epithelium. Investigations into the role of *Gata3* using drug-rescued mutants, to circumvent embryonic lethality, have revealed that while limited morphogenesis and sensory development is possible in the vestibular regions, the cochlea remains immature and devoid of any neurosensory development [Haugas et al., 2012]. Critical genes required for normal patterning of the developing cochlea like *Neurod1*, *Fgf10*, *Lmx1a*, *Pax2* and *Sox2* are severely disrupted, as are the peripheral efferent connections [Duncan et al., 2011]. Inactivating *Gata3* during early otocyst development at E8.5 results in a truncated cochlear duct, again devoid of sensory patches and innervation. ATOH1 is completely absent as are SOX2 and TECTA [Duncan and Fritzsch, 2013]. TECTA absence leads to the formation of a cochlear duct without the tectorial membrane. In the same study, use of a $Pax2^{Cre}$ driver line resulted in a slightly delayed suppression of *Gata3* function, resulting in small cochlear HC patches innervated by nerve bundles. These HCs have defective stereociliary bundles, and *Fgf8* expression is perturbed. Fgf8 is a ligand expressed by IHCs to activate radial patterning in the organ of Corti [Jacques et al., 2007]. The reduced size of the cochlear duct, prosensory domain and depletion of spiral ganglion neurons is a result of elevated cell death [Luo et al., 2013]. The studies outlined above attempt to elucidate *Gata3* function by removing it very early during otic development. The resultant multitude effects are a consequence of an early removal of an essential player of otic systemic development. Insight into specific roles of *Gata3* in the different cell types of the cochlea entails its removal from individual cell populations in a controlled temporal fashion.

Although the knock-out strategy has traditionally been employed to study the function of genes, this method alone is not without its limitations. For an important gene like *Gata3*, which is expressed very early on during development in several different compartments of a developing system, a direct knock-out yields pleiotropic

effects. It is difficult to differentiate between direct and indirect, primary and secondary and autonomous and non-cell autonomous effects. Although there are ways to control the spatial and/or temporal patterns of such knock-outs, combining such an approach with more subtle knock-down experiments (such as those provided by *Gata3*$^{+/-}$ animals in the previous chapters) can often yield more meaningful and reliable information.

We have used *Otoferlin* to drive *Cre*-mediated excision of the floxed *Gata3* allele *in vivo* in an IHC-specific manner. *Otoferlin* expression is detected in IHCs from E16 onwards, and this expression persists into adulthood [Roux et al., 2006], making it an essential tool to study the IHC-specific effects of both *Gata3* heterozygosity and deletion. In OHCs however, weak *Otoferlin* expression is first observed at E18, which then peaks at P6 after which its immunoreactivity disappears from OHCs [Roux et al., 2006].

The *Otof*^{Cre} line specifically targets IHCs. Moreover, IHCs could potentially influence the development of OHCs via FGF signalling [Jacques et al., 2007], confounding our observations with the possibility of an indirect effect in OHCs. We therefore, decided to focus upon any potential intrinsic effect *Gata3* might have on IHCs.

To accomplish this, IHCs were investigated at three different stages encompassing pre-hearing, young hearing and older stages (hereafter referred to as 'pre-hearing', 'young' and 'old') for their basolateral membrane properties, as a read-out of their functionality.

5.2 Results

5.2.1 *Otoferlin* mediates recombination of floxed stop codon in *Rosa26R Eyfp* animals

Cochlear cryosections from E17.5 embryos from the *Rosa26R Eyfp* and *Otof*^{Cre} cross were used to confirm the activation of *Cre recombinase*. Immunolabeling for EYFP showed that in knockout animals, HCs specifically expressed EYFP protein, indicating that *Otoferlin* successfully mediated the recombination of the floxed stop codon at least as early as E17.5, within a day of *Otoferlin* expression in IHCs [Roux et al., 2006] Figure 5-1A). Another lab showed that in whole-mount cochlear immunolabeling of P3 animals from the *Rosa26R-tdTomato* and *Otof*^{Cre} cross, *tdTomato* was expressed specifically in most IHCs, while affecting only about 5% of OHCs (Muller, personal communication; Figure 5-1C).

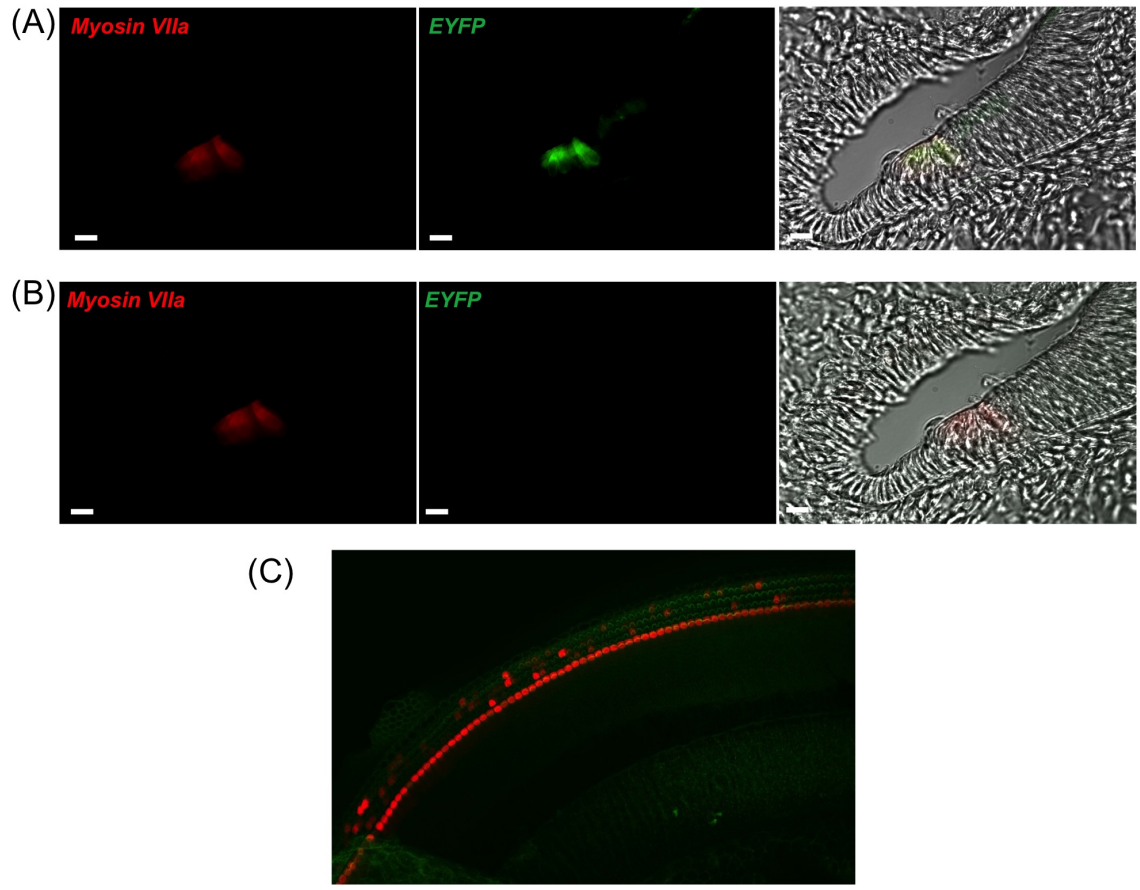

Figure 5-1: *Otoferlin* successfully recombines the floxed stop codon in *Rosa26R Eyfp* animals
(A) Cryosection from E17.5 $Otof^{Cre}$:$Rosa26R\ Eyfp^{flox/flox}$ animal - Myosin VIIa-positive (red) HCs are seen to express *Eyfp* (green) indicating activation of Cre recombinase. The phase contrast image shows the merged red and green channels.
(B) Cryosection from E17.5 $Otof^{Cre}$:$Rosa26R\ Eyfp^{+/+}$ - Myosin VIIa-positive (red) HCs do not express *Eyfp* (green) as they do not carry the floxed stop codon. Phase contrast image shows only the red channel
(C) Whole-mount organ of Corti from P3 $Otof^{Cre}$:$tdTomato^{flox/flox}$ animal showing expression of the fluorescent protein in most IHCs but only in a very small number of OHCs (Muller, personal communication). Hair bundles have been stained with phalloidin.

5.2.2 Inwardly rectifying I_{k1} conductance in immature *Gata3*$^{\Delta/\Delta}$ IHCs is reduced

I_{k1} was elicited from IHCs of prehearing animals by hyperpolarising voltage steps of 170 ms duration from a holding potential of -64 mV, in nominal 10 mV steps (Figure 5-2A). In *Gata3*$^{+/+}$ and *Gata3*$^{+/\Delta}$ cells, the voltage step protocol elicited large inward currents showing a voltage-dependent rectification (black and blue traces in Figure 5-2B), consistent with previous reports [Marcotti et al., 1999]. However, in IHCs from *Gata3*$^{\Delta/\Delta}$ animals, these large currents were not observed (light grey trace in Figure 5-2B). We compared the steady-state current (calculated as the mean current over 20 ms of the voltage step towards the end of the step protocol) at -150 mV between the three genotypes (Table 5.1). In *Gata3*$^{\Delta/\Delta}$ IHCs, inward currents remained, but these were considerably smaller compared to *Gata3*$^{+/+}$ and *Gata3*$^{+/\Delta}$ IHCs (Table 5.1; Figure 5-3; one-way ANOVA followed by Tukey's post test, $p < 0.05$). The reduction of I_{k1} in *Gata3*$^{\Delta/\Delta}$ IHCs can be appreciated from Figure 5-2C, which shows the cumulative I-V curves of the steady-state and peak current values of all the cells recorded from the three genotypes for comparison.

TABLE 5.1: *Steady-state I_{k1} current in pre-hearing mice*

Genotype	Mean (nA)	S.E.M	N
Gata3$^{+/+}$	-568.2	34.05	18
Gata3$^{+/\Delta}$	-590.7	137.8	3
Gata3$^{\Delta/\Delta}$	-108.0	13.8	3

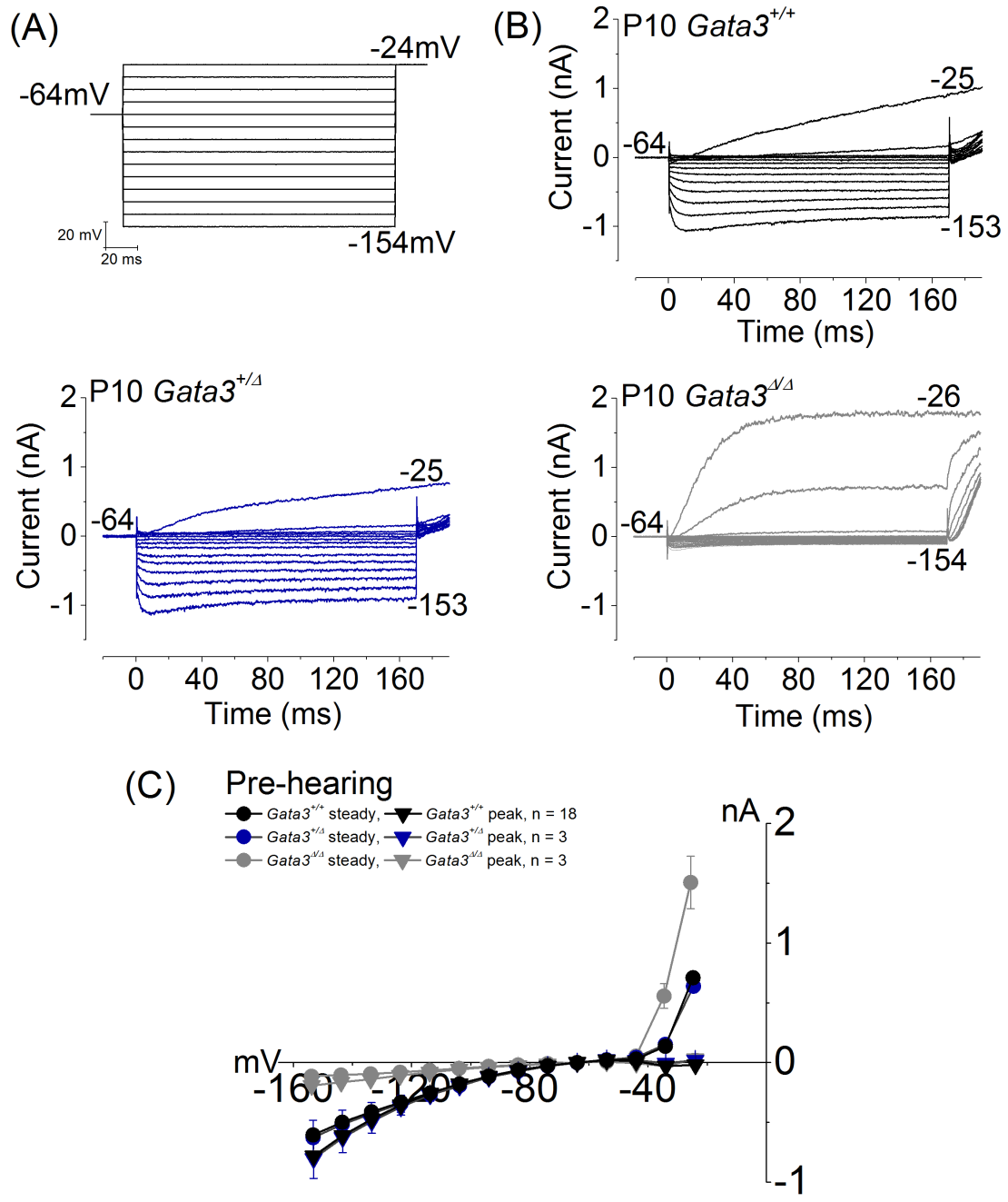

Figure 5-2: Inward rectifier K^+ current (I_{k1}) in pre-hearing IHCs (P9 - P10)
(A) The step protocol applied to elicit I_{k1}. Cells were referred to a holding potential of -64 mV, and stepped to different potentials from a potential of -154 mV, in increments of 10 mV. The duration of each voltage step was 170 ms
(B) I_{k1} recordings IHC from control (black), *Gata3*$^{+/\Delta}$ (blue) and *Gata3*$^{\Delta/\Delta}$ (light grey) pre-hearing mouse in response to the above protocol
(C) Cumulative average peak (inverted triangles) and steady state (circles) I-V curves for I_{k1} from control (n = 18), *Gata3*$^{+/\Delta}$ (n = 3) and *Gata3*$^{\Delta/\Delta}$ (n = 3) pre-hearing mice. Note the smaller size of the current in *Gata3*$^{\Delta/\Delta}$ IHCs compared to their control and *Gata3*$^{+/\Delta}$ counterparts. Error bars represent ± S.E.M.

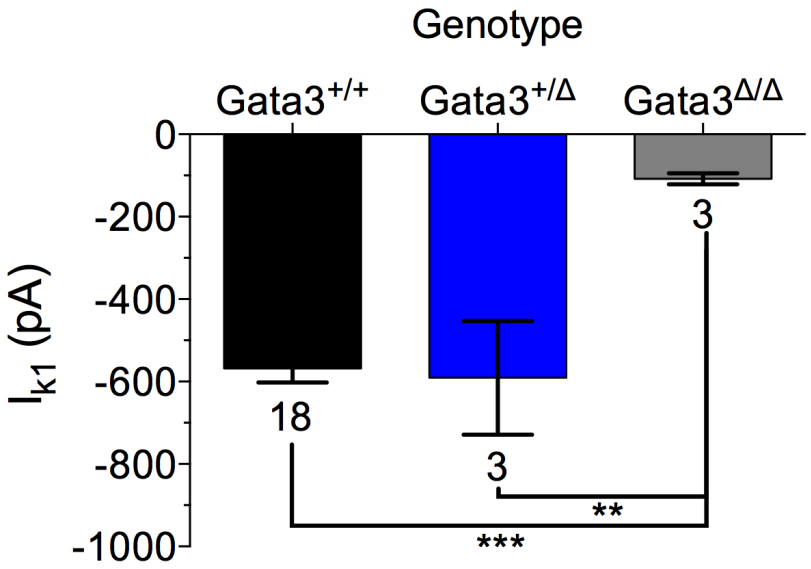

Figure 5-3: Bar graph showing the steady-state values of I_{k1} in pre-hearing IHCs (P9 - P10)
Comparison of the size of steady-state I_{k1} at 150 mV between the three genotypes at the pre-hearing stage shows that this conductance is significantly reduced in IHCs from *Gata3*$^{\Delta/\Delta}$ mice compared to their counterparts from control and *Gata3*$^{+/\Delta}$ mice (One-way ANOVA followed by Tukey's post test, p <0.05). N numbers are written below individual columns and error bars represent ± S.E.M. ** indicates $p \leq 0.01$ and *** indicates $p \leq 0.001$.

5.2.3 Total outward K^+ currents in *Gata3*$^{\Delta/\Delta}$ IHCs were smaller

Whole cell voltage clamp recordings were conducted from patch clamped IHCs at two different time points: at pre-hearing stages between P9 and P10, and at newly hearing stages between P16 and P20. The physiology of HCs was investigated at these ages to study the development of membrane properties of cells from which *Gata3* had either been knocked down or completely knocked out, and also to enable comparisons with the *Gata3*$^{+/-}$ HCs (in chapters 3 and 4).

The voltage step protocol employed was the same as that used previously (Figure 3-2A). Steady-state values of the outward currents were measured towards the end of each test pulse (160 ms from the start of the voltage step) and plotted against the

corresponding membrane potential to construct a current-voltage (I-V) relationship curve.

At pre-hearing stages, there were no differences between the total steady currents at 0 mV between control, *Gata3*$^{+/\Delta}$ and *Gata3*$^{\Delta/\Delta}$ IHCs (Figure 5-4A-B; two-way ANOVA, $p < 0.05$). This observation was similar to newly hearing stages, when again there were no differences between the total currents at 0 mV between the three genotypes investigated (Figure 5-5A-B; Table 5.2; two-way ANOVA, $p < 0.05$).

TABLE 5.2: *Total outward K^+ currents*

Age	Genotype	Mean (nA)	S.E.M	N
P9 - 10	Gata3$^{+/+}$	6.232	0.2607	19
	Gata3$^{+/\Delta}$	6.230	0.3970	3
	Gata3$^{\Delta/\Delta}$	7.567	1.258	3
P16 - 20	Gata3$^{+/+}$	11.09	1.536	12
	Gata3$^{+/\Delta}$	9.868	0.8757	8
	Gata3$^{\Delta/\Delta}$	9.210	1.716	7

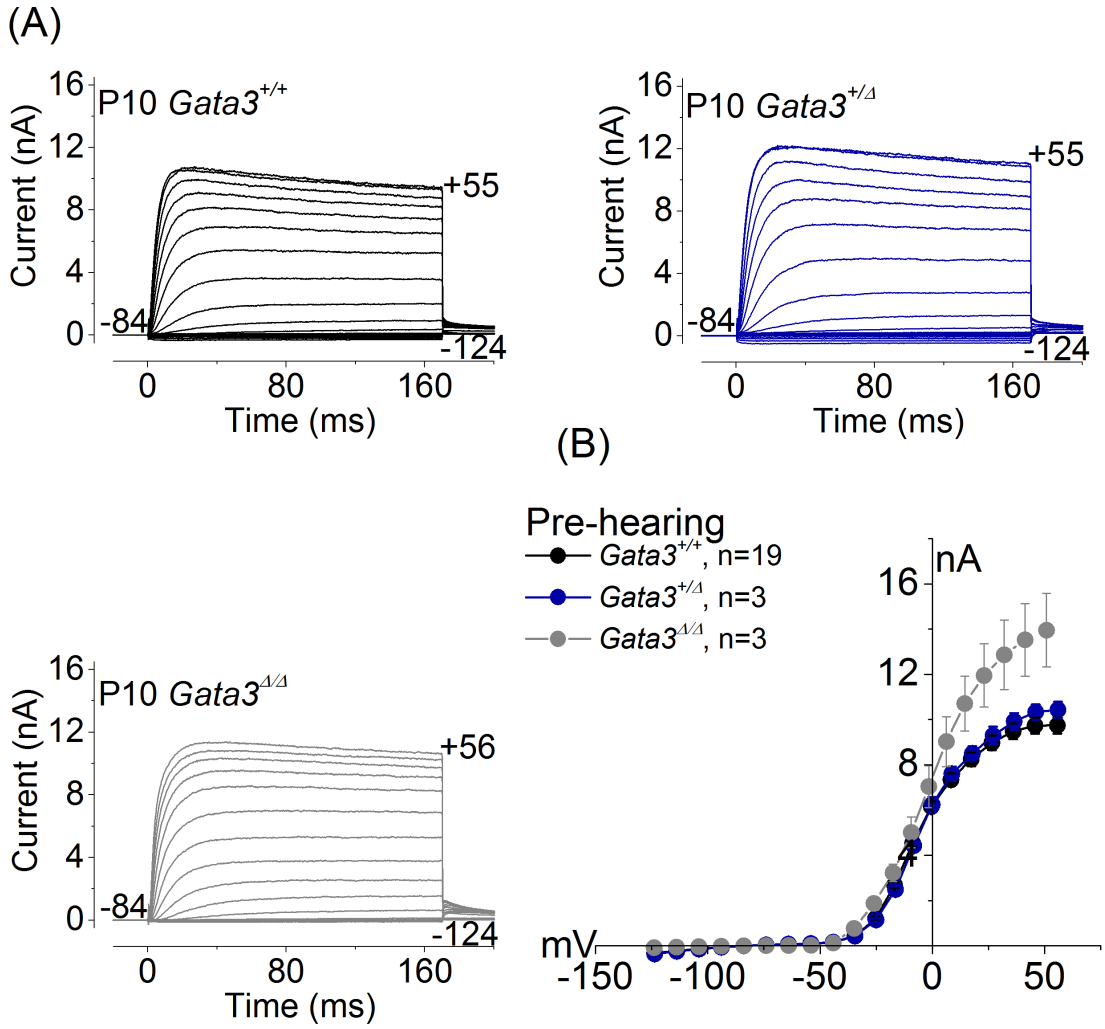

Figure 5-4: Outward K^+ currents from apical-coil mouse IHCs from the pre-hearing stage (P9 - P10)
(A) Typical current responses of an IHC from control (black), $Gata3^{+/\Delta}$ (blue) and $Gata3^{\Delta/\Delta}$ (light grey) pre-hearing mouse.
(B) Cumulative average steady-state I-V relationship curves for control (n = 19), $Gata3^{+/\Delta}$ (n = 3) and $Gata3^{\Delta/\Delta}$ (n = 3) IHCs from prehearing mice. Error bars represent ± S.E.M values.

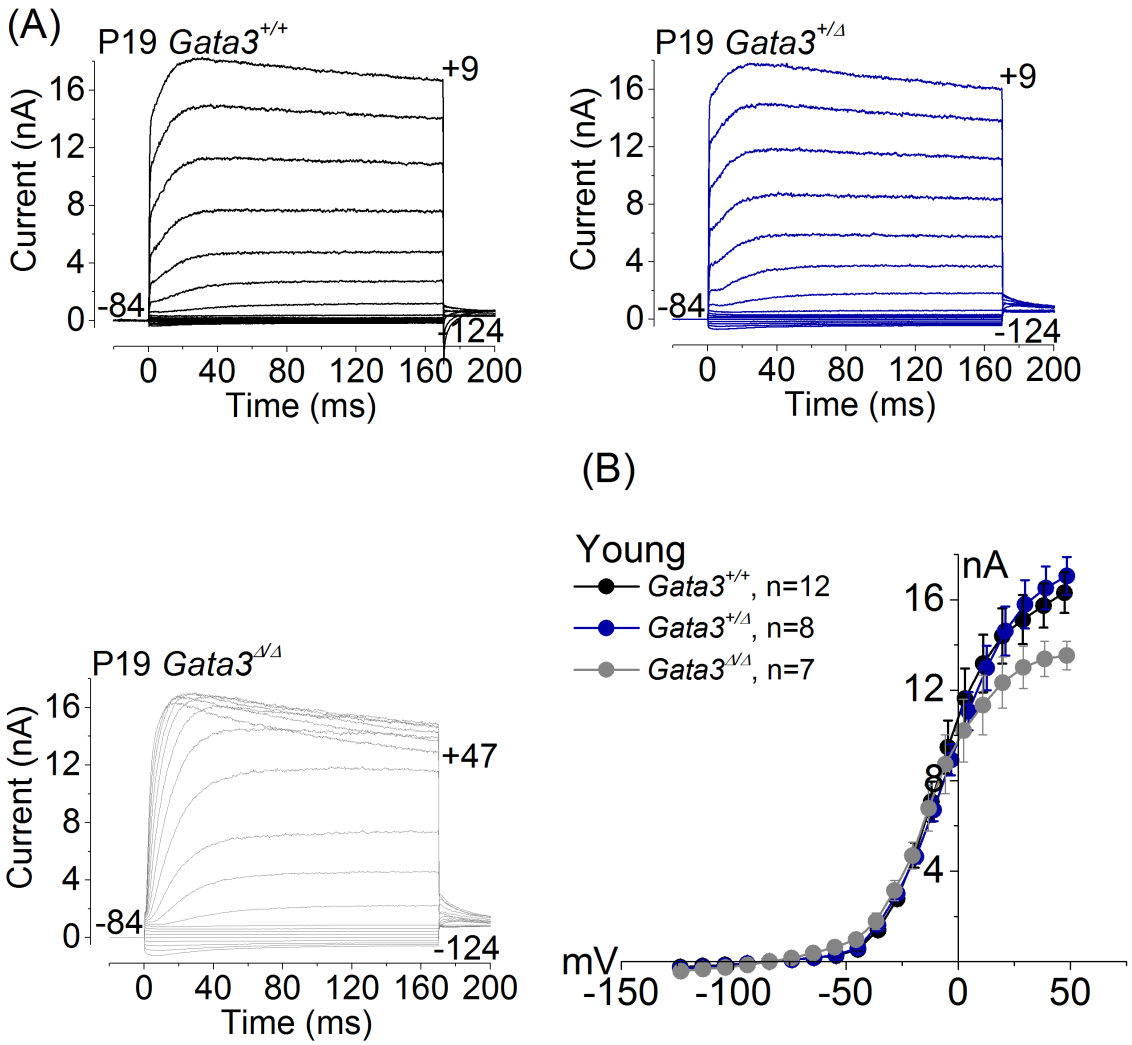

Figure 5-5: Outward K^+ currents from apical-coil IHCs from newly hearing young mice (P16 - P20)
(A) Typical current responses of an IHC from control (black), $Gata3^{+/\Delta}$ (blue) and $Gata3^{\Delta/\Delta}$ (light grey) prehearing mouse.
(B) Cumulative average steady-state I-V relationship curves for control (n = 12), $Gata3^{+/\Delta}$ (n = 8) and $Gata3^{\Delta/\Delta}$ (n = 7) IHCs from young mice. Error bars represent ± S.E.M values.

However, despite the similarity in average current sizes between all three groups at the newly hearing stages, I-V curves from *Gata3*$^{\Delta/\Delta}$ IHCs were distinct from their control and *Gata3*$^{+/Delta}$ counterparts (Figure 5-5B). While the I-V curves from control and *Gata3*$^{+/\Delta}$ IHCs showed a linear relationship, those from *Gata3*$^{\Delta/\Delta}$ IHCs showed a bell-shaped curve.

In order to further look at the development of the whole cell currents at older ages, we recorded from a few IHCs from *Gata3*$^{+/\Delta}$ and *Gata3*$^{\Delta/\Delta}$ animals at older time-points (Table 5.3), beyond P38. At this stage, there was a decrease in the average current size at 0 mV between the two genotypes (Figure 5-6A-B; Mann Whitney two-tailed test, $p < 0.05$), and the typical bell-shaped curve of the I-V relationship *Gata3*$^{\Delta/\Delta}$ IHCs was observed to be more pronounced. The development of the outward K^+ currents is represented in a bar graph in Figure 5-7.

TABLE 5.3: *Total steady outward K^+ currents in older P38+ mice*

Genotype	Mean (nA)	S.E.M	N
Gata3$^{+/\Delta}$	20.59	2.483	6
Gata3$^{\Delta/\Delta}$	10.15	1.685	6

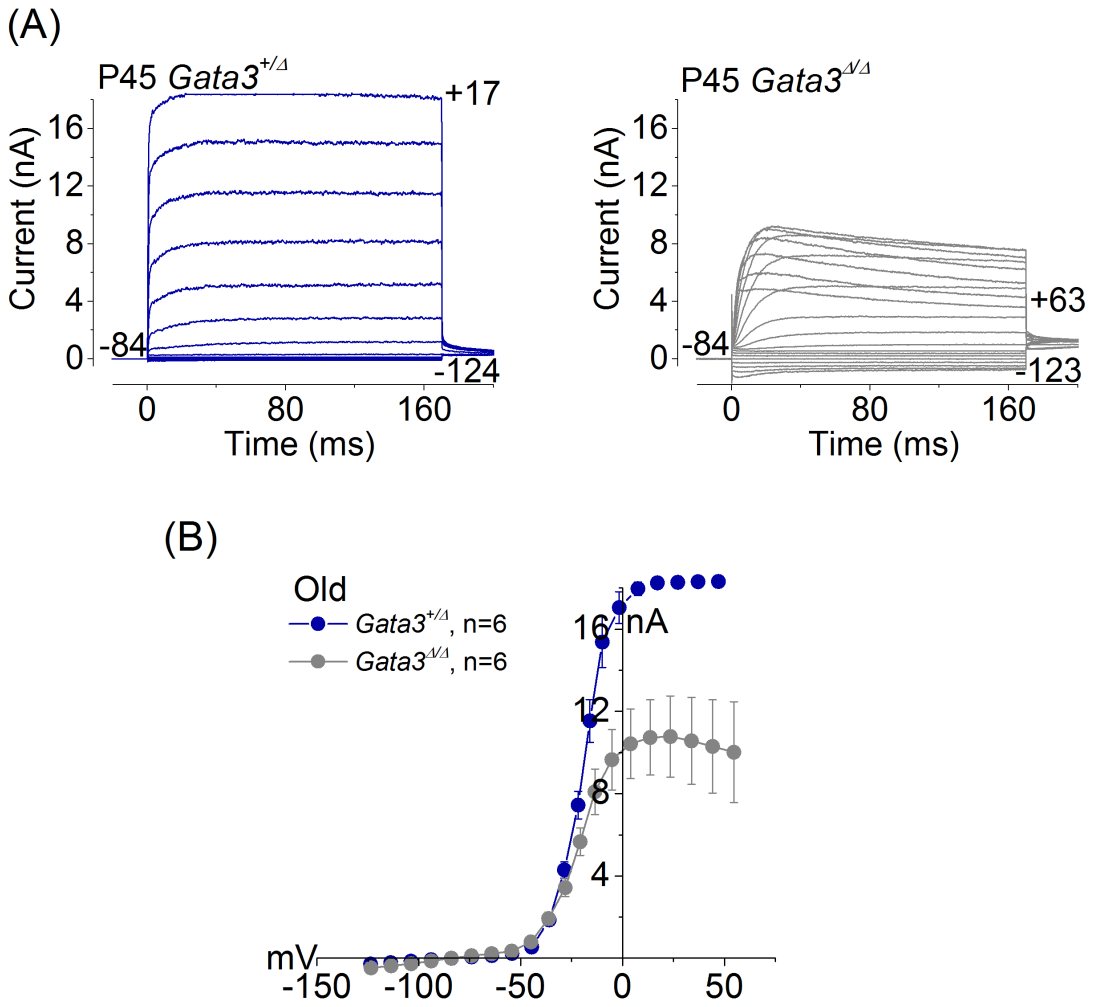

Figure 5-6: Outward K^+ currents from apical-coil IHCs from older adult mice (P38+)
(A) Typical current responses of an IHC from *Gata3*$^{+/\Delta}$ (blue) and *Gata3*$^{\Delta/\Delta}$ (light grey) old mouse.
(B) Cumulative average steady-state I-V relationship curves for *Gata3*$^{+/\Delta}$ (n = 6) and *Gata3*$^{\Delta/\Delta}$ (n = 6) IHCs from older mice. The I-V curve is bell-shaped for *Gata3*$^{\Delta/\Delta}$ IHCs. Note that the plateau effect of the curve positive to 0 mV in the case of *Gata3*$^{+/\Delta}$ recordings is an artefact caused due to the upper limit of the operational range of the Axopatch 200B amplifier (18 nA). Error bars represent ± S.E.M values.

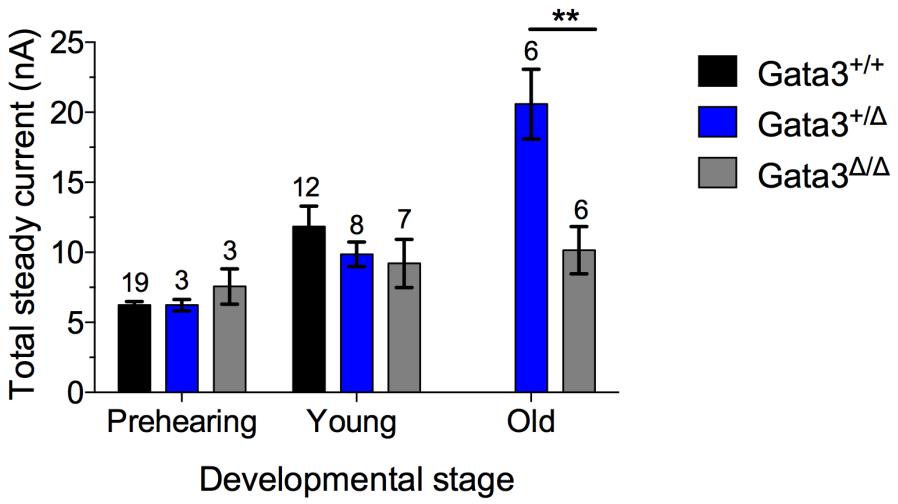

Figure 5-7: Development of outward K^+ currents from apical-coil IHCs
Bar graph showing average steady-state currents at 0 mV of wild type (black) and *Gata3*$^{+/\Delta}$ (blue) and *Gata3*$^{\Delta/\Delta}$ (light grey) IHCs at different postnatal ages. Current sizes in *Gata3*$^{\Delta/\Delta}$ IHCs were significantly smaller at the older ages (two-way ANOVA followed by Tukey's post-test, p <0.05). N numbers are written above individual columns, and error bars represent ± S.E.M values. ** indicates $p \leq 0.01$.

5.2.4 Fast activating $I_{k,f}$ conductance in *Gata3*$^{\Delta/\Delta}$ IHCs is severely reduced

To understand the basis of the altered I-V relationship in IHCs from *Gata3*$^{\Delta/\Delta}$ animals, we isolated the $I_{k,f}$ conductance as before, by measuring its amplitude at 1.5 ms from the start of the voltage step at the membrane potential of -25 mV.

At the younger time-point between P16 and P20, while $I_{k,f}$ size was similar between control and *Gata3*$^{+/\Delta}$ IHCs, there was a significant decrease in the magnitude of $I_{k,f}$ in *Gata3*$^{\Delta/\Delta}$ IHCs (Table 5.4; Figure 5-8; one-way ANOVA followed by Tukey's post-test, p <0.05). This characteristic persisted into the older time-point investigated (Table 5.4; Figure 5-8; two-way ANOVA followed by Tukey's post-test, p <0.05).

TABLE 5.4: $I_{k,f}$ *conductance*

Age	Genotype	Mean (nA)	S.E.M	N
P16 - 20	*Gata3*$^{+/+}$	1.775	0.2604	12
	Gata3$^{+/\Delta}$	1.761	0.1523	8
	Gata3$^{\Delta/\Delta}$	0.8043	1.308	7
P38+	*Gata3*$^{+/\Delta}$	2.907	0.4162	6
	Gata3$^{\Delta/\Delta}$	0.6367	0.0727	6

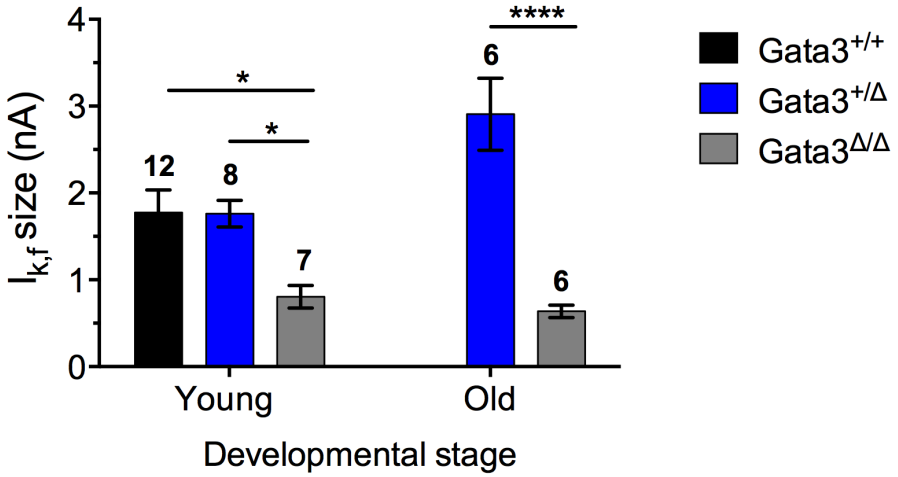

Figure 5-8: $I_{k,f}$ is reduced in *Gata3*$^{\Delta/\Delta}$ animals
Bar graph showing the comparison between average $I_{k,f}$ amplitudes from control (black), *Gata3*$^{+/\Delta}$ (blue) and *Gata3*$^{\Delta/\Delta}$ (light grey) IHCs, measured at 1.5 ms from the start of the voltage step. $I_{k,f}$ size is significantly smaller in IHCs from *Gata3*$^{\Delta/\Delta}$ animals compared to age-matched counterparts at both, the young and older ages investigated (two-way ANOVA followed by Tukey's post-hoc test, p <0.05). N numbers are written above individual columns, and error bars represent ± S.E.M values. * indicates p<0.05, ** indicates $p \leq 0.01$, *** indicates $p \leq 0.001$ and **** indicates $p \leq 0.0001$.

5.2.5 $I_{k,n}$ conductance is reduced in *Gata3*$^{\Delta/\Delta}$ IHCs

Since the $I_{k,f}$ conductance from *Gata3*$^{\Delta/\Delta}$ animals showed an impaired profile, we wanted to study the concomitant development of the $I_{k,n}$ conductance in these cells. $I_{k,n}$ was elicited as described before (Figure 3-8A) by depolarizing voltage steps of 170 ms duration from -154 mV to -34 mV in 10 mV increments, from the holding potential of -64 mV. Steady-state values of the current were measured towards the end of the test pulse, and peak values were individually calculated for each recording. Current size was measured as the difference between the instantaneous and steady-state deactivating currents at a fixed potential of -125 mV for control and *Gata3*$^{+/\Delta}$ IHCs, and at -150 mV for *Gata3*$^{\Delta/\Delta}$.

In the case of the newly hearing animals (between P16 and P20), $I_{k,n}$ size was comparable between control and *Gata3*$^{+/\Delta}$ IHCs (Table 5.5; black and blue traces in Figure 5-9; two-way ANOVA, $p < 0.05$). Interestingly at these ages, $I_{k,n}$ never developed in *Gata3*$^{\Delta/\Delta}$ IHCs. These cells showed the current profile of the inwardly rectifying I_{k1} (evident from its I-V curve in Figure 5-9, light grey), reminiscent of immature IHCs [Marcotti et al., 1999], instead of the acquisition of the $I_{k,n}$ conductance. This feature was also observed in *Gata3*$^{\Delta/\Delta}$ IHCs from the older time-points investigated (Figure 5-10).

TABLE 5.5: *$I_{k,n}/I_{k1}$ conductance*

Age	Genotype	Mean (pA)	S.E.M	N
P16 - 20	*Gata3*$^{+/+}$	-304.3	64.40	11
	Gata3$^{+/\Delta}$	-292.8	37.52	4
	Gata3$^{\Delta/\Delta}$	-1158.40	159.93	5
P38+	*Gata3*$^{+/\Delta}$	-204.6	41.46	5
	Gata3$^{\Delta/\Delta}$	-741.40	163.14	5

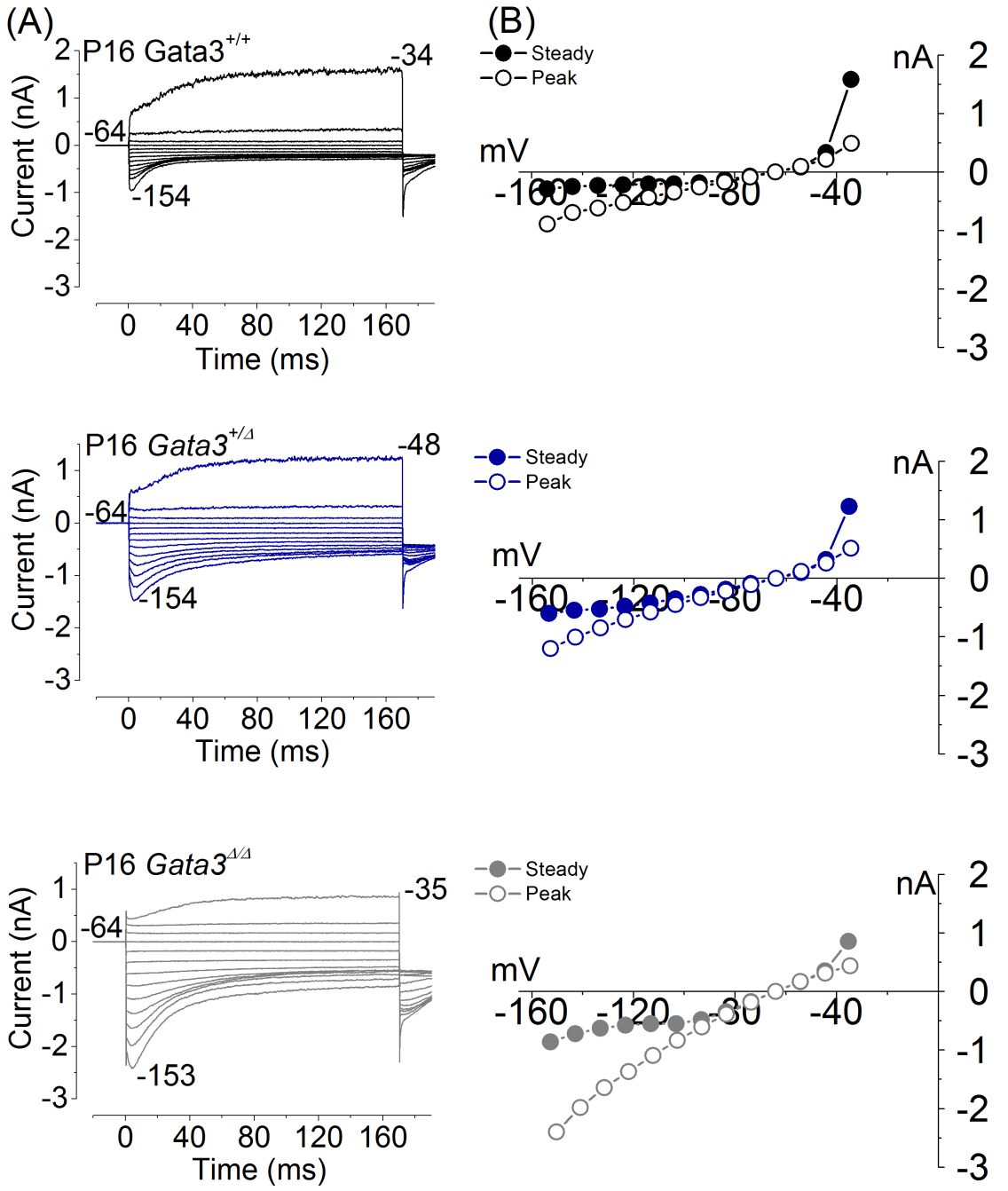

Figure 5-9: Negatively-activating inward K^+ current ($I_{k,n}$) does not develop in IHCs from newly hearing young *Gata3*$^{\Delta/\Delta}$ mice (P16 - P20)
(A) Typical examples of negatively-activating inward currents measured from control (black), *Gata3*$^{+/\Delta}$ (blue) and *Gata3*$^{\Delta/\Delta}$ (light grey) IHCs from young mice
(B) I-V curves of the traces shown above, showing the steady-state (measured towards the end of the voltage step, filled circle symbol) and peak (hollow circle symbol) inward currents from control (black) and *Gata3*$^{+/\Delta}$ (blue) and *Gata3*$^{\Delta/\Delta}$ (light grey) IHCs. Note the I-V curve of the inwardly activating current from the *Gata3*$^{\Delta/\Delta}$ IHC is reminiscent of I_{k1} in prehearing control and *Gata3*$^{+/\Delta}$ mice (black and blue traces in Figure 5-2).

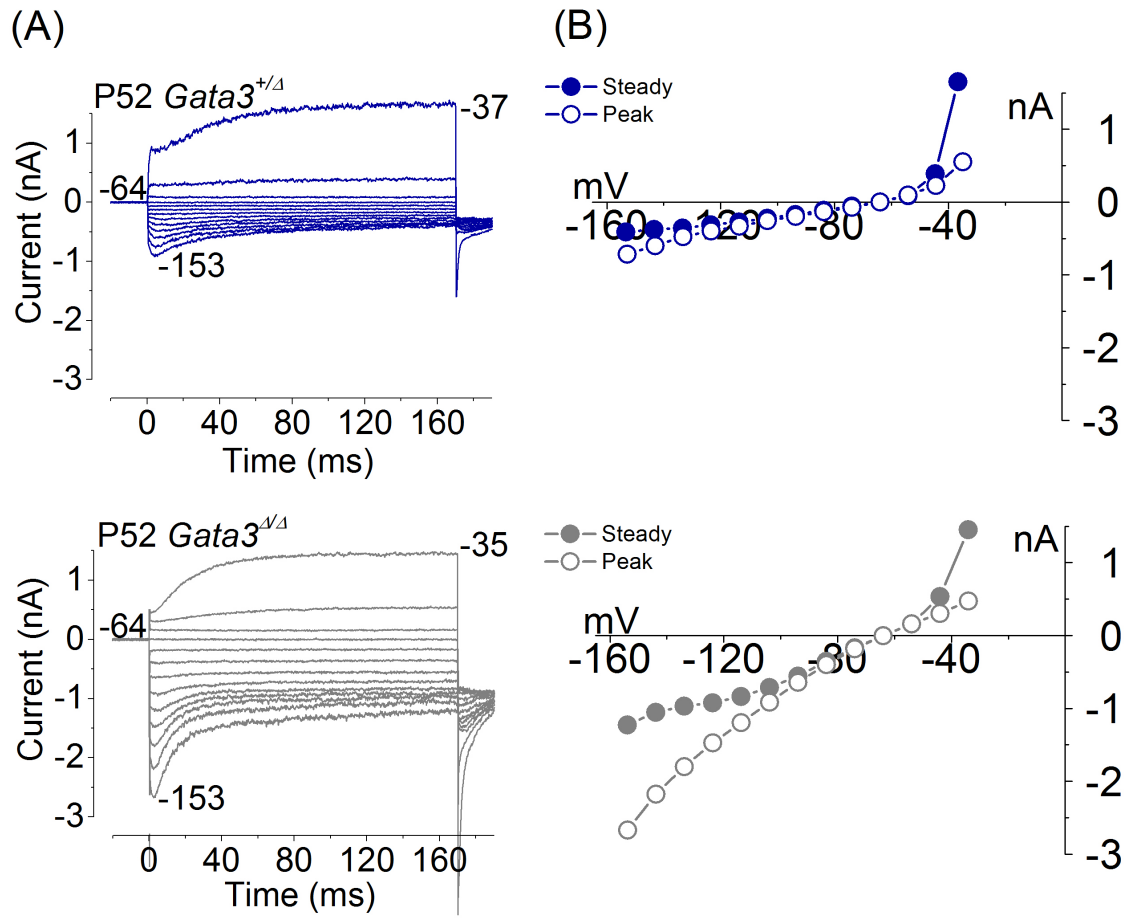

Figure 5-10: Negatively-activating inward K^+ current ($I_{k,n}$) does not develop in IHCs from older *Gata3*$^{\Delta/\Delta}$ mice (P38+)
(A) Typical examples of negatively activating inward K^+ currents measured from *Gata3*$^{+/\Delta}$ (blue) and *Gata3*$^{\Delta/\Delta}$ (light grey) IHCs from older mice.
(B) I-V relationship curves of the individual traces shown above, showing the steady-state (measured towards the end of the voltage step, filled circle symbol) and peak (hollow circle symbol) inward currents from *Gata3*$^{+/\Delta}$ (blue) and *Gata3*$^{\Delta/\Delta}$ (light grey) IHCs. Note the I-V curve of the inwardly activating current from the *Gata3*$^{\Delta/\Delta}$ IHC is reminiscent of I_{k1} in prehearing control and *Gata3*$^{+/\Delta}$ mice (black and dark grey traces in Figure 5-2).

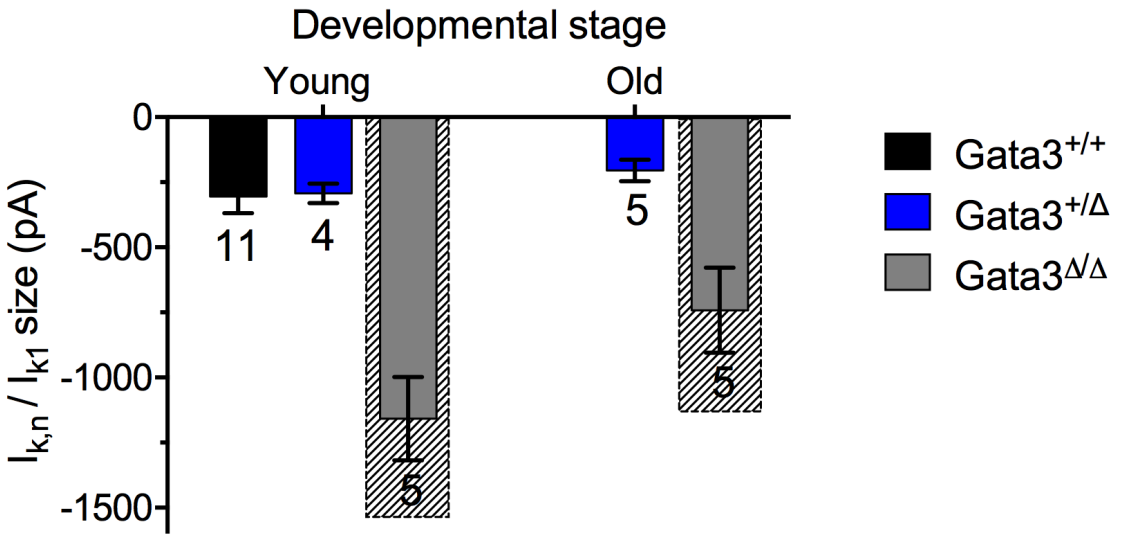

Figure 5-11: Inwardly rectifying I_{k1} conductance remains in IHCs from older *Gata3*$^{\Delta/\Delta}$ animals
Bar graph showing the average size of the inward current of control (black), *Gata3*$^{+/\Delta}$ (blue) and *Gata3*$^{\Delta/\Delta}$ (light grey) in young (P16 - P20) and older (P38+) mice, in response to voltage step protocol in order to elicit $I_{k,n}$. $I_{k,n}$ size, in the case of control and *Gata3*$^{+/\Delta}$ IHCs, was calculated as the difference between the instantaneous peak and the deactivating steady state current, at a fixed potential of -125 mV. Inward current size, in the case of IHCs from *Gata3*$^{\Delta/\Delta}$ animals, was calculated as the difference between the peak and the steady state currents at -150 mV for comparison (bars with hatched background). This current had an I-V curve resembling that of I_{k1} from immature IHCs of prehearing animals (refer to Figure 5-2). N numbers are written above individual columns, and error bars represent ± S.E.M values.

Figure 5-11 is the graphical representation of the average amplitudes of $I_{k,n}$ (for wild type and *Gata3*$^{+/\Delta}$ IHCs) and I_{k1} (for *Gata3*$^{\Delta/\Delta}$ IHCs) at the young and older stages investigated. Statistical tests were not conducted for this as they were two different current types.

5.2.6 Voltage responses of *Gata3*$^{\Delta/\Delta}$ IHCs are altered

To understand the consequence of the altered current profiles of the IHCs from *Gata3*$^{\Delta/\Delta}$ animals, we studied their responses to current injections. Cells were held in current clamp configuration and subjected to current clamp protocol as described previously. The resting membrane potential of cells were first measured by averaging the voltage of the cell before current was injected. Cells were then stimulated from their resting membrane potentials with current injections which ranged from -100 pA to + 900 pA, in 100 pA increments. At the prehearing stages, the resting membrane potentials were comparable between control, *Gata3*$^{+/\Delta}$ and *Gata3*$^{\Delta/\Delta}$ IHCs (Table 5.6; two-way ANOVA, p <0.05). Cells from all three genotypes responded with an initial spike followed by a sustained depolarisation in response to positive current injections (Figure 5-12). In response to negative current injections, *Gata3*$^{\Delta/\Delta}$ IHCs were unable to clamp the changing voltage fluctuation as efficiently as cells from control and *Gata3*$^{+/\Delta}$ animals (arrow in light grey trace in Figure fig:prehearingrmA and 5-12B).

TABLE 5.6: *Resting membrane potential*

Age	Genotype	Mean (mV)	S.E.M	N
P9 - 10	*Gata3*$^{+/+}$	-76.74	0.7051	19
	Gata3$^{+/\Delta}$	-73.47	0.4792	3
	Gata3$^{\Delta/\Delta}$	-79.59	2.887	3
P16 - 20	*Gata3*$^{+/+}$	-69.32	2.359	9
	Gata3$^{+/\Delta}$	-71.61	3.257	3
	Gata3$^{\Delta/\Delta}$	-73.36	2.340	8
P38+	*Gata3*$^{+/\Delta}$	-74.52	0.9437	6
	Gata3$^{\Delta/\Delta}$	-68.85	3.526	7

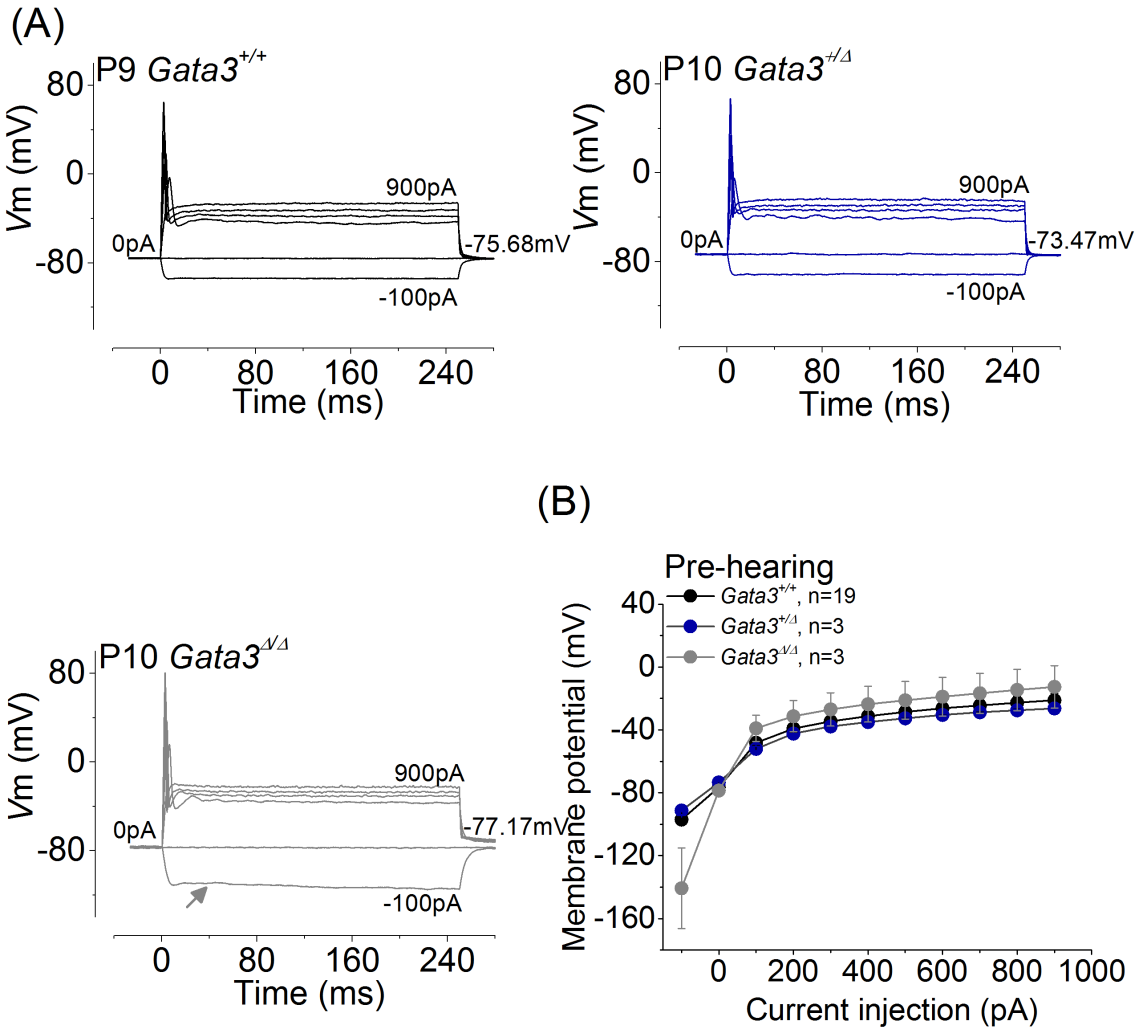

Figure 5-12: Voltage responses of IHCs from the pre-hearing stage (P9 - P10)
(A) Typical examples of voltage responses of IHCs from control (black), *Gata3*$^{+/\Delta}$ (blue) and *Gata3*$^{\Delta/\Delta}$ (light grey) IHCs from pre-hearing mice. Arrow indicates the larger voltage excursion in response to the hyperpolarising current injection in the case of *Gata3*$^{\Delta/\Delta}$ IHCs.
(B) Cumulative average steady-state voltage responses measured from control (n = 19), *Gata3*$^{+/\Delta}$ (n = 3) and *Gata3*$^{\Delta/\Delta}$ (n = 3) pre-hearing mice in response to the protocol described above. Steady values plotted are the mean voltages over the last 25 ms of the current injection. Note the larger fluctuation of the membrane potential in response to the -100 pA injection. There were no differences in the resting membrane potentials between the three groups. Error bars represent ± S.E.M.

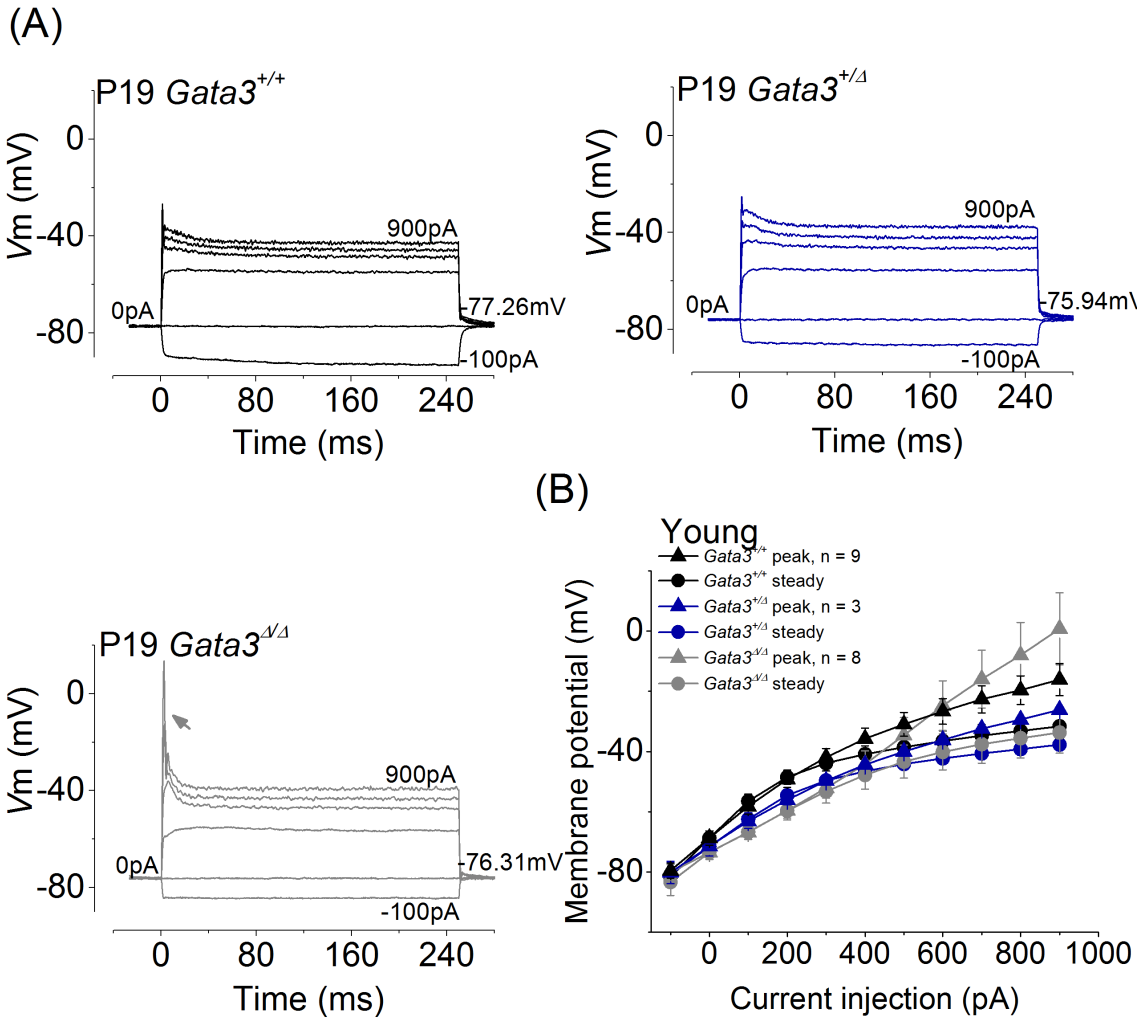

Figure 5-13: Voltage responses of IHCs from newly hearing young mice (P16 - P20) (A) Typical examples of voltage responses of IHCs from control (black), $Gata3^{+/\Delta}$ (blue) and $Gata3^{\Delta/\Delta}$ (light grey) IHCs from young mice. Arrow indicates the larger voltage fluctuation in response to depolarising current injections in IHCs from $Gata3^{\Delta/\Delta}$ mice.
(B) Cumulative average peak (triangles) and steady-state (circles) voltage responses measured from young control (n = 9), $Gata3^{+/\Delta}$ (n = 3) and $Gata3^{\Delta/\Delta}$ (n = 8). The difference between the peak and steady voltage response at +900 pA in $Gata3^{\Delta/\Delta}$ IHCs was nearly double that of the control or $Gata3^{+/\Delta}$ groups. There were no differences in the resting membrane potentials between the three groups. Error bars represent ± S.E.M.

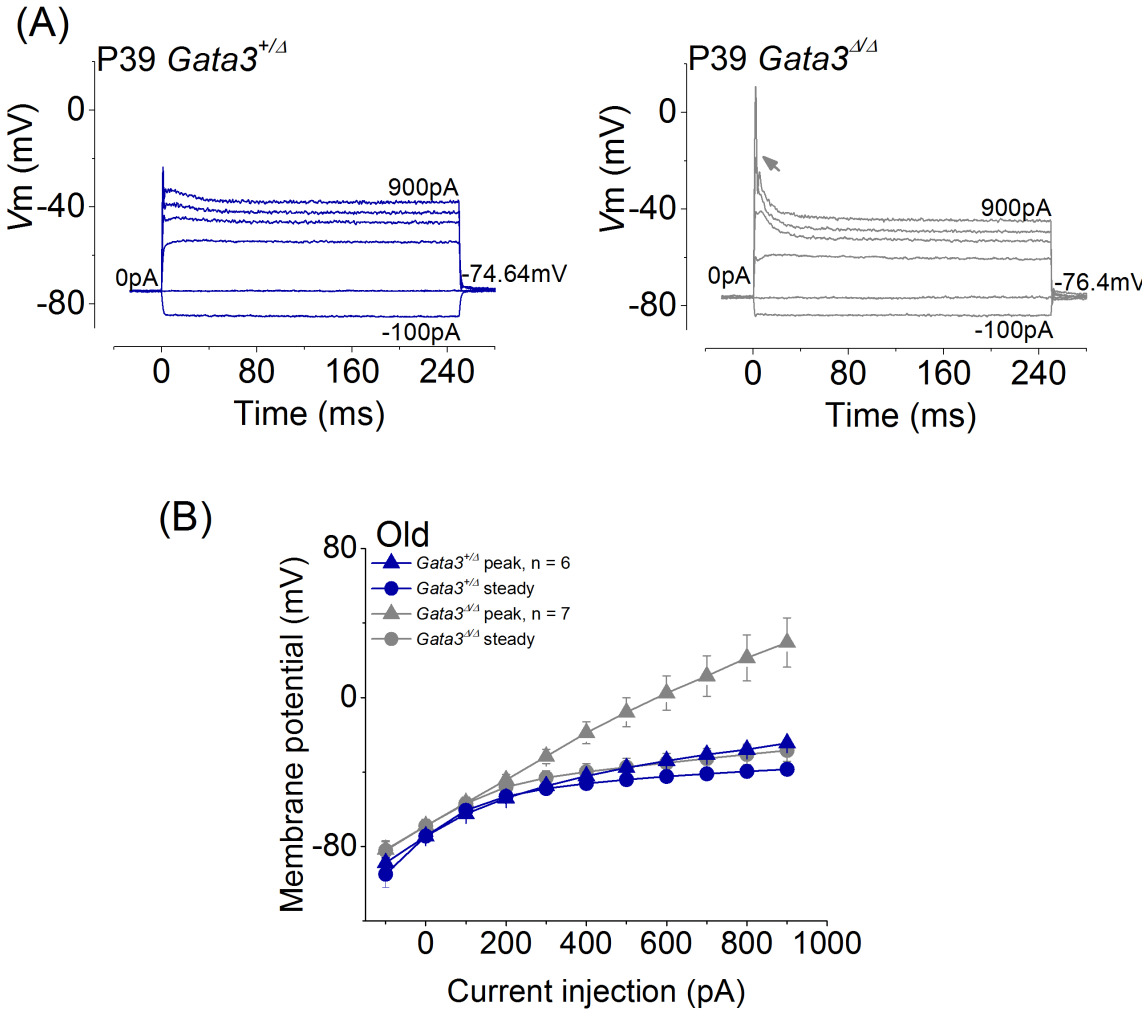

Figure 5-14: Voltage responses of IHCs from older mice (P38+)
(A) Typical examples of voltage responses of IHCs from *Gata3*$^{+/\Delta}$ (blue) and *Gata3*$^{\Delta/\Delta}$ (light grey) IHCs from older mice. Arrow indicates the larger voltage fluctuation in response to depolarising current injections in IHCs from *Gata3*$^{\Delta/\Delta}$ mice.
(B) Cumulative average peak (triangles) and steady-state (circles) voltage responses measured from older *Gata3*$^{+/\Delta}$ (n = 6) and *Gata3*$^{\Delta/\Delta}$ (n = 7) IHCs. The differences between the peak and steady voltage responses were consistently larger in *Gata3*$^{\Delta/\Delta}$ IHCs than the *Gata3*$^{+/\Delta}$ group. There were no differences in the resting membrane potentials between the two groups. Error bars represent ± S.E.M.

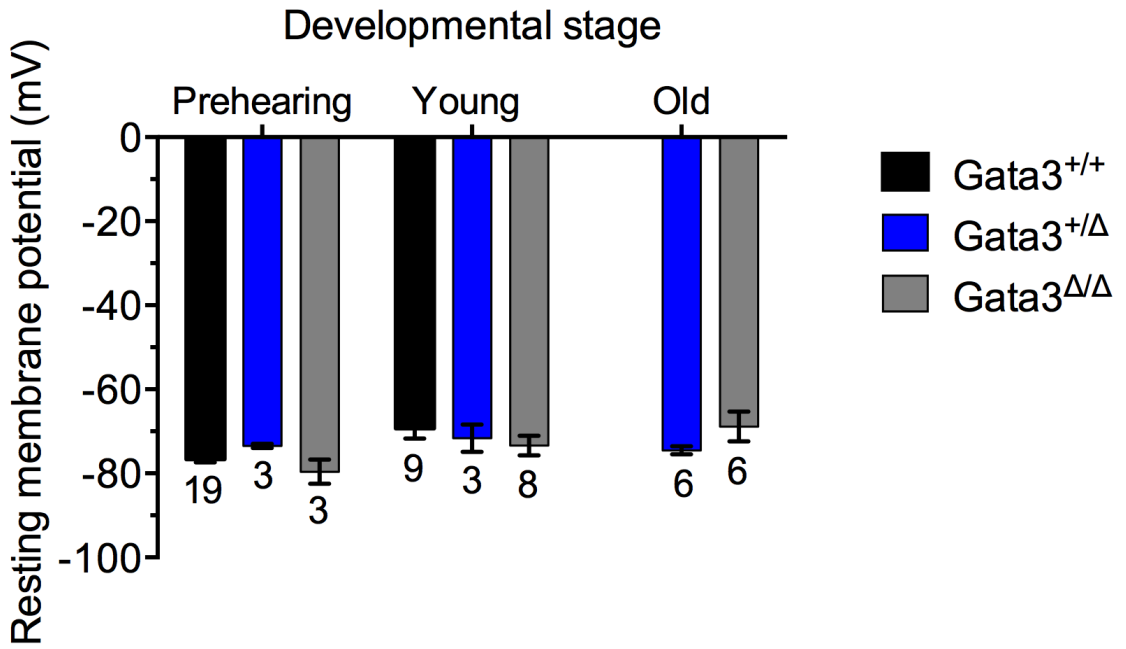

Figure 5-15: Resting membrane potentials of *Gata3*$^{\Delta/\Delta}$ IHCs are normal
Bar graph showing the comparison between resting membrane potentials of wild type(black), *Gata3*$^{+/\Delta}$ (blue) and *Gata3*$^{\Delta/\Delta}$ (light grey) IHCs from pre-hearing (P9 - P10), newly hearing young (P16 - P20) and older (P38+) mice. The resting membrane potentials between the three genotypes at each age were comparable to each other. N numbers are written above individual columns, and error bars represent ± S.E.M values.

Young animals (between P16 and P20) also showed comparable resting membrane potentials between all three genotypes investigated (Table 5.6; Figure 5-15; two-way ANOVA, $p < 0.05$). However, in response to current injections, *Gata3*$^{\Delta/\Delta}$ IHCs showed a much larger voltage change than their *Gata3*$^{+/\Delta}$ and wild type counterparts (Figure 5-13A), similar to *Gata3*$^{+/-}$ IHCs in Chapter 4. This attribute persisted in the older *Gata3*$^{\Delta/\Delta}$ IHCs investigated (Figure 5-14A). The larger fluctuation is evident in the graphs showing the peak and steady-state voltage responses corresponding to the injected current (Figures 5-13B and 5-14B)

5.3 Discussion

The physiology of *Gata3*-inactivated IHCs in the cochlea, after their initial differentiation show the following:

1. Near-complete absence of inward rectifier (I_{k1}) currents during immature stages
2. Delayed development of the normal I_{k1} current profile
3. Persistence of I_{k1} into older adult stages
4. Failure of the development of the mature inward rectifying conductance, $I_{k,n}$
5. Reduction of the total cell currents at older ages, and
6. Reduction of $I_{k,f}$ at the older ages

The severe reduction of I_{k1} conductance in pre-hearing *Gata3*$^{\Delta/\Delta}$ IHCs is very similar to the pharmacological block of this current by barium or cesium [Marcotti et al., 1999]. The strong initial reduction and delay in the onset of the normal phenotype of I_{k1} reflects a cell autonomous effect of the complete loss of GATA3 in IHCs. The anomalous I_{k1} profile in knockout IHCs suggests a developmental cause triggered by the absence of GATA3, as the onset of I_{k1} is first seen in

murine embryonic IHCs by E15.5 [Marcotti et al., 2003]. Concomitant voltage responses from pre-hearing cells revealed a larger passive response to negative current injections, as a consequence of the reduced I_{k1} (arrow in the light grey trace in Figure 5-2). Lack of an abnormal I_{k1} profile from *Gata3*$^{+/-}$ IHCs (chapter 4) suggests that half the dose of normal levels of GATA3 is adequate to retain the normal phenotype of I_{k1}.

During subsequent postnatal development, I_{k1} size increases in *Gata3*$^{\Delta/\Delta}$ IHCs, but is retained far beyond the onset of hearing, at a time when it should be replaced by $I_{k,n}$ [Marcotti et al., 2003]. This coincides with the downregulation of Kir2.1 channels underlying I_{k1} [Ruan et al., 2008], and the upregulation of KCNQ4 channels. IHCs from the *Gata3*$^{+/\Delta}$ group develop $I_{k,n}$ similar to the *Gata3*$^{+/+}$ group, and do not exhibit intermediate phenotypes. The replacement of one conductance by another during functional maturity of IHCs is deregulated in the absence of GATA3. However, it is uncertain if this is a knock-on effect due to the delayed onset of I_{k1}, or whether this is a mutually exclusive phenomenon caused by a lack of normal protein levels during postnatal development. Whether this is due to a delayed development of Kir2.1 channels or channel functionality remains to be investigated.

While *Gata3*$^{+/-}$ IHCs showed smaller overall currents at younger ages between P16 - P20 (Figure 4-5), reduction of the total steady current at 0 mV was first observed in IHCs from *Gata3*$^{\Delta/\Delta}$ animals at the older ages investigated. This could be tentatively explained: most *Gata3*$^{+/-}$ animals were P20, while most *Gata3*$^{\Delta/\Delta}$ were between P16-18, the knockout group thus reflected a more immature profile compared to the *Gata3*$^{+/-}$ group. Additionally, IHCs from *Gata3*$^{+/\Delta}$ animals did not appear to be affected, unlike *Gata3*$^{+/-}$ IHCs. This would indicate that the impaired phenotype of the total outward K^+ currents in *Gata3*$^{+/-}$ IHCs was due to a compounded effect of the reduction of GATA3 from HCs as well as other cell

populations within the cochlea, and accumulated defects over a longer period of time (from the birth of HCs until the onset of *cre recombinase*) .

Another attribute common between *Gata3* haploinsufficiency (in $Gata3^{+/-}$ animals) and complete inactivation in $Gata3^{\Delta/\Delta}$ IHCs, was the diminished $I_{k,f}$. Again, $Gata3^{+/\Delta}$ IHCs were similar to wild type controls, while $Gata3^{Delta/Delta}$ IHCs were affected. The defective development of $I_{k,f}$ in $Gata3^{\Delta/\Delta}$ cells points to a cell autonomous effect due to complete suppression of *Gata3* function in these cells. The abnormal effect in $Gata3^{+/-}$ IHCs is most likely a more pronounced cumulative effect due to both the chronic and global lack of GATA3 from the cochlea. Similar to $Gata3^{+/-}$ IHCs, the consequence of the smaller $I_{k,f}$ in $Gata3^{\Delta/\Delta}$ cells is reflected in the larger amplitude of the voltage responses to depolarising current injections.

It is perhaps important to note that the size of $I_{k,f}$ is approximately unchanged from the time of its onset from P12 onwards, until the oldest stages investigated, in both $Gata3^{+/-}$ and $Gata3^{\Delta/\Delta}$ animals. This would mean that the residual outward currents in these cells, the delayed rectifier current, which during this time (from P12 onwards) should follow a slower growth pattern than $I_{k,f}$ [Kros et al., 1998], also remains unchanged in the case of the affected IHCs (Figure 5-7 and 4-5).

The Drosophila homologue of *Gata*, *pannier*, is a critical embryonic cardiogenic transcriptional regulator, and is re-deployed during postnatal development to establish certain aspects of adult cardiac physiology [Qian and Bodmer, 2009]. Interestingly, *Kcnq*, *slo* (encodes for the pore-forming BK channel subunit) and the fly homologue of smooth endoplasmic reticulum calcium ATP-ase (SERCA) were significantly down-regulated in *pannier* heterozygote flies in the same study.

SERCA localises to the main intracellular stores of HCs, the endoplasmic reticulum (ER) [Spicer et al., 1999]. Inhibition of SERCA by a drug called thapsigargin

induces an initial increase in free cytosolic Ca^{2+} and hinders their subsequent re-filling [Thastrup et al., 1990]. The activation of BK channels is mainly dependant upon intracellular Ca^{2+}, which can be modulated by the stores [Marcotti et al., 2004a]. A depleted ER, due to decreased function of *Serca*, could throw the critically regulated process of Ca^{2+} homeostasis within the cells out of sync, and induce the ER stress response to trigger apoptosis [Sartori et al., 2013; Mekahli et al., 2011; Fujinami et al., 2012; Wang et al., 2015].

Elevated intracellular Ca^{2+} levels have been observed to inhibit KCNQ4 channels [Chambard and Ashmore, 2005]. Raised Ca^{2+} is able to hydrolyse phosphatidylinositol-bis-phosphate (PIP_2) [Allen et al., 1997], a component closely associated with the plasma membrane. Although it makes up less than 1% of the plasma membrane, it functions as a second messenger to regulate several important cellular processes, including the activation of KCNQ4 [Zhang et al., 2003] and Kir2.1 [Xie et al., 2008; Zhang et al., 1999] channels, conductances mediated by both being affected by the deficiency of GATA3.

The evidence presented here suggests not only a developmental role for *Gata3*, but is also the first study to report a role for *Gata3* in postnatal HCs, further lending support for its continued expression in this cell population. Our next logical step was to develop an *in vitro* model system that would allow investigations into direct and indirect regulation by *Gata3*.

Chapter 6

Derivation of a *Gata3* reporter cell line

6.1 Introduction

The expression level of *Gata3* is clearly important for *Gata3* function [Ku et al., 2015] and the haploinsufficiency that underlies HDR syndrome might be treated by up-regulation of *Gata3*. Furthermore, *Gata3* enhances the action of *Atoh1* in the production of hair cells [Masuda et al., 2012] and its upregulation in adult tissue might be an effective part of sensory regeneration [Milo et al., 2009]. Interleukin 4 (IL-4) is known to upregulate *Gata3* in lymphocyte differentiation [Zhu et al., 2004], and we decided to develop a screening tool to discover other agents that could do the same. An appropriate drug could potentially be used not only for treating haploinsufficiency but also as part of a treatment for regeneration.

Conditionally immortal cell lines can be effective models for auditory cell function [Rivolta and Holley, 2002; Nicholl et al., 2005; Helyer et al., 2007]. They can be cultured and screened in unlimited numbers to identify molecules and drugs that modulate specific genes or influence signaling pathways [Milo et al., 2009]. They can also be used to study the physiological properties of cochlear cells [Jagger et al., 2000; Lawlor et al., 1999] and used to explore the mechanisms by which *Gata3* influences the expression of functional K^+ channels *in vitro*.

We aimed to characterise a transgenic mouse carrying an *Egfp* reporter for *Gata3* [Panayi et al., 2010], to cross it with the *Immortomouse* and then to derive *Gata3 Egfp* reporter lines from embryonic otic tissue.

The *Immortomouse* carries a temperature-sensitive variant of the Simian Virus 40 (SV40) large *T Antigen* transgene under the control of an interferon-inducible promoter. This allows for tissue-specific cells to be derived directly from the *Immortomouse* [Kern, 2005]. Under 'permissive' conditions of 33°C in the presence of γ-interferon, cells undergo reversible immortalization, and can thus proliferate. Higher temperatures of 37 to 39°C do not facilitate immortalization, instead causes them to differentiate [Kern, 2005]. One transgene is enough to cause immortalization of cells. Derivation of cell lines from *Immortomouse* is a well established procedure, and has been done for several different tissue types [Gray et al., 1999; Whitehead and Robinson, 2009; Zeichner-David et al., 2003], including the inner ear in the past [Rivolta and Holley, 2002], where they have been observed to retain characterics of the native tissue [Nicholl et al., 2005; Helyer et al., 2007].

The *Gata3 Egfp* mouse carries a Bacterial Artificial Chromosome (BAC)-modified *Gata3* locus, where the first exon of the gene has been replaced by *Egfp* [Panayi et al., 2010], such that reporter activity is driven by the *Gata3* gene. The fidelity of expression of *Enhanced Green Fluorescent Protein (EGFP)* to mirror endogenous *Gata3* expression has never been studied.

We chose to derive cells at embryonic day E10.5, as this is an appropriate stage for cells that express *Gata3* prior to hair cell differentiation [Helyer et al., 2007].

6.2 Results

6.2.1 *Gata3egfp* reporter mouse recapitulates expected Gata3 expression

At E10.5, the earliest stage investigated, strong *Egfp* expression was observed in the midline dorsal aorta, somites and in the mesonephric ridge (Figure 6-1D). Distinct expression was noted in endothelial cells around the region of the neural lumen and the neurons of the central nervous system (Figure 6-1B). On either side of the floorplate in the rhombomere 4 region of the medulla, EGFP-positive neurons were seen to extend laterally (Figure 6-1A). Fibres were seen to also cross the floorplate at this stage. The otic vesicle (Figure 6-1C) and lens of the eye (Figure 6-1E) both expressed *gfp*.

At E12.5, in cross sections of the embryo heads, we noted significant *Egfp* expression in the mesencephalon (Figure 6-2C). More caudally, two bilaterally symmetric groups of neurons were positive for *Egfp* in the pons and the diencephalon (Figure 6-2D). At this stage the vomeronasal organ (Figure 6-2E) and lens of the eye (Figure 6-2A) also showed strong *Egfp* expression. The organ of Corti and the spiral ganglion neurons were strongly labelled (Figure 6-2B). Figure 6-2F is an image of the whole head of the embryo showing expression in the olfactory region, lens, midbrain, hindbrain and spinal cord.

At E14.5, *Egfp* expression was found to be similar to E12.5. Expression was noted in GABAergic neurons in the pons , trigeminal ganglion (Figure 6-3B) and the ventral aspect of the spinal cord (Figure 6-3A). The thyroid glands were seen to be *Egfp*-expressing as well (Figure 6-3C). Interestingly, the muscle of the tongue was positive for *Egfp* at this stage (Figure 6-3D). Expression persisted in the vomeronasal organ (Figure 6-3E) of the olfactory region. The organ of Corti and

spiral ganglion neurons (Figure 6-3F) remained positive for *Egfp*.

At E16.5, *Egfp* expression was observed in the diencephalon, pons (Figure 6-4A), the spinal cord, organ of Corti and associated spiral ganglion neurons (Figure 6-5B-E). Expression in the lens (Figure 6-4B), tongue (Figure 6-4D) and olfactory region (Figure 6-4E) persisted. Very strong expression was noted in the thymus (Figure 6-4C), and expression in hair follicles of the whiskers (Figure 6-5A and 6-4D) was also detected.

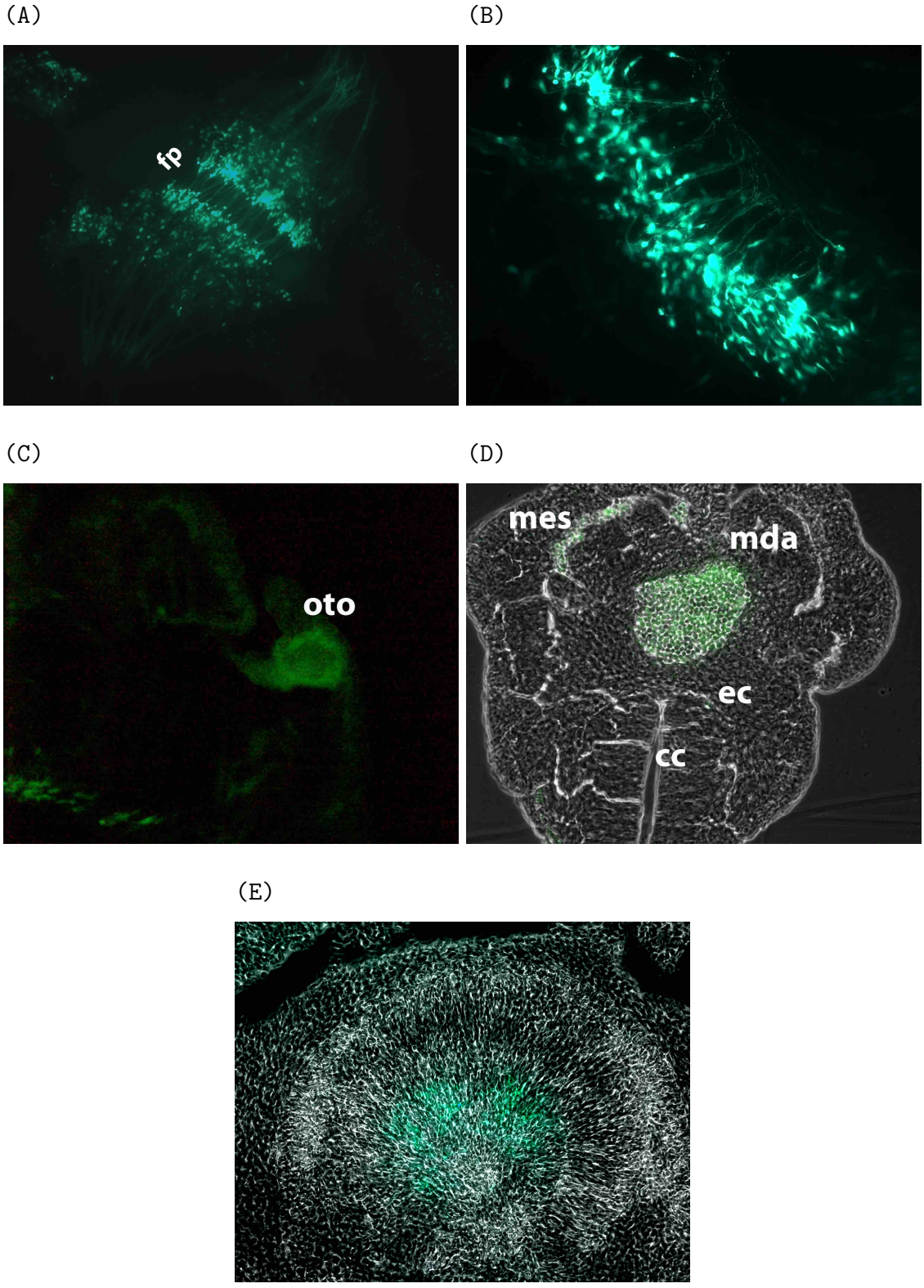

Figure 6-1: Expression of *Egfp* in E10.5 *Gata3 Egfp* mouse embryos. (A-C, E) GFP fluorescence is observed in unfixed preparations of tissue in the medullary raphae where neural fibres are seen to cross the floorplate (fp; A), CNS neurons (B), otocyst (oto; C) and lens of the eye (E). (D) Transverse section through the embryo shows GFP fluorescence in the midline dorsal aorta (mda), mesonephric duct (mes) and in endothelial cells (ec) surrounding the neural tube. cc: central canal.

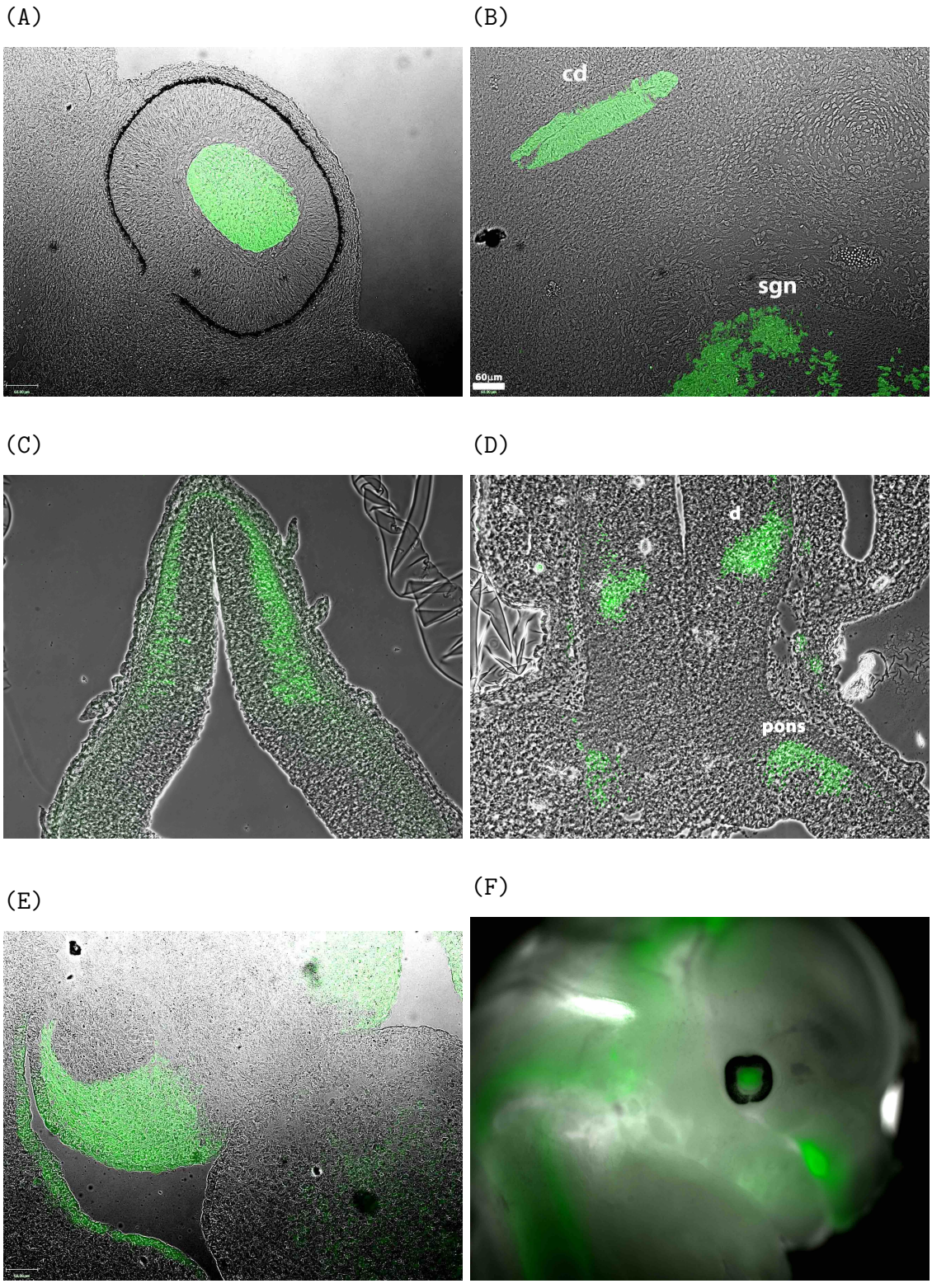

Figure 6-2: Expression of *Egfp* in E12.5 *Gata3 Egfp* mouse embryos. (A-E) GFP fluorescence is observed in transverse sections through the embryo in the lens (A); cochlear duct (cd) and spiral ganglion neurons (sgn; B); outer half of the mesencephalon (C); diencephalon (d) and pons (D) and the vomeronasal organ (vno; E). (F) Whole head of the *Gata3 Egfp* embryo showing EGFP in the eye, olfactory region, brain and spinal cord.

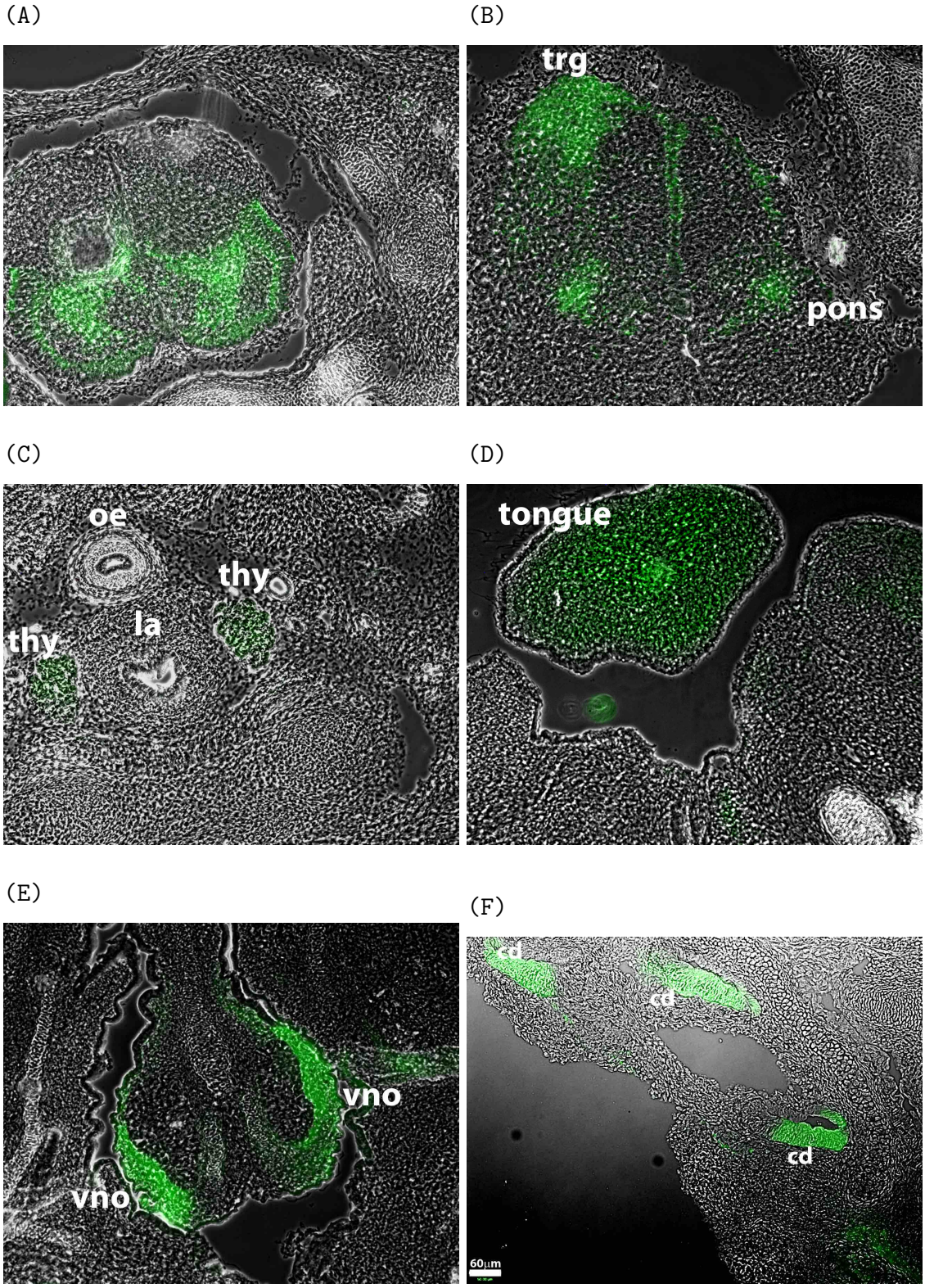

Figure 6-3: Expression of *Egfp* in E14.5 *Gata3 Egfp* mouse embryos. GFP fluorescence is observed in transverse sections through the embryo in the ventral spinal cord (A); trigeminal ganglion (trg) and pons (B); thyroid glands (thy; C); tongue (D) vomeronasal organ (vno; E); and the cochlear duct (cd) within the organ of Corti (F). oe: oesophagus; la: laryngeal aditus

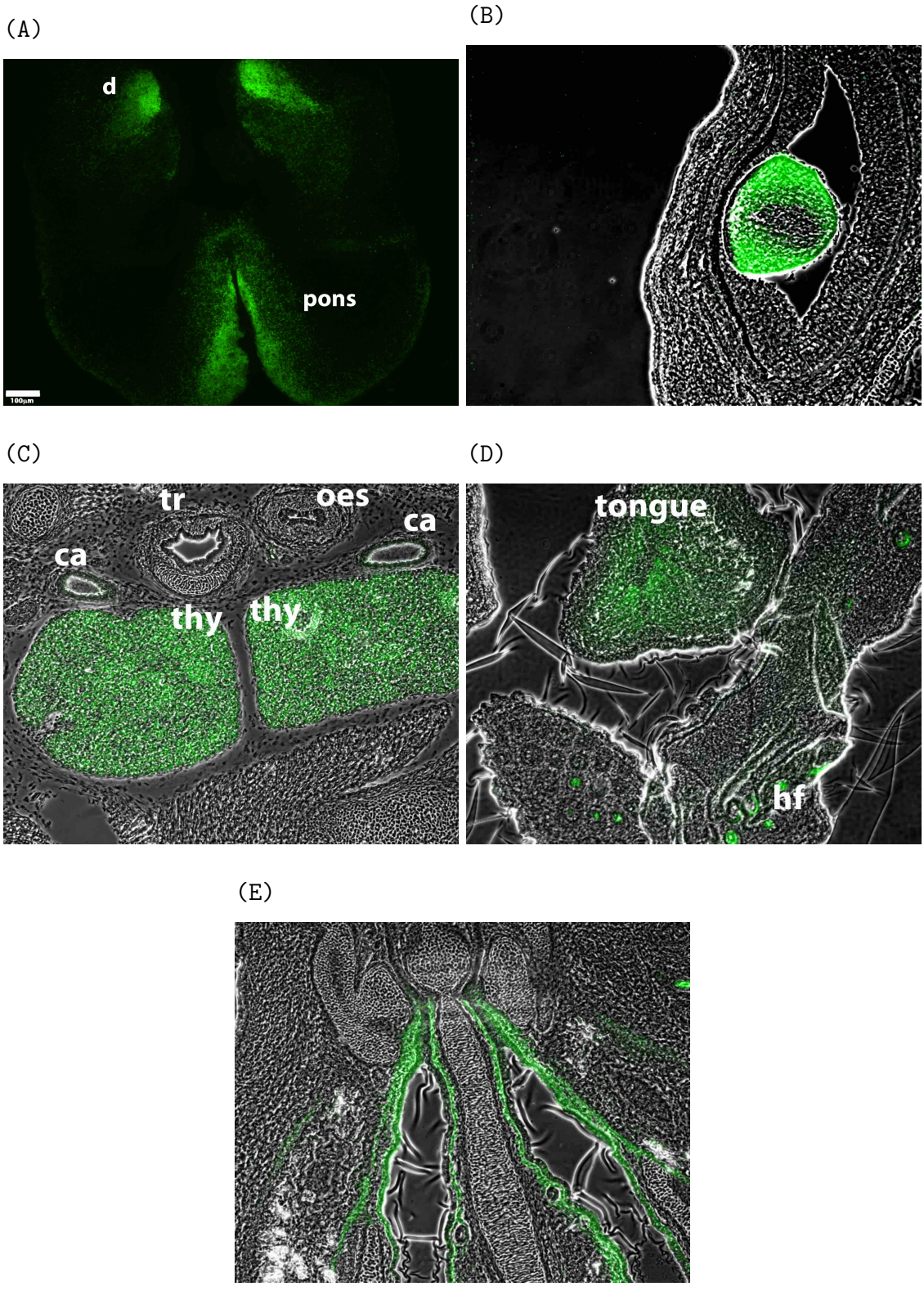

Figure 6-4: Expression of *Egfp* in E16.5 *Gata3 Egfp* mouse embryos. GFP fluorescence is observed in transverse sections through the embryo in the junctional region between the midbrain and pons, and more rostrally in the diencephalon (d; A); lens of the eye (B); thymus (thy) and carotid arteries (ca; C); tongue and hair follicles (hf; D); and the serous tubules of olfactory epithelium (E). oes: oesophagus; tr: trachea

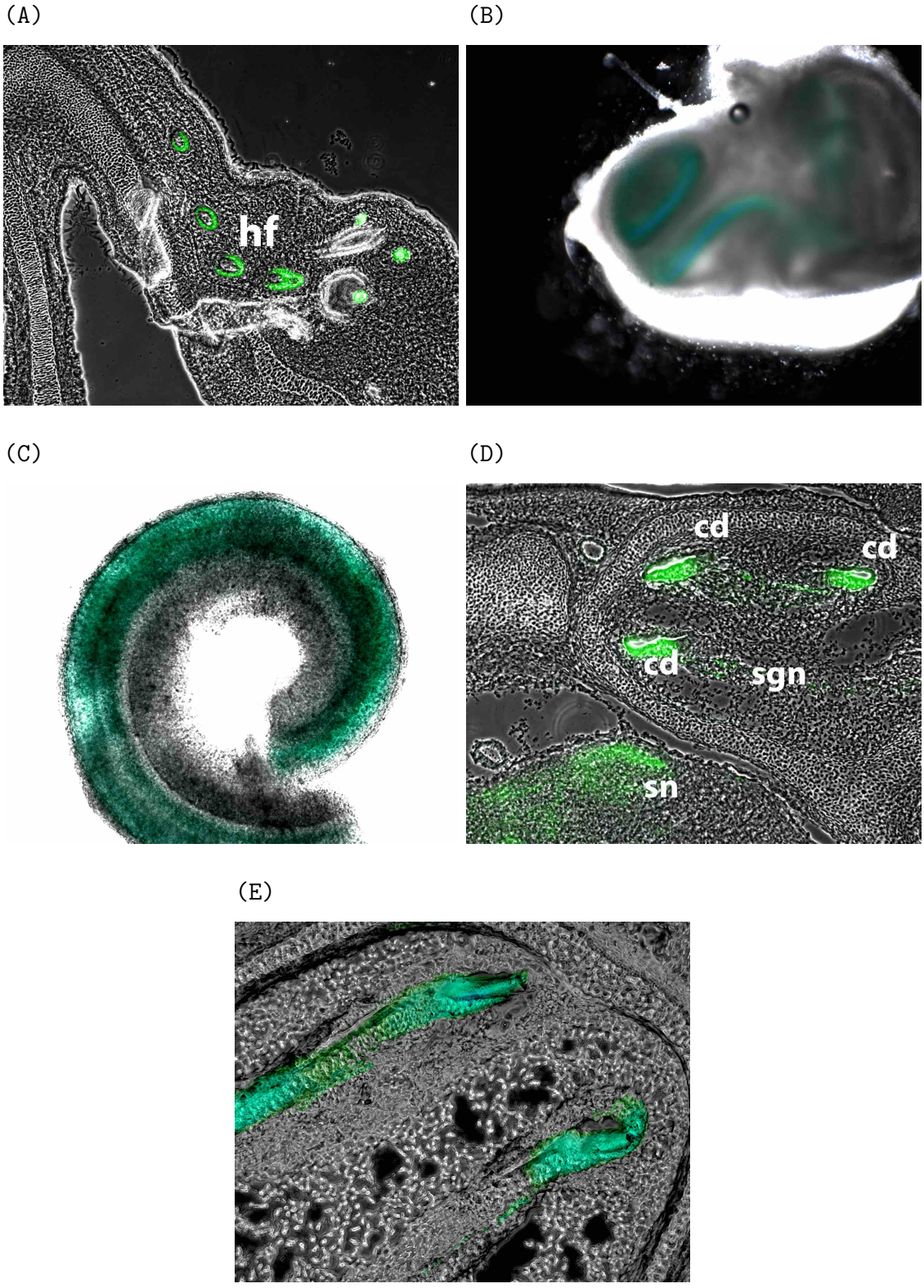

Figure 6-5: Expression of *Egfp* in E16.5 *Gata3 Egfp* mouse embryos (contd..) (A-D) *Egfp* is expressed in the hair follicles (hf) of the whiskers(A); observed in the gross dissection of the cochleo-vestibular apparatus (B); unfixed preparation of the organ of Corti (C); cochlear ducts (cd), spiral ganglion neurons (sgn) and spinal neurons (sn). (E) Magnified view of the floor of the cochlear duct.

6.2.2 *Gata3 Egfp* reporter mouse X *Immortomouse* crosses

Breeding pairs of *Gata3 Egfp* and *Immortomouse* transgenic mice were established. *Gata3 Egfp* mice were homozygous for the *Egfp* transgene and the *Immortomouse* were either homozygous or heterozygous for the *T Antigen*. Therefore all offspring were expected to be heterozygous for *Egfp* while the inheritance of the *T Antigen* was expected to be gender-dependant [Kern, 2005].

Homozygous and heterozygous females for the *T Antigen* gene often demonstrated poor health, reduced fertility and decreased lifespan. As a result, we switched to using only heterozygous *Immortomouse* males and *Gata3 Egfp* females for the breeding routine. While the *Gata3 Egfp* mice efficiently interbred amongst themselves, the same was not found to be true for the cross breeding. We often had to wait for several weeks to detect a pregnancy.

6.2.3 Establishment of the *Gata3 Egfp* reporter cell line

Cells derived directly from the embryos displayed a range of morphological characteristics. Some showed evidence of epithelial properties - regular flat polygonal shapes with distinct borders closely associated with other such cells, forming isolated colonies, which quickly grew as large sheets. Others showed more neural form - multipolar or bipolar projections from a distinct cell body.

After dissecting 15 embryos at E10.5, 8 embryos at E11.5, 10 embryos at E12.5, 9 embryos at E13.5 and 11 embryos at E16.5, a few of them were discarded due to insufficient growth. The remainder were expanded and frozen down, and can be recovered at any time. One animal (animal number 2) from E10.5 was chosen for subsequent derivation of clones. Several attempts were made to derive clones from this animal by the limiting dilution method and FACS, but were all unsuccessful. The main difficulties were that the cells either did not grow well enough or the

population was too heterogenous. We then tested different media for expansion of the cells: MEM (Gibco UK), F12 (Gibco, UK), Neurobasal medium (Gibco, UK) and Ultraculture (Sartorius Stedim Biotech, UK).

Ultraculture medium, supplemented with rock kinase inhibitor and 10% FCS allowed cells to proliferate, survive and then be dilution cloned. 10 clones were finally derived, out of which one expressed *Egfp* at a high level (clone 5; Figure 6-7) and another expressed low *Egfp* levels but looked more clonal (clone 11; Figure 6-6).

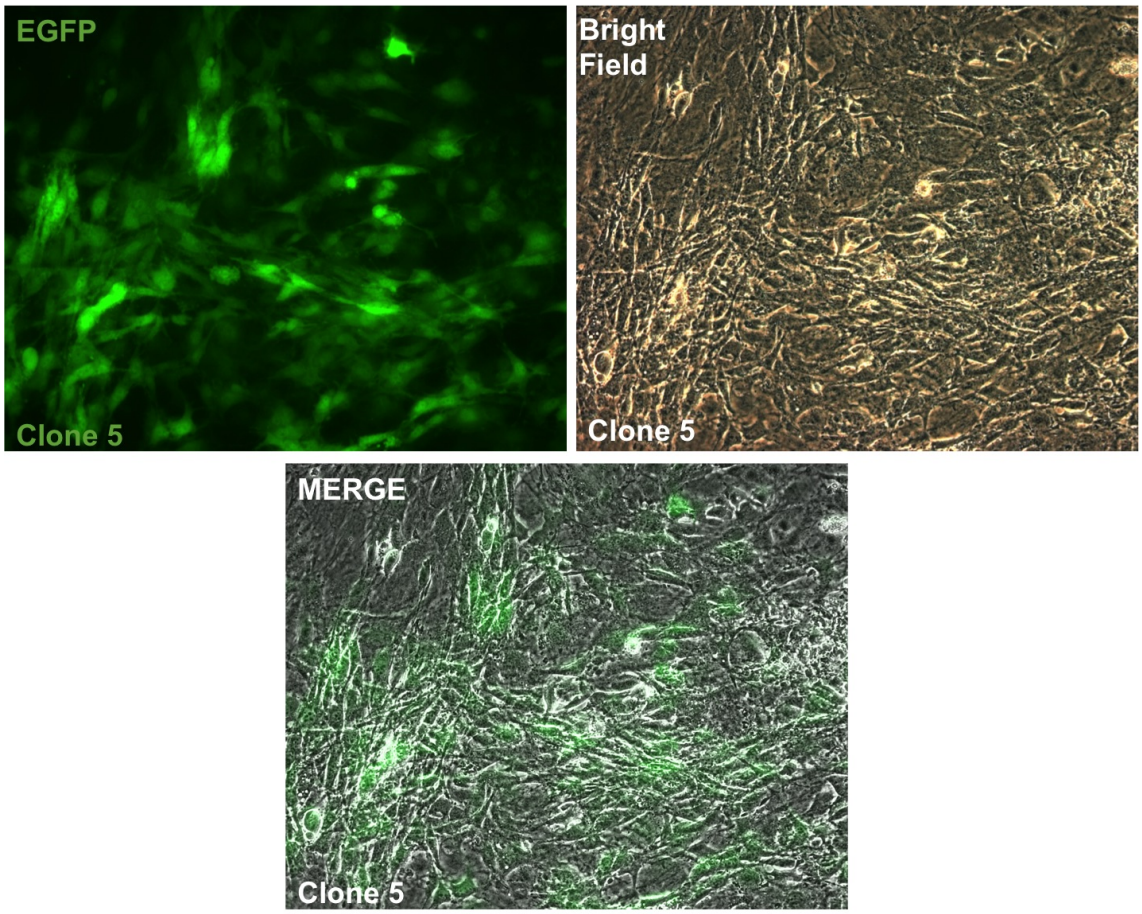

Figure 6-6: Clone expressing high levels of *Egfp*
Endogenous EGFP fluorescence from clone 5, expressing high levels of *Egfp*

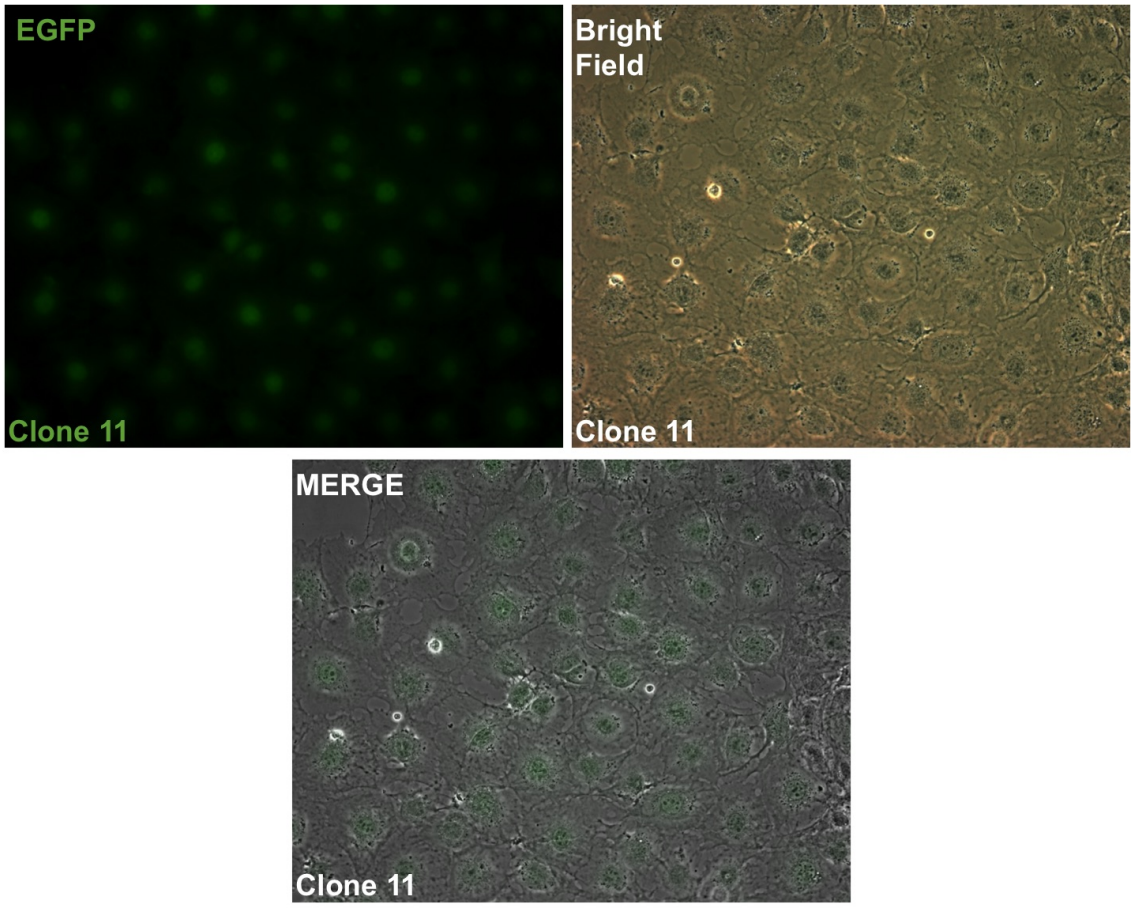

Figure 6-7: Clone expressing low levels of *Egfp*
Endogenous EGFP fluorescence from clone 11, expressing low levels of *Egfp*

6.2.4 Characterising the *Gata3 Egfp* reporter cell line

The two most important factors that required investigation were the correlation between *Gata3* expression and the reporter (EGFP) signal, and the expression of *T Antigen*. EGFP expression appeared to faithfully correlate with GATA3 (Figure 6-8). These cells also expressed *T Antigen* (Figure 6-9).

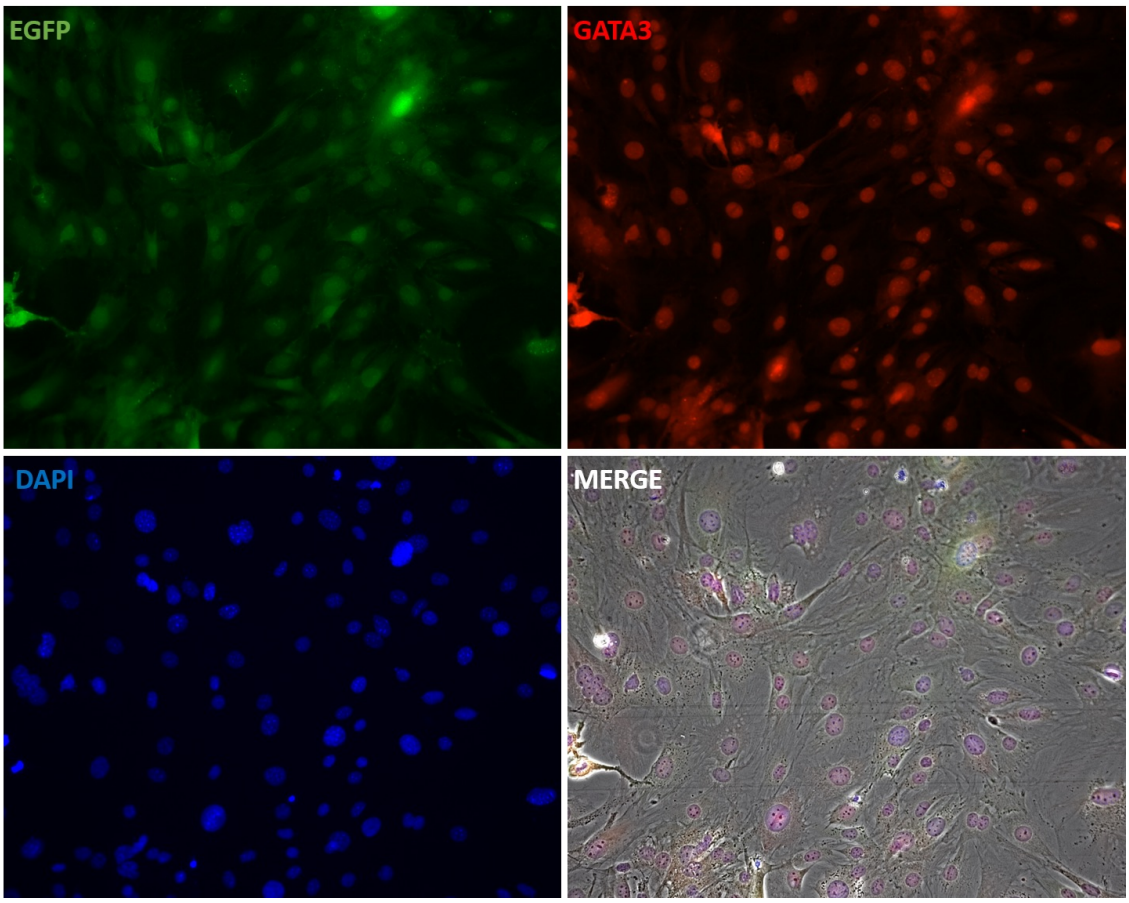

Figure 6-8: *Egfp* expression correlates with the expression of *Gata3*
The green panel shows cells immunolabelled with anti-Egfp antibody, the red panel with anti-Gata3 antibody, the blue panel with DAPI and the last panel shows a merge of the three channels. *Egfp* expression correlates with that of *Gata3*.

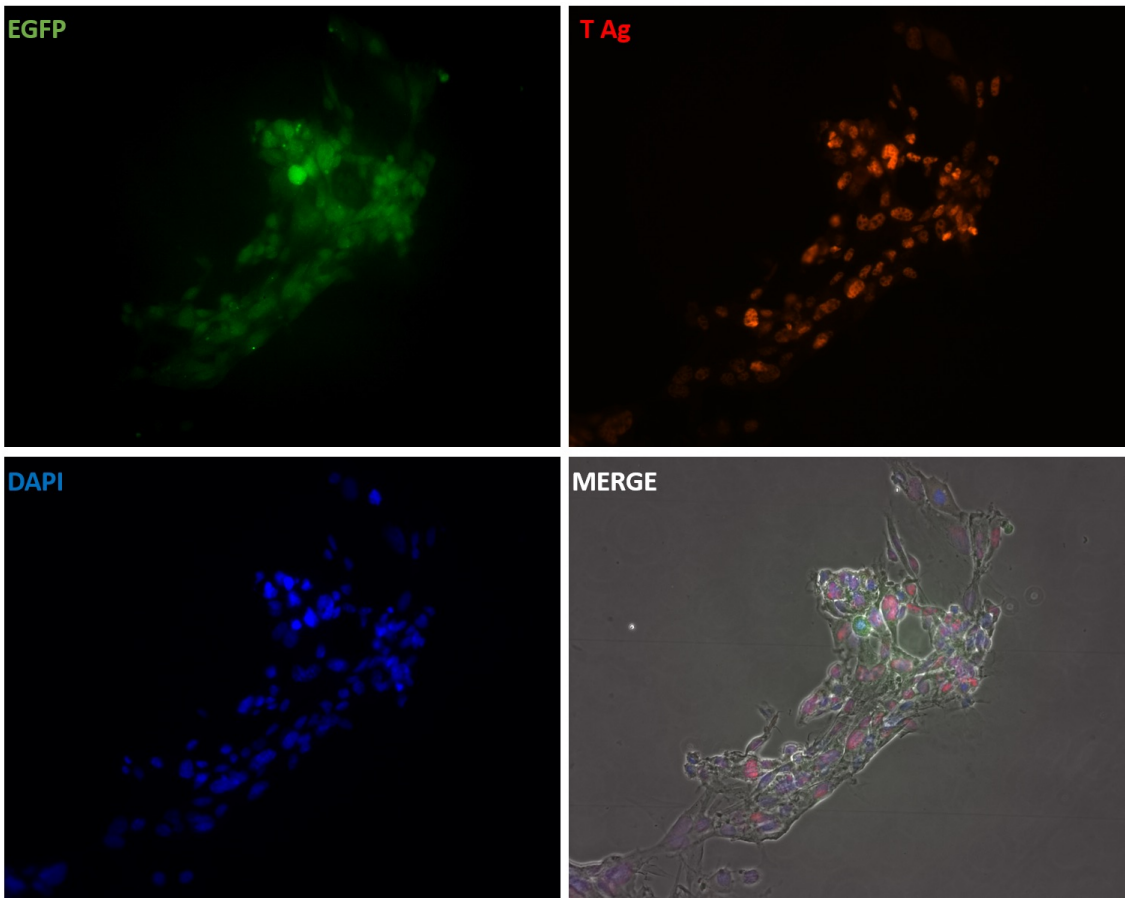

Figure 6-9: Expression of *T Antigen*
Cell lines expressed EGFP as well as T Antigen. EGFP expression observed here was the native endogenous fluorescence from the reporter, while cells were labelled for the expression of *T Antigen*.

6.3 Discussion

6.3.1 *Gata3* reporter cell line reliably reports *Gata3* expression

A critical requirement for developing a *Gata3* reporter cell line was the faithful expression of *Egfp* to mirror *Gata3* expression. The homozygous *Gata3 Egfp* mouse had robust *Egfp* expression allowing for an easily detectable signal, evident in fresh tissue and cryosections. *Egfp* expression was observed in tissues (including the inner ear) that have previously been reported to express *Gata3* (Section 6.2.1), fulfiling an essential prerequisite of the reporter cell line derivation process [Debacker et al., 1999; George et al., 1994; Lieuw et al., 1997; Grote et al., 2006; Fuchs, 2007; Karis et al., 2001; Lawoko-Kerali et al., 2002; van der Wees et al., 1999]. EGFP fluorescence was observed to overlap with that of *Gata3* in our cell lines.

Offspring of *Gata3 Egfp* and *Immortomouse* mice, from which cell lines have been derived, carried only one copy of *Egfp* resulting in a reduction of signal strength. It is to be noted that *Gata3* expression is highly dynamic during these developmental stages (Section 1.5.3). A combination of these two factors resulted in the derivation of cells expressing different intensities of EGFP fluorescence (Figures 6-6 and 6-7, which persisted as long as the cells were passaged.

The immortalising gene is most effective if activated (by the right temperature and γ-interferon) before cells have carried out their final mitotic division [Ikram et al., 1994]. Our cell lines fulfilled the criterion of expressing the *T Antigen* which would allow cells to continue proliferating under the right culture conditions.

6.3.2 Uses of *Gata3* reporter cell line

The physiological and histological assays have detected two of the earliest discrepancies that arise as a consequence of *Gata3* manipulation: OHCs fail to survive from a very early age and IHC physiology is deregulated. The desired goal is to identify agents through a screen, using our cell lines as a model system, that would be able to rescue these detected phenotypes. For example, IL-4 has been shown to be able to upregulate *Gata3* expression in the blood system [Zhu et al., 2004]. Preliminary studies in our laboratory have indicated that the same holds true for auditory cell lines in culture. In the future, we plan to use IL-4 in our cell lines to observe for changes in *Egfp* expression as a readout of *Gata3* modulation. Additionally organotypic cultures derived from *Gata3 Egfp* mice can be incubated in the presence or absence of IL-4 to check for any obvious quantifiable differences. The ideal model system should be sensitive enough to detect changes and differences of expression between different cell types, distinct developmental stages and upon the application of different factors.

However, it is plausible that agents that may regulate *Gata3* in certain ways *in vivo* may not behave the same way in culture. A reasonable explanation for this is cell lines are essentially detached preparations from their host systems, causing the complete loss of intrinsic regulation from neighbouring tissues [Pan et al., 2009]. Also, variables introduced by culture conditions may negatively intervene with the normal processes as they occur *in vivo*. Another possibility could be that that the loss of the first exon of the *Gata3* gene during the designing of the transgenic mouse could contain essential elements vital for the activity of said agents. This is a potential limitation of our system.

Cell lines should ideally retain the endogenous properties of gene expression profiles of their parent cell populations at the time of their extraction. Defining not only

the identity of the source tissue, but also the developmental time frame of isolation would ensure that any information gleaned from such studies would reflect as closely as possible, the scenario *in vivo*, accounting for the fact that these investigations were made under more controlled culture conditions. In order to further set up cell lines as an effective model system, we need to be able to define and properly control most variables associated with it.

This study has been complicated by a few factors. We have encountered delays in the breeding program and have been unable to maintain several breeding pairs to compensate for breeding issues due to funding limitations. However, in principle we have cell lines that could be used a model system to screen for agents that could potentially modulate GATA3 levels in culture. Our dissection techniques could be further refined to use enzymes like collagenase and/or dispase to help separate the otic epithelia from the underlying connective tissue to allow for cleaner isolation of cells of interest.

Chapter 7

Conclusion

Through this study, I have provided the first novel insight of the role of *Gata3* in regulating HC function. Using two different but partially overlapping approaches, I have demonstrated that *Gata3*, in addition to its critical role in HC survival, is required for the complete physiological maturation of differentiated HCs.

A chronic and global inactivation of a single allele of the gene resulted in the perturbation of the normal complement of OHCs while not affecting their basolateral or transduction properties. Potassium ion conductances in IHCs, on the other hand, were misregulated, with reduction of the $I_{k,f}$ conductance being the more severely affected phenotype. $I_{k,n}$ was also affected, but to a more modest degree. The mechanism underlying the differential effects on the same ionic conductances (in the case of $I_{k,n}$) in the two sub-populations of HCs could potentially be explained by the distinct regulation of KCNQ4 channels [Chambard and Ashmore, 2005] in the two HC sub-types. These results could partially explain the basis of HL in HDR Syndrome.

Endogenous GATA3 protein levels are different in the two HC populations, being higher in IHCs than in OHCs [Milo et al., 2009]. While this could explain the differential effects of haploinsufficiency on the two cell types, it is also plausible that *Gata3* allelic switching, previously observed in the context of the immune system [Ku et al., 2015], allows the maturation of OHCs and IHCs to be managed

differentially. Stringent regulation of GATA3 levels is critical. GATA3 protein levels are different in the cell types, and so is the effect of having only a single copy of the gene.

In order to preclude the contribution of other cell types towards the resultant phenotypes observed in *Gata3* haploinsufficiency, we strategically partially or completely suppressed *Gata3* function in IHCs. $Otof^{Cre}$ was chosen to study the effects of manipulating *Gata3* levels in an IHC-specific manner. OHCs, inefficiently targeted by this system, were purposefully left out of this study to circumvent the influence of IHCs on their development [Jacques et al., 2007]. Contrary to our expectations, $Gata3^{+/\Delta}$ IHCs did not produce quantifiable differences, and were comparable to wild type controls. Phenotypes observed in $Gata3^{\Delta/\Delta}$ IHCs appeared to be reminiscent of $Gata3^{+/-}$ cells. $Gata3^{\Delta/\Delta}$ IHCs demonstrated an earlier phenotype with an impaired I_{k1} profile, the onset of which was developmentally delayed and thereafter not replaced by $I_{k,n}$. $I_{k,f}$ was reduced like in $Gata3^{+/-}$ IHCs. Although $Gata3^{+/-}$ and $Gata3^{+/\Delta}$ IHCs, both had one functional allele, they differed in terms of their membrane properties. A reasonable explanation for this is not only that $Gata3^{+/-}$ IHCs were subjected to a reduction of GATA3 levels in a tissue-wide manner, but perhaps more importantly from the very beginning of the gene expression. On the contrary, protein levels were reduced specifically in IHCs from $Gata3^{+/\Delta}$ animals, only after precursors and newly differentiated HCs had been exposed to wild type levels of GATA3 until E16. The $Gata3^{\Delta/\Delta}$ IHC phenotype is in a way a more exacerbated effect compared to the $Gata3^{+/-}$ IHCs, as *Gata3* was completely knocked out in these cells, albeit after E16. These investigations indicate *Gata3* has an important role in the complete functional maturation of IHCs, and this influence is in part exerted in the postnatal context, upto two weeks after the initial differentiation of HCs from the sensory epithelium, coinciding with the onset of hearing in most altricial rodents.

Although *Gata3* regulates different aspects of development during embryogenesis, a role for *Gata3* in the context of differentiated cells has been reported before. In mammary glands, *Gata3* is essential in maintaining the differentiated status of the lumenal epithelium [Kouros-Mehr et al., 2006], and has a similar role in adult prostate glands [Nguyen et al., 2013]. In both cases, loss of expression of *Gata3* is correlated with de-differentiation of the tissue and progression to cancerous states [Dydensborg et al., 2009; Nguyen et al., 2013]. In the immune system, not only is it required for the development of T-helper cells, but its maintenance is essential to sustain the differentiated phenotype of these cells [Pai et al., 2004]. There is evidence that *Gata3* can act as a 'pioneer' transcription factor in order to remodel inaccessible regions of chromatin, to effect cellular reprogramming [Takaku et al., 2016], a mechanistic insight into its role in metastatic cancer. These examples indicate that the multiple functions mediated by *Gata3* is highly context-driven, being dependent upon its temporal activation and molecular environment.

Given that *Gata3* regulates diverse processes in multiple tissue systems at different stages of maturation, it is plausible to suggest that it mediates its effects through a common signaling pathway, which in turn has multiple targets. It has been postulated that *Gata3* acts via the Protein Kinase B (PKB) or Akt signalling pathway in order to exert its effects [Milo et al., 2009]. Downregulation of *Gata3* correlates inversely with Akt pathway activation in otic epithelial cells [Milo et al., 2009]. This pathway is known to govern several key processes like apoptosis, survival, proliferation, metabolism, growth, etc.[Manning and Cantley, 2007], and its components are widely expressed, including in the inner ear [Brand et al., 2015].

In the future, the *Gata3 Egfp* cell line can be used a tool to elucidate the signaling pathway/s that *Gata3* might interact with in the auditory epithelium. It can be exploited as a potent means to reveal its downstream molecular targets. In the context of the inner ear, *Gata3* shares similarities with *Pten*, not only as a

suppressor of Akt pathway activation but also as a tumour suppressor in several forms of cancer [Dydensborg et al., 2009; Yan et al., 2010]. The link between *Gata3* and Akt pathway has also been demonstrated in the context of prostrate cancers [Nguyen et al., 2013].

The *modus operandi* of *Gata3* is likely to be of a complex nature, given its diverse roles and molecular targets. The variable nature of the penetrance of the pathophysiological symptoms of HDR syndrome could be in part due to the myriad mutations in the gene (Section 1.5.7), with more being discovered on a regular basis; but could also be because of a stable non-stochastic mono-allelic to bi-allelic transcriptional switch, like in the case of T helper cells in the thymus [Ku et al., 2015].

Finally, its is attractive to speculate that the comprehensive deregulation of ionic conductances that we have observed due to a deficiency of *Gata3*, is due to perturbed calcium homeostasis in HCs. Possible factors underlying this have been suggested in Section 5.3, and would be interesting to test experimentally. Interestingly, PIP2 is a component of the Akt signalling pathway.

Ideally, I would have liked to supplement the information presented here with deletion of *Gata3* from HCs and supporting cells in a mutually exclusive manner by using the relevant *Cre* lines. However, identification and import of appropriate *Cre* drivers have proved to be challenging. Dissection of the role of *Gata3* in the organ of Corti has to be executed in several parts, due to the different cells types, their inter-dependence, and its dynamic temporal profile in them. An inducible system which allows inactivation of *Gata3* function from the different cell types, at different time-points, in a mutually exclusive fashion, would provide the most information about its possibly background-dependent evolving role in the epithelium, in the context of development, growth, survival, differentiation and function of the cell types in

question.

Bibliography

[Abba et al., 2006] Abba, M. C., Nunez, M. I., Colussi, A. G., Croce, M. V., Segal-Eiras, A., and Aldaz, C. M. (2006). Gata3 protein as a muc1 transcriptional regulator in breast cancer cells. *Breast Cancer Res*, 8(6):R64.

[Ali et al., 2007] Ali, A., Christie, P. T., Grigorieva, I. V., Harding, B., Van Esch, H., Ahmed, S. F., Bitner-Glindzicz, M., Blind, E., Bloch, C., Christin, P., et al. (2007). Functional characterization of gata3 mutations causing the hypoparathyroidism-deafness-renal (hdr) dysplasia syndrome: insight into mechanisms of dna binding by the gata3 transcription factor. *Human molecular genetics*, 16(3):265–275.

[Allen et al., 1997] Allen, V., Swigart, P., Cheung, R., Cockroft, S., and Katan, M. (1997). Regulation of inositol lipid-specific phospholipase cδ by changes in ca2+ ion concentrations. *Biochemical Journal*, 327(2):545–552.

[Alzahrani et al., 2015] Alzahrani, M., Tabet, P., and Saliba, I. (2015). Pediatric hearing loss: common causes, diagnosis and therapeutic approach. *Minerva pediatrica*, 67(1):75–90.

[Anniko, 1983] Anniko, M. (1983). Cytodifferentiation of cochlear hair cells. *American journal of otolaryngology*, 4(6):375–388.

[Anttonen et al., 2014] Anttonen, T., Belevich, I., Kirjavainen, A., Laos, M., Brakebusch, C., Jokitalo, E., and Pirvola, U. (2014). How to bury the dead: Elimination of apoptotic hair cells from the hearing organ of the mouse. *Journal of the Association for Research in Otolaryngology*, pages 1–18.

[Appler et al., 2013] Appler, J. M., Lu, C. C., Druckenbrod, N. R., Yu, W.-M., Koundakjian, E. J., and Goodrich, L. V. (2013). Gata3 is a critical regulator of cochlear wiring. *The Journal of Neuroscience*, 33(8):3679–3691.

[Aronson et al., 2014] Aronson, B. E., Stapleton, K. A., and Krasinski, S. D. (2014). Role of gata factors in development, differentiation, and homeostasis of the small intestinal epithelium. *American Journal of Physiology-Gastrointestinal and Liver Physiology*, 306(6):G474–G490.

[Ashmore, 1987] Ashmore, J. (1987). A fast motile response in guinea-pig outer hair cells: the cellular basis of the cochlear amplifier. *The Journal of Physiology*, 388:323.

[Asmar et al., 2008] Asmar, J., Biryukova, I., and Heitzler, P. (2008). Drosophila dlmo-pa isoform acts as an early activator of achaete/scute proneural expression. *Developmental biology*, 316(2):487–497.

[Atkinson et al., 2014] Atkinson, P. J., Wise, A. K., Flynn, B. O., Nayagam, B. A., and Richardson, R. T. (2014). Hair cell regeneration after atoh1 gene therapy in the cochlea of profoundly deaf adult guinea pigs. *PloS one*, 9(7):e102077.

[Bermingham et al., 1999] Bermingham, N. A., Hassan, B. A., Price, S. D., Vollrath, M. A., Ben-Arie, N., Eatock, R. A., Bellen, H. J., Lysakowski, A., and Zoghbi, H. Y. (1999). Math1: an essential gene for the generation of inner ear hair cells. *Science*, 284(5421):1837–1841.

[Beurg et al., 2008] Beurg, M., Safieddine, S., Roux, I., Bouleau, Y., Petit, C., and Dulon, D. (2008). Calcium-and otoferlin-dependent exocytosis by immature outer hair cells. *The Journal of Neuroscience*, 28(8):1798–1803.

[Bilous et al., 1992] Bilous, R. W., Murty, G., Parkinson, D. B., Thakker, R. V., Coulthard, M. G., Burn, J., Mathias, D., and Kendall-Taylor, P. (1992). Autosomal dominant familial hypoparathyroidism, sensorineural deafness, and renal dysplasia. *New England Journal of Medicine*, 327(15):1069–1074.

[Bok et al., 2007] Bok, J., Chang, W., and Wu, D. K. (2007). Patterning and morphogenesis of the vertebrate inner ear. *International Journal of Developmental Biology*, 51(6/7):521.

[Bossard and Zaret, 1998] Bossard, P. and Zaret, K. S. (1998). Gata transcription factors as potentiators of gut endoderm differentiation. *Development*, 125(24):4909–4917.

[Brand et al., 2015] Brand, Y., Levano, S., Radojevic, V., Naldi, A. M., Setz, C., Ryan, A. F., Pak, K., Hemmings, B. A., and Bodmer, D. (2015). All akt isoforms (akt1, akt2, akt3) are involved in normal hearing, but only akt2 and akt3 are involved in auditory hair cell survival in the mammalian inner ear. *PloS one*, 10(3):e0121599.

[Brignull et al., 2009] Brignull, H. R., Raible, D. W., and Stone, J. S. (2009). Feathers and fins: non-mammalian models for hair cell regeneration. *Brain research*, 1277:12–23.

[Bryant et al., 2002] Bryant, J., Goodyear, R. J., and Richardson, G. P. (2002). Sensory organ development in the inner ear: molecular and cellular mechanisms. *British medical bulletin*, 63(1):39–57.

[Chambard and Ashmore, 2005] Chambard, J.-M. and Ashmore, J. (2005). Regulation of the voltage-gated potassium channel kcnq4 in the auditory pathway. *Pflügers Archiv*, 450(1):34–44.

[Chen et al., 2002] Chen, P., Johnson, J. E., Zoghbi, H. Y., and Segil, N. (2002). The role of math1 in inner ear development: Uncoupling the establishment of the sensory primordium from hair cell fate determination. *Development*, 129(10):2495–2505.

[Chen et al., 2012] Chen, Y., Bates, D. L., Dey, R., Chen, P.-H., Machado, A. C. D., Laird-Offringa, I. A., Rohs, R., and Chen, L. (2012). Dna binding by gata transcription factor suggests mechanisms of dna looping and long-range gene regulation. *Cell reports*, 2(5):1197–1206.

[Coate and Kelley, 2013] Coate, T. M. and Kelley, M. W. (2013). Making connections in the inner ear: recent insights into the development of spiral ganglion neurons and their connectivity with sensory hair cells. In *Seminars in cell & developmental biology*, volume 24, pages 460–469. Elsevier.

[Cole et al., 2000] Cole, L. K., Le Roux, I., Nunes, F., Laufer, E., Lewis, J., and Wu, D. K. (2000). Sensory organ generation in the chicken inner ear: contributions of bone morphogenetic protein 4, serrate1, and lunatic fringe. *Journal of Comparative Neurology*, 424(3):509–520.

[Corns et al., 2014] Corns, L. F., Johnson, S. L., Kros, C. J., and Marcotti, W. (2014). Calcium entry into stereocilia drives adaptation of the mechanoelectrical transducer current of mammalian cochlear hair cells. *Proceedings of the National Academy of Sciences*, 111(41):14918–14923.

[Dabdoub et al., 2008] Dabdoub, A., Puligilla, C., Jones, J. M., Fritzsch, B., Cheah, K. S., Pevny, L. H., and Kelley, M. W. (2008). Sox2 signaling in prosensory domain specification and subsequent hair cell differentiation in the developing cochlea. *Proceedings of the National Academy of Sciences*, 105(47):18396–18401.

[Dallos and Evans, 1995] Dallos, P. and Evans, B. N. (1995). High-frequency motility of outer hair cells and the cochlear amplifier. *Science*, 267(5206):2006–2009.

[Dallos et al., 2008] Dallos, P., Wu, X., Cheatham, M. A., Gao, J., Zheng, J., Anderson, C. T., Jia, S., Wang, X., Cheng, W. H., Sengupta, S., et al. (2008). Prestin-based outer hair cell motility is necessary for mammalian cochlear amplification. *Neuron*, 58(3):333–339.

[Dallos et al., 2006] Dallos, P., Zheng, J., and Cheatham, M. A. (2006). Prestin and the cochlear amplifier. *The Journal of physiology*, 576(1):37–42.

[Daniel, 2007] Daniel, E. (2007). Noise and hearing loss: a review. *Journal of School Health*, 77(5):225–231.

[Debacker et al., 1999] Debacker, C., Catala, M., and Labastie, M.-C. (1999). Embryonic expression of the human gata-3 gene. *Mechanisms of development*, 85(1):183–187.

[Driver and Kelley, 2009] Driver, E. C. and Kelley, M. W. (2009). Specification of cell fate in the mammalian cochlea. *Birth Defects Research Part C: Embryo Today: Reviews*, 87(3):212–221.

[Duncan and Fritzsch, 2013] Duncan, J. S. and Fritzsch, B. (2013). Continued expression of gata3 is necessary for cochlear neurosensory development. *PloS one*, 8(4):e62046.

[Duncan et al., 2011] Duncan, J. S., Lim, K.-C., Engel, J. D., and Fritzsch, B. (2011). Limited inner ear morphogenesis and neurosensory development are possible in the absence of gata3. *International Journal of Developmental Biology*, 55(3):297.

[Dydensborg et al., 2009] Dydensborg, A., Rose, A., Wilson, B., Grote, D., Paquet, M., Giguere, V., Siegel, P., and Bouchard, M. (2009). Gata3 inhibits breast cancer growth and pulmonary breast cancer metastasis. *Oncogene*, 28(29):2634–2642.

[Echteler et al., 1989] Echteler, S. M., Arjmand, E., and Dallos, P. (1989). Developmental alterations in the frequency map of the mammalian cochlea.

[Edge and Chen, 2008] Edge, A. S. and Chen, Z.-Y. (2008). Hair cell regeneration. *Current opinion in neurobiology*, 18(4):377–382.

[Elgoyhen et al., 2001] Elgoyhen, A. B., Vetter, D. E., Katz, E., Rothlin, C. V., Heinemann, S. F., and Boulter, J. (2001). $\alpha 10$: a determinant of nicotinic cholinergic receptor function in mammalian vestibular and cochlear mechanosensory hair cells. *Proceedings of the National Academy of Sciences*, 98(6):3501–3506.

[Fettiplace and Fuchs, 1999] Fettiplace, R. and Fuchs, P. (1999). Mechanisms of hair cell tuning. *Annual review of physiology*, 61(1):809–834.

[Fettiplace and Hackney, 2006] Fettiplace, R. and Hackney, C. M. (2006). The sensory and motor roles of auditory hair cells. *Nature Reviews Neuroscience*, 7(1):19–29.

[Forge et al., 1993] Forge, A., Li, L., Corwin, J. T., and Nevill, G. (1993). Ultrastructural evidence for hair cell regeneration in the mammalian inner ear. *Science*, 259(5101):1616–1619.

[Freeland et al., 2010] Freeland, A., Jones, J., and Mohammed, N. K. (2010). Sensorineural deafness in tanzanian children is ototoxicity a significant cause? a pilot study. *International journal of pediatric otorhinolaryngology*, 74(5):516–519.

[Fuchs, 2007] Fuchs, E. (2007). Scratching the surface of skin development. *Nature*, 445(7130):834–842.

[Fujinami et al., 2012] Fujinami, Y., Mutai, H., Mizutari, K., Nakagawa, S., and Matsunaga, T. (2012). A novel animal model of hearing loss caused by acute endoplasmic reticulum stress in the cochlea. *Journal of pharmacological sciences*, 118(3):363–372.

[Fukai et al., 2013] Fukai, R., Ochi, N., Murakami, A., Nakashima, M., Tsurusaki, Y., Saitsu, H., Matsumoto, N., and Miyake, N. (2013). Co-occurrence of 22q11 deletion syndrome and hdr syndrome. *American Journal of Medical Genetics Part A*, 161(10):2576–2581.

[Fukui and Raphael, 2013] Fukui, H. and Raphael, Y. (2013). Gene therapy for the inner ear. *Hearing research*, 297:99–105.

[García-Bellido and de Celis, 2009] García-Bellido, A. and de Celis, J. F. (2009). The complex tale of the achaete–scute complex: a paradigmatic case in the analysis of gene organization and function during development. *Genetics*, 182(3):631–639.

[George et al., 1994] George, K. M., Leonard, M. W., Roth, M. E., Lieuw, K. H., Kioussis, D., Grosveld, F., and Engel, J. D. (1994). Embryonic expression and cloning of the murine gata-3 gene. *Development*, 120(9):2673–2686.

[Glowatzki and Fuchs, 2000] Glowatzki, E. and Fuchs, P. A. (2000). Cholinergic synaptic inhibition of inner hair cells in the neonatal mammalian cochlea. *Science*, 288(5475):2366–2368.

[Gomes et al., 2012] Gomes, T., Gortner, L., Dockter, G., Leitner, D., Thakker, R., and Rohrer, T. (2012). Hdr syndrome–a follow-up genotype-phenotype analysis of a de novo missense thr272ile mutation in exon 4 of gata3. *Klinische Pädiatrie*, 224(07):452–454.

[Gray et al., 1999] Gray, J., Grigoryan, G., Virley, D., Patel, S., Sinden, J., and Hodges, H. (1999). Conditionally immortalized, multipotential and multifunctional neural stem cell lines as an approach to clinical transplantation. *Cell transplantation*, 9(2):153–168.

[Gross et al., 2010] Gross, J., Stute, K., Moller, R., Fuchs, J., Amarjargal, N., Pohl, E. E., Angerstein, M., Smorodchenko, A., and Mazurek, B. (2010). Expression of prestin and gata-3,-2,-1 mrna in the rat organ of corti during the postnatal period and in culture. *Hearing research*, 261(1):9–21.

[Grote et al., 2006] Grote, D., Souabni, A., Busslinger, M., and Bouchard, M. (2006). Pax2/8-regulated gata3 expression is necessary for morphogenesis and guidance of the nephric duct in the developing kidney. *Development*, 133(1):53–61.

[Groves and Fekete, 2012] Groves, A. K. and Fekete, D. M. (2012). Shaping sound in space: the regulation of inner ear patterning. *Development*, 139(2):245–257.

[Guinan Jr, 2010] Guinan Jr, J. J. (2010). Cochlear efferent innervation and function. *Current opinion in otolaryngology & head and neck surgery*, 18(5):447.

[Hackney and Furness, 1995] Hackney, C. M. and Furness, D. N. (1995). Mechanotransduction in vertebrate hair cells: structure and function of the stereociliary bundle. *American Journal of Physiology-Cell Physiology*, 37(1):C1.

[Hafidi et al., 2005] Hafidi, A., Beurg, M., and Dulon, D. (2005). Localization and developmental expression of bk channels in mammalian cochlear hair cells. *Neuroscience*, 130(2):475–484.

[Haugas et al., 2012] Haugas, M., Lilleväli, K., and Salminen, M. (2012). Defects in sensory organ morphogenesis and generation of cochlear hair cells in¡ i¿ gata3¡/i¿-deficient mouse embryos. *Hearing research*, 283(1):151–161.

[Helyer et al., 2007] Helyer, R., Cacciabue-Rivolta, D., Davies, D., Rivolta, M., Kros, C., and Holley, M. (2007). A model for mammalian cochlear hair cell differentiation in vitro: effects of retinoic acid on cytoskeletal proteins and potassium conductances. *European Journal of Neuroscience*, 25(4):957–973.

[Hendriks et al., 1999] Hendriks, R. W., Nawijn, M. C., Engel, J. D., van Doorninck, H., Grosveld, F., and Karis, A. (1999). Expression of the transcription factor gata-3 is required for the development of the earliest t cell progenitors and correlates with stages of cellular proliferation in the thymus. *European journal of immunology*, 29(6):1912–1918.

[Ho et al., 2009] Ho, I.-C., Tai, T.-S., and Pai, S.-Y. (2009). Gata3 and the t-cell lineage: essential functions before and after t-helper-2-cell differentiation. *Nature Reviews Immunology*, 9(2):125–135.

[Hosoya et al., 2010] Hosoya, T., Maillard, I., and Engel, J. D. (2010). From the cradle to the grave: activities of gata-3 throughout t-cell development and differentiation. *Immunological reviews*, 238(1):110–125.

[Hudspeth, 2014] Hudspeth, A. (2014). Integrating the active process of hair cells with cochlear function. *Nature Reviews Neuroscience*, 15(9):600–614.

[Ikram et al., 1994] Ikram, Z., Norton, T., and Jat, P. S. (1994). The biological clock that measures the mitotic life-span of mouse embryo fibroblasts continues to function in the presence of simian virus 40 large tumor antigen. *Proceedings of the National Academy of Sciences*, 91(14):6448–6452.

[Izumikawa et al., 2005] Izumikawa, M., Minoda, R., Kawamoto, K., Abrashkin, K. A., Swiderski, D. L., Dolan, D. F., Brough, D. E., and Raphael, Y. (2005). Auditory hair cell replacement and hearing improvement by atoh1 gene therapy in deaf mammals. *Nature medicine*, 11(3):271–276.

[Jacques et al., 2007] Jacques, B. E., Montcouquiol, M. E., Layman, E. M., Lewandoski, M., and Kelley, M. W. (2007). Fgf8 induces pillar cell fate and regulates cellular patterning in the mammalian cochlea. *Development*, 134(16):3021–3029.

[Jagger et al., 2000] Jagger, D., Griesinger, C., Rivolta, M., Holley, M., and Ashmore, J. (2000). Calcium signalling mediated by the $\alpha 9$ acetylcholine receptor in a cochlear cell line from the immortomouse. *The Journal of physiology*, 527(1):49–54.

[Jiang et al., 2008] Jiang, S.-Y., Xu, M., and Zhang, Y.-Y. (2008). [role of gata-4 in cardiac development and remodeling]. *Sheng li ke xue jin zhan [Progress in physiology]*, 39(4):302–306.

[Johnson et al., 1997] Johnson, K. R., Erway, L. C., Cook, S. A., Willott, J. F., and Zheng, Q. Y. (1997). A major gene affecting age-related hearing loss in c57bl/6j mice. *Hearing research*, 114(1):83–92.

[Johnson et al., 2011a] Johnson, S. L., Beurg, M., Marcotti, W., and Fettiplace, R. (2011a). Prestin-driven cochlear amplification is not limited by the outer hair cell membrane time constant. *Neuron*, 70(6):1143–1154.

[Johnson et al., 2011b] Johnson, S. L., Eckrich, T., Kuhn, S., Zampini, V., Franz, C., Ranatunga, K. M., Roberts, T. P., Masetto, S., Knipper, M., Kros, C. J., et al. (2011b). Position-dependent patterning of spontaneous action potentials in immature cochlear inner hair cells. *Nature neuroscience*, 14(6):711–717.

[Johnson et al., 2008] Johnson, S. L., Forge, A., Knipper, M., Münkner, S., and Marcotti, W. (2008). Tonotopic variation in the calcium dependence of neurotransmitter release and vesicle pool replenishment at mammalian auditory ribbon synapses. *The Journal of Neuroscience*, 28(30):7670–7678.

[Johnson et al., 2012] Johnson, S. L., Kennedy, H. J., Holley, M. C., Fettiplace, R., and Marcotti, W. (2012). The resting transducer current drives spontaneous activity in prehearing mammalian cochlear inner hair cells. *The Journal of Neuroscience*, 32(31):10479–10483.

[Johnson et al., 2005] Johnson, S. L., Marcotti, W., and Kros, C. J. (2005). Increase in efficiency and reduction in ca2+ dependence of exocytosis during development of mouse inner hair cells. *The Journal of physiology*, 563(1):177–191.

[Johnson et al., 2013] Johnson, S. L., Wedemeyer, C., Vetter, D. E., Adachi, R., Holley, M. C., Elgoyhen, A. B., and Marcotti, W. (2013). Cholinergic efferent synaptic transmission regulates the maturation of auditory hair cell ribbon synapses. *Open biology*, 3(11):130163.

[Jones and Chen, 2007] Jones, C. and Chen, P. (2007). Planar cell polarity signaling in vertebrates. *Bioessays*, 29(2):120–132.

[Jones et al., 2006] Jones, J. M., Montcouquiol, M., Dabdoub, A., Woods, C., and Kelley, M. W. (2006). Inhibitors of differentiation and dna binding (ids) regulate math1 and hair cell formation during the development of the organ of corti. *The Journal of neuroscience*, 26(2):550–558.

[Kachar et al., 1985] Kachar, B., Brownell, W. E., Altschuler, R., and Fex, J. (1985). Electrokinetic shape changes of cochlear outer hair cells. *Nature*, 322(6077):365–368.

[Kachar et al., 2000] Kachar, B., Parakkal, M., Kurc, M., Zhao, Y.-d., and Gillespie, P. G. (2000). High-resolution structure of hair-cell tip links. *Proceedings of the National Academy of Sciences*, 97(24):13336–13341.

[Kaltenbach et al., 1994] Kaltenbach, J. A., Falzarano, P. R., and Simpson, T. H. (1994). Postnatal development of the hamster cochlea. ii. growth and differentiation of stereocilia bundles. *Journal of Comparative Neurology*, 350(2):187–198.

[Karis et al., 2001] Karis, A., Pata, I., van Doorninck, J. H., Grosveld, F., de Zeeuw, C. I., de Caprona, D., and Fritzsch, B. (2001). Transcription factor gata-3 alters

pathway selection of olivocochlear neurons and affects morphogenesis of the ear. *Journal of Comparative Neurology*, 429(4):615–630.

[Kazmierczak et al., 2007] Kazmierczak, P., Sakaguchi, H., Tokita, J., Wilson-Kubalek, E. M., Milligan, R. A., Müller, U., and Kachar, B. (2007). Cadherin 23 and protocadherin 15 interact to form tip-link filaments in sensory hair cells. *Nature*, 449(7158):87–91.

[Kelley, 2006] Kelley, M. W. (2006). Regulation of cell fate in the sensory epithelia of the inner ear. *Nature Reviews Neuroscience*, 7(11):837–849.

[Kelley et al., 1993] Kelley, M. W., Xu, X.-M., Wagner, M. A., Warchol, M. E., and Corwin, J. T. (1993). The developing organ of corti contains retinoic acid and forms supernumerary hair cells in response to exogenous retinoic acid in culture. *Development*, 119(4):1041–1053.

[Kern, 2005] Kern, F. (2005). Localization of transgenes and genotyping of h-2kb-tsa58 transgenic mice. *Biotechniques*, 38(1):38–42.

[Kharkovets et al., 2000] Kharkovets, T., Hardelin, J.-P., Safieddine, S., Schweizer, M., El-Amraoui, A., Petit, C., and Jentsch, T. J. (2000). Kcnq4, a k+ channel mutated in a form of dominant deafness, is expressed in the inner ear and the central auditory pathway. *Proceedings of the National Academy of Sciences*, 97(8):4333–4338.

[Khimich et al., 2005] Khimich, D., Nouvian, R., Pujol, R., tom Dieck, S., Egner, A., Gundelfinger, E. D., and Moser, T. (2005). Hair cell synaptic ribbons are essential for synchronous auditory signalling. *Nature*, 434(7035):889–894.

[Kiernan et al., 2001] Kiernan, A. E., Ahituv, N., Fuchs, H., Balling, R., Avraham, K. B., Steel, K. P., and de Angelis, M. H. (2001). The notch ligand jagged1 is required for inner ear sensory development. *Proceedings of the National Academy of Sciences*, 98(7):3873–3878.

[Kiernan et al., 2005] Kiernan, A. E., Pelling, A. L., Leung, K. K., Tang, A. S., Bell, D. M., Tease, C., Lovell-Badge, R., Steel, K. P., and Cheah, K. S. (2005). Sox2 is required for sensory organ development in the mammalian inner ear. *Nature*, 434(7036):1031–1035.

[Kong et al., 2008] Kong, J.-H., Adelman, J. P., and Fuchs, P. A. (2008). Expression of the sk2 calcium-activated potassium channel is required for cholinergic function in mouse cochlear hair cells. *The Journal of Physiology*, 586(22):5471–5485.

[Kouros-Mehr et al., 2006] Kouros-Mehr, H., Slorach, E. M., Sternlicht, M. D., and Werb, Z. (2006). Gata-3 maintains the differentiation of the luminal cell fate in the mammary gland. *Cell*, 127(5):1041–1055.

[Kros and Crawford, 1990] Kros, C. and Crawford, A. (1990). Potassium currents in inner hair cells isolated from the guinea-pig cochlea. *The Journal of Physiology*, 421(1):263–291.

[Kros et al., 1992] Kros, C., Rusch, A., and Richardson, G. (1992). Mechano-electrical transducer currents in hair cells of the cultured neonatal mouse cochlea. *Proceedings of the Royal Society of London B: Biological Sciences*, 249(1325):185–193.

[Kros et al., 1998] Kros, C. J., Ruppersberg, J. P., and Rüsch, A. (1998). Expression of a potassium current in inner hair cells during development of hearing in mice. *Nature*, 394(6690):281–284.

[Ku et al., 2015] Ku, C.-J., Lim, K.-C., Kalantry, S., Maillard, I., Engel, J. D., and Hosoya, T. (2015). A monoallelic-to-biallelic t-cell transcriptional switch regulates gata3 abundance. *Genes & development*, 29(18):1930–1941.

[Kubisch et al., 1999] Kubisch, C., Schroeder, B. C., Friedrich, T., Lütjohann, B., El-Amraoui, A., Marlin, S., Petit, C., and Jentsch, T. J. (1999). Kcnq4, a novel potassium channel expressed in sensory outer hair cells, is mutated in dominant deafness. *Cell*, 96(3):437–446.

[Kurt et al., 2012] Kurt, S., Sausbier, M., Rüttiger, L., Brandt, N., Moeller, C. K., Kindler, J., Sausbier, U., Zimmermann, U., van Straaten, H., Neuhuber, W., et al. (2012). Critical role for cochlear hair cell bk channels for coding the temporal structure and dynamic range of auditory information for central auditory processing. *The FASEB Journal*, 26(9):3834–3843.

[Lawlor et al., 1999] Lawlor, P., Marcotti, W., Rivolta, M. N., Kros, C. J., and Holley, M. C. (1999). Differentiation of mammalian vestibular hair cells from conditionally immortal, postnatal supporting cells. *The Journal of neuroscience*, 19(21):9445–9458.

[Lawoko-Kerali et al., 2002] Lawoko-Kerali, G., Rivolta, M. N., and Holley, M. (2002). Expression of the transcription factors gata3 and pax2 during development of the mammalian inner ear. *Journal of Comparative Neurology*, 442(4):378–391.

[Lawoko-Kerali et al., 2004] Lawoko-Kerali, G., Rivolta, M. N., Lawlor, P., Cacciabue-Rivolta, D. I., Langton-Hewer, C., Hikke van Doorninck, J., and Holley, M. C. (2004). Gata3 and neurod distinguish auditory and vestibular neurons during development of the mammalian inner ear. *Mechanisms of development*, 121(3):287–299.

[Lefebvre et al., 1993] Lefebvre, P. P., Malgrange, B., Staecker, H., Moonen, G., and Van de Water, T. R. (1993). Retinoic acid stimulates regeneration of mammalian auditory hair cells. *Science*, 260(5108):692–695.

[Liberman et al., 1990] Liberman, M. C., Dodds, L. W., and Pierce, S. (1990). Afferent and efferent innervation of the cat cochlea: quantitative analysis with light and electron microscopy. *Journal of comparative neurology*, 301(3):443–460.

[Liberman et al., 2002] Liberman, M. C., Gao, J., He, D. Z., Wu, X., Jia, S., and Zuo, J. (2002). Prestin is required for electromotility of the outer hair cell and for the cochlear amplifier. *Nature*, 419(6904):300–304.

[Lieuw et al., 1997] Lieuw, K. H., Li, G.-l., Zhou, Y., Grosveld, F., and Engel, J. D. (1997). Temporal and spatial control of murine gata-3 transcription by promoter-proximal regulatory elements. *Developmental biology*, 188(1):1–16.

[Lilleväli et al., 2006] Lilleväli, K., Haugas, M., Matilainen, T., Pussinen, C., Karis, A., and Salminen, M. (2006). Gata3 is required for early morphogenesis and fgf10 expression during otic development. *Mechanisms of development*, 123(6):415–429.

[Lilleväli et al., 2004] Lilleväli, K., Matilainen, T., Karis, A., and Salminen, M. (2004). Partially overlapping expression of gata2 and gata3 during inner ear development. *Developmental dynamics*, 231(4):775–781.

[Lim et al., 2000] Lim, K.-C., Lakshmanan, G., Crawford, S. E., Gu, Y., Grosveld, F., and Engel, J. D. (2000). Gata3 loss leads to embryonic lethality due to noradrenaline deficiency of the sympathetic nervous system. *Nature genetics*, 25(2):209–212.

[Liu et al., 2005] Liu, H., Corrales, C. E., Wang, Z., Zhao, Y., Wang, Y., Liu, H., and Heller, S. (2005). Bmp4 signaling is involved in the generation of inner ear sensory epithelia. *BMC developmental biology*, 5(1):1.

[Lonsbury-Martin et al., 1990] Lonsbury-Martin, B. L., Harris, F., Stagner, B., Hawkins, M., and Martin, G. (1990). Distortion product emissions in humans. i. basic properties in normally hearing subjects. *The Annals of otology, rhinology & laryngology. Supplement*, 147:3–14.

[Lu et al., 2013] Lu, N., Chen, Y., Wang, Z., Chen, G., Lin, Q., Chen, Z.-Y., and Li, H. (2013). Sonic hedgehog initiates cochlear hair cell regeneration through downregulation of retinoblastoma protein. *Biochemical and biophysical research communications*, 430(2):700–705.

[Luo et al., 2013] Luo, X.-j., Deng, M., Xie, X., Huang, L., Wang, H., Jiang, L., Liang, G., Hu, F., Tieu, R., Chen, R., et al. (2013). Gata3 controls the specification of prosensory domain and neuronal survival in the mouse cochlea. *Human molecular genetics*, 22(18):3609–3623.

[Maeda et al., 2009] Maeda, A., Moriguchi, T., Hamada, M., Kusakabe, M., Fujioka, Y., Nakano, T., Yoh, K., Lim, K.-C., Engel, J. D., and Takahashi, S. (2009). Transcription factor gata-3 is essential for lens development. *Developmental Dynamics*, 238(9):2280–2291.

[Maison et al., 2013] Maison, S. F., Pyott, S. J., Meredith, A. L., and Liberman, M. C. (2013). Olivocochlear suppression of outer hair cells in vivo: evidence for combined action of bk and sk2 channels throughout the cochlea. *Journal of neurophysiology*, 109(6):1525–1534.

[Manning and Cantley, 2007] Manning, B. D. and Cantley, L. C. (2007). Akt/pkb signaling: navigating downstream. *Cell*, 129(7):1261–1274.

[Marcotti, 2012] Marcotti, W. (2012). Functional assembly of mammalian cochlear hair cells. *Experimental physiology*, 97(4):438–451.

[Marcotti et al., 1999] Marcotti, W., Géléoc, G. S., Lennan, G. W., and Kros, C. J. (1999). Transient expression of an inwardly rectifying potassium conductance in developing inner and outer hair cells along the mouse cochlea. *Pflügers Archiv*, 439(1-2):113–122.

[Marcotti et al., 2003] Marcotti, W., Johnson, S. L., Holley, M. C., and Kros, C. J. (2003). Developmental changes in the expression of potassium currents of embryonic, neonatal and mature mouse inner hair cells. *The Journal of physiology*, 548(2):383–400.

[Marcotti et al., 2004a] Marcotti, W., Johnson, S. L., and Kros, C. J. (2004a). Effects of intracellular stores and extracellular ca2+ on ca2+-activated k+ currents in mature mouse inner hair cells. *The Journal of physiology*, 557(2):613–633.

[Marcotti et al., 2004b] Marcotti, W., Johnson, S. L., and Kros, C. J. (2004b). A transiently expressed sk current sustains and modulates action potential activity in immature mouse inner hair cells. *The Journal of physiology*, 560(3):691–708.

[Marcotti and Kros, 1999] Marcotti, W. and Kros, C. J. (1999). Developmental expression of the potassium current ik, n contributes to maturation of mouse outer hair cells. *The Journal of Physiology*, 520(3):653–660.

[Masuda et al., 2012] Masuda, M., Pak, K., Chavez, E., and Ryan, A. F. (2012). Tfe2 and gata3 enhance induction of pou4f3 and myosin viia positive cells in nonsensory cochlear epithelium by atoh1. *Developmental biology*, 372(1):68–80.

[Mejia et al., 2014] Mejia, J. D., Cervantes, L., Puerta, H., Bauer, M., and Diaz, A. (2014). Neonatal diagnosis of a patient with hypoparathyroidism, sensorineural deafness and renal dysplasia (hdr) syndrome associated with cerebral infarction. *Journal of Pediatric Endocrinology and Metabolism*.

[Mekahli et al., 2011] Mekahli, D., Bultynck, G., Parys, J. B., De Smedt, H., and Missiaen, L. (2011). Endoplasmic-reticulum calcium depletion and disease. *Cold Spring Harbor perspectives in biology*, 3(6):a004317.

[Mescher, 2010] Mescher, A. L. (2010). *Junqueira's basic histology: text & atlas*, volume 12. McGraw-Hill Medical New York.

[Middlebrooks and Green, 1991] Middlebrooks, J. C. and Green, D. M. (1991). Sound localization by human listeners. *Annual review of psychology*, 42(1):135–159.

[Milo et al., 2009] Milo, M., Cacciabue-Rivolta, D., Kneebone, A., Van Doorninck, H., Johnson, C., Lawoko-Kerali, G., Niranjan, M., Rivolta, M., and Holley, M. (2009). Genomic analysis of the function of the transcription factor gata3 during development of the mammalian inner ear. *PLoS One*, 4(9):e7144.

[Møller, 1974] Møller, A. R. (1974). The acoustic middle ear muscle reflex. In *Auditory system*, pages 519–548. Springer.

[Morsli et al., 1998] Morsli, H., Choo, D., Ryan, A., Johnson, R., and Wu, D. K. (1998). Development of the mouse inner ear and origin of its sensory organs. *The Journal of neuroscience*, 18(9):3327–3335.

[Nakamura et al., 2007] Nakamura, Y., Suzuki, T., and Sasano, H. (2007). Transcription factor gata-6 in the human adrenocortex: association with adrenal development and aging. *Endocrine journal*, 54(5):783–789.

[Nanba et al., 2013] Nanba, K., Usui, T., Nakamura, M., Toyota, Y., Hirota, K., Tamanaha, T., Kawashima, S.-T., Nakao, K., Yuno, A., Tagami, T., et al. (2013). A novel gata3 nonsense mutation in a newly diagnosed adult patient of hypoparathyroidism, deafness, and renal dysplasia (hdr) syndrome. *Endocrine Practice*, 19(1):e17–e20.

[Neher, 1992] Neher, E. (1992). [6] correction for liquid junction potentials in patch clamp experiments. *Methods in enzymology*, 207:123–131.

[Nguyen et al., 2013] Nguyen, A. H., Tremblay, M., Haigh, K., Koumakpayi, I. H., Paquet, M., Pandolfi, P. P., Mes-Masson, A.-M., Saad, F., Haigh, J. J., and Bouchard, M. (2013). Gata3 antagonizes cancer progression in pten-deficient prostates. *Human molecular genetics*, page ddt088.

[Nicholl et al., 2005] Nicholl, A., Kneebone, A., Davies, D., Cacciabue-Rivolta, D., Rivolta, M., Coffey, P., and Holley, M. (2005). Differentiation of an auditory neuronal cell line suitable for cell transplantation. *European Journal of Neuroscience*, 22(2):343–353.

[Nishida et al., 1998] Nishida, Y., Rivolta, M. N., and Holley, M. C. (1998). Timed markers for the differentiation of the cuticular plate and stereocilia in hair cells from the mouse inner ear. *The Journal of comparative neurology*, 395(1):18–28.

[Noramly and Grainger, 2002] Noramly, S. and Grainger, R. M. (2002). Determination of the embryonic inner ear. *Journal of neurobiology*, 53(2):100–128.

[Ohyama et al., 2006] Ohyama, T., Mohamed, O. A., Taketo, M. M., Dufort, D., and Groves, A. K. (2006). Wnt signals mediate a fate decision between otic placode and epidermis. *Development*, 133(5):865–875.

[Oliver et al., 2000] Oliver, D., Klöcker, N., Schuck, J., Baukrowitz, T., Ruppersberg, J. P., and Fakler, B. (2000). Gating of ca¡ sup¿ 2+¡/sup¿-activated k¡ sup¿+¡/sup¿ channels controls fast inhibitory synaptic transmission at auditory outer hair cells. *Neuron*, 26(3):595–601.

[Oliver et al., 2003] Oliver, D., Knipper, M., Derst, C., and Fakler, B. (2003). Resting potential and submembrane calcium concentration of inner hair cells in the isolated mouse cochlea are set by kcnq-type potassium channels. *The Journal of neuroscience*, 23(6):2141–2149.

[Oliver et al., 2006] Oliver, D., Taberner, A. M., Thurm, H., Sausbier, M., Arntz, C., Ruth, P., Fakler, B., and Liberman, M. C. (2006). The role of bkca channels in electrical signal encoding in the mammalian auditory periphery. *The Journal of neuroscience*, 26(23):6181–6189.

[Pai et al., 2004] Pai, S.-Y., Truitt, M. L., and Ho, I.-C. (2004). Gata-3 deficiency abrogates the development and maintenance of t helper type 2 cells. *Proceedings of the National Academy of Sciences of the United States of America*, 101(7):1993–1998.

[Pan et al., 2009] Pan, C., Kumar, C., Bohl, S., Klingmueller, U., and Mann, M. (2009). Comparative proteomic phenotyping of cell lines and primary cells to assess preservation of cell type-specific functions. *Molecular & Cellular Proteomics*, 8(3):443–450.

[Panayi et al., 2010] Panayi, H., Panayiotou, E., Orford, M., Genethliou, N., Mean, R., Lapathitis, G., Li, S., Xiang, M., Kessaris, N., Richardson, W. D., et al. (2010). Sox1 is required for the specification of a novel p2-derived interneuron subtype in the mouse ventral spinal cord. *The Journal of Neuroscience*, 30(37):12274–12280.

[Pandolfi et al., 1995] Pandolfi, P. P., Roth, M. E., Karis, A., Leonard, M. W., Dzierzak, E., Grosveld, F. G., Engel, J. D., and Lindenbaum, M. H. (1995). Targeted disruption of the gata3 gene causes severe abnormalities in the nervous system and in fetal liver haematopoiesis. *Nature genetics*, 11(1):40–44.

[Pangršič et al., 2012] Pangršič, T., Reisinger, E., and Moser, T. (2012). Otoferlin: a multi-c¡ sub¿ 2¡/sub¿ domain protein essential for hearing. *Trends in neurosciences*, 35(11):671–680.

[Pevny et al., 1995] Pevny, L., Lin, C.-S., D'Agati, V., Simon, M. C., Orkin, S. H., and Costantini, F. (1995). Development of hematopoietic cells lacking transcription factor gata-1. *Development*, 121(1):163–172.

[Pevny et al., 1991] Pevny, L., Simon, M. C., Robertson, E., Klein, W. H., Tsai, S.-F., D'Agati, V., Orkin, S. H., and Costantini, F. (1991). Erythroid differentiation in chimaeric mice blocked by a targeted mutation in the gene for transcription factor gata-1.

[Probst et al., 1991] Probst, R., Lonsbury-Martin, B. L., and Martin, G. K. (1991). A review of otoacoustic emissions. *The Journal of the Acoustical Society of America*, 89(5):2027–2067.

[Pujol et al., 1998] Pujol, R., Lavigne-Rebillard, M., and Lenoir, M. (1998). Development of sensory and neural structures in the mammalian cochlea. In *Development of the auditory system*, pages 146–192. Springer.

[Pyott et al., 2007] Pyott, S. J., Meredith, A. L., Fodor, A. A., Vázquez, A. E., Yamoah, E. N., and Aldrich, R. W. (2007). Cochlear function in mice lacking the bk channel α, $\beta 1$, or $\beta 4$ subunits. *Journal of Biological Chemistry*, 282(5):3312–3324.

[Qian and Bodmer, 2009] Qian, L. and Bodmer, R. (2009). Partial loss of gata factor pannier impairs adult heart function in drosophila. *Human molecular genetics*, 18(17):3153–3163.

[Ramekers et al., 2015] Ramekers, D., Versnel, H., Strahl, S. B., Klis, S. F., and Grolman, W. (2015). Temporary neurotrophin treatment prevents deafness-induced auditory nerve degeneration and preserves function. *The Journal of Neuroscience*, 35(36):12331–12345.

[Raphael and Altschuler, 2003] Raphael, Y. and Altschuler, R. A. (2003). Structure and innervation of the cochlea. *Brain research bulletin*, 60(5):397–422.

[Riccomagno et al., 2005] Riccomagno, M. M., Takada, S., and Epstein, D. J. (2005). Wnt-dependent regulation of inner ear morphogenesis is balanced by the opposing and supporting roles of shh. *Genes & development*, 19(13):1612–1623.

[Rivolta and Holley, 1998] Rivolta, M. N. and Holley, M. C. (1998). Gata3 is downregulated during hair cell differentiation in the mouse cochlea. *Journal of neurocytology*, 27(9):637–647.

[Rivolta and Holley, 2002] Rivolta, M. N. and Holley, M. C. (2002). Cell lines in inner ear research. *Journal of neurobiology*, 53(2):306–318.

[Roberson et al., 2004] Roberson, D. W., Alosi, J. A., and Cotanche, D. A. (2004). Direct transdifferentiation gives rise to the earliest new hair cells in regenerating avian auditory epithelium. *Journal of neuroscience research*, 78(4):461–471.

[Rohmann et al., 2015] Rohmann, K. N., Wersinger, E., Braude, J. P., Pyott, S. J., and Fuchs, P. A. (2015). Activation of bk and sk channels by efferent synapses on outer hair cells in high-frequency regions of the rodent cochlea. *The Journal of Neuroscience*, 35(5):1821–1830.

[Roux et al., 2006] Roux, I., Safieddine, S., Nouvian, R., Grati, M., Simmler, M.-C., Bahloul, A., Perfettini, I., Le Gall, M., Rostaing, P., Hamard, G., et al. (2006). Otoferlin, defective in a human deafness form, is essential for exocytosis at the auditory ribbon synapse. *Cell*, 127(2):277–289.

[Roux et al., 2011] Roux, I., Wersinger, E., McIntosh, J. M., Fuchs, P. A., and Glowatzki, E. (2011). Onset of cholinergic efferent synaptic function in sensory hair cells of the rat cochlea. *The Journal of Neuroscience*, 31(42):15092–15101.

[Ruan et al., 2008] Ruan, Q., Chen, D., Wang, Z., Chi, F., Yin, S., and Wang, J. (2008). Topological and developmental expression gradients of kir2. 1, an inward rectifier k+ channel, in spiral ganglion and cochlear hair cells of mouse inner ear. *Developmental neuroscience*, 30(6):374–388.

[Rubel and Fritzsch, 2002] Rubel, E. W. and Fritzsch, B. (2002). Auditory system development: primary auditory neurons and their targets. *Annual review of neuroscience*, 25(1):51–101.

[Ruben, 1967] Ruben, R. J. (1967). Development of the inner ear of the mouse: a radioautographic study of terminal mitoses. *Acta oto-laryngologica*, pages Suppl–220.

[Rüttiger et al., 2004] Rüttiger, L., Sausbier, M., Zimmermann, U., Winter, H., Braig, C., Engel, J., Knirsch, M., Arntz, C., Langer, P., Hirt, B., et al. (2004). Deletion of the ca2+-activated potassium (bk) α-subunit but not the bkβ1-subunit leads to progressive hearing loss. *Proceedings of the National Academy of Sciences of the United States of America*, 101(35):12922–12927.

[Safieddine et al., 2012] Safieddine, S., El-Amraoui, A., and Petit, C. (2012). The auditory hair cell ribbon synapse: from assembly to function. *Annual review of neuroscience*, 35:509–528.

[Sánchez-Calderón et al., 2007] Sánchez-Calderón, H., Milo, M., León, Y., Varela-Nieto, I., et al. (2007). A network of growth and transcription factors controls neuronal differentation and survival in the developing ear. *International Journal of Developmental Biology*, 51(6-7):557–570.

[Santos-Sacchi and Dilger, 1988] Santos-Sacchi, J. and Dilger, J. (1988). Whole cell currents and mechanical responses of isolated outer hair cells. *Hearing research*, 35(2):143–150.

[Sartori et al., 2013] Sartori, D. J., Wilbur, C. J., Long, S. Y., Rankin, M. M., Li, C., Bradfield, J. P., Hakonarson, H., Grant, S. F., Pu, W. T., and Kushner, J. A. (2013). Gata factors promote er integrity and β-cell survival and contribute to type 1 diabetes risk. *Molecular Endocrinology*, 28(1):28–39.

[Sau et al., 2013] Sau, T., Chatterjee, A., Ghosh, K., and Dey, S. (2013). Seizure, deafness and renal agenesis: A rare case of barakat syndrome. *Annals of Indian Academy of Neurology*, 16(1):91.

[Schimmang et al., 2007] Schimmang, T. et al. (2007). Expression and functions of fgf ligands during early otic development. *International Journal of Developmental Biology*, 51(6-7):473–481.

[Schmitz, 2009] Schmitz, F. (2009). The making of synaptic ribbons: how they are built and what they do. *The Neuroscientist*.

[Schrott et al., 1991] Schrott, A., Puel, J.-L., and Rebillard, G. (1991). Cochlear origin of 21- 2 distortion products assessed by using 2 types of mutant mice. *Hearing research*, 52(1):245–253.

[Sheehan-Rooney et al., 2013] Sheehan-Rooney, K., Swartz, M. E., Zhao, F., Liu, D., and Eberhart, J. K. (2013). Ahsa1 and hsp90 activity confers more severe craniofacial phenotypes in a zebrafish model of hypoparathyroidism, sensorineural deafness and renal dysplasia (hdr). *Disease models & mechanisms*, 6(5):1285–1291.

[Shen et al., 2004] Shen, Z., Liang, F., Hazen-Martin, D. J., and Schulte, B. A. (2004). Bk channels mediate the voltage-dependent outward current in type i spiral ligament fibrocytes. *Hearing research*, 187(1):35–43.

[Shi and Edge, 2013] Shi, F. and Edge, A. S. (2013). Prospects for replacement of auditory neurons by stem cells. *Hearing research*, 297:106–112.

[Shivdasani et al., 1998] Shivdasani, R. A., Mcdevitt, M. A., Fujiwara, Y., and Orkin, S. H. (1998). Transcription factor gata-1 in megakaryocyte development. *Stem Cells*, 16(S1):79–83.

[Shnerson et al., 1981] Shnerson, A., Devigne, C., and Pujol, R. (1981). Age-related changes in the c57bl/6j mouse cochlea. ii. ultrastructural findings. *Developmental Brain Research*, 2(1):77–88.

[Simmons, 2002] Simmons, D. D. (2002). Development of the inner ear efferent system across vertebrate species. *Journal of neurobiology*, 53(2):228–250.

[Sobkowicz et al., 1982] Sobkowicz, H. M., Rose, J. E., Scott, G. E., and Slapnick, S. M. (1982). Ribbon synapses in the developing intact and cultured organ of corti in the mouse. *The Journal of Neuroscience*, 2(7):942–957.

[Spektor et al., 1991] Spektor, Z., Leonard, G., Kim, D., Jung, M. D., and Smurzynski, J. (1991). Otoacoustic emissions in normal and hearing-impaired children and normal adults. *The Laryngoscope*, 101(9):965–976.

[Spicer et al., 1999] Spicer, S. S., Thomopoulos, G. N., and Schulte, B. A. (1999). Novel membranous structures in apical and basal compartments of inner hair cells. *Journal of Comparative Neurology*, 409(3):424–437.

[Sterbing and Schrott-Fischer, 2002] Sterbing, S. and Schrott-Fischer, A. (2002). Electrophysiological characteristics of inferior colliculus neurons in mutant mice with hereditary absence of cochlear outer hair cells. *Hearing research*, 170(1):179–189.

[Takaku et al., 2016] Takaku, M., Grimm, S. A., Shimbo, T., Perera, L., Menafra, R., Stunnenberg, H. G., Archer, T. K., Machida, S., Kurumizaka, H., and Wade, P. A. (2016). Gata3-dependent cellular reprogramming requires activation-domain dependent recruitment of a chromatin remodeler. *Genome biology*, 17(1):1.

[Thastrup et al., 1990] Thastrup, O., Cullen, P. J., Drøbak, B., Hanley, M. R., and Dawson, A. P. (1990). Thapsigargin, a tumor promoter, discharges intracellular ca2+ stores by specific inhibition of the endoplasmic reticulum ca2 (+)-atpase. *Proceedings of the National Academy of Sciences*, 87(7):2466–2470.

[Torres et al., 1996] Torres, M., Gómez-Pardo, E., and Gruss, P. (1996). Pax2 contributes to inner ear patterning and optic nerve trajectory. *Development*, 122(11):3381–3391.

[Úlehlová et al., 1987] Úlehlová, L., Voldřich, L., and Janisch, R. (1987). Correlative study of sensory cell density and cochlear length in humans. *Hearing research*, 28(2):149–151.

[van Beelen et al., 2014] van Beelen, E., Leijendeckers, J., Admiraal, R., Huygen, P., Hoefsloot, L., Pennings, R., Snik, A., and Kunst, H. (2014). Audiometric characteristics of a dutch family with a new mutation in gata3 causing hdr syndrome. *Audiology and Neurotology*, 19(2):106–114.

[van der Wees et al., 1999] van der Wees, J., Karis, A., Goedknegt, E., Rutteman, M., Grosveld, F., Doorninck, J., and Zeeuw, C. (1999). Gata-3 is involved in the development of serotonergic neurons in the caudal raphe nuclei. *The Journal of Neuroscience*, 19(12):1–8.

[van der Wees et al., 2004] van der Wees, J., van Looij, M. A., de Ruiter, M. M., Elias, H., van der Burg, H., Liem, S.-S., Kurek, D., Engel, J. D., Karis, A., van Zanten, B. G., et al. (2004). Hearing loss following¡ i¿ gata3¡/i¿ haploinsufficiency is caused by cochlear disorder. *Neurobiology of disease*, 16(1):169–178.

[Van Esch and Devriendt, 2001] Van Esch, H. and Devriendt, K. (2001). Human genome and diseases: Review transcription factor gata3 and the human hdr syndrome. *Cellular and Molecular Life Sciences CMLS*, 58(9):1296–1300.

[Van Esch et al., 2000] Van Esch, H., Groenen, P., Nesbit, M. A., Schuffenhauer, S., Lichtner, P., Vanderlinden, G., Harding, B., Beetz, R., Bilous, R. W., Holdaway, I., et al. (2000). Gata3 haplo-insufficiency causes human hdr syndrome. *NATURE-LONDON-*, pages 419–421.

[van Looij et al., 2005] van Looij, M. A., van der Burg, H., van der Giessen, R. S., de Ruiter, M., van der Wees, J., van Doorninck, J., De Zeeuw, C., and van Zanten, G. (2005). Gata3 haploinsufficiency causes a rapid deterioration of distortion product otoacoustic emissions (dpoaes) in mice. *Neurobiology of disease*, 20(3):890–897.

[Vicente et al., 2012] Vicente, C., Conchillo, A., García-Sánchez, M. A., and Odero, M. D. (2012). The role of the gata2 transcription factor in normal and malignant hematopoiesis. *Critical reviews in oncology/hematology*, 82(1):1–17.

[Von Békésy and Wever, 1960] Von Békésy, G. and Wever, E. G. (1960). *Experiments in hearing*, volume 8. McGraw-Hill New York.

[Wakabayashi et al., 2003] Wakabayashi, J., Yomogida, K., Nakajima, O., Yoh, K., Takahashi, S., Engel, J. D., Ohneda, K., and Yamamoto, M. (2003). Gata-1 testis activation region is essential for sertoli cell-specific expression of gata-1 gene in transgenic mouse. *Genes to Cells*, 8(7):619–630.

[Wan et al., 2013] Wan, G., Corfas, G., and Stone, J. S. (2013). Inner ear supporting cells: Rethinking the silent majority. In *Seminars in cell & developmental biology*, volume 24, pages 448–459. Elsevier.

[Wang et al., 2015] Wang, W., Sun, Y., Chen, S., Zhou, X., Wu, X., Kong, W., and Kong, W. (2015). Impaired unfolded protein response in the degeneration of cochlea cells in a mouse model of age-related hearing loss. *Experimental gerontology*, 70:61–70.

[Wangemann, 2006] Wangemann, P. (2006). Supporting sensory transduction: cochlear fluid homeostasis and the endocochlear potential. *The Journal of physiology*, 576(1):11–21.

[Warchol, 2011] Warchol, M. E. (2011). Sensory regeneration in the vertebrate inner ear: differences at the levels of cells and species. *Hearing research*, 273(1):72–79.

[Wersinger and Fuchs, 2011] Wersinger, E. and Fuchs, P. A. (2011). Modulation of hair cell efferents. *Hearing research*, 279(1):1–12.

[Wersinger et al., 2010] Wersinger, E., McLean, W. J., Fuchs, P. A., and Pyott, S. J. (2010). Bk channels mediate cholinergic inhibition of high frequency cochlear hair cells. *PLoS One*, 5(11):e13836.

[Whitehead and Robinson, 2009] Whitehead, R. H. and Robinson, P. S. (2009). Establishment of conditionally immortalized epithelial cell lines from the intestinal tissue of adult normal and transgenic mice. *American Journal of Physiology-Gastrointestinal and Liver Physiology*, 296(3):G455–G460.

[Woods et al., 2004] Woods, C., Montcouquiol, M., and Kelley, M. W. (2004). Math1 regulates development of the sensory epithelium in the mammalian cochlea. *Nature neuroscience*, 7(12):1310–1318.

[Xie et al., 2008] Xie, L.-H., John, S. A., Ribalet, B., and Weiss, J. N. (2008). Phosphatidylinositol-4, 5-bisphosphate (pip2) regulation of strong inward rectifier kir2. 1 channels: multilevel positive cooperativity. *The Journal of physiology*, 586(7):1833–1848.

[Xu et al., 2011] Xu, M., Millard, R. W., and Ashraf, M. (2011). Role of gata-4 in differentiation and survival of bone marrow mesenchymal stem cells. *Progress in molecular biology and translational science*, 111:217–241.

[Yan et al., 2010] Yan, W., Cao, Q. J., Arenas, R. B., Bentley, B., and Shao, R. (2010). Gata3 inhibits breast cancer metastasis through the reversal of epithelial-mesenchymal transition. *Journal of Biological Chemistry*, 285(18):14042–14051.

[Zeichner-David et al., 2003] Zeichner-David, M., Oishi, K., Su, Z., Zakartchenko, V., Chen, L.-S., Arzate, H., and Bringas, P. (2003). Role of hertwig's epithelial root sheath cells in tooth root development. *Developmental dynamics*, 228(4):651–663.

[Zhang et al., 2003] Zhang, H., Craciun, L. C., Mirshahi, T., Rohács, T., Lopes, C. M., Jin, T., and Logothetis, D. E. (2003). Pip 2 activates kcnq channels, and its hydrolysis underlies receptor-mediated inhibition of m currents. *Neuron*, 37(6):963–975.

[Zhang et al., 1999] Zhang, H., He, C., Yan, X., Mirshahi, T., and Logothetis, D. E. (1999). Activation of inwardly rectifying k+ channels by distinct ptdins (4, 5) p2 interactions. *Nature cell biology*, 1(3):183–188.

[Zheng and Gao, 2000] Zheng, J. L. and Gao, W.-Q. (2000). Overexpression of math1 induces robust production of extra hair cells in postnatal rat inner ears. *Nature neuroscience*, 3(6):580–586.

[Zheng et al., 1999] Zheng, Q. Y., Johnson, K. R., and Erway, L. C. (1999). Assessment of hearing in 80 inbred strains of mice by abr threshold analyses. *Hearing research*, 130(1):94–107.

[Zhu et al., 2004] Zhu, J., Min, B., Hu-Li, J., Watson, C. J., Grinberg, A., Wang, Q., Killeen, N., Urban, J. F., Guo, L., and Paul, W. E. (2004). Conditional deletion of gata3 shows its essential function in th1-th2 responses. *Nature immunology*, 5(11):1157–1165.

[Zhu et al., 2014] Zhu, Z.-Y., Zhou, Q.-L., Ni, S.-N., and Gu, W. (2014). Gata3 mutation in a family with hypoparathyroidism, deafness and renal dysplasia syndrome. *World Journal of Pediatrics*, 10(3):278–280.

[Zou et al., 2008] Zou, D., Erickson, C., Kim, E.-H., Jin, D., Fritzsch, B., and Xu, P.-X. (2008). Eya1 gene dosage critically affects the development of sensory epithelia in the mammalian inner ear. *Human molecular genetics*, 17(21):3340–3356.